REPORT SERIES IN AEROSOL SCIENCE
N:o 220 (2019)

# Biogenic New Particle Formation: Field Observations and Chamber Experiments

LUBNA DADA

Institute for Atmospheric and Earth System Research / Physics
Faculty of Science,
University of Helsinki,
Helsinki, Finland

Academic dissertation

*To be presented, with the permission of the Faculty of Science of the University of Helsinki, for public criticism in auditorium E204, Gustaf Hällströmin katu 2, on June 14th, 2019, at 12 o'clock noon.*

**Helsinki 2019**

Author's Address: Institute for Atmospheric and Earth System Research / Physics
P.O. box 64
FI-00140 University of Helsinki
lubna.dada@helsinki.fi

Supervisors: Academician, Professor Markku Kulmala, Ph.D.
Institute for Atmospheric and Earth System Research / Physics
University of Helsinki
Professor Veli-Matti Kerminen, Ph.D.
Institute for Atmospheric and Earth System Research / Physics
University of Helsinki
Assistant Professor Pauli Paasonen, Ph.D.
Institute for Atmospheric and Earth System Research / Physics
University of Helsinki

Reviewers: Professor Hannele Korhonen, Ph.D.
Climate Research Programme
Finnish Meteorological Institute
Professor Miikka Dal Maso, Ph.D.
Laboratory of Physics, Tampere University

Opponent: Director, Professor Maria Cristina Facchini, Ph.D
Institute of Atmospheric Sciences and Climate,
Italian National Research Council

ISBN 978-952-7276-22-8 (printed version)
ISSN 0784-3496
Helsinki 2019
Unigrafia Oy

ISBN 978-952-7276-23-5 (pdf version)
http://www.atm.helsinki.fi/FAAR
Helsinki 2019
Helsingin yliopiston verkkojulkaisut

## Acknowledgements

The research work for this thesis was done within the premises of INAR and Hyytiälä SMEAR II measurement station. I would like to thank all the technical staff that made these measurements happen. I would like to also thank all my co-authors and collaborators. A special thanks goes to Professor Hannele Korhonen and Professor Miikka Dal Maso for reviewing my thesis.

Please let me express my gratitude to my supervisor and the Director of INAR Academician Professor Markku Kulmala for not only employing me at INAR but for welcoming me within the group. Thank you for giving me the opportunity to participate in many different projects that made me broaden my horizons and pushed me to explore my full potential. Thank you for the trust you have placed me in. Thank you for your curiosity and vision that kept me going; besides, you have taught me not only science, but also life.

I would like to thank Professor Veli-Matti Kerminen for keeping his door open for whatever questions I had, and for giving me the most helpful comments throughout my PhD experience. Thank you for guiding me, teaching me and correcting me when I was wrong. It was very helpful.

When I first joined the division, I was helpless, Assistant Professor Pauli Paasonen didn't give up on me. You didn't get bored from the million questions I asked or the bugs in my MATLAB code. Thank you for that. Thank you for your support and for teaching me patience.

I would also like to thank Professor Tareq Hussein for introducing me to INAR as a whole. Thank you for always involving me in interesting science regardless of how busy both of us were. Moving to Helsinki for my PhD was one of the hardest yet the best decisions ever.

I would also like to thank Professor Tuukka Petäjä, Professor Douglas Worsnop, Assistant Professor Tuomo Nieminen, Associate Professor Katrianne Lehtipalo, Dr. Jenni Kontkanen, Dr. Juha Kangasluoma and Dr. Hanna Manninen for passing on their knowledge and for training me. Thank you for holding my hand when needed while teaching me to be independent. Thank you for your "let's do this" attitude.

I have enjoyed every bit of science that I did together with Dr. Chao Yan and Dr. Clèmence Rose, we were the most efficient group of people with maximum sync.

My PhD track has also brought me to work with Aerosol and Haze project at the Beijing University of chemical technology. The group welcomed me as part of the team. Thank you for making the Chinese experience worthwhile! Thanks to Dr. Tommy Chan, Dr. Tom Kokkonen, Simo Hakala, Mona Kurppa, Dr. Yonghong Wang, Ying Zhou, Dr. Biwu Chu, Dr. Wei Du, Dr. Xiaolong Fan, Dr. Jing Cai and many others.

The CLOUD experiment would not have been endured without the awesome people whom I met and became close friends with. Many thanks to the late night chats, the cooking and the endless support I got from Dr. Andrea Wagner, Dr. Martin Heinritzi, Mario Simon, Dr. Dominik Stolzenburg, Mao Xiao, Xucheng He, Antonio Dias, Dr. Jonathan Duplissy and the whole CLOUD collaboration. After all, the 3

o’clock meetings were worth it. In particular, I would like to thank Professor Jasper Kirkby for his wonderful support during the four years, your dedication and enthusiasm to always discover new things is contagious.

I would like to thank my friends/superwomen in the division, who are dedicated to lift spirit, spread positivity and eat cake. Thanks to Stephany, Lauriane, Rima, Anna, Daniela, Olga and many others who made it feel like home! Thank you for eating the cake no matter how lousy it tasted. Regardless of the distance and the time zones, my Lebanese friends still managed to always remind me why I am going through this journey and were passing on all the love and support to Finland. Many thanks to Ali, Bilal, Nour, Rasha and Reem.

None of this work, or status of life, would have become possible without the endless support of my mother Mariam. Your selfless thinking helped me reach places I never thought I would. You are an extraordinary, open-minded, strong, and one of a kind wonder woman that I always looked up to.

In the end, I would like to thank my partner Kaspar moving to Helsinki, and for bearing my stress levels. Thank you for encouraging my insane ideas and for going with me on this crazy roller coaster of aerosol science. Thank you for always reminding me that things will work out and that there is life outside the PhD.

**Biogenic New Particle Formation: Field Observations and Chamber Experiments**

Lubna Dada

University of Helsinki, 2019

## Abstract

New particle formation (NPF) is an atmospheric phenomenon, observed in many environments globally, and it contributes to a major fraction of the global aerosol number budget thereby affecting both climate and human health. In this thesis, we investigate the mechanisms behind NPF in the boreal forest environment and analyze the long-term behavior of the variables associated with the occurrence of this phenomenon.

In order to improve the classification of atmospheric NPF events, especially when considering the increasing number of measurement campaigns and stations, we developed an automatic framework to classify NPF events based on the 2–4 nm ion and 7–25 nm aerosol particle concentrations in the atmosphere. This approach categorizes days into four defined classes: Regional NPF events, transported NPF events, ion bursts and non-events. For regional NPF events, the approach additionally determined the precise period (start and end-time) during which the event occurred. We show that, in the boreal forest, NPF events tend to occur under clear sky conditions with low condensation sinks and moderate temperatures.

Using chamber simulations, we further investigated the mechanisms of new particle formation and growth in the boreal forest environment. While sulfuric acid is known to be the driver of NPF, we found that pure biogenic NPF is possible in the absence of sulfuric acid, and that the nucleation is mediated by dimers of highly oxygenated monoterpene oxidation products. We also found that anthropogenic vapors, such as $NO_x$, attenuate the particle formation and growth by modifying the chemical composition of highly oxygenated molecules (HOMs) necessary for nucleation and growth.

In the present-day-time atmosphere, we found that highly oxygenated molecules (HOMs) govern ion-induced new particle formation in the boreal forest when the ratio of biogenic HOMs to $H_2SO_4$ is greater than 30. Our results show that non-nitrate HOM dimers mediate ion-induced nucleation not only during daytime but also during night-time. In the absence of $H_2SO_4$, we observed pure biogenic ion-induced clustering mediated by non-nitrate HOM dimers and trimers; however, these clusters did not grow past 6 nm due to insufficient photochemistry needed for producing condensable vapors that would ensure cluster survival.

Key Words: NPF, IIN, HOM, CLOUD, cloudiness, condensation sink, $H_2SO_4$

## Contents

## List of publications

This thesis consists of an introductory section, followed by five research articles. In the introduction part, these articles are cited according to their roman numbers. Papers III and V are reprinted with the approval of all co-authors. Papers I, II and IV are reprinted under the Creative Commons Attribution 4.0 International license.

I **Dada, L**., Chellapermal, R., Buenrostro Mazon, S., Paasonen, P., Lampilahti, J., Manninen, H. E., Junninen, H., Petäjä, T., Kerminen, V. M., and Kulmala, M.: Refined classification and characterization of atmospheric new-particle formation events using air ions, *Atmospheric Chemistry and Physics*, doi: 10.5194/acp-18-17883-2018, 2018.

II **Dada, L**., Paasonen, P., Nieminen, T., Mazon, S. B., Kontkanen, J., Perakyla, O., Lehtipalo, K., Hussein, T., Petaja, T., Kerminen, V. M., Back, J., and Kulmala, M.: Long-term analysis of clear-sky new particle formation events and nonevents in Hyytiala, *Atmospheric Chemistry and Physics*, doi: 10.5194/acp-17-6227-2017, 2017.

III Lehtipalo, K., Yan, C., **Dada, L**., Bianchi, F., Xiao, M., Wagner, R., Stolzenburg, D., Ahonen, L. R., Amorim, A., Baccarini, A., Bauer, P. S., Baumgartner, B., Bergen, A., Bernhammer, A.-K., Breitenlechner, M., Brilke, S., Buchholz, A., Mazon, S. B., Chen, D., Chen, X., Dias, A., Dommen, J., Draper, D. C., Duplissy, J., Ehn, M., Finkenzeller, H., Fischer, L., Frege, C., Fuchs, C., Garmash, O., Gordon, H., Hakala, J., He, X., Heikkinen, L., Heinritzi, M., Helm, J. C., Hofbauer, V., Hoyle, C. R., Jokinen, T., Kangasluoma, J., Kerminen, V.-M., Kim, C., Kirkby, J., Kontkanen, J., Kürten, A., Lawler, M. J., Mai, H., Mathot, S., Mauldin, R. L., Molteni, U., Nichman, L., Nie, W., Nieminen, T., Ojdanic, A., Onnela, A., Passananti, M., Petäjä, T., Piel, F., Pospisilova, V., Quéléver, L. L. J., Rissanen, M. P., Rose, C., Sarnela, N., Schallhart, S., Schuchmann, S., Sengupta, K., Simon, M., Sipilä, M., Tauber, C., Tomé, A., Tröstl, J., Väisänen, O., Vogel, A. L., Volkamer, R., Wagner, A. C., Wang, M., Weitz, L., Wimmer, D., Ye, P., Ylisirniö, A., Zha, Q., Carslaw, K. S., Curtius, J., Donahue, N. M., Flagan, R. C., Hansel, A., Riipinen, I., Virtanen, A., Winkler, P. M., Baltensperger, U., Kulmala, M., and Worsnop, D. R.: Multicomponent new particle formation from sulfuric acid, ammonia, and biogenic vapors, *Science Advances*, doi: 10.1126/sciadv.aau5363, 2018

IV Yan, C., **Dada, L**., Rose, C., Jokinen, T., Nie, W., Schobesberger, S., Junninen, H., Lehtipalo, K., Sarnela, N., Makkonen, U., Garmash, O., Wang, Y., Zha, Q., Paasonen, P., Bianchi, F., Sipilä, M., Ehn, M., Petäjä, T., Kerminen, V. M., Worsnop, D. R., and Kulmala, M.: The role of $H_2SO_4$-$NH_3$ anion clusters in ion-induced aerosol nucleation mechanisms in the boreal forest, *Atmospheric Chemistry and Physics*, doi: 10.5194/acp-18-13231-2018, 2018.

V Rose C., Zha Q., **Dada L**., Yan C., Lehtipalo K., Junninen H., Buenrostro Mazon S., Jokinen T., Sarnela N., Sipilä M., PetäjäT., KerminenV.-M., Bianchi F., Kulmala M.: Observations of biogenic ion-induced cluster formation in the atmosphere, *Science Advances*, doi: 11.1126/sciadv.aar5218, 2018.

# 1. Introduction

Aerosol particles are solid particles or liquid droplets suspended in a carrier gas. These particles have diameters ranging between about one nanometer and several tens of micrometers, and they have varying chemical composition (Putaud et al., 2004) and morphologies (Dada et al., 2013). Scientists associate elevated particle concentrations with increased death rates (Pope et al., 1995; Apte et al., 2015; Burnett et al., 2018). However, it is still controversial which specific characteristic of atmospheric particles (mass or number concentration, or chemical composition) has the strongest impact on human health (Lelieveld et al., 2015). While it has been thought that the smallest particles do not have a large impact on health, they have been observed to penetrate the respiratory tract towards the blood circulation and finally deposit into the brain (Oberdörster et al., 2004; Künzli and Tager, 2005). In addition to their health effects, aerosol particles affect climate directly by scattering or absorbing incoming solar radiation, and indirectly by modifying many cloud properties (IPCC, 2013; Murphy and Ravishankara, 2018).

Atmospheric aerosol particles originate from a large variety of different sources and formation pathways. They can be emitted directly to the atmosphere as primary particles via natural phenomena or because of anthropogenic activities. The two most important natural primary particle sources in the atmosphere are sea spray production and wind-blown dust emissions (Huneeus et al., 2011; Grythe et al., 2014), while globally-important anthropogenic primary particle sources include a variety of biomass burning activities, traffic and other transportation activities, power generation, various industrial activities, etc. (Schauer et al., 1996; Andreae and Merlet, 2001; Kumar et al., 2013; Paasonen et al., 2016; Vicente and Alves, 2018). In addition to primary particle emissions, particulate matter or entirely new aerosol particles can be formed secondarily in the atmosphere via heterogeneous and homogenous nucleation pathways, respectively. New particle formation (NPF) is a type of secondary particle formation where low-volatility gas-phase precursor compounds produce stable clusters and eventually aerosol particles (Kulmala, 2003). Specifically, a new particle formation event is defined by the appearance of stable clusters that show signs of growth (Dal Maso et al., 2005). NPF has been observed in different environments around the world, ranging from relatively pristine environments to heavily-polluted megacities (Kulmala et al., 2004; Kerminen et al., 2018; Chu et al., 2019). In practice, whether NPF occurs or not is a result of the competition between the sources and sinks of initially-formed clusters (about 0.8 nm in diameter), and this phenomenon is typically observed once these clusters start to grow past a few nanometers to be classified as a NPF event. Depending on the environmental conditions, the frequency and intensity of such NPF events can vary considerably (Nieminen et al., 2018). While the frequency of NPF events at a specific location is determined by event classification (**Paper I**), the intensity of such events is quantified by determining particle formation and growth rates (**Paper II**).

Recently, thorough research activities have been carried out in order to understand the drivers of NPF, as this phenomenon was found to contribute to a large fraction of the global aerosol particle number budget (Spracklen et al., 2010). Furthermore, particles formed by NPF were found to influence cloud properties by contributing to the concentration of cloud condensation nuclei (Merikanto et al., 2009; Pierce and Adams, 2009; Kerminen et al., 2012). Measurement campaigns and continuous measurement

stations have thus been established at various locations around the world in order to understand the mechanisms behind NPF (Kulmala et al., 2004; Kulmala, 2018). Scientists have also studied the impact of NPF on the pre-industrial aerosol by laboratory experiments using atmospheric simulation chambers in order to improve future climate predictions of global models (Liao et al., 2006; Dunne et al., 2016; Gordon et al., 2016; Kirkby et al., 2016). Indeed, with the development of instrumentation, such as proton-transfer reaction mass spectrometer (PTR-MS, Hansel et al., 1995) and atmospheric-pressure-interface time-of-flight mass spectrometer (APi-TOF, Junninen et al., 2010), it has become possible to follow the process of NPF even before the actual particle is born. Such instruments measure, for example, concentrations of available precursor vapors and the chemical composition of freshly formed clusters. The development of additional instrumentation, such as the Particle Size Magnifier (PSM, Vanhanen et al., 2011), allows us to follow the size evolution of the newly formed particles starting from about 1 nm in particle diameter.

Sulfuric acid ($H_2SO_4$) has been identified as the major precursor vapor influencing atmospheric NPF (Weber et al., 1995; Birmili et al., 2003; Kulmala et al., 2006; Sihto et al., 2006; Sipilä et al., 2010; Riccobono et al., 2012; Kuang et al., 2010; Yao et al., 2018). The main reason for this is the low saturation vapor pressure of $H_2SO_4$, making it capable of forming small clusters and condensing onto them effectively. When $H_2SO_4$ is stabilized by a base, such as ammonia ($NH_3$) or amines, the new particle formation rate is enhanced (Ortega et al., 2008; Almeida et al., 2013; Jen et al., 2014; Kürten et al., 2016). Recently, low volatility highly oxygenated molecules (HOMs) (Ehn et al., 2014; Bianchi et al., 2019) have been discovered as oxidation products of many kinds of volatile organic vapors. Via chamber experiments, HOMs of biogenic origin were proven to contribute to particle growth and even particle formation in the absence of sulfuric acid (Riccobono et al., 2012; Riipinen et al., 2012; Schobesberger et al., 2013; Kirkby et al., 2016). More recently, after being stabilized by ions, HOMs were found to contribute to the early stages of particle formation in the ambient atmosphere, including the free troposphere (Bianchi et al., 2016) and boreal forest environment (**Papers IV** and **V**). The synergistic roles of HOMs, $H_2SO_4$ and $NH_3$, when present simultaneously in particle formation, have been simulated in chamber experiments (**Paper III**) and observed in the field (**Paper IV**). A schematic summary of the processes involved in new particle formation from precursors, such as $SO_2$ and biogenic organic compounds, is demonstrated in Figure 1.

The aims of this thesis are to:

(i) develop a new method for automatically classifying new particle formation event days using their characteristic air ion and particle concentrations,
(ii) quantify the effect of cloudiness on the frequency of NPF events,
(iii) determine the parameters that affect the probability of NPF in the boreal forest environment,
(iv) quantify how HOMs, $H_2SO_4$ and $NH_3$ affect daytime and night-time NPF in a boreal forest environment using chamber experiments and field observations.

In the first step of this thesis, a data handling framework is introduced, which allows for classifying NPF event and non-event days, as well as two other classes: transported NPF events and ion bursts (**Paper I**).

The method relies on the cluster mode ion concentration (initial steps of clustering) and is therefore able to categorize all measurement days, including those which are usually undefined and are excluded from further analysis. This procedure is made automatic, which makes it possible to analyze long-term data sets while minimizing both analysis biases and manpower required (**Paper I**). After classifying the days, long-term evidence of the effect of cloudiness on reducing the occurrence of NPF events is presented (**Paper II**). Also, upon defining the exact time window during which NPF events in the boreal forest occur (**Paper I**), and under clear sky conditions, the impact of several environmental parameters such as condensation sink and ambient temperature is analyzed (**Paper II**). Moreover, the participation of several gaseous precursors (HOMs, $H_2SO_4$ and $NH_3$) in nucleation and growth are simulated in laboratory experiments, each individually and in a mixture (**Paper III**). Lastly, the impact of these precursors, on parameters describing NPF, such as NPF event frequency, formation rates, and growth rates are presented and are quantified in the ambient under different conditions (day-time (**Paper IV**) vs night-time (**Paper V**)).

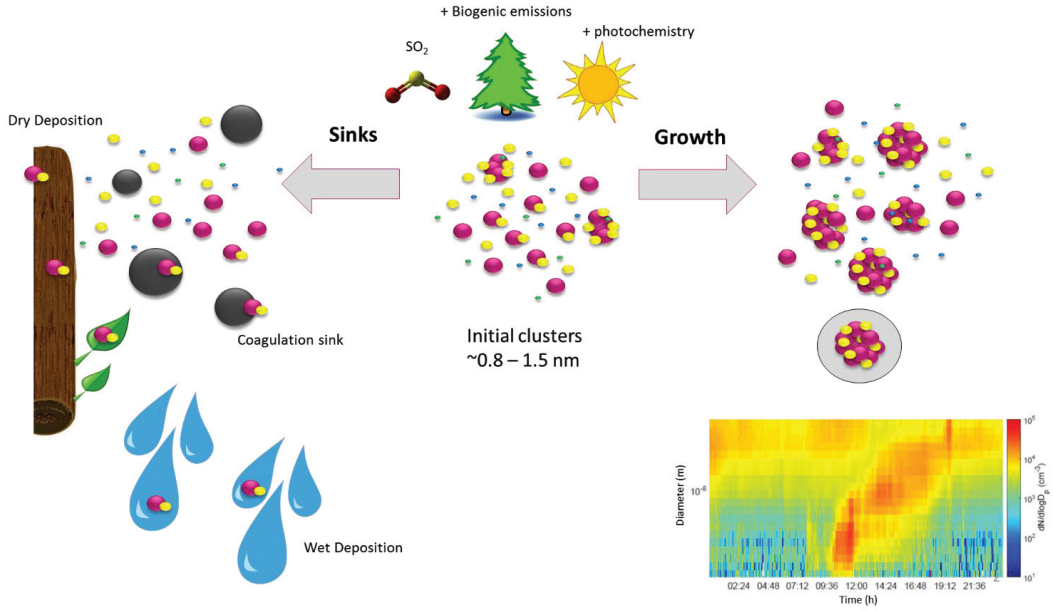


Figure 1 Pathway from precursor vapor emissions to new particle formation.

# 2. Methods

## 2.1. Measurement facilities and instrumentation

### 2.1.1. Station for Measuring Ecosystem – Atmosphere Relations (SMEAR II)

The main conclusions of this thesis cover new particle formation and growth as well as their governing mechanisms in the boreal forest. The observations reported in **Papers I, II, IV** and **V** were made at the SMEAR II station and the experiments described in **Paper III** replicated the same environment in terms of gaseous precursors, temperature and condensation sink. The station provides more than 20 years of continuous comprehensive measurements of variables describing atmosphere–forest–ecosystem interactions (Hari and Kulmala, 2005). The station is located in Hyytiälä, southern Finland (61◦510 N, 24◦170 E, 181 m a.s.l.). The largest nearest city, Tampere, is located 60 km SW of Hyytiälä. The station is insignificantly influenced by direct anthropogenic emissions and could then be considered a rural background site representative of the northern hemisphere boreal forests (Asmi et al., 2011). Additionally, the station is surrounded by a homogenous green-belt of Scots pines ideal for studying biogenic new particle formation under low levels of air pollutants (**Papers I, II, III, IV** and **V)**.

Since January 1996, the station has provided continuous measurements of parameters including aerosol particle number size distributions, concentration of the trace gases, and meteorological parameters (solar radiation, temperature and relative humidity). The aerosol number size distributions were measured with a twin DMPS (Differential Mobility Particle Sizer) system (Wang et al., 1990; Aalto et al., 2001) over the size range of 3–500 nm until the year 2004 and over the size range of 3–1000 nm from 2005 onwards. Additionally, the mobility distributions of neutral and charged aerosol particles and clusters in the size ranges of 2–42 nm and 0.8–47 nm, respectively, were measured with a Neutral cluster and Air Ion Spectrometer (NAIS, Airel Ltd., Estonia, Manninen et al. (2009); (2016); Mirme and Mirme (2013)) since 2006. Trace gas concentrations are being measured at six different heights on a 74 m-high mast (extended to 126 m in summer 2010). Recently, more advanced instruments, such as proton-transfer reaction mass spectrometer (PTR-MS, Hansel et al., (1995); Jordan et al., (2009); Rantala et al., (2014)), Aerosol Chemical Speciation Monitor (ACSM, Ng et al., (2011)), and atmospheric-pressure-interface time-of-flight mass spectrometer with and without a chemical ionization inlet (CI-APi-TOF (Jokinen et al., (2012); APi-TOF, Junninen et al., (2010); Ehn et al., (2010)) have also been deployed for the continuous measurement of precursor vapors responsible of clustering.

### 2.1.2. CLOUD (Cosmics Leaving OUtdoor Droplets) chamber

The CLOUD chamber is a 26.1 $m^3$, well-controlled, stainless-steel cylinder with electro-polished walls (Kirkby et al., 2011; Duplissy et al., 2016) located at CERN (European Center for Nuclear Research), Geneva, Switzerland. The chamber has extremely low contamination levels (Kirkby et al., 2016; Schnitzhofer et al., 2014), suitable for studying atmospheric-relevant mechanisms at molecular levels. In order to ensure ultra-cleanliness inside the chamber, the walls are occasionally rinsed with ultrapure water at 373 K, right before the start of a new experiment. The carrier and mixing flow synthetic air, used

throughout the experiments, were produced by mixing cryogenic liquid nitrogen and oxygen. Furthermore, the CLOUD chamber allows for studying both neutral and ion induced/mediated pathways of NPF by controlling the ion concentration. On one hand, the neutral (N) pathway can be isolated by operating the high voltage field (20 kV $m^{-1}$) that removes all charged species. On the other hand, tropospheric levels of ions are produced when the high voltage is switched off, reproducing nucleation under atmospherically-relevant galactic cosmic rays (GCR) conditions in the chamber. Additionally, higher layers of the troposphere can be simulated by generating more ions utilizing CERN's proton synchrotron. Moreover, several UV lights were utilized to mimic the photochemistry that occurs during daytime in the boreal forest environment. The light system includes but is not limited to a Krypton-Fluoride (KrF) excimer UV-laser (3 W, $\lambda$ = 248 nm) to produce OH via $O_3$ photolysis, two UV LEDs (16.5W, $\lambda$ = 370-390 nm) to photolyze $NO_2$ into NO, and four Hamamatsu Xenon arc lamps (200W, $\lambda$ = 250-580 nm) to provide a broad range of UV light and make the overall UV spectrum closer to atmospheric levels.

### 2.1.3. Measurement of atmospheric particles and ions

#### *2.1.3.1. Neutral cluster and Air Ion Spectrometer*

A Neutral cluster and Air Ion Spectrometer was used to measure the mobility distributions of neutral and charged aerosol particles and clusters in the size ranges of 2–42 nm and 0.8–47 nm, respectively (NAIS, Airel Ltd., Estonia, Manninen et al. (2009); Mirme and Mirme (2013); Manninen et al. (2016)). The data collected at the SMEAR II station between 2006 and 2016 were used for the event classification in **Paper I** (Section 3), and for determining atmospheric particle and ion formation and growth rates in **Papers IV** and **V**. The NAIS instrument uses two identical differential mobility analyzers (DMA, Knutson and Whitby (1975)) for simultaneous measurement of positive and negative ions. The instrument is operated at a sample flow rate of 30 $L.min^{-1}$ and at a sheath flow rate of 60 L $min^{-1}$. In ion mode, only naturally-charged clusters are measured, while in total mode, atmospheric neutral particles are pre-charged by ions from a corona discharge unit introduced before the DMAs.

#### *2.1.3.2. Differential mobility particle sizer*

For calculating the condensation sink (CS), in **Papers I, II, IV** and **V**, which is equal to the rate at which non-volatile vapors condense onto pre-existing aerosol particles (Kulmala et al., 2012), the particle number concentration size distributions were measured with a twin-DMPS (Differential Mobility Particle Sizer) system (Aalto et al., 2001) over the size ranges of 3–500 nm until the year 2004 and over the size range of 3–1000 nm from 2005 onwards. The data were also used to classify days as NPF events and non-events following the original method proposed by Dal Maso et al. (2005), for **Papers I, II,** and **IV**.

#### *2.1.3.3. Particle Size Magnifier*

For the determination of sub-3 nm particles concentrations around the sizes at which the particle formation is measured, as in **Paper III**, a Particle Size Magnifier (PSM, Vanhanen et al., 2011, Airmodus

Ltd.) in series with a condensation particle counter (CPC) was utilized. Within the PSM, diethylene glycol (DEG) is used as working fluid. The sample flow is mixed with a heated, saturated air to ensure DEG supersaturation, which results in a particle growth due to condensation in the growth tube. The particles then reach a size of around 90 nm, which allows them to be counted by the CPC. The cut-off diameter (the smallest diameter at which 50% of particles are detected) of the PSM depends on the saturation ratio and thus on the flow rate of the saturated air, which can be varied. The PSMs can be operated in scanning mode (periodically ramping up and down the saturation flow), which allows determining the particle concentration at several different cut-off sizes for the calculation of particle formation rates at different sizes, for example at 1.7 nm in **Paper III** (see section 2.2.5).

#### 2.1.4. Measurement of atmospheric ion composition

An atmospheric-pressure-interface time-of-flight mass spectrometer (APi-TOF, Junninen et al., 2010) was used to measure the composition of atmospheric ions reported in **Papers III** and **IV**. The APi-TOF measures naturally-charged molecules only. Once drawn into the inlet, the ions are focused and guided through two quadrupole chambers and one ion lens assembly, and then detected by the time-of-flight mass analyzer. The data from APi-TOF were used to assess the variability of naturally-charged clusters (anions), such as $H_2SO_4$, $H_2SO_4$-$NH_3$, and charged Highly Oxygenated Molecules (HOMs), in chamber experiments and field measurements as in **Papers III** and **IV**, respectively. The extracted data were processed with the tofTools package (version 6.08) (Junninen et al., 2010). In **Paper IV**, the identification of HOM signals was performed using the same ion peak list as reported in Bianchi et al. (2017), and the total signal of HOM ions is the sum of all high resolution signals of identified HOMs.

#### 2.1.5. Measurement of new particle precursors ($H_2SO_4$ and HOMs)

In **Papers III, IV** and **V**, the concentrations of $H_2SO_4$ and HOMs were measured by chemical ionization atmospheric-pressure-interface time-of-flight mass spectrometer (CI-APi-TOF). Chemical ionization is the artificial charging of molecular clusters in the sample by nitrate ions ($NO_3^-$) (Jokinen et al., 2012). $H_2SO_4$ quantification was performed following the method proposed in Jokinen et al. (2012). HOMs quantification followed the method in Kirkby et al. (2016).

### 2.2. Data analysis

#### 2.2.1. Cloudiness parameter

For isolating clear sky days, the cloudiness parameter ($P$) was calculated as the ratio of measured global radiation ($R_d$) to the theoretical global irradiance ($R_g$):

$$P = \frac{R_d}{R_g} \quad (1)$$

The theoretical global irradiance or theoretical maximum global radiation (Rg) is calculated using the latitude and the seasonal solar cycle at a specific location. The days with a daytime median $P < 0.3$ were

identified as having a complete cloud cover while those with $P > 0.7$ were classified as clear sky days (Perez et al., 1990; Sogacheva et al., 2008; Sánchez et al., 2012).These data were used in **Papers I, II and IV**. Although in this thesis work we stick to using Equation 1 for the calculation of cloudiness, we suggest that in the future the cloudiness parameter will be calculated as $P = 1 - \frac{R_d}{R_g}$ so that it explicitly represents cloudiness.

### 2.2.2. Precursor vapors proxies

The concentrations of biogenic oxidation products, used in **Paper II**, called oxidized organic compounds (OxOrg), were estimated using a proxy developed by Kontkanen et al. (2016). This proxy is calculated by using the concentrations of oxidants such as measured ozone ($O_3$) and proxies for the hydroxyl (OH) and nitrate radical concentration ($NO_3$), respectively and their reaction rates, $k_i$, with the monoterpenes:

$$[\mathrm{OxOrg}]_{\mathrm{proxy}} = \frac{(k_{\mathrm{OH+MT}}[\mathrm{OH}]+k_{\mathrm{O3+MT}}[\mathrm{O_3}]+k_{\mathrm{NO3+MT}}[\mathrm{NO_3}])\cdot \mathrm{MT_{proxy}}}{\mathrm{CS}}. \quad (2)$$

Here, the monoterpene proxy ($MT_{proxy}$) is calculated from temperature-driven emissions by taking into account the effect of the boundary layer and monoterpenes oxidation, and CS is the condensation sink (Kulmala et al., 2012).

Gas phase sulfuric acid concentration, used in **Paper II**, was calculated from a pseudo-steady-state-approximation proxy developed by Petäjä et al. (2009) which includes the sulfuric acid source and sink terms:

$$[\mathrm{H_2SO_4}]_{\mathrm{proxy}} = k \cdot \frac{[\mathrm{SO_2}]\cdot \mathrm{UVB}}{\mathrm{CS}}. \quad (3)$$

Here UVB (W $m^{-2}$) is the fraction of the UV radiation (280 – 320 nm), CS is the condensation sink ($s^{-1}$) and the coefficient $k$ ($m^2$ $W^{-1}$ $s^{-1}$) has a median value of $9.9\times10^{-7}$ $m^2$ $W^{-1}$ $s^{-1}$ obtained from the comparison of the proxy concentration to the available measured $H_2SO_4$ data at SMEAR II station. Proxy concentrations were used when the measurements did not cover the whole time period of the analysis (20 years - **Paper II**).

### 2.2.3. Contribution of gaseous precursors to particle formation and growth

The estimated value of the formation rates of 1.5 nm particles ($J_{1.5,C}$) in **Paper II** was calculated by assuming heteromolecular nucleation between $H_2SO_4$ and OxOrg as follows:

$$J_{1.5,\mathrm{C}} = K_{\mathrm{het}}[\mathrm{H_2SO_4}]_{\mathrm{proxy}}[\mathrm{OxOrg}]_{\mathrm{proxy}} . \quad (4)$$

The heterogeneous nucleation coefficient used in Eq. (4) is the median estimated coefficient for Hyytiälä $K_{het} = 9.2\times10^{-14}$ $cm^3$ $s^{-1}$ scaled from Paasonen et al. (2010).

The formation rate of nucleation mode particles ($J_{3,C}$, particle diameter > 3 nm) was calculated based on the inverse of the equation introduced by Kerminen and Kulmala (2002) and by using the calculated formation rate of 1.5 nm sized particles ($J_{1.5,C}$) (Kerminen and Kulmala, 2002):

$$J_{3,C} = J_{1.5,C}\exp\left(-\gamma \frac{CS'}{GR_{1.5-3}}\left(\frac{1}{1.5}-\frac{1}{3}\right)\right). \quad (5)$$

Here CS' ($s^{-1}$) is the condensation sink calculated as suggested by Kerminen and Kulmala (2002) and Kulmala et al. (2012) and $\gamma$ is a coefficient with an approximate value of 0.23 $m^3\,nm^2\,s^{-1}$.The growth rates (GR) of particles between 1.5 and 3 nm were estimated using the size of the condensing vapor molecules ($H_2SO_4$ and OxOrg) and the thermal speed of the particle (Nieminen et al., 2010). The growth rates were calculated as the sum of the growth rates of each of the condensing vapors while assuming the density of the particle to be constant (1440 $kg/m^3$). For $H_2SO_4$, the mass of hydrated $H_2SO_4$, at the present RH, and its density (Kurtén et al., 2007) were used to determine the $H_2SO_4$ concentration needed to make the particles grow at the rate of 1 nm/h. Thus, the GR of the particles due to $H_2SO_4$ condensation was calculated by using the $H_2SO_4$ proxy concentration. The same method was applied to OxOrg condensation (using the OxOrg proxy), where the vapor density was assumed to be 1200 $kg/m^3$ (Kannosto et al., 2008; Hallquist et al., 2009).

#### 2.2.4. Growth rates from atmospheric observations

For the daytime data, the growth rates of ions were calculated using the maximum concentration method (Lehtinen and Kulmala, 2003). Using the latter method and the NAIS data in ion mode, the peak of the ion concentration in each size bin was fitted by a Gaussian function, followed by determining the time at which the maximum concentration is reached within each size bin. The growth rate was then determined by fitting a linear least square fit through diameters as a function of the 'maximum concentration' times. This method was used for calculating the GR of 1.5–3 nm particles in **Paper IV**. In addition, the same method was applied to estimate the growth rate of the $H_2SO_4$-$NH_3$ clusters detected with the APi-TOF during daytime, which was done by converting the cluster masses into diameters in order to get growth rate values in nm $h^{-1}$ instead of amu $h^{-1}$, using a cluster density of 1840 kg $m^{-3}$ (Ehn et al., 2011).

For the night time data, when the ion concentrations are lower, the growth rates were calculated using the appearance time method (Lehtipalo et al., 2014; Dal Maso et al., 2016). For this method, the ion concentration from the NAIS in each size bin was fitted by a sigmoid fit function, followed by determining the time at which 50% of the maximum concentration is reached within each size bin. The growth rate was then determined by fitting a linear least square fit through diameters as a function of the 50% appearance times. This method was used for calculating GR of 1.5–6 nm ions in **Paper V**. Moreover, the growth rate of charged molecules, measured by the APi-TOF, was determined by identifying the masses with the highest normalized signal intensity, and then plotting the probability distribution by fitting a Gaussian function to these masses. After that, the growth rate was determined by a linear least square fit through the mean of the Gaussians obtained at each hour. In **Paper V**, the growth

rate calculation was restricted to a night-time period between 18:00 and 21:00. Particle formation rates from atmospheric observation

The formation rate of atmospheric particles ($J_i$) was calculated and used in **Paper IV** from the following equation (Kulmala et al., 2012):

$$J_i = \frac{dN_{i-j}}{dt} + CoagS_{i-j} \times N_{i-j} + \frac{1}{\Delta(i-j)} GR_j \times N_{i-j} \quad , \tag{6}$$

where $N_{i\text{-}j}$ is the particle concentration between the diameters *i* and *j* measured with the NAIS in particle mode, CoagS is the coagulation sink of particles, which is the rate at which particles in the size bin *i-j* are lost to pre-existing particles, and is derived from DMPS measurements (Kulmala et al., 2012). $GR_j$ is the particle growth rate out of the bin calculated from NAIS measurements in ion mode described in sections 2.2.4.

### 2.2.5. Ion formation rates from atmospheric observation

The formation rate of atmospheric ions ($J_i^{\pm}$) was calculated in **Papers IV and V** from the following equation:

$$J_i^{\pm} = \frac{dN_{i-j}^{\pm}}{dt} + CoagS_{i-j} \times N_{i-j}^{\pm} + \frac{1}{\Delta(i-j)} GR_j \times N_{i-j}^{\pm} + \alpha \times N_{i-j}^{\pm} N_{<j}^{\mp} - \beta \times N_{i-j} N_{<i}^{\pm}. \tag{7}$$

Here $N_{i\text{-}j}^{\pm}$ is the concentration of positive or negative ions between diameters *i* and *j* measured with the NAIS in ion mode, $\alpha$ is the ion-ion recombination coefficient assumed to be equal to $1.6 \times 10^{-6}$ cm$^3$ s$^{-1}$, $N_{<j}^{\pm}$ is the concentration of positive or negative ions with diameters smaller than j, $\beta$ is the ion-neutral attachment coefficient assumed to be equal to $0.01 \times 10^{-6}$ cm$^3$ s$^{-1}$ and $N_{<i}^{\pm}$ is the concentration of positive or negative ions with diameters smaller than i. Assumptions were made considering the ambient temperature, pressure and relative humidity as well as the sizes of the colliding objects, i.e. ion-ion or ion-aerosol particle collisions (Hoppel, 1985; Tammet and Kulmala, 2005).

### 2.2.6. Particle formation rates from CLOUD experiments

For chamber experiments, as in **Paper III**, the formation rate of particles was calculated from total particle concentration measured with PSM (See section 2.1.3.3). The nucleation rates (*J*) were calculated by using the time derivative of total particle concentrations above a certain threshold and accounting for losses in the chamber:

$$J = \frac{dN}{dt} + S_{dil} + S_{wall} + S_{coag} \; [cm^{-3}\, s^{-1}] \, . \tag{8}$$

Here, $S_{dil}$ was used to describe the dilution of particles due to the synthetic air continuously flowing into the chamber in order to account for the sample flow of the instruments. The dilution results in a lower particle concentration and is calculated as follows:

$$S_{dil} = N_{tot} \cdot k_{dil}\ [cm^{-3}\ s^{-1}]\ . \tag{9}$$

In **Paper III**, the total flow inside the chamber alternated between 225 and 250 lpm resulting in dilution coefficients of $k_{dil} = 1.437 \cdot 10^{-4}\ s^{-1}$ and $k_{dil} = 1.596 \cdot 10^{-4}\ s^{-1}$, respectively.

Wall losses due to diffusion ($S_{wall}$) were determined by observing the decay of sulfuric acid monomer of diameter ($d_{p,ref} = 0.82$ nm) concentrations in the chamber. The obtained loss rate coefficient is inversely proportional to the mobility diameter of the particles ($d_p$), and can therefore be scaled and applied to correct for the losses of small clusters at chamber temperature using a reference temperature ($T_{ref} = 278$ K):

$$S_{wall}(d_p, T) = N(d_p) \cdot k_{wall}(d_p, T)\ [cm^{-3}\ s^{-1}] \tag{10}$$

$$k_{wall}(d_p, T) = 2.116 \cdot 10^{-3} \cdot \left(\frac{T}{T_{ref}}\right)^{0.875} \cdot \left(\frac{d_{p,ref}}{d_p}\right)\ [s^{-1}] \tag{11}$$

The coagulation sink term, which is the loss of freshly formed particles and clusters to pre-existing aerosols, ($S_{coag}$) was calculated from the measured number size distribution present in the chamber and the coagulation coefficient $K(d_p,d_p')$ is the coagulation coefficient for particles sizes $d_p$ and $d_p'$(Seinfeld and Pandis, 2016):

$$S_{coag}(d_p) = \int K\left(d_p, d_p'\right) n(d_p') dd_p' \cong \sum_{d_p'=d_p}^{d_p'=max} K(d_p, d_p') N_{d_p'}\, N_{dp} [cm^{-3}\ s^{-1}] \tag{12}$$

# 3. Classification of new particle formation using characteristic air ions

New particle formation events have been observed all over the world (Kulmala et al., 2004; Kerminen et al., 2018; Chu et al., 2019), and their analyses requires intensive labor, especially with the increased number of measurement stations (Kulmala, 2018). Originally, days were classified as NPF events or non-events following the method proposed by Dal Maso et al. (2005), in which days are visually inspected for the appearance of a new mode in the size distribution within the nucleation mode size range (3–25 nm), and whether this new mode prevails for several hours while showing signs of further growth. Although this method has been widely used, it still has some limitations. Apart from the fact that it is labor intensive and requires long hours, it leaves a large group of days undefined due to incomprehensive characteristics. In fact, the fraction of undefined days classified at SMEAR II station was around 50% between the years 1996 and 2016 (Buenrostro Mazon et al., 2009). The latter limitation is mainly the result of the instrumentation used in this kind of analyses, the DMPS (section 2.1.3.2), which does not measure completely below 3 nm and effectively below 6 nm, and thus misses the initial steps of NPF and clustering. Moreover, a visual classification method is subject to errors and human biases. Accordingly, we developed, in **Paper I**, an automatic method which classifies days into NPF events, non-events and two classes in between by extending the observation to sub-3 nm charged clusters (See NAIS, section 2.1.3.1). Our method, therefore, minimizes the number of undefined days which are usually excluded from further analyses.

## 3.1. Development of an automatic event classification method

In order to validate our automated classification method, described in **Paper I**, we used 10 years of data collected at the SMEAR II station, see section 2.1.1. Using the 2–4 nm ion concentration and their subsequent growth, we were able to access the initial steps of clustering and thus estimate whether a regional NPF event has occurred within the air mass during which the observation was made (regional event, RE) or was carried to our measurement location (transported event, TE). In addition, some days were classified as ion bursts (IB), where an increase of ion concentration (2–4 nm) was observed but was not followed by growth. Days with none of the aforementioned criteria were classified as non-event days (NE). The decision pathway of the event classification is shown in Figure 2.

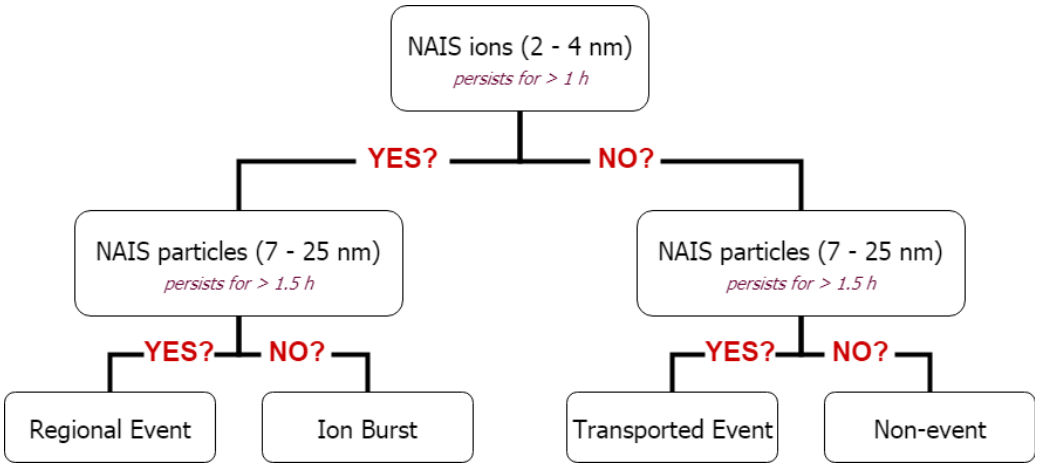


Figure 2. A flow chart for the decision pathway for event classification using the new classification method. The figure is adopted from **Paper I**.

## 3.2. Description of automated method

First, the method searches for a notable increase in the 2–4 nm ion concentration lasting for at least 1 hour above the threshold value detected from early morning observations. The ion concentration is considered significant in case it exceeds 20 $cm^{-3}$ (Leino et al., 2016). Next, the method searches for an increase in 7–25 nm particle concentration that should persists for at least 1.5 hours and reach a value higher than 3000 $cm^{-3}$. So, if the ion concentration increases and is followed by an increase in the particle concentration, a regional event (RE) is identified. However, if the ion concentration increases with no subsequent increase in the particle concentration, the time period is classified as an ion burst. In parallel, if the particle concentration increases without a prior increase in the ion concentration, the period is defined as a transported event (TE), previously identified as a tail event (Buenrostro Mazon et al., 2009). If neither 2–4 nm ions nor 7–25 nm particles are present in sufficient intensities, the period is then classified as a non-event (NE).

# 4. Long term observations of new particle formation events in the boreal forest

Using 20 years of data measured at the SMEAR II station, we investigated the parameters affecting NPF formation events during daytime, which is the time period during which growing NPF events have been observed in Hyytiälä (Lehtipalo et al., 2011; Buenrostro Mazon et al., 2016; and **Paper V**). After determining the start, peak and end times of NPF event days in **Paper I** using the presence of ions (2 – 4 nm), (See section 4.1), we restricted our further analyses to the NPF occurrence time of 9:00–12:00 local time and narrowed it down further to the time of most intense NPF (11:00–12:00 local time). Within the specified time window, we studied the effect of cloudiness on the NPF frequency and found that most RE occur under a clear sky conditions (**Paper I**). However, under clear-sky conditions, NPF events were not always detected. We therefore investigated what parameters inhibit the occurrence of NPF under clear-sky conditions in **Paper II**.

## 4.1. Start, peak and end times of new particle events

We applied the automated method, described in **Paper I** and Section 4, to 10 years of data measured with the NAIS (Section 2.1.3.1) in order to identify the start, peak and end times of regional NPF events observed at the SMEAR II station. During spring, most events started concurrent with the sunrise, peaked before the noon and lasted for 9 to 11 hours before they completely diminished, as shown in Figure 3. In comparison, during summer, RE started, peaked and ended later than events in spring, which could be attributed to longer daylight hours and fewer clouds. However, during autumn and winter, the events started earlier than the ones in spring or summer. The importance of identifying the exact time window during which NPF events occurs enhances our understanding of the characteristic variables governing the occurrence of an event by focusing on a specific time frame. For instance, the studies on NPF in the boreal forest at SMEAR II station were restricted to daylight hours, specifically those during which the events are occurring as in **Papers II** and **IV**.

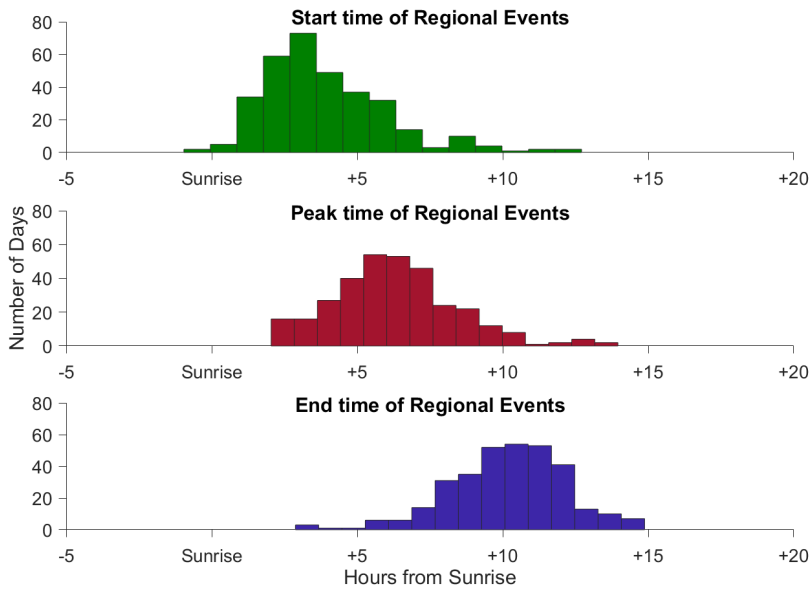


Figure 3. Frequency of days during spring at which regional events start, peak and end past sunrise. For example, most events start within 3 hours from sunrise. Figure is adopted from **Paper I.**

## 4.2. Effect of cloudiness on NPF frequency

In **Paper II**, we calculated the cloudiness parameter (*P*), described in section 2.2.1, during the 20 years of measurements at the SMEAR II station. On one hand, our results show that 75% of the NPF events had at least a semi clear sky ($P > 0.5$) (Figure 4b). Moreover, on cloudy days ($P< 0.3$) NPF events occurred on less than 10% of the days (Figure 4a). On the other hand, NPF non-events were characterized by lower values of *P* (Figure 4b). In specific, the median *P* value on non-event days was 0.25, in comparison to median *P* value of 0.75 on event days. Thus, we conclude that clear sky conditions favor the occurrence of NPF events. Furthermore, we found that *P* values were lower for TE than for RE, which indicates that a semi-cloudy day is unfavorable for NPF within the measured air mass or inside the boundary layer, which resulted in the occurrence of a NPF in another location where the conditions are more favorable as shown in **Paper I**. The same conclusion also applies to more clouds (demonstrated by a lower *P* value in **Paper I**) during ion bursts, classified using the automated method and NAIS ion data in section 3. Indeed, ion bursts are attempts of a NPF event, which could have been interrupted due to the appearance of a cloud during the formation or growth process. Under clear sky conditions, more radiation necessary for photochemistry is available, resulting in more $H_2SO_4$ and HOMs leading to higher frequency and intensity of NPF as discussed later in section 5, and Papers **II, IV** and **V**.

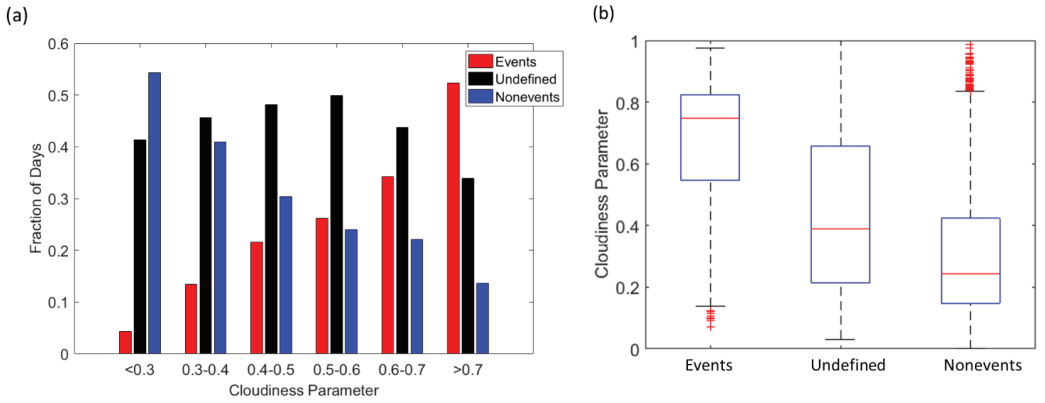


Figure 4. (a) The fraction of days which are classified as NPF events, non-events, and undefined days during different sky cloudiness conditions. (b) Cloudiness daytime (9:00–12:00) medians and percentiles during NPF event, undefined and non-event days. The red line represents the median of the data and the lower and upper edges of the box represent 25th and 75$^{th}$ percentiles of the data respectively. The length of the whiskers represents 1.5 times the interquartile range which includes 99.3% of the data. Data outside the whiskers are considered outliers and are marked with red pluses. Figure adopted from **Paper II**.

## 4.3. Monthly variations of NPF gaseous precursor proxies

Under clear-sky conditions, when most NPF events take place, we found that sulfuric acid proxy (SA proxy) had the highest concentration during February (Figure 5a). The higher concentration of SA proxy during winter can be attributed to higher $SO_2$ concentrations and lower boundary height. In contrast, biogenic oxidized organics proxy (OxOrg proxy) concentrations followed the temperature profiles in the boreal forest environment, with the maximum in July (Figure 5b). Thus, neither precursor vapor concentrations coincided with the highest frequency of NPF events, i.e. during spring as shown in **Paper II**. Accordingly, we hypothesize that neither of these two precursors is the limiting factor in the NPF process at the SMEAR II station, and that instead they play a synergistic role resulting in the observed NPF, described in **Papers III** and **IV**.

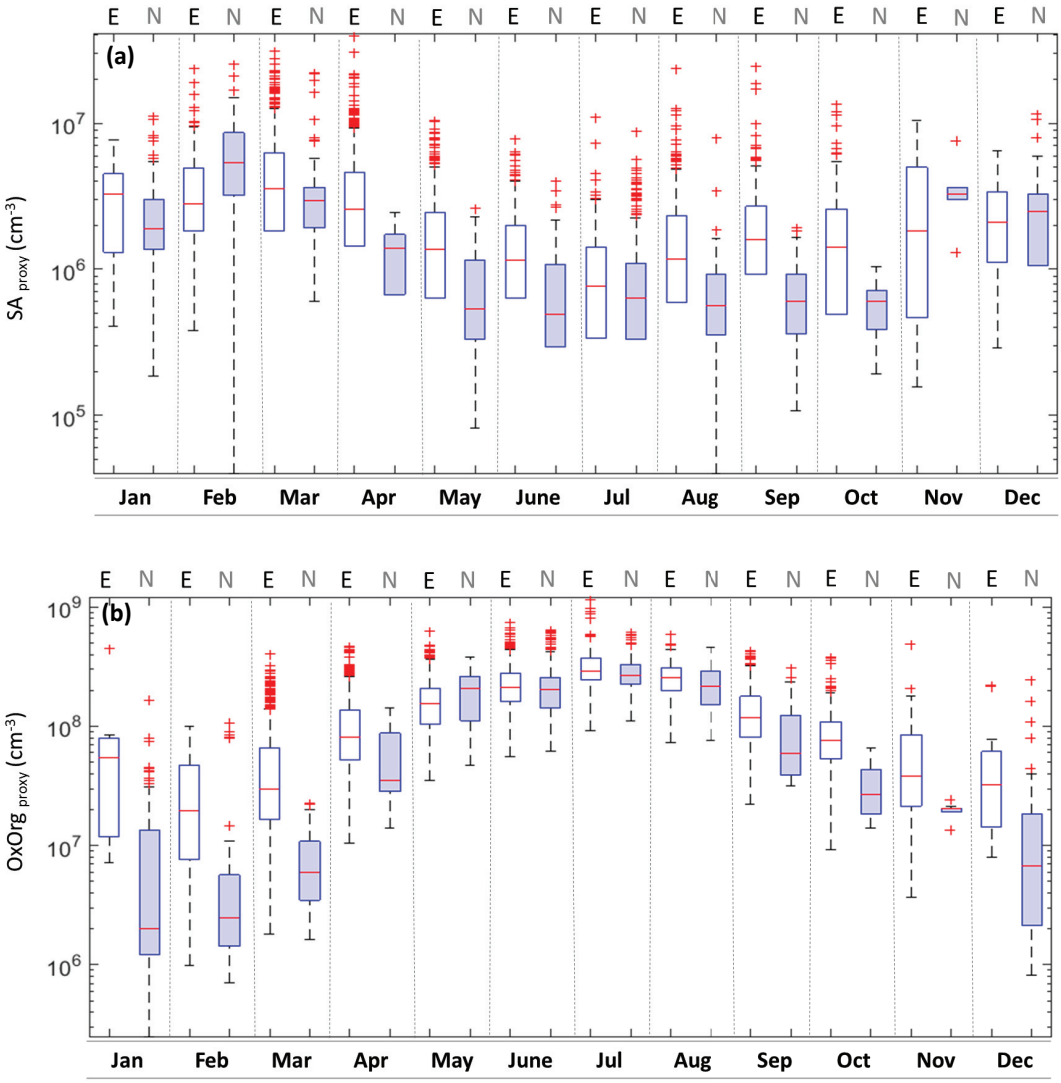


Figure 5. Monthly variation of medians and percentiles of daytime (9:00–12:00) concentrations of (a) SA proxy and (b) OxOrg proxy under clear sky conditions ($P$>0.7) during NPF events (E, white) and non-events (N, blue). Figure is adopted from **Paper II**.

## 4.4. Probability of NPF events and nonevents

Cloudiness affects the frequency of NPF as it obscures radiation and thus decreases the photochemistry needed for providing the precursors for NPF. Therefore, in order to study the effect of other variables on NPF at SMEAR II station, we concentrated on clear-sky conditions, particularly to understand the absence of events during some clear-sky days (**Paper II**). For that purpose, we focused on the peak time of NPF found in **Paper I** (11:00–12:00), and found out that temperature (*T*) and condensation sink (CS) both play a role in determining NPF probability. In specific, we came to an equation (Equation 13) relating *T* and CS above which no NPF events could occur, in **Paper II**.

$$\text{CS (in the unit } s^{-1}) > -3.091\times10^{-5} \times \text{T (in K)} + 0.0120 \quad (13)$$

Finally, we found that the highest probability of occurrence of NPF events corresponded to moderate *T* and low CS (Figure 6). At low *T*, less biogenic volatile organic compounds are emitted, reducing the precursor concentrations. However, at high *T*, HOMs are less likely to condense onto clusters, hindering stabilization and further growth of freshly formed particles (Stolzenburg et al., 2018). However, when CS is high, precursor vapors are lost much faster, thus decreasing their efficiency in participating in the clustering process.

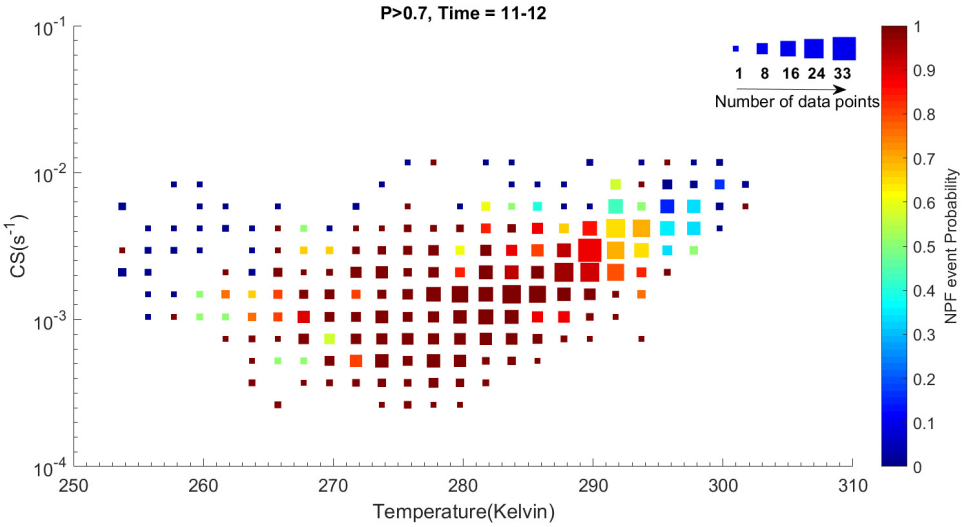


Figure 6. NPF probability distribution based on the CS and *T* during clear-sky days at NPF peak time (11:00 -12:00). Marker size indicates number of days included in the probability calculation within every cell. Figure is adopted from **Paper II**.

# 5. Mechanism of New particle formation in the boreal forest environment

## 5.1. Experimental simulations from the CLOUD chamber

Using a well-controlled simulation chamber (**Paper III)**, we simulated the possible mechanisms of NPF in the boreal forest environment, in an attempt to mimic the mechanisms occurring at SMEAR II station (e.g. **Papers IV** and **V**). First, we injected a mixture of pure biogenic monoterpenes α-pinene and Δ-3-carene, which are the most abundant monoterpenes measured at SMEAR II station (Hakola et al., 2003; Jokinen et al., 2016). The formation rates of these particles, during neutral (N) and galactic cosmic rays (GCR) conditions, were similar in magnitude to those in a pure α-pinene systems conducted in earlier experiments at CLOUD (Kirkby et al., 2016). However, although the SMEAR II station is relatively clean, it is still affected by anthropogenic pollutants, including $SO_2$, $NH_3$ and $NO_x$ (**Paper II**). Accordingly, we studied the impact of these vapors on biogenic NPF using experiments done within the CLOUD chamber (Figure 7). $SO_2$ is the precursor of $H_2SO_4$, which is a low-volatility vapor that governs NPF in many environments (Weber et al., 1995; Birmili et al., 2003; Kulmala et al., 2006; Sihto et al., 2006; Sipilä et al., 2010; Riccobono et al., 2012; Kuang et al., 2010; Yao et al., 2018). Interestingly, under GCR conditions, the addition of $SO_2$, and thus $H_2SO_4$, was found to enhance particle formation only slightly in the absence of ammonia ($NH_3$) and immensely in the presence of few 100 ppts of $NH_3$. Furthermore, no ion effect was seen under these conditions, proving that the quaternary mechanism of NPF ($H_2O$, HOMs, $H_2SO_4$ and $NH_3$) proceeds through a neutral dominated pathway, while the ion induced nucleation (IIN) pathway is rather minor. At the same time, $NO_x$, which is mainly emitted from traffic-related activities, was found to suppress new particle formation. In general, we hypothesize that $NO_x$ interferes with the biogenic particle formation pathway by altering the chemistry of HOMs. Indeed, not all HOMs contributed to the particle formation, in specific, non-nitrate HOM dimers correlated the best with $J_{1.7}$, which lead to our conclusion that the latter (non-nitrate HOM dimers) govern the nucleation pathway. In the presence of $NO_x$, the auto-oxidation pathway of HOM formation is inhibited and more nitrate-containing HOMs were measured. Nitrate-containing HOMs were found to be more volatile, and therefore less efficient in participating in clustering, slowing down the total particle formation rates. Regardless of their higher volatility, these nitrate-containing HOMs still contributed to particle growth rates. In addition, the particle growth was found to be independent of the ammonia concentration but was mainly dependent on the HOM concentration, and mainly enhanced with an increasing non-nitrate HOM dimer concentration. We therefore concluded that in the boreal forest environment, a synergistic role of HOMs, $H_2SO_4$ and $NH_3$ is present. The highest rate of particle formation was observed in the presence of all the three components together, without the need of ions for stabilization. In the absence of $NH_3$, the ion effect was enhanced, and HOM concentrations mediate the particle formation, through an IIN pathway, which was confirmed through atmospheric observations in **Paper IV**.

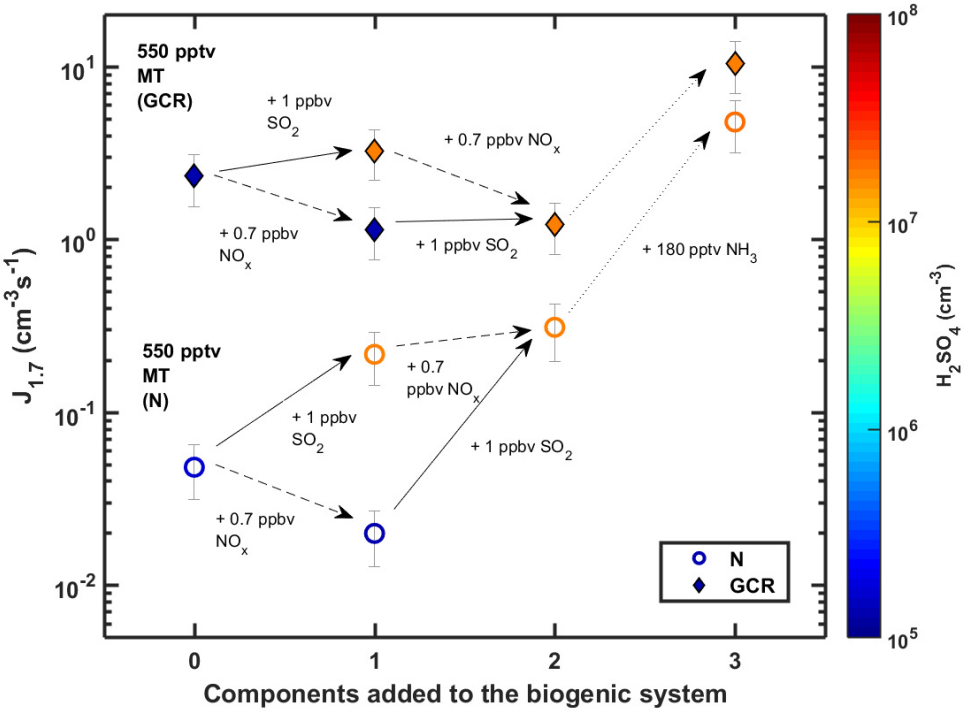


Figure 7. The effect of adding different vapors on biogenic nucleation rates ($J_{1.7}$). All points have similar monoterpene (about 550 pptv) and ozone (40 ppbv) mixing ratios. The leftmost points were measured with only monoterpenes added to the chamber, and each step to the right represents addition of one more component to the system. Solid, dashed and dotted arrows describe the addition of about 1 ppbv of $SO_2$, 0.7 ppbv of $NO_x$ and 180 pptv of $NH_3$, respectively. Circles are experiments at neutral (N) and diamonds at GCR conditions. Colors of the symbols indicate the measured sulfuric acid concentration. The error bars describe the uncertainty in the nucleation rates, which was calculated similar to earlier CLOUD publications, taking into account both the systematic and statistical errors and run-to-run repeatability. Figure is adopted from **Paper III**.

## 5.2. Daytime ion induced nucleation from field Measurements at SMEAR II

Provided that pure biogenic NPF is possible under atmospherically relevant conditions with the aid of ions (Kirkby et al., 2016), we studied in **Paper IV** the possible mechanisms of IIN measured at the SMEAR II station. Our focus was on the $H_2SO_4$-$NH_3$ clusters and the factors that govern their clustering and participation in IIN in the boreal forest. Indeed, we found that clusters of combined $H_2SO_4$-$NH_3$ were present when the ratio between the concentrations of biogenic HOMs and $H_2SO_4$ was less than 30 and that $NH_3$ is not the limiting factor. $NH_3$-free clusters were visible up to 6 $H_2SO_4$ molecules. However, in

the presence of $NH_3$, the cluster could contain up to 13 $H_2SO_4$ molecules. On ~50% of the measurement days, when IIN was observed in the NAIS, $H_2SO_4$-$NH_3$ clusters were observed ($H_2SO_4$ -Ev). Therefore, we deduce that an $NH_3$-free mechanism governs the IIN during the other 50% portion of the days (Other-Ev). Interestingly, the intensity of IIN increased with an increasing HOM concentration which in turn increased with an increasing temperature (Figure 8). While $H_2SO_4$–Ev contributed to higher total particle formation (IIN + neutral, $J_{TOT}$), Other-Ev show higher $J_{ION}/J_{TOT}$, which indicated the role of ions in governing HOM driven IIN. We conclude that at higher $H_2SO_4$ concentrations, $NH_3$ contributes to the stabilization of the $H_2SO_4$ clusters, leading to a $H_2SO_4$-$NH_3$ mediated IIN pathway. Conversely, when the HOM concentration was dominant ([HOM]/[$H_2SO_4$] > 30), $NH_3$ played no role and ions stabilized the HOM clusters, leading to a pure biogenic IIN pathway. Finally, we found that the probability of ion induced nucleation increased with an increasing size of the $H_2SO_4$-$NH_3$ cluster, reaching the 100% probability of IIN when the cluster contained at 6 or more $H_2SO_4$ molecules.

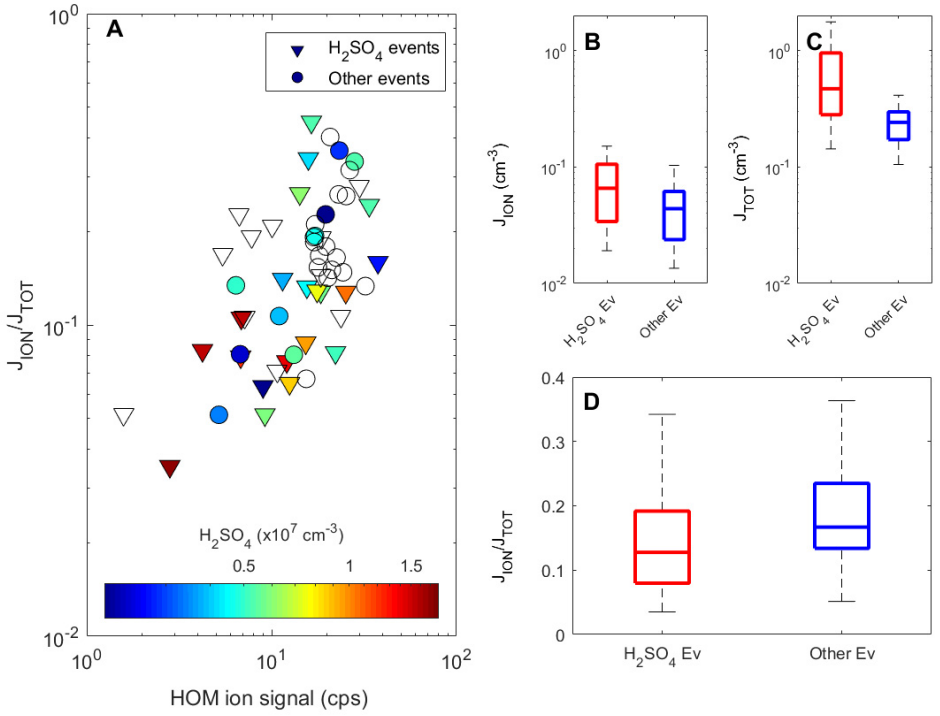


Figure 8. Formation rate of 2.5 nm ions and total particles (both ions and neutral clusters) under different nucleation mechanisms. A) Charged fraction of the formation rate of 2.5 nm particles as a function of the total signal of HOM ions color-coded by the $H_2SO_4$ concentration, and (B, C and D) the differences in $J_{ION}$, $J_{TOT}$, and $J_{ION}/J_{TOT}$ between the $H_2SO_4$–$NH_3$-involved events ($H_2SO_4$-Ev) and other events (Other-Ev). Figure is adopted from **Paper IV**.

## 5.3. Night-time ion induced nucleation from field Measurements at SMEAR II

In **Paper V**, we show clear evidence of pure biogenic NPF in the boreal forest environment within few hours around sunset. Under low $H_2SO_4$ conditions, biogenic HOMs originating from monoterpene oxidation are able to form stable clusters, consistent with **Paper IV**. However, these clusters do not grow past 6 nm, due to the lack of precursor vapors essential for their further growth. The latter is due to lack of photochemistry during dark hours. These clusters were able to grow at a rate of 181.1 amu $h^{-1}$, which is equivalent to 0.14 nm $h^{-1}$ in mobility diameter of clusters. In this study, we defined the products from monoterpene oxidation as naturally-charged monomers (number of carbons = 9–10), dimers (number of carbons = 16–20) and trimers (number of carbons = 27–30) in the ranges of m/z=300–400Th, 500–650Th and 75–850Th, respectively. Naturally-charged dimers and trimers were found to increase ion concentrations detected by the NAIS in the size bins centred at 1.44 nm and 1.66 nm, respectively (Figure 9). Regardless of the GR and the $H_2SO_4$ concentration, the slope between the concentrations of above-mentioned HOMs and ions was approximately constant. At the same time, a clear relation was visible between charged HOM dimers and formation rate of 1.5 nm ions, consistent with observations in **Paper III**. Furthermore, we investigated the chemical speciation of the HOM dimers involved in the process of ion formation. Indeed, we found a strong correlation between the number concentration of 1.44 nm ion clusters and non-nitrate dimers. However, no correlation was observed with nitrate-containing dimers, indicating weak condensation of nitrate containing HOMs, dominant during night-time (Bianchi et al., 2017), onto small clusters. Our findings are consistent with **Paper III**, during which we found that $NO_x$ supresses NPF by forming nitrate HOMs that do not contribute as much to vapor condensation, and therefore to the particle growth, as non-nitrate HOMs.

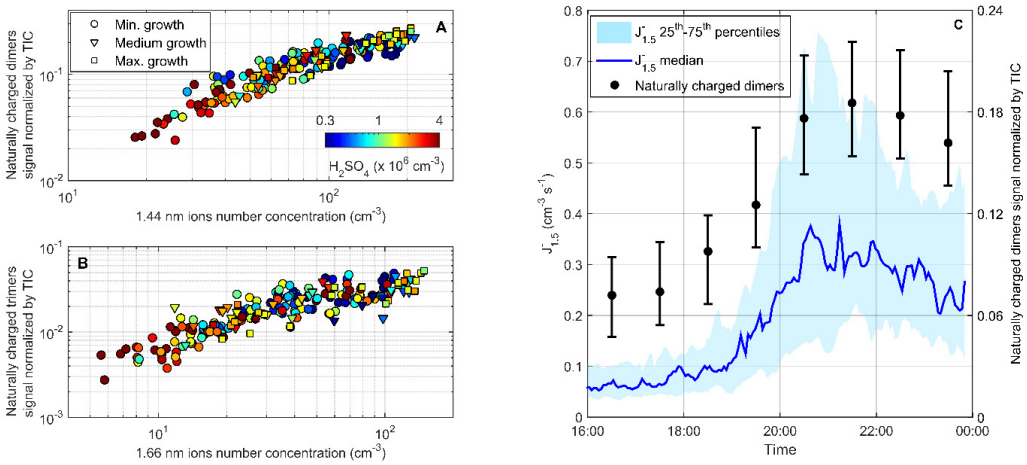


**Figure 9.** Relationship between ion and mass spectrometers observations. **(A)** Normalized HOM dimers signal as a function of the NAIS negative ion number concentration in the size bin centred at 1.44 nm. Concentrations and signal intensities are one-hour averages from all event evenings between 16:00 and 00:00. **(B)** Normalized HOM trimers as a function of NAIS negative ion number concentration in the size bin centred at 1.66 nm negative ion number concentration. **(C)** Averaged time series of the HOM dimers signal normalized by total ion count (TIC) and formation rate of 1.5-nm negatively charged clusters on event evenings. Black circles represent the median of the normalized HOM dimers signal, while lower and upper limits of the error bars represent 25th and 75th percentiles, respectively. Figure is adopted from **Paper V**.

# 6. Review of papers and author's contribution

**Paper I** is the first step of analyzing atmospherically observed new particle formation events in the boreal forest environment and elsewhere in the world. **Paper I** explains how days can be automatically classified into NPF events or non-events using characteristic air ions. Accordingly, 10 years of days measured in the boreal forest at the SMEAR II station were classified into NPF events, non-events and two classes in between: 'transported events' and ion bursts. The importance of this method lies in its ability to minimize the errors created by human biases during the manual classification process, as well as in minimizing the number of undefined days usually excluded from further analysis. Furthermore, the study identifies the exact start, peak and end times of NPF events observed at SMEAR II station. For **Paper I**, I elaborated the original idea, evaluated the automatic code, analyzed the data output and wrote the manuscript.

In **Paper II**, 20 years of data collected at the SMEAR II station were analyzed for the effect of clouds on the occurrence of NPF events. Together with **Paper I**, the results show that clouds interrupt, if not completely inhibit, the formation of particles. After considering only the days with clear sky conditions, both condensation sink and temperature were found to govern the probability of NPF events. The study was a continuation from the work that started, back when I was a student at Hyytiälä winter school, on advanced data analyses in March 2015, where I contributed to most of the data analyses and wrote most of the text.

**Paper III** explains how NPF and growth, under boreal forest daytime conditions, were simulated via experiments in the CLOUD chamber at CERN. Within this paper, the roles of anthropogenic pollutants ($SO_2$, $NO_x$ and $NH_3$) on biogenic NPF and growth were studied individually and in a mixture. While $SO_2$ was found out to enhance NPF together with $NH_3$, NOx was found to attenuate particle formation and early growth. Accordingly, human activities interchangeably enhance and suppress NPF, depending on the available conditions. I participated in the coordination of the campaigns, participated in the experiment, prepared the particle data and the corresponding formation rates, and commented on the manuscript.

In **Paper IV,** the synergistic effects of biogenic HOMs, $H_2SO_4$ and $NH_3$ during daytime ion induced NPF observed at SMEAR II station were studied. During daytime, $H_2SO_4$-$NH_3$ clusters were found to be important for both ion induced new particle formation and cluster growth rate. In fact, when clusters contained 6 or more $H_2SO_4$ molecules, IIN was observed at almost 100% probability. In addition to $H_2SO_4$-$NH_3$ clusters, another pathway of IIN is proposed, with evidence of HOM-driven IIN. They could well be HOM dimers, as suggested by **Paper III** and other complementary studies. I interpreted the IIN growth and formation rates, contributed to the scientific discussions and wrote a portion of the text.

**Paper V** elucidates the night-time atmospheric observation of IIN at the SMEAR II station. While the daytime pathway was found to involve HOMs and $H_2SO_4$-$NH_3$ clusters, as found in **Paper IV**, observations during the night-time at Hyytiälä were the first atmospheric evidence of a pure HOM driven nucleation pathway. As HOMs include a wide range of molecules, a detailed analyses of the chemical

specificities showed that only the HOM non-nitrate dimers were the ones most likely contributing to nucleation. However, these freshly formed clusters did not show evidence of further growth, partly explained by the lack of photochemistry responsible for forming $H_2SO_4$ and higher concentrations of HOMs required for keeping the mechanism going. I interpreted the IIN growth and formation rates, contributed to the scientific discussions and wrote part of the paper.

# 7. Conclusions and outlook

New particle formation is an atmospheric phenomenon, observed in many environments (Kulmala et al., 2004; Kerminen et al., 2018; Chu et al., 2019), and contributes to a major fraction of the global aerosol number budget (Spracklen et al., 2010). The formed particles affect the climate by interfering with the incoming solar radiation and by altering cloud properties (IPCC, 2013; Murphy and Ravishankara, 2018). Besides, by forming high loading of nano-particles, NPF could be directly associated with deteriorating human health (Oberdörster et al., 2004; Künzli and Tager, 2005; Apte et al., 2015; Burnett et al., 2018). In this thesis, we investigate the driver behind NPF in a boreal forest environment and analyze the atmospheric parameters that enhance or attenuate this phenomenon.

As a starting point of any atmospherically observed NPF-related analysis, and in order to quantify this phenomenon, days are classified according to whether a NPF event had occurred or not. Originally, event classification was done manually. Events were identified visually by the appearance of a persistent nucleation particle mode followed by continuous growth (Dal Maso et al., 2005). However, such procedure is labor intensive and is subject to human biases, especially when considering the increasing number of measurement campaigns and stations. In addition, the visual method leaves a large fraction of the days undefined, and such days are usually excluded from further analyses. In this thesis, as stated in *objective i*, we made use of the development of particle instruments, such as the NAIS which accesses the initial steps of NPF, in order to automatically classify NPF events based on their characteristic air ion concentrations (**Paper I**). As a result of this framework, all days at the SMEAR II station were classified into NPF events, nonevents and two classes in between. The automatic method also determined the start, peak and end times of NPF regional events, and thus generated a time series during which an NPF event had occurred at the SMEAR II station.

Using the defined time periods, we concentrated on the times during which an event had occurred in order to understand which parameters affect the long-term behavior of the occurrence of NPF in the boreal forest environment (**Paper II**). For example, clouds are known to attenuate the incoming solar radiation and thus to prevent the photochemistry needed for producing precursors for NPF. Our results showed that NPF events tend to occur under clear sky conditions, while cloudy days were mostly nonevents (*objective ii*). However, on some clear sky days NPF did not occur. We therefore investigated other meteorological parameters that define the NPF probability. In this thesis, we showed that NPF events require a clear-sky environment with low condensation sink and a moderate temperature (*objective iii*). Under these conditions, we observed that neither $H_2SO_4$ nor oxidized organics are the limiting factor in the NPF process.

After considering the general environment necessary for NPF events to occur in the boreal forest, we went into molecular level analyses in an attempt to understand the pathway from gaseous precursors to stable clusters. $H_2SO_4$, supported by its very low saturation vapor pressure, has been identified as the precursor vapor responsible for NPF in many environments globally (Sihto et al., 2006; Sipilä et al., 2010). $H_2SO_4$ mediated nucleation and particle formation involved the stabilization of $H_2SO_4$ by

ammonia or amines (Ortega et al., 2008; Kirkby et al., 2011; Almeida et al., 2013). Recently, highly oxygenated molecules were found to contribute to the formation and growth of clusters, even in the absence of sulfuric acid (Kirkby et al., 2016). Therefore, in order to understand the contribution of each of $H_2SO_4$, $NH_3$ and HOMs to NPF, we simulated the boreal forest environment in the CLOUD chamber (**Paper III**).

In **Paper III**, a mixture of monoterpenes (α-pinene and Δ-3-carene) was first injected into the chamber and, in the presence of $O_3$, particle formation was observed. $SO_2$ was then injected and, in the absence of $NH_3$, only slight enhancement in the formation rate of particles was observed. However, with the addition of only few 100 ppts of $NH_3$, the particle formation rate was intensely enhanced. The results also showed that biogenic non-nitrate HOM dimers are the major contributor to particle formation and growth. The experiment was indicative of an interplay between all three components (biogenic HOMs, $H_2SO_4$ and $NH_3$) and the importance of their simultaneous presence for the formation and survival of particles (*objective iv*). In **Paper III**, besides $SO_2$, the effect of other anthropogenic vapors, such as $NO_x$, on biogenic NPF was examined. Our results showed that $NO_x$ attenuates the particle formation and growth by interfering with the chemical composition of HOMs and by reducing the concentration of non-nitrate dimers necessary for nucleation and growth.

Chamber studies, however, do not fully replicate our atmospheric conditions because of the missing micrometeorology and unmeasurable and unidentified species. We therefore revisited the IIN at SMEAR II in order to verify the particle formation mechanism in the daytime atmosphere (**Paper IV**). Our results showed that $NH_3$ is needed for the stabilization of $H_2SO_4$ clusters in order to ensure a sulfuric acid-mediated pathway of NPF (*objective iv*). However, $H_2SO_4$-$NH_3$ clusters were not observed when the ratio of biogenic HOMs to $H_2SO_4$ exceeded 30, indicating another IIN mechanism which we hypothesized to be HOM-mediated. In a cluster, up to 6 $H_2SO_4$ molecules were observed in the absence of $NH_3$ and are sought to be big enough to ensure a 100% probability of IIN.

In order to isolate the effect of biogenic HOMs on clustering in the atmosphere, we studied the chemical composition of clusters accompanying nocturnal nucleation. In the boreal forest, post sunset $H_2SO_4$ concentrations are usually low, which explains the absence of night-time NPF (*objective iv*). However, in **Paper V** we still observed ion induced clustering molecules incapable of growing past 6 nm. The formation of these clusters was found to be driven by pure biogenic HOM dimers and trimers, confirming our chamber observations in **Paper III**. The lack of growth of these clusters was tentatively attributed to the lack of solar radiation needed for photochemistry, consistent with our observations in **Paper II**.

All papers verified that a sufficient intensity of solar radiation is crucial for providing the photochemistry needed for the survival of freshly formed particles. In addition, the papers indicate a synergistic role of all quaternary components ($H_2O$, $H_2SO_4$, $NH_3$ and HOMs) of NPF in the boreal forest environment. In particular, biogenic non-nitrate dimers are found to be the most relevant HOMs for participating in particle formation.

With the establishment of long term stations (Kulmala, 2018), the effects of pollution mitigation policies, such as the $SO_2$ directive, on the concentration of precursor vapors will become more visible in our measurements (Glachant, 2001). This leaves room for investigating long-term trends in new particle formation frequencies and mechanisms and raises the question: will we go back to pre-industrial, low-$H_2SO_4$ character of new particle formation? Similarly, using long-term data, we could examine the effects of radiation intensity attenuation by clouds on the chemical composition of precursor vapors and their mechanisms of oxidation.

Moreover, the experiments in **Paper III** were done at a temperature of 5 degrees Celsius, mimicking the spring-time boreal forest environment. This leaves room for similar experiments simulating conditions typical for other seasons. Furthermore, with the development of recent trace-gas-measuring instrumentation, biogenic vapors other than monoterpenes, such as sesquiterpenes and isoprenes, have been measured in the boreal forest (Jokinen et al., 2016; Hellén et al., 2018). These could be simulated in the chamber experiments for their role in NPF individually and in a biogenic mixture. Moreover, similar experiments could be carried out in the presence of both amines and ammonia. Using such chamber experiments combined with atmospheric observations, we could further investigate the mechanisms of HOM formation and their relative volatilities in an attempt to answer: why HOM non-nitrate dimers?!

# 8. References


Aalto, P., Hämeri, K., Becker, E., Weber, R., Salm, J., Mäkelä, J. M., Hoell, C., O'dowd, C. D., Hansson, H.-C., Väkevä, M., Koponen, I. K., Buzorius, G., and Kulmala, M.: Physical characterization of aerosol particles during nucleation events, Tellus B, 53, 344-358 10.1034/j.1600-0889.2001.530403.x, 2001.

Almeida, J., Schobesberger, S., Kürten, A., Ortega, I. K., Kupiainen-Määttä, O., Praplan, A. P., Adamov, A., Amorim, A., Bianchi, F., and Breitenlechner, M. J. N.: Molecular understanding of sulphuric acid–amine particle nucleation in the atmosphere, 502, 359, 2013.

Andreae, M. O., and Merlet, P.: Emission of trace gases and aerosols from biomass burning, Global Biogeochem. Cycl., 15, 955-966, 10.1029/2000gb001382, 2001.

Apte, J. S., Marshall, J. D., Cohen, A. J., and Brauer, M.: Addressing global mortality from ambient PM2. 5, Environmental Science and Technology, 49, 8057-8066, 2015.

Asmi, A., Wiedensohler, A., Laj, P., Fjaeraa, A.-M., Sellegri, K., Birmili, W., Weingartner, E., Baltensperger, U., Zdimal, V., and Zikova, N.: Number size distributions and seasonality of submicron particles in Europe 2008–2009, Atmos. Chem. Phys., 11, 5505-5538, 10.5194/acp-11-5505-2011, 2011.

Bianchi, F., Tröstl, J., Junninen, H., Frege, C., Henne, S., Hoyle, C., Molteni, U., Herrmann, E., Adamov, A., Bukowiecki, N., Chen, X., Duplissy, J., Gysel, M., Hutterli, M., Kangasluoma, J., Kontkanen, J., Kürten, A., Manninen, H. E., Münch, S., Peräkylä, O., Petäjä, T., Rondo, L., Williamson, C., Weingartner, E., Curtius, J., Worsnop, D. R., Kulmala, M., Dommen, J., and Baltensperger, U.: New particle formation in the free troposphere: A question of chemistry and timing, Science, 352, 1109-1112, 10.1126/science.aad5456, 2016.

Bianchi, F., Garmash, O., He, X., Yan, C., Iyer, S., Rosendahl, I., Xu, Z., Rissanen, M. P., Riva, M., Taipale, R. J. A. C., and Physics: The role of highly oxygenated molecules (HOMs) in determining the composition of ambient ions in the boreal forest, 17, 13819-13831, 2017.

Bianchi, F., Kurtén, T., Riva, M., Mohr, C., Rissanen, M. P., Roldin, P., Berndt, T., Crounse, J. D., Wennberg, P. O., and Mentel, T. F. J. C. r.: Highly Oxygenated Organic Molecules (HOM) from Gas-Phase Autoxidation Involving Peroxy Radicals: A Key Contributor to Atmospheric Aerosol, 2019.

Birmili, W., Berresheim, H., Plass-Dülmer, C., Elste, T., Gilge, S., Wiedensohler, A., and Uhrner, U.: The Hohenpeissenberg aerosol formation experiment (HAFEX): a long-term study including

size-resolved aerosol, H2SO4, OH, and monoterpenes measurements, Atmos. Chem. Phys., 3, 361-376, 10.5194/acp-3-361-2003, 2003.

Buenrostro Mazon, S., Riipinen, I., Schultz, D., Valtanen, M., Maso, M. D., Sogacheva, L., Junninen, H., Nieminen, T., Kerminen, V.-M., and Kulmala, M.: Classifying previously undefined days from eleven years of aerosol-particle-size distribution data from the SMEAR II station, Hyytiälä, Finland, Atmos. Chem. Phys., 9, 667-676, 10.5194/acp-9-667-2009, 2009.

Buenrostro Mazon, S., Kontkanen, J., Manninen, H. E., Nieminen, T., Kerminen, V.-M., and Kulmala, M.: A long-term comparison of nighttime cluster events and daytime ion formation in a boreal forest, Boreal Env. Res., 21, 242-261, 2016.

Burnett, R., Chen, H., Szyszkowicz, M., Fann, N., Hubbell, B., Pope, C. A., Apte, J. S., Brauer, M., Cohen, A., and Weichenthal, S.: Global estimates of mortality associated with long-term exposure to outdoor fine particulate matter, Proceedings of the National Academy of Sciences, 115, 9592-9597, 2018.

Chu, B., Kerminen, V. M., Bianchi, F., Yan, C., Petäjä, T., and Kulmala, M.: Atmospheric new particle formation in China, Atmos. Chem. Phys., 19, 115-138, 10.5194/acp-19-115-2019, 2019.

Dada, L., Mrad, R., Siffert, S., and Saliba, N.: Atmospheric markers of African and Arabian dust in an urban eastern Mediterranean environment, Beirut, Lebanon, Journal of Aerosol Science, 66, 187-192, 2013.

Dal Maso, M., Kulmala, M., Riipinen, I., Wagner, R., Hussein, T., Aalto, P. P., and Lehtinen, K. E.: Formation and growth of fresh atmospheric aerosols: eight years of aerosol size distribution data from SMEAR II, Hyytiala, Finland, Boreal Env. Res., 10, 323, 2005.

Dal Maso, M., Liao, L., Wildt, J., Kiendler-Scharr, A., Kleist, E., Tillmann, R., Sipilä, M., Hakala, J., Lehtipalo, K., Ehn, M., Kerminen, V. M., Kulmala, M., Worsnop, D., and Mentel, T.: A chamber study of the influence of boreal BVOC emissions and sulfuric acid on nanoparticle formation rates at ambient concentrations, Atmos. Chem. Phys., 16, 1955-1970, 10.5194/acp-16-1955-2016, 2016.

Dunne, E. M., Gordon, H., Kürten, A., Almeida, J., Duplissy, J., Williamson, C., Ortega, I. K., Pringle, K. J., Adamov, A., Baltensperger, U., Barmet, P., Benduhn, F., Bianchi, F., Breitenlechner, M., Clarke, A., Curtius, J., Dommen, J., Donahue, N. M., Ehrhart, S., Flagan, R. C., Franchin, A., Guida, R., Hakala, J., Hansel, A., Heinritzi, M., Jokinen, T., Kangasluoma, J., Kirkby, J., Kulmala, M., Kupc, A., Lawler, M. J., Lehtipalo, K., Makhmutov, V., Mann, G., Mathot, S., Merikanto, J., Miettinen, P., Nenes, A., Onnela, A., Rap, A., Reddington, C. L. S., Riccobono, F., Richards, N. A. D., Rissanen, M. P., Rondo, L., Sarnela, N., Schobesberger, S., Sengupta, K.,

Simon, M., Sipilä, M., Smith, J. N., Stozkhov, Y., Tomé, A., Tröstl, J., Wagner, P. E., Wimmer, D., Winkler, P. M., Worsnop, D. R., and Carslaw, K. S.: Global atmospheric particle formation from CERN CLOUD measurements, 354, 1119-1124, 10.1126/science.aaf2649 %J Science, 2016.

Duplissy, J., Merikanto, J., Franchin, A., Tsagkogeorgas, G., Kangasluoma, J., Wimmer, D., Vuollekoski, H., Schobesberger, S., Lehtipalo, K., Flagan, R. C., Brus, D., Donahue, N. M., Vehkamäki, H., Almeida, J., Amorim, A., Barmet, P., Bianchi, F., Breitenlechner, M., Dunne, E. M., Guida, R., Henschel, H., Junninen, H., Kirkby, J., Kürten, A., Kupc, A., Määttänen, A., Makhmutov, V., Mathot, S., Nieminen, T., Onnela, A., Praplan, A. P., Riccobono, F., Rondo, L., Steiner, G., Tome, A., Walther, H., Baltensperger, U., Carslaw, K. S., Dommen, J., Hansel, A., Petäjä, T., Sipilä, M., Stratmann, F., Vrtala, A., Wagner, P. E., Worsnop, D. R., Curtius, J., and Kulmala, M.: Effect of ions on sulfuric acid-water binary particle formation: 2. Experimental data and comparison with QC-normalized classical nucleation theory, 121, 1752-1775, 10.1002/2015jd023539, 2016.

Ehn, M., Junninen, H., Petäjä, T., Kurtén, T., Kerminen, V.-M., Schobesberger, S., Manninen, H., Ortega, I., Vehkamäki, H., Kulmala, M. J. A. C., and Physics: Composition and temporal behavior of ambient ions in the boreal forest, 10, 8513-8530, 2010.

Ehn, M., Junninen, H., Schobesberger, S., Manninen, H. E., Franchin, A., Sipilä, M., Petäjä, T., Kerminen, V.-M., Tammet, H., Mirme, A. J. A. S., and Technology: An instrumental comparison of mobility and mass measurements of atmospheric small ions, 45, 522-532, 2011.

Ehn, M., Thornton, J. A., Kleist, E., Sipilä, M., Junninen, H., Pullinen, I., Springer, M., Rubach, F., Tillmann, R., Lee, B., Lopez-Hilfiker, F., Andres, S., Acir, I.-H., Rissanen, M., Jokinen, T., Schobesberger, S., Kangasluoma, J., Kontkanen, J., Nieminen, T., Kurtén, T., Nielsen, L. B., Jørgensen, S., Kjaergaard, H. G., Canagaratna, M., Maso, M. D., Berndt, T., Petäjä, T., Wahner, A., Kerminen, V.-M., Kulmala, M., Worsnop, D. R., Wildt, J., and Mentel, T. F.: A large source of low-volatility secondary organic aerosol, Nature, 506, 476-479, 10.1038/nature13032, 2014.

Glachant, M.: Implementing European environmental policy: The impacts of directives in the Member States, Edward Elgar Publishing, 2001.

Gordon, H., Sengupta, K., Rap, A., Duplissy, J., Frege, C., Williamson, C., Heinritzi, M., Simon, M., Yan, C., and Almeida, J. J. P. o. t. N. A. o. S.: Reduced anthropogenic aerosol radiative forcing caused by biogenic new particle formation, Proc Natl Acad Sci U S A, 113, 12053-12058, 10.1073/pnas.1602360113, 2016.

Grythe, H., Ström, J., Krejčí, R., Quinn, P. K., and Stohl, A.: A review of sea-spray aerosol source functions using a large global set of sea salt aerosol concentration measurements, Atmos. Chem. Phys., 14, 1277-1297, 2014.

Hakola, H., Tarvainen, V., Laurila, T., Hiltunen, V., Hellén, H., and Keronen, P.: Seasonal variation of VOC concentrations above a boreal coniferous forest, Atmospheric Environment, 37, 1623-1634, 2003.

Hallquist, M., Wenger, J., Baltensperger, U., Rudich, Y., Simpson, D., Claeys, M., Dommen, J., Donahue, N., George, C., and Goldstein, A.: The formation, properties and impact of secondary organic aerosol: current and emerging issues, Atmos. Chem. Phys., 9, 5155-5236, 10.5194/acp-9-5155-2009, 2009.

Hansel, A., Jordan, A., Holzinger, R., Prazeller, P., Vogel, W., Lindinger, W. J. I. J. o. M. S., and Processes, I.: Proton transfer reaction mass spectrometry: on-line trace gas analysis at the ppb level, 149, 609-619, 1995.

Hari, P., and Kulmala, M.: Station for measuring ecosystem-atmosphere relations, Boreal Env. Res., 10, 315-322, 2005.

Hellén, H., Praplan, A. P., Tykkä, T., Ylivinkka, I., Vakkari, V., Bäck, J., Petäjä, T., Kulmala, M., Hakola, H. J. A. C., and Physics: Long-term measurements of volatile organic compounds highlight the importance of sesquiterpenes for the atmospheric chemistry of a boreal forest, 18, 13839-13863, 2018.

Hoppel, W. A.: Ion-aerosol attachment coefficients, ion depletion, and the charge distribution on aerosols, Journal of Geophysical Research: Atmospheres, 90, 5917-5923, 1985.

Huneeus, N., Schulz, M., Balkanski, Y., Griesfeller, J., Prospero, J., Kinne, S., Bauer, S., Boucher, O., Chin, M., Dentener, F., Diehl, T., Easter, R., Fillmore, D., Ghan, S., Ginoux, P., Grini, A., Horowitz, L., Koch, D., Krol, M. C., Landing, W., Liu, X., Mahowald, N., Miller, R., Morcrette, J. J., Myhre, G., Penner, J., Perlwitz, J., Stier, P., Takemura, T., and Zender, C. S.: Global dust model intercomparison in AeroCom phase I, Atmos. Chem. Phys., 11, 7781-7816, 10.5194/acp-11-7781-2011, 2011.

IPCC: Climate Change 2013: The Physical Science Basis. Contribution of Working Group I to the Fifth Assessment Report of the Intergovernmental Panel on Climate Change, Cambridge University Press, Cambridge, United Kingdom and New York, NY, USA, 1535 pp., 2013.

Jen, C. N., McMurry, P. H., and Hanson, D. R. J. J. o. G. R. A.: Stabilization of sulfuric acid dimers by ammonia, methylamine, dimethylamine, and trimethylamine, 119, 7502-7514, 2014.

Jokinen, T., Sipilä, M., Junninen, H., Ehn, M., Lönn, G., Hakala, J., Petäjä, T., Mauldin Iii, R. L., Kulmala, M., and Worsnop, D. R.: Atmospheric sulphuric acid and neutral cluster measurements using CI-APi-TOF, Atmos. Chem. Phys., 12, 4117-4125, 10.5194/acp-12-4117-2012, 2012.

Jokinen, T., Kausiala, O., Garmash, O., Peräkylä, O., Junninen, H., Schobesberger, S., Chao, Y., Sipilä, M., and Rissanen, M. P.: Production of highly oxidized organic compounds from ozonolysis of β-caryophyllene: laboratory and field measurements, 2016.

Jordan, A., Haidacher, S., Hanel, G., Hartungen, E., Märk, L., Seehauser, H., Schottkowsky, R., Sulzer, P., and Märk, T. J. I. J. o. M. S.: A high resolution and high sensitivity proton-transfer-reaction time-of-flight mass spectrometer (PTR-TOF-MS), 286, 122-128, 2009.

Junninen, H., Ehn, M., Petäjä, T., Luosujärvi, L., Kotiaho, T., Kostiainen, R., Rohner, U., Gonin, M., Fuhrer, K., and Kulmala, M. J. A. M. T.: A high-resolution mass spectrometer to measure atmospheric ion composition, Atmos Meas Tech, 3, 1039-1053, 10.5194/amt-3-1039-2010, 2010.

Kannosto, J., Virtanen, A., Lemmetty, M., Mäkelä, J. M., Keskinen, J., Junninen, H., Hussein, T., Aalto, P., and Kulmala, M.: Mode resolved density of atmospheric aerosol particles, Atmos. Chem. Phys., 8, 5327-5337, 10.5194/acp-8-5327-2008, 2008.

Kerminen, V.-M., and Kulmala, M.: Analytical formulae connecting the “real” and the “apparent” nucleation rate and the nuclei number concentration for atmospheric nucleation events, Journal of Aerosol Science, 33, 609-622, 10.1016/S0021-8502(01)00194-X, 2002.

Kerminen, V.-M., Paramonov, M., Anttila, T., Riipinen, I., Fountoukis, C., Korhonen, H., Asmi, E., Laakso, L., Lihavainen, H., Swietlicki, E., Svenningsson, B., Asmi, A., Pandis, S. N., Kulmala, M., and Petäjä, T.: Cloud condensation nuclei production associated with atmospheric nucleation: a synthesis based on existing literature and new results, Atmos. Chem. Phys., 12, 12037-12059, 10.5194/acp-12-12037-2012, 2012.

Kerminen, V.-M., Chen, X., Vakkari, V., Petäjä, T., Kulmala, M., and Bianchi, F.: Atmospheric new particle formation and growth: review of field observations, Environ Res Lett, 13, 103003, ARTN 103003, 10.1088/1748-9326/aadf3c, 2018.

Kirkby, J., Curtius, J., Almeida, J., Dunne, E., Duplissy, J., Ehrhart, S., Franchin, A., Gagné, S., Ickes, L., Kürten, A., Kupc, A., Metzger, A., Riccobono, F., Rondo, L., Schobesberger, S., Georgios Tsagkogeorgas, Daniela Wimmer, Antonio Amorim, Bianchi, F., Martin Breitenlechner, André David, Josef Dommen, Downard, A., Ehn, M., Flagan, R. C., Haider, S., Hansel, A., Hauser, D., Jud, W., Junninen, H., Kreissl, F., Kvashin, A., Laaksonen, A., Lehtipalo, K., Lima, J., Lovejoy, E. R., Makhmutov, V., Mathot, S., Mikkilä, J., Minginette, P., Sandra Mogo, Nieminen, T.,

Onnela, A., Pereira, P., Petäjä, T., Schnitzhofer, R., Seinfeld, J. H., Sipilä, M., Stozhkov, Y., Stratmann, F., Tomé, A., Vanhanen, J., Viisanen, Y., Vrtala, A., Wagner, P. E., Walther, H., Weingartner, E., Wex, H., Winkler, P. M., Carslaw, K. S., Worsnop, D. R., Baltensperger, U., and Kulmala, M.: Role of sulphuric acid, ammonia and galactic cosmic rays in atmospheric aerosol nucleation, Nature, 476, 429-433, 10.1038/nature10343, 2011.

Kirkby, J., Duplissy, J., Sengupta, K., Frege, C., Gordon, H., Williamson, C., Heinritzi, M., Simon, M., Yan, C., and Almeida, J. J. N.: Ion-induced nucleation of pure biogenic particles, Nature, 533, 521, 10.1038/nature17953, 2016.

Knutson, E., and Whitby, K.: Aerosol classification by electric mobility: apparatus, theory, and applications, Journal of Aerosol Science, 6, 443-451, 1975.

Kontkanen, J., Paasonen, P., Aalto, J., Bäck, J., Rantala, P., Petäjä, T., and Kulmala, M.: Simple proxies for estimating the concentrations of monoterpenes and their oxidation products at a boreal forest site, Atmos. Chem. Phys., 16, 13291-13307, 10.5194/acp-16-13291-2016, 2016.

Kuang, C., Riipinen, I., Sihto, S. L., Kulmala, M., McCormick, A. V., and McMurry, P. H.: An improved criterion for new particle formation in diverse atmospheric environments, Atmos. Chem. Phys., 10, 8469-8480, 10.5194/acp-10-8469-2010, 2010.

Kulmala, M.: How Particles Nucleate and Grow, 302, 1000-1001, 10.1126/science.1090848 %J Science, 2003.

Kulmala, M., Vehkamäki, H., Petäjä, T., Dal Maso, M., Lauri, A., Kerminen, V.-M., Birmili, W., and McMurry, P. H.: Formation and growth rates of ultrafine atmospheric particles: a review of observations, Journal of Aerosol Science, 35, 143-176, 10.1016/j.jaerosci.2003.10.003, 2004.

Kulmala, M., Lehtinen, K. E. J., and Laaksonen, A.: Cluster activation theory as an explanation of the linear dependence between formation rate of 3nm particles and sulphuric acid concentration, Atmos. Chem. Phys., 6, 787-793, 10.5194/acp-6-787-2006, 2006.

Kulmala, M., Petäjä, T., Nieminen, T., Sipilä, M., Manninen, H. E., Lehtipalo, K., Dal Maso, M., Aalto, P. P., Junninen, H., and Paasonen, P.: Measurement of the nucleation of atmospheric aerosol particles, Nature protocols, 7, 1651-1667, 10.1038/nprot.2012.091, 2012.

Kulmala, M.: Build a global Earth observatory, Nature, 553, 21-23, 10.1038/d41586-017-08967-y, 2018.

Kumar, P., Pirjola, L., Ketzel, M., and Harrison, R. M.: Nanoparticle emissions from 11 non-vehicle exhaust sources – A review, Atmospheric Environment, 67, 252-277, 2013.

Künzli, N., and Tager, I. B. J. S. M. W.: Air pollution: from lung to heart, 135, 697-702, 2005.

Kürten, A., Bianchi, F., Almeida, J., Kupiainen-Määttä, O., Dunne, E. M., Duplissy, J., Williamson, C., Barmet, P., Breitenlechner, M., and Dommen, J. J. J. o. G. R. A.: Experimental particle formation rates spanning tropospheric sulfuric acid and ammonia abundances, ion production rates, and temperatures, 121, 12,377-312,400, 2016.

Kurtén, T., Torpo, L., Ding, C. G., Vehkamäki, H., Sundberg, M. R., Laasonen, K., and Kulmala, M.: A density functional study on water-sulfuric acid-ammonia clusters and implications for atmospheric cluster formation, J. Geophys. Res. Atmos, 112, 10.1029/2006JD007391, 2007.

Lehtinen, K. E. J., and Kulmala, M.: A model for particle formation and growth in the atmosphere with molecular resolution in size, Atmos Chem Phys, 3, 251-257, DOI 10.5194/acp-3-251-2003, 2003.

Lehtipalo, K., Sipilä, M., Junninen, H., Ehn, M., Berndt, T., Kajos, M., Worsnop, D., Petäjä, T., Kulmala, M. J. A. S., and Technology: Observations of nano-CN in the nocturnal boreal forest, 45, 499-509, 2011.

Lehtipalo, K., Leppa, J., Kontkanen, J., Kangasluoma, J., Franchin, A., Wimnner, D., Schobesberger, S., Junninen, H., Petaja, T., Sipila, M., Mikkila, J., Vanhanen, J., Worsnop, D. R., and Kulmala, M.: Methods for determining particle size distribution and growth rates between 1 and 3 nm using the Particle Size Magnifier, Boreal Environ Res, 19, 215-236, 2014.

Lelieveld, J., Evans, J. S., Fnais, M., Giannadaki, D., and Pozzer, A.: The contribution of outdoor air pollution sources to premature mortality on a global scale, Nature, 525, 367, 10.1038/nature15371, 2015.

Liao, H., Chen, W. T., and Seinfeld, J. H. J. J. o. G. R. A.: Role of climate change in global predictions of future tropospheric ozone and aerosols, 111, 2006.

Manninen, H. E., Petaja, T., Asmi, E., Riipinen, I., Nieminen, T., Mikkila, J., Horrak, U., Mirme, A., Mirme, S., Laakso, L., Kerminen, V. M., and Kulmala, M.: Long-term field measurements of charged and neutral clusters using Neutral cluster and Air Ion Spectrometer (NAIS), Boreal Environ Res, 14, 591-605, 2009.

Manninen, H. E., Mirme, S., Mirme, A., Petäjä, T., and Kulmala, M.: How to reliably detect molecular clusters and nucleation mode particles with Neutral cluster and Air Ion Spectrometer (NAIS), Atmos Meas Tech, 9, 3577-3605, 10.5194/amt-9-3577-2016, 2016.

Merikanto, J., Spracklen, D., Mann, G., Pickering, S., and Carslaw, K.: Impact of nucleation on global CCN, Atmos. Chem. Phys., 9, 8601-8616, 10.5194/acp-9-8601-2009, 2009.

Mirme, S., and Mirme, A.: The mathematical principles and design of the NAIS–a spectrometer for the measurement of cluster ion and nanometer aerosol size distributions, Atmos Meas Tech, 6, 1061-1071, 2013.

Murphy, D., and Ravishankara, A.: Trends and patterns in the contributions to cumulative radiative forcing from different regions of the world, Proceedings of the National Academy of Sciences, 115, 13192-13197, 2018.

Ng, N. L., Herndon, S. C., Trimborn, A., Canagaratna, M. R., Croteau, P., Onasch, T. B., Sueper, D., Worsnop, D. R., Zhang, Q., Sun, Y. J. A. S., and Technology: An Aerosol Chemical Speciation Monitor (ACSM) for routine monitoring of the composition and mass concentrations of ambient aerosol, 45, 780-794, 2011.

Nieminen, T., Lehtinen, K., and Kulmala, M.: Sub-10 nm particle growth by vapor condensation–effects of vapor molecule size and particle thermal speed, Atmos. Chem. Phys., 10, 9773-9779, 10.5194/acp-10-9773-2010, 2010, 2010.

Nieminen, T., Kerminen, V. M., Petäjä, T., Aalto, P. P., Arshinov, M., Asmi, E., Baltensperger, U., Beddows, D. C. S., Beukes, J. P., Collins, D., Ding, A., Harrison, R. M., Henzing, B., Hooda, R., Hu, M., Hõrrak, U., Kivekäs, N., Komsaare, K., Krejci, R., Kristensson, A., Laakso, L., Laaksonen, A., Leaitch, W. R., Lihavainen, H., Mihalopoulos, N., Németh, Z., Nie, W., O'Dowd, C., Salma, I., Sellegri, K., Svenningsson, B., Swietlicki, E., Tunved, P., Ulevicius, V., Vakkari, V., Vana, M., Wiedensohler, A., Wu, Z., Virtanen, A., and Kulmala, M.: Global analysis of continental boundary layer new particle formation based on long-term measurements, Atmos. Chem. Phys., 18, 14737-14756, 10.5194/acp-18-14737-2018, 2018.

Oberdörster, G., Sharp, Z., Atudorei, V., Elder, A., Gelein, R., Kreyling, W., and Cox, C. J. I. t.: Translocation of inhaled ultrafine particles to the brain, 16, 437-445, 2004.

Ortega, I. K., Kurtén, T., Vehkamäki, H., Kulmala, M. J. A. C., and Physics: The role of ammonia in sulfuric acid ion induced nucleation, 8, 2859-2867, 2008.

Paasonen, P., Nieminen, T., Asmi, E., Manninen, H., Petäjä, T., Plass-Dülmer, C., Flentje, H., Birmili, W., Wiedensohler, A., Horrak, U., Metzger, A., Hamed, A., Laaksonen, A., Facchini, M. C., Kerminen, V.-M., and Kulmala, M.: On the roles of sulphuric acid and low-volatility organic vapours in the initial steps of atmospheric new particle formation, Atmos. Chem. Phys., 10, 11223-11242, 10.5194/acp-10-11223-2010, 2010.

Paasonen, P., Kupiainen, K., Klimont, Z., Visschedijk, A., Denier van der Gon, H. A. C., and Amann, M.: Continental anthropogenic primary particle number emissions, Atmos. Chem. Phys., 16, 6823-6840, 10.5194/acp-16-6823-2016, 2016.

Perez, R., Ineichen, P., Seals, R., and Zelenka, A.: Making full use of the clearness index for parameterizing hourly insolation conditions, Sol Energy, 45, 111-114, 10.1016/0038-092X(90)90036-C, 1990.

Petäjä, T., Mauldin Iii, R., Kosciuch, E., McGrath, J., Nieminen, T., Paasonen, P., Boy, M., Adamov, A., Kotiaho, T., and Kulmala, M.: Sulfuric acid and OH concentrations in a boreal forest site, Atmos. Chem. Phys., 9, 7435-7448, 10.5194/acp-9-7435-2009, 2009.

Pierce, J. R., and Adams, P. J.: Uncertainty in global CCN concentrations from uncertain aerosol nucleation and primary emission rates, Atmos. Chem. Phys., 9, 1339-1356, 10.5194/acp-9-1339-2009, 2009.

Pope, C. A., Thun, M. J., Namboodiri, M. M., Dockery, D. W., Evans, J. S., Speizer, F. E., Heath, C. W. J. A. j. o. r., and medicine, c. c.: Particulate air pollution as a predictor of mortality in a prospective study of US adults, 151, 669-674, 1995.

Putaud, J.-P., Raes, F., Van Dingenen, R., Brüggemann, E., Facchini, M. C., Decesari, S., Fuzzi, S., Gehrig, R., Hüglin, C., Laj, P., Lorbeer, G., Maenhaut, W., Mihalopoulos, N., Müller, K., Querol, X., Rodriguez, S., Schneider, J., Spindler, G., Brink, H. t., Tørseth, K., and Wiedensohler, A.: A European aerosol phenomenology—2: chemical characteristics of particulate matter at kerbside, urban, rural and background sites in Europe, Atmospheric Environment, 38, 2579-2595, https://doi.org/10.1016/j.atmosenv.2004.01.041, 2004.

Rantala, P., Taipale, R., Aalto, J., Kajos, M. K., Patokoski, J., Ruuskanen, T. M., and Rinne, J.: Continuous flux measurements of VOCs using PTR-MS—reliability and feasibility of disjunct-eddy-covariance, surface-layer-gradient, and surface-layer-profile methods, 2014.

Riccobono, F., Rondo, L., Sipilä, M., Barmet, P., Curtius, J., Dommen, J., Ehn, M., Ehrhart, S., Kulmala, M., Kürten, A. J. A. C., and Physics: Contribution of sulfuric acid and oxidized organic compounds to particle formation and growth, 12, 9427-9439, 2012.

Riipinen, I., Yli-Juuti, T., Pierce, J. R., Petäjä, T., Worsnop, D. R., Kulmala, M., and Donahue, N. M. J. N. G.: The contribution of organics to atmospheric nanoparticle growth, 5, 453, 2012.

Sánchez, G., Serrano, A., and Cancillo, M.: Effect of cloudiness on solar global, solar diffuse and terrestrial downward radiation at Badajoz (Southwestern Spain), Optica pura y aplicada, 45, 33-38, 2012.

Schauer, J. J., Rogge, W. F., Hildemann, L. M., Mazurek, M. A., Cass, G. R., and Simoneit, B. R. T.: Source apportionment of airborne particulate matter using organic compounds as tracers, Atmospheric Environment, 30, 3837-3855, https://doi.org/10.1016/1352-2310(96)00085-4, 1996.

Schnitzhofer, R., Metzger, A., Breitenlechner, M., Jud, W., Heinritzi, M., De Menezes, L.-P., Duplissy, J., Guida, R., Haider, S., and Kirkby, J. J. A. M. T.: Characterisation of organic contaminants in the CLOUD chamber at CERN, 7, 2159-2168, 2014.

Schobesberger, S., Junninen, H., Bianchi, F., Lönn, G., Ehn, M., Lehtipalo, K., Dommen, J., Ehrhart, S., Ortega, I. K., and Franchin, A. J. P. o. t. N. A. o. S.: Molecular understanding of atmospheric particle formation from sulfuric acid and large oxidized organic molecules, 110, 17223-17228, 2013.

Seinfeld, J. H., and Pandis, S.: Atmospheric Chemistry and Physics: From Air Pollution to Climate Change, 3rd Edition, John Wiley & Sons, Inc., 2016.

Sihto, S.-L., Kulmala, M., Kerminen, V.-M., Maso, M. D., Petäjä, T., Riipinen, I., Korhonen, H., Arnold, F., Janson, R., Boy, M. J. A. C., and Physics: Atmospheric sulphuric acid and aerosol formation: implications from atmospheric measurements for nucleation and early growth mechanisms, 6, 4079-4091, 2006.

Sipilä, M., Berndt, T., Petäjä, T., Brus, D., Vanhanen, J., Stratmann, F., Patokoski, J., Mauldin, R. L., Hyvärinen, A.-P., Lihavainen, H., and Kulmala, M.: The Role of Sulfuric Acid in Atmospheric Nucleation, 327, 1243-1246, 10.1126/science.1180315 %J Science, 2010.

Sogacheva, L., Saukkonen, L., Nilsson, E., Dal Maso, M., Schultz, D. M., De Leeuw, G., and Kulmala, M.: New aerosol particle formation in different synoptic situations at Hyytiälä, southern Finland, Tellus B, 60, 485-494, 10.1111/j.1600-0889.2008.00364.x, 2008.

Spracklen, D. V., Carslaw, K. S., Merikanto, J., Mann, G. W., Reddington, C. L., Pickering, S., Ogren, J. A., Andrews, E., Baltensperger, U., Weingartner, E., Boy, M., Kulmala, M., Laakso, L., Lihavainen, H., Kivekäs, N., Komppula, M., Mihalopoulos, N., Kouvarakis, G., Jennings, S. G., O'Dowd, C., Birmili, W., Wiedensohler, A., Weller, R., Gras, J., Laj, P., Sellegri, K., Bonn, B., Krejci, R., Laaksonen, A., Hamed, A., Minikin, A., Harrison, R. M., Talbot, R., and Sun, J.: Explaining global surface aerosol number concentrations in terms of primary emissions and particle formation, Atmos. Chem. Phys., 10, 4775-4793, 10.5194/acp-10-4775-2010, 2010.

Stolzenburg, D., Fischer, L., Vogel, A. L., Heinritzi, M., Schervish, M., Simon, M., Wagner, A. C., Dada, L., Ahonen, L. R., and Amorim, A. J. P. o. t. N. A. o. S.: Rapid growth of organic aerosol nanoparticles over a wide tropospheric temperature range, 115, 9122-9127, 2018.

Tammet, H., and Kulmala, M.: Simulation tool for atmospheric aerosol nucleation bursts, Journal of Aerosol Science, 36, 173-196, 2005.

Vanhanen, J., Mikkila, J., Lehtipalo, K., Sipila, M., Manninen, H. E., Siivola, E., Petaja, T., and Kulmala, M.: Particle Size Magnifier for Nano-CN Detection, Aerosol Sci Tech, 45, 533-542, 10.1080/02786826.2010.547889, 2011.

Vicente, E. D., and Alves, C. A.: An overview of particulate emissions from residential biomass combustion, Atmospheric Research, 199, 159-185, https://doi.org/10.1016/j.atmosres.2017.08.027, 2018.

Wang, S. C., Flagan, R. C. J. A. S., and Technology: Scanning electrical mobility spectrometer, 13, 230-240, 1990.

Weber, R. J., McMurry, P. H., Eisele, F. L., and Tanner, D. J.: Measurement of Expected Nucleation Precursor Species and 3–500-nm Diameter Particles at Mauna Loa Observatory, Hawaii, J. Atmos. Sci., 52, 2242-2257, 10.1175/1520-0469(1995)052<2242:Moenps>2.0.Co;2, 1995.

Yao, L., Garmash, O., Bianchi, F., Zheng, J., Yan, C., Kontkanen, J., Junninen, H., Mazon, S. B., Ehn, M., Paasonen, P., Sipilä, M., Wang, M., Wang, X., Xiao, S., Chen, H., Lu, Y., Zhang, B., Wang, D., Fu, Q., Geng, F., Li, L., Wang, H., Qiao, L., Yang, X., Chen, J., Kerminen, V.-M., Petäjä, T., Worsnop, D. R., Kulmala, M., and Wang, L.: Atmospheric new particle formation from sulfuric acid and amines in a Chinese megacity, 361, 278-281, 10.1126/science.aao4839 %J Science, 2018.

# Paper I

Atmos. Chem. Phys., 18, 17883–17893, 2018
https://doi.org/10.5194/acp-18-17883-2018


Atmospheric Chemistry and Physics
Open Access
EGU

# Refined classification and characterization of atmospheric new-particle formation events using air ions

**Lubna Dada[1], Robert Chellapermal[1], Stephany Buenrostro Mazon[1], Pauli Paasonen[1], Janne Lampilahti[1], Hanna E. Manninen[1,2], Heikki Junninen[1,3], Tuukka Petäjä[1,4], Veli-Matti Kerminen[1], and Markku Kulmala[1,4,5]**

[1]Institute for Atmospheric and Earth System Research/Physics, University of Helsinki, Helsinki, Finland
[2]Experimental Physics Department, CERN, 1211 Geneva, Switzerland
[3]Institute of Physics, University of Tartu, Ülikooli 18, 50090 Tartu, Estonia
[4]Aerosol and Haze Laboratory, Beijing Advanced Innovation Center for Soft Matter Science and Engineering, Beijing University of Chemical Technology, Beijing, China
[5]Joint International Research Laboratory of Atmospheric and Earth System Sciences, Nanjing University, Nanjing, China

**Correspondence:** Lubna Dada (lubna.dada@helsinki.fi)

Received: 25 June 2018 – Discussion started: 9 August 2018
Revised: 19 November 2018 – Accepted: 27 November 2018 – Published: 17 December 2018

**Abstract.** Atmospheric new-particle formation (NPF) is a worldwide-observed phenomenon that affects the human health and the global climate. With a growing network of global atmospheric measurement stations, efforts towards investigating NPF have increased. In this study, we present an automated method to classify days into four categories including NPF events, non-events and two classes in between, which then ensures reproducibility and minimizes the hours spent on manual classification. We applied our automated method to 10 years of data collected at the SMEAR II measurement station in Hyytiälä, southern Finland using a Neutral cluster and Air Ion Spectrometer (NAIS). In contrast to the traditionally applied classification methods, which categorize days into events and non-events and ambiguous days as undefined days, our method is able to classify the undefined days as it accesses the initial steps of NPF at sub-3 nm sizes. Our results show that, on $\sim$24 % of the days in Hyytiälä, a regional NPF event occurred and was characterized by nice weather and favourable conditions such as a clear sky and low condensation sink. Another class found in Hyytiälä is the transported event class, which seems to be NPF carried horizontally or vertically to our measurement location and it occurred on 17 % of the total studied days. Additionally, we found that an ion burst, wherein the ions apparently fail to grow to larger sizes, occurred on 18 % of the days in Hyytiälä. The transported events and ion bursts were characterized by less favourable ambient conditions than regional NPF events and thus experienced interrupted particle formation or growth. Non-events occurred on 41 % of the days and were characterized by complete cloud cover and high relative humidity. Moreover, for regional NPF events occurring at the measurement site, the method identifies the start time, peak time and end time, which helps us focus on variables within an exact time window to better understand NPF at a process level. Our automated method can be modified to work in other measurement locations where NPF is observed.

## 1 Introduction

New-particle formation (NPF) is an atmospheric phenomenon that results in a big addition to aerosol load in the global troposphere (Spracklen et al., 2010; Kerminen et al., 2018). NPF is observed frequently in different environments around the globe, ranging from pristine locations (Siberia – Kulmala et al., 2011; Asmi et al., 2016) to boreal forests (Hyytiälä – Kulmala et al., 2013; Nieminen et al., 2014), tropical forests (Amazon – Artaxo et al., 2013; Wimmer et al., 2018), mountaintops (Jungfraujoch – Bianchi et al., 2016), semi-polluted cities (European cities – Manninen et al., 2010) and even heavily polluted megacities (China

– Kulmala et al., 2016, 2017; Wang et al., 2017). The freshly formed particles that grow to larger sizes contribute largely to the cloud condensation nuclei load in the atmosphere (Merikanto et al., 2009; Kerminen et al., 2012; Salma et al., 2016) and thus indirectly affect the climate (IPCC, 2013).

In order to comprehend the phenomenon of NPF in a specific location, we first need to understand its frequency and characteristics as well as the particle formation and growth rates associated with it. With a growing number of global stations (Kulmala, 2018), an automatic method is needed to classify the days into events and non-events. In addition to minimizing the effort of manual event classification, an automated method tends to also reduce any human error. In this study, we present an automated method which classifies days into four classes according to the observed characteristics of 2–4 nm sized air ions and 7–25 nm sized particles. The original classification method of days as events, non-events and undefined days was proposed by Dal Maso et al. (2005), later modified by Kulmala et al. (2012) and is based on particle measurements starting from about 3 nm in particle mobility diameter, thus missing the initial steps of NPF. With the increased development of instrumentation, we are able to access sub-3 nm clusters and refine our classification method to account for the very initial steps of NPF. The classification proposed here divides days into regional events, transported events, ion bursts and non-events, thus excluding any undefined days, which minimizes the number of days usually excluded from further data analysis. Furthermore, our automated method identifies the start, peak and end times of daytime regional events or ion bursts. By identifying the start and end times, we are able to concentrate on the conditions present during the actual NPF time window.

Our study focuses on the NPF occurring in Hyytiälä, a boreal forest site in southern Finland where the SMEAR II (Station for Measuring Forest Ecosystem-Atmosphere Relations) measurement station is located (Hari and Kulmala, 2005). The data set collected at the station sums up more than 22 years of particle, meteorological and gas data, making extensive analyses of NPF and related parameters possible. Besides studying NPF occurrence in Hyytiälä, our method can be applied to other locations where NPF is observed, enabling scientists studying particle formation to focus on specific time windows by which active NPF occurs. Our specific aims in this study are (i) to automatically classify days in Hyytiälä according to their initial NPF steps, (ii) to minimize the number of undefined days by refining the classification, (iii) to investigate different characteristics of classified days, (iv) to identify the start, peak and end times of regional events and, thereby, (v) to create a time series which allows us to focus on the exact time period during which a regional new-particle formation event has occurred.

## 2 Materials and methods

### 2.1 Measurement location

The main results of our study are based on the measurements collected at the SMEAR II station located in the boreal forest site in Hyytiälä, southern Finland (61°51′ N, 24°17′ E, 181 m a.s.l.). The station has accumulated 22 years of comprehensive measurements including particle, radiation, gas, meteorological and complementary data. This study analyses 10 years of data collected between 2006 and 2016. The location is considered a semi-clean boreal forest environment as it is far from anthropogenic pollutants (Asmi et al., 2011) and thus represents the Northern Hemisphere boreal forests. A more detailed description of the site and the ongoing measurements can be found in Hari and Kulmala (2005) and Nieminen et al. (2014).

### 2.2 Instrumentation

The traditional classification of days as NPF events and non-events follows the method proposed by Dal Maso et al. (2005) and Kulmala et al. (2012). For this classification method, the particle number-size distributions measured with a twin DMPS (Differential Mobility Particle Sizer) system (Aalto et al., 2001) were used. The twin DMPS system measured the aerosol number-size distribution over the size range 3–500 nm until 2004 and over the size range 3–1000 nm from 2005 onwards. The DMPS measurements are also used to calculate the condensation sink (CS), which is the rate at which non-volatile vapours condense onto pre-existing particles (Kulmala et al., 2012).

For our proposed automated classification method, the mobility distributions of neutral and charged aerosol particles and clusters in the size ranges of 2–42 nm and 0.8–47 nm, respectively, were measured with a Neutral cluster and Air Ion Spectrometer (NAIS, Airel Ltd., Estonia, Manninen et al., 2009, 2016; Mirme and Mirme, 2013) between 2006 and 2016. No measurements using the NAIS were made during 2008 when the instrument was used for an intensive campaign. Particle and air ion data are available in 2 min time steps.

The air temperature and the relative humidity are measured with 4-wired PT-100 sensors and relative humidity sensors (Rotronic Hygromet MP102H with Hygroclip HC2-S3, Rotronic AG, Bassersdorf, Switzerland) on a mast at a height level of 16.8 m. The temperature and relative humidity data are provided as 30 min averages. Solar radiation in the wavelengths of global radiation (0.30–4.8 µm) is monitored using pyranometers (SL 501A UVB, Solar Light, Philadelphia, PA, USA; Reeman TP 3, Astrodata, Tõravere, Tartumaa, Estonia until June 2008, and Middleton Solar SK08, Middleton Solar, Yarraville, Australia since June 2008) above the forest at 18 m. We used global radiation data for calculating the cloudiness parameter ($P$), which is the ratio of global radia-

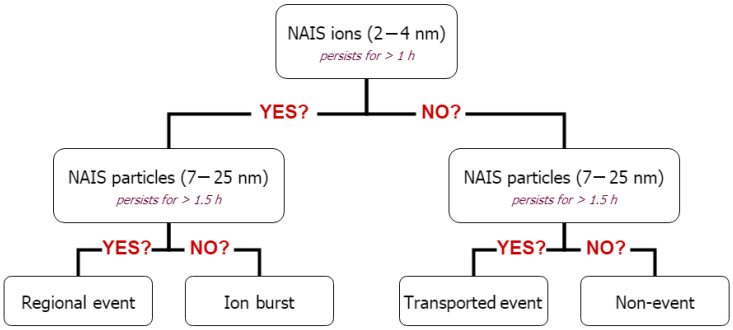


**Figure 1.** A flow chart for the decision path during event classification in Hyytiälä using the new classification method.

tion to theoretical maximum radiation arriving at Hyytiälä, by following the method proposed by Dada et al. (2017). Values of $P \leq 0.3$ represent a complete cloud cover, while values of $P \geq 0.8$ can be considered to represent clear-sky conditions.

### 2.3 Event classification decision tree

Based on the concentrations of 2–4 nm ions, we are able to detect the initial steps of cluster formation (see Leino et al., 2016), which would not be possible using the DMPS system alone and the traditional classification. This small size window available from the NAIS operating in ion mode gives an additional opportunity to investigate sub-3 nm clusters. Accordingly, we are able to estimate whether a regional NPF event occurred within the air mass in which the observations were made or if it occurred elsewhere and was then carried to our measurement location. Similarly, undefined days are identified based on their sub-3 nm characteristics. In Fig. 1 we present our refined classification decision tree and apply it to Hyytiälä data in this study. In order to attain this classification, we rely on the initial steps of cluster formation and their further growth, which we monitor using an automatic method. Since in our study we are interested in daytime NPF, we chose a time window between 06:00 and 19:00 LT (local time) when monitoring aerosol number concentrations. However, the automated method can be tweaked to include evening or night-time event classification in places where these event types are present.

Our decision tree (Fig. 1) first examines 2–4 nm ion concentrations representing the initial step of new-particle formation. A notable increase in their concentration is interpreted as ion clustering on site. To be counted as an increase, the number concentration of ions after 06:00 LT must increase above a relative threshold and persist for more than 1 h. This threshold is calculated from ion concentration averaged over the time period 00:00–04:00 LT multiplied by a scaling factor (Fig. 2a); we chose this time window as the background as it is outside the time window in which night-time ion clusters are observed (Buenrostro Mazon et al., 2016; Rose et al., 2018). To be counted as a notable increase past the threshold value, a concentration of 20 ions $cm^{-3}$ should be reached and should last for at least 1 h. We chose the aforementioned value as it has been found to be an indicator for NPF in Hyytiälä (Leino et al., 2016). If this criterion is met, these ions are expected to either grow to bigger sizes and lead to regional NPF events (REs) or fail to grow further. In this case the events are identified as ion bursts (IBs) that do not form new particles.

To decide whether the particle growth is observed, particle concentrations in the size range of 7–25 nm are examined. These particles represent the growth phase of freshly formed clusters. Since in Hyytiälä growth rates of 4–7 nm particles are reported to lie between 0.8 and 17 nm $h^{-1}$ (average of 3.8 nm $h^{-1}$ ) (Yli-Juuti et al., 2011), we considered a time delay of 1 to 8 h between the initial increase of ion (2–4 nm) concentrations and particle (7–25 nm) concentrations. To be considered as an increase, the particle number concentration should exceed a relative threshold, which in this case is the number concentration averaged over the time period of 03:00–05:00 (Fig. 2b). We determined the background time window by comparing the automatic method to a manual classification that we performed for the years 2013–2014 from our data set. The increase in concentration should last for $\sim$ 1.5 h (100 min) and reach a peak of at least 3000 particles $cm^{-3}$. On one hand, if both 2–4 nm ions and 7–25 nm particles are present, the time period is considered to be an RE. On the other hand, if the 2–4 nm ions are present but they do not grow to form 7–25 nm particles, the time period is classified as an ion burst (IB). Moreover, if 2–4 nm ions are not present, but we observe an increase in the particles, this leads to the assumption that the NPF event did not occur at the measurement location but was carried horizontally or vertically to our site (Leino et al., 2018). The latter has been previously described as a tail event (Buenrostro Mazon et al., 2009) or a TE. However, if neither criterion is met, which means that neither 2–4 nm ions nor 7–25 nm par-

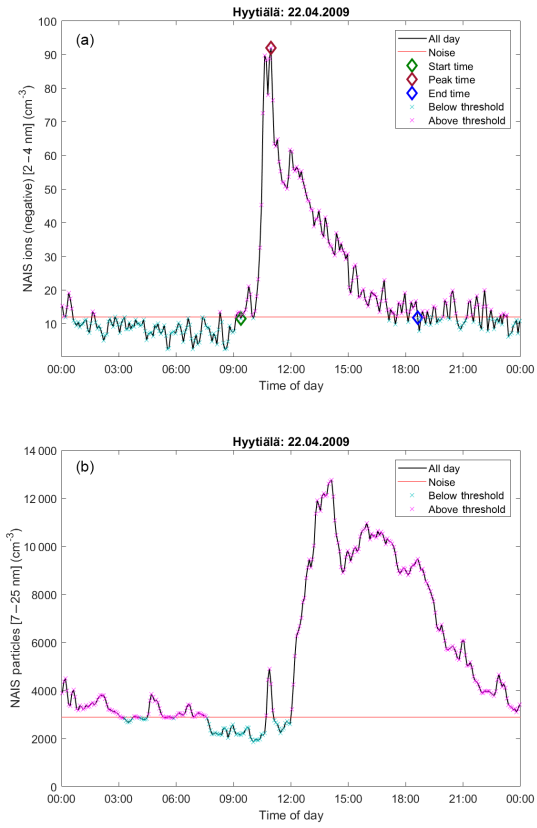


**Figure 2.** Example of an automatic method applied to **(a)** 2–4 nm ions (negative); ion concentration passed threshold and persisted for more than 1 h. **(b)** Example of 7–25 nm particles; particle concentration passed threshold and persisted for more than 1.5 h.

ticles are present in sufficient concentrations, the time period is then classified as an NE.

### 2.4 Description of the automated method

Our automatic method selects the start time, peak time and end time of negative NAIS ions in the size range 2–4 nm. The growth to an event is confirmed by an accompanying peak in the 7–25 nm particles measured by the NAIS. The outcome of the automatic method is the classification of days into the four classes, as well as a time series that identifies the time period of regional events and ion bursts in Hyytiälä (pathways of REs and IBs in Fig. 1). Once the ion and particle data are smoothed and the precipitation time stamps are eliminated using the new automated method, the classified time series is generated within a couple of minutes with a click of a button. This is in contrast to the manual method, which could use several hours and at least two people in order to classify 1 year of data.

First, to investigate the appearance of 2–4 nm ions, the precipitation time stamps are excluded from our analysis as they interfere with the ion data (Leino et al., 2016), resulting in misinterpretations. After that, the ion concentrations are smoothed using a Savitzky–Golay filter (Orfanidis, 1995). We then search for an increase in the ion concentration that lasts for 12 consecutive points (5 min each) above a threshold value and reaches values greater than 20 cm$^{-3}$ (Leino et al., 2016). A maximum of three drops below the threshold value is allowed (Fig. 2a). Finally, the method looks for a peak in the 7–25 nm particle concentration to identify the appearance of a growth phase (Fig. 2b). The peak requires 15 consecutive points (5 min each) with concentrations larger than the threshold value and that reach a value larger than 3000 cm$^{-3}$. Also, a maximum of 3 drops below the threshold value are allowed. Accordingly, each time stamp is classified.

### 2.5 Start time, peak time and end time determination

The start time, peak times and end times for regional events and ion bursts are defined based on the 2–4 nm ion concentration as follows: (i) the start time is the first crossing of the threshold line which lasts for more than 12 consecutive points, (ii) the peak time is when the concentration reaches the maximum and (iii) the end time is the first trough after crossing the threshold line into lower concentrations which remains below the threshold for more than three consecutive points. An example day is demonstrated in Fig. 2a. The threshold is taken as the 2–4 nm ion concentration averaged over the time period 00:00–04:00 multiplied by a scaling factor of 7. Our scaling factor was determined after a comparison with the manual classification of the data for the years 2013–2014.

## 3 Results and discussion

### 3.1 Event classification

Our classification puts the days in Hyytiälä into four different categories following the pathway chart in Fig. 1. REs, or regional NPF events, are those which are initiated over a large area, including the measurement location, and the particles continue to grow to bigger sizes. The type TE, or transported events (also known as tail events by Buenrostro Mazon et al., 2009), are events with an undetected beginning as it does not occur at the immediate vicinity of our measurement site. Such events could have been initiated outside our measurement site and transported to Hyytiälä (Leino et al., 2018). The aforementioned hypotheses could explain the observation that TE typically occur at around midday or later in the afternoon, while REs tend to occur concurrent with sunrise. The type IB, or ion bursts, is an attempt at NPF, during which clusters form in Hyytiälä; however, they do not grow beyond

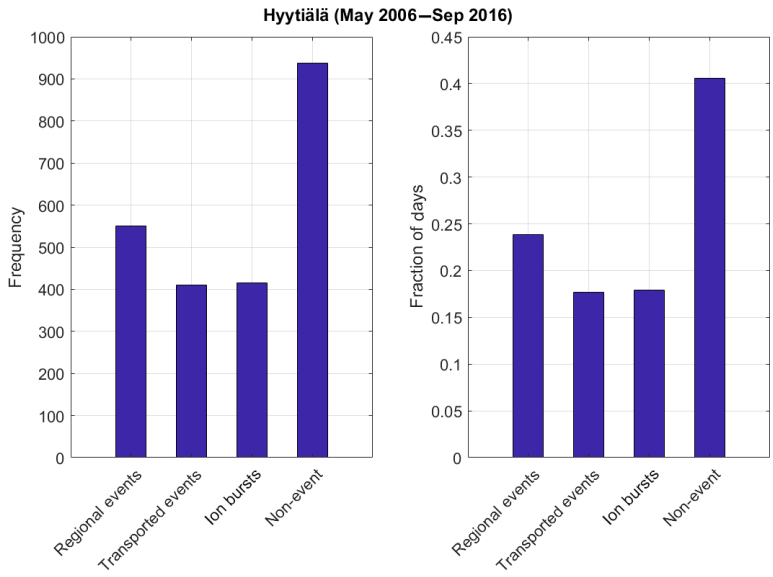


**Figure 3.** Frequency and fraction of events, ion burst and non-events in Hyytiälä using the new classification method.

a few nanometres in diameter. Changes in atmospheric conditions that could cause the limited, or interrupted, growth of the clusters are assessed in more detail in Sect. 3.3. Finally, non-events (NEs) are days on which we do not observe a forming mode of 2–4 nm ions nor a growing mode of 7–25 particles.

### 3.2 Frequency of events

For 10 years of data (2006–2016), excluding the days with missing NAIS data when the instrument was under maintenance or on campaigns, we classified a total of 2134 days. Using our refined classification method, we were able to classify the days into four categories as follows (Fig. 3): 551 REs (24 %), 410 TEs (18 %), 415 IBs (18 %) and 938 NEs (40 %). This refined classification is able to place all days into categories and thus eliminate the undefined days that usually constitute around 40 % of all the days in our location (Dal Maso et al., 2005; Buenrostro Mazon et al., 2009).

Moreover, we studied the interannual variation of each of the classes (Fig. 4a). In general, REs constitute 20 %–30 % of the total classified days. In 2006, the measurement started in September, which explains a lower fraction of REs. The gap in the analysis in 2008 is explained by a campaign during which the NAIS data is not available (Manninen et al., 2010). The data in 2009 includes data from spring only, which explains the high frequency of REs in 2009. While we can observe changes in the frequency of REs over the years, no clear trend exists. The annual variation of TEs follows that of REs, also having no specific trend over the years. The type IB appears to have an almost constant fraction over the years. Finally, NEs constitute between 40 % and 50 % of the days, except in 2009, which has a spring bias, favouring REs.

The monthly variation of REs follows the typical yearly cycle of NPF, with a peak in spring, followed by a smaller peak in autumn (Dal Maso et al., 2005; Nieminen et al., 2014; Dada et al., 2017). Interestingly, the refined classification shows that the events occurring in spring are mostly REs, while those in autumn are dominated by TEs. Additionally, REs rarely occur in winter, appearing on less than 5 % of the days. IBs have a steady 10 %–20 % occurrence during the year. Finally, NEs occur on 60 % to 70 % of winter days and less than 30 % during spring. Interestingly, while previously it was understood that summer is dominated by NEs (Nieminen et al., 2014; Dada et al., 2017), the refined classification shows that both TEs and IBs are frequent during summer, complementing observations by Buenrostro Mazon et al. (2009), who reported "failed events" during summer.

### 3.3 Characteristics of REs, TEs, IBs and NEs

For a regional event to take place, favourable conditions need to be present. These include a low condensation sink, low relative humidity, moderate temperature and plenty of radiation available during a clear sky (Dada et al., 2017; Hyvönen et al., 2005; Nieminen et al., 2014; Nieminen et al., 2015). In Fig. 5, we present the characteristics of each type of event classified in terms of condensation sink (CS), relative humidity (RH), temperature (T) and cloudiness (P). The data in the plots represent half-hour averages of each variable between

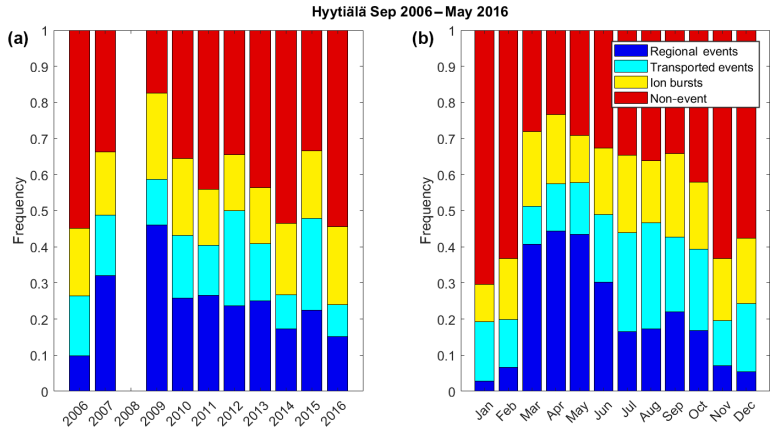


**Figure 4.** **(a)** Yearly and **(b)** monthly fraction of days classified as regional events (REs), transported events (TEs), ion bursts (IBs) and non-events (NEs) using the new classification method. The data from 2009 are biased towards spring months, which could explain the much higher number of events. No data were available during 2008.

07:00 and 12:00 during spring (March–May). We chose this season in order to capture the maximum NPF events and this time window in order to be consistent for all four studied classes. As expected, the median CS observed in REs was $1.7 \times 10^{-3}$ s$^{-1}$, which is a factor of 2 lower than CS observed on TE days or on NE days ($3 \times 10^{-3}$ s$^{-1}$). To our understanding, high CS inhibits NPF, so that its higher values during the days classified as TEs forbid the initial formation of particles at the measurement site. IBs, on the other hand, are potential regional events with interrupted growth. Since the median CS during IBs was not high ($2.5 \times 10^{-3}$ s$^{-1}$), it does not explain the discontinuous growth of the clusters during these events. We proceed to study the effect of T on the occurrence of each class of events. Since the data in Fig. 5 are measurements during spring, the median value of temperature (2–7 °C) was rather similar on all days and no specific trend or exception could be found.

In addition to CS and T, RH and cloudiness (P) play an important role in the occurrence of NPFs (Hamed et al., 2011; Dada et al., 2017). A regional NPF event is more likely to occur on a clear-sky day rather than on a cloudy day. This conclusion is demonstrated nicely in Fig. 5, which shows that the median value of $P$ was close to 0.8 on the RE days and closer to 0.3 on NE days. TE usually took place when the conditions within the boundary layer were not favourable for a regional NPF to occur. However, the particle growth was much less sensitive to environmental conditions: a particle growth was often observed during all times of the day and in every season, but also on days (and nights) on which NPF did not take place (Paasonen et al., 2018). Combined with a higher CS, the value of $P$ was much lower on TE days than on RE days, describing a semi-cloudy day as one that is unfavourable for NPF to occur within the boundary layer, which could result in the occurrence of a TE in locations where the conditions are conducive enough to NPF. It is, however, important to mention that it is possible to have a regional NPF episode taking place simultaneously with a transported one, and when the latter is transported it gets mixed with the regional NPF so that this situation will be classified as an RE. Finally, since ion bursts are the attempt of an event but do not grow, an interrupted clear sky could explain this phenomenon: for instance a sudden appearance of a cloud would result in the interruption of NPF (Baranizadeh et al., 2014), which then remains as an ion burst only. Finally, the RH, which in general correlates with cloudiness, showed a nice pattern between the event classes: RH was lowest for REs and highest for NEs, and it reflects cloudiness fairly well.

### 3.4 Start times, peak time and end time of RE

Our method makes it possible to detect the start, peak and end times of every regional event classified during our study period. Although several previous studies state that the occurrence of NPF starts with sunrise and peaks around midday, very few investigations have considered occurrence times accurately. We derived the start, peak and end times from 2–4 nm ions automatically, as mentioned in Sect. 2.4 and 2.5. During spring, when most of the NPF events occur, our results (Fig. 6) show that indeed REs occur after sunrise and prior to noon, with the maximum number of days occurring between the sunrise and 5 h past sunrise. The peak times of the events had the most frequent occurrence at 5 to 6 h after sunrise, which is between 10:30 and 11:30 LT (local time), complementing our previous assumption that NPF peaks before noon. Finally, the ending times of the events had the most frequent occurrence at 9 to 11 h after sunrise. During summer the events tend to start, peak and end later than

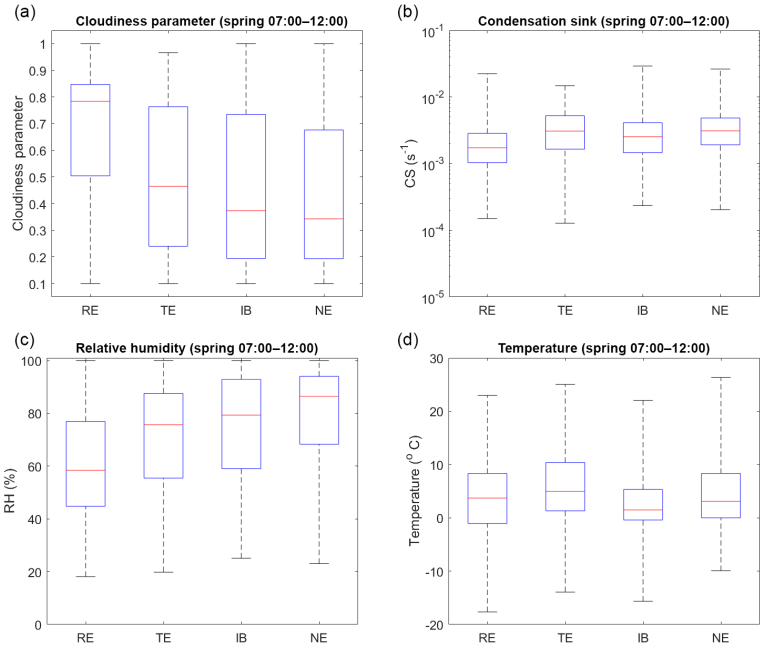


**Figure 5.** **(a)** Cloudiness parameter, **(b)** condensation sink, **(c)** relative humidity and **(d)** temperature on different days classified with the new classification method for spring (March–May) of 2006–2016 during the maximum NPF window (07:00–12:00). The acronyms RE, TE, IB and NE stand for regional event, transported event, ion burst and non-event. The red line represents the median of the data and the lower and upper edges of the box represent the 25th and 75th percentiles of the data. The lines extending from the central box represent the minimum and the maximum of the data.

in spring, and they show lower variability in comparison to spring. This observation could be attributed to longer daylight hours and fewer clouds. Whereas in autumn, the events start, peak and end earlier than in spring. Exceptionally, during winter, ion concentrations might be affected by the accumulation of snow on or around the inlets. Overall, the variability of the event start, peak and end times can be affected by the solar cycle, degree of cloudiness and seasonality. The importance of the identification of the exact start and end times of the process helps to increase our understanding of the processes governing the NPF phenomenon. More specifically, they allow us to form a time series in which NPF is separated from non-event times, making it possible to compare the parameters responsible for the NPF process within appropriate time frames.

### 3.5 Comparison to previous classification

In order to estimate the goodness of our automatic method, it is crucial to compare our results with the previous classifications (Dal Maso et al., 2005; Kulmala et al., 2012). Although such a comparison is not straightforward, we show one version of it in Fig. 7. On the $x$ axis, the original classified days are shown, and the refined classes are shown on the $y$ axis

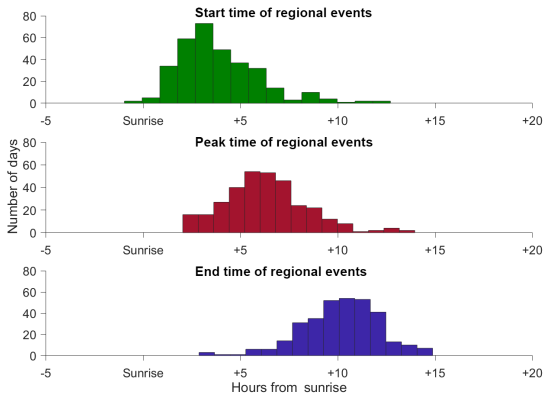


**Figure 6.** Frequency of days during spring at which regional events start, peak and end past sunrise. For example, most events start within 3 h from sunrise.

as a fraction of each original class. For example, 65 % of the originally classified event days (event days make 25 % of the total days in Hyytiälä according to the original classification) were found to be REs, 10 % were TEs and 14 % were IBs. The remaining 11 % were considered as misclassified or bad data (by manual classification) and were excluded from the plot. In total, our automatic method was able to classify 89 % of the original NPF events into some of the new event classes (RE, TE or IB). The original non-events (which made 40 % of the total days) were split between the TEs (20 %), IBs (19 %) and NEs (53 %). The remaining 8 % were bad data according to the manual classification and were excluded from the plot.

Finally, undefined days, which according to the traditional classification were 35 % of the total days, were split between all the classes. Our results show that 17 % of those were REs, 21 % were TEs, 19 % were IBs and 42 % were non-events. Those days were usually excluded from further analysis because they did not belong to a defined class according to the original classification method. Previous extensive studies of undefined days in Hyytiälä by Buenrostro Mazon et al. (2009) showed that a fraction of undefined days resemble interrupted events which, in our case, were 83 % of the days (TEs, IBs or NEs), and which all in all were related to unfavourable conditions for regional NPF. The interruption mechanisms may include the appearance of clouds (Baranizadeh et al., 2014; Dada et al., 2017), resulting in decreased radiation essential for particle formation and growth (Jokinen et al., 2017), or a change in the origin of arriving air masses from a clean to a rather polluted sector (Sogacheva et al., 2005). Our automated method fails sometimes as the result of the simultaneous appearance of an ion burst and a pollution plume. While the misjudgment of these days as regional events is largely minimized by correcting for the background concentrations of 7–25 nm particles, erroneous classification is still possible in some cases.

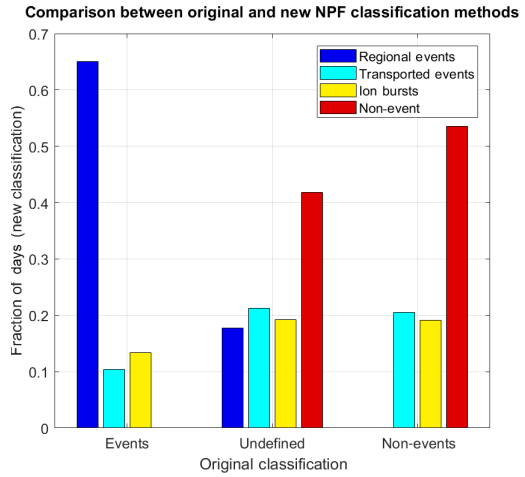


**Figure 7.** Comparison between original and new NPF classification methods. The refined classification matches 94 % with original event and non-event classification.

## 4 Conclusions

Using 10 years of measurements using the NAIS at the SMEAR II station, we were able to create an automated method to classify days into four classes based on their ion (2–4 nm) and particle (7–25 nm) number concentrations, including regional events, transported events, ion bursts and non-events. Our method minimizes the efforts used in manual day-by-day classification as well as the errors due to human bias. In addition, our method allows for the complete classification (sub-3 nm) of all days, i.e. reduces the number of previously known "undefined days", which have always been excluded from previous analyses.

Our results show that on ∼ 40 % of the days during spring in Hyytiälä, a regional NPF event occurs and is characterized by a set of favourable conditions, such as a clear sky, low condensation sink, medium temperature and low relative humidity. On the contrary, NEs were ∼ 25 % of the days and were characterized by a complete cloud cover, high RH and high CS. Interestingly, TEs and IBs fall into the category between REs and NEs in this respect. While IBs are interrupted growth of REs that were initially started due to a probable change in polluted air mass or the appearance of a cloud, TEs occurred on days when there was little chance for the cluster to form within our measurement location but they still had a chance to grow if they reached our site. Both IBs and TEs were characterized by intermediate values of CS, RH and $P$ compared with REs and NEs. Moreover, using the new method we are able to identify the start time, peak time and end time of events occurring in Hyytiälä. Our results show that most REs started within 5 h from the sunrise, peaked before noon and ended 10 h after sunrise. Finally, with small changes the classification method can be applied to other places around the globe where NPF takes place, providing a deeper understanding yet less effort for atmospheric scientists.

*Data availability.* Data measured at the SMEAR II station are available on the web page: https://avaa.tdata.fi/web/smart/ (Junninen et al., 2009). The classification, start times, peak times and end times are available from Lubna Dada (lubna.dada@helsinki.fi) upon request.

*Author contributions.* LD and VMK: manuscript writing. LD: data analysis. SBM, HEM and JL: NAIS data collection and interpretation. LD, RC and HJ: development of the method. LD, PP, HEM, JL, TP, VMK and MK: scientific discussions and conclusions.

*Competing interests.* The authors declare that they have no conflict of interest.

*Special issue statement.* This article is part of the special issue "Pan-Eurasian Experiment (PEEX)". It is not associated with a conference.

*Acknowledgements.* Lubna Dada acknowledges the doctoral programme in Atmospheric Sciences (ATM-DP, University of Helsinki) for financial support. This project has received funding from the European Union's Horizon 2020 research (ERA-PLANET 689443) and innovation programme under grant agreement no. 654109. This work was supported by the European Commission via projects ACTRIS2, European Research Council via ATM-GTP (742206), and Academy of Finland Centre of Excellence in Atmospheric Sciences (grant number: 272041).

Edited by: Imre Salma
Reviewed by: two anonymous referees

## References

Aalto, P., Hämeri, K., Becker, E., Weber, R., Salm, J., Mäkelä, J. M., Hoell, C., O'dowd, C. D., Hansson, H.-C., Väkevä, M., Koponen, I. K., Buzorius, G., and Kulmala, M.: Physical characterization of aerosol particles during nucleation events, Tellus B, 53, 344–358, https://doi.org/10.1034/j.1600-0889.2001.530403.x, 2001.

Artaxo, P., Rizzo, L. V., Brito, J. F., Barbosa, H. M., Arana, A., Sena, E. T., Cirino, G. G., Bastos, W., Martin, S. T., and Andreae, M. O.: Atmospheric aerosols in Amazonia and land use change: from natural biogenic to biomass burning conditions, Faraday Discuss., 165, 203–235, 2013.

Asmi, A., Wiedensohler, A., Laj, P., Fjaeraa, A.-M., Sellegri, K., Birmili, W., Weingartner, E., Baltensperger, U., Zdimal, V., Zikova, N., Putaud, J.-P., Marinoni, A., Tunved, P., Hansson, H.-C., Fiebig, M., Kivekäs, N., Lihavainen, H., Asmi, E., Ulevicius, V., Aalto, P. P., Swietlicki, E., Kristensson, A., Mihalopoulos, N., Kalivitis, N., Kalapov, I., Kiss, G., de Leeuw, G., Henzing, B., Harrison, R. M., Beddows, D., O'Dowd, C., Jennings, S. G., Flentje, H., Weinhold, K., Meinhardt, F., Ries, L., and Kulmala, M.: Number size distributions and seasonality of submicron particles in Europe 2008–2009, Atmos. Chem. Phys., 11, 5505–5538, https://doi.org/10.5194/acp-11-5505-2011, 2011.

Asmi, E., Kondratyev, V., Brus, D., Laurila, T., Lihavainen, H., Backman, J., Vakkari, V., Aurela, M., Hatakka, J., Viisanen, Y., Uttal, T., Ivakhov, V., and Makshtas, A.: Aerosol size distribution seasonal characteristics measured in Tiksi, Russian Arctic, Atmos. Chem. Phys., 16, 1271–1287, https://doi.org/10.5194/acp-16-1271-2016, 2016.

Baranizadeh, E., Arola, A., Hamed, A., Nieminen, T., Mikkonen, S., Virtanen, A., Kulmala, M., Lehtinen, K., and Laaksonen, A.: The effect of cloudiness on new-particle formation: investigation of radiation levels, Boreal Env. Res., 19, 343–354, 2014.

Bianchi, F., Tröstl, J., Junninen, H., Frege, C., Henne, S., Hoyle, C., Molteni, U., Herrmann, E., Adamov, A., Bukowiecki, N., Chen, X., Duplissy, J., Gysel, M., Hutterli, M., Kangasluoma, J., Kontkanen, J., Kürten, A., Manninen, H. E., Münch, S., Peräkylä, O., Petäjä, T., Rondo, L., Williamson, C., Weingartner, E., Curtius, J., Worsnop, D. R., Kulmala, M., Dommen, J., and Baltensperger, U.: New particle formation in the free troposphere: A question of chemistry and timing, Science, 352, 1109–1112, https://doi.org/10.1126/science.aad5456, 2016.

Buenrostro Mazon, S., Riipinen, I., Schultz, D. M., Valtanen, M., Dal Maso, M., Sogacheva, L., Junninen, H., Nieminen, T., Kerminen, V.-M., and Kulmala, M.: Classifying previously undefined days from eleven years of aerosol-particle-size distribution data from the SMEAR II station, Hyytiälä, Finland, Atmos. Chem. Phys., 9, 667–676, https://doi.org/10.5194/acp-9-667-2009, 2009.

Buenrostro Mazon, S., Kontkanen, J., Manninen, H. E., Nieminen, T., Kerminen, V.-M., and Kulmala, M.: A long-term comparison of nighttime cluster events and daytime ion formation in a boreal forest, Boreal Env. Res., 21, 242–261, 2016.

Dada, L., Paasonen, P., Nieminen, T., Buenrostro Mazon, S., Kontkanen, J., Peräkylä, O., Lehtipalo, K., Hussein, T., Petäjä, T., Kerminen, V.-M., Bäck, J., and Kulmala, M.: Long-term analysis of clear-sky new particle formation events and non-events in Hyytiälä, Atmos. Chem. Phys., 17, 6227–6241, https://doi.org/10.5194/acp-17-6227-2017, 2017.

Dal Maso, M., Kulmala, M., Riipinen, I., Wagner, R., Hussein, T., Aalto, P. P., and Lehtinen, K. E.: Formation and growth of fresh atmospheric aerosols: eight years of aerosol size distribution data from SMEAR II, Hyytiala, Finland, Boreal Env. Res., 10, 323–336, 2005.

Hamed, A., Korhonen, H., Sihto, S. L., Joutsensaari, J., Järvinen, H., Petäjä, T., Arnold, F., Nieminen, T., Kulmala, M., and Smith, J. N.: The role of relative humidity in continental new particle formation, J. Geophys. Res.-Atmos., 116, D03202, https://doi.org/10.1029/2010JD014186, 2011.

Hari, P. and Kulmala, M.: Station for measuring ecosystem-atmosphere relations, Boreal Env. Res., 10, 315–322, 2005.

Hyvönen, S., Junninen, H., Laakso, L., Dal Maso, M., Grönholm, T., Bonn, B., Keronen, P., Aalto, P., Hiltunen, V., Pohja, T., Launiainen, S., Hari, P., Mannila, H., and Kulmala, M.: A look at aerosol formation using data mining techniques, Atmos. Chem. Phys., 5, 3345–3356, https://doi.org/10.5194/acp-5-3345-2005, 2005.

IPCC: Climate Change 2013: The Physical Science Basis, Contribution of Working Group I to the Fifth Assessment Report of the Intergovernmental Panel on Climate Change, Cambridge University Press, Cambridge, UK and New York, USA, 1535 pp., 2013.

Jokinen, T., Kontkanen, J., Lehtipalo, K., Manninen, H. E., Aalto, J., Porcar-Castell, A., Garmash, O., Nieminen, T., Ehn, M., Kangasluoma, J., Junninen, H., Levula, J., Duplissy, J., Ahonen, L. R., Rantala, P., Heikkinen, L., Yan, C., Sipilä, M., Worsnop, D. R., Bäck, J., Petäjä, T., Kerminen, V.-M., and Kulmala, M.: Solar eclipse demonstrating the importance of photochemistry in new particle formation, Sci. Rep.-UK, 7, 45707, https://doi.org/10.1038/srep45707, 2017.

Junninen, H., Lauri, A., Keronen, P., Aalto, P., Hiltunen, V., Hari, P., and Kulmala, M.: Smart-SMEAR: on-line data exploration and visualization tool for SMEAR stations, Boreal Environ. Res., 14, 447–457, 2009 (data available at: https://avaa.tdata.fi/web/smart/, last access: 1 June 2018).

Kerminen, V.-M., Paramonov, M., Anttila, T., Riipinen, I., Fountoukis, C., Korhonen, H., Asmi, E., Laakso, L., Lihavainen, H., Swietlicki, E., Svenningsson, B., Asmi, A., Pandis, S. N., Kulmala, M., and Petäjä, T.: Cloud condensation nuclei production associated with atmospheric nucleation: a synthesis based on existing literature and new results, Atmos. Chem. Phys., 12, 12037–12059, https://doi.org/10.5194/acp-12-12037-2012, 2012.

Kerminen, V.-M., Chen, X., Vakkari, V., Petäjä, T., Kulmala, M., and Bianchi, F.: Atmospheric new particle formation and growth: review of field observations, 13, 103003, https://doi.org/10.1088/1748-9326/aadf3c, 2018.

Kulmala, M.: Build a global Earth observatory, Nature, 553, 21–23, 2018.

Kulmala, M., Alekseychik, P., Paramonov, M., Laurila, T., Asmi, E., Arneth, A., Zilitinkevich, S., and Kerminen, V.-M.: On measurements of aerosol particles and greenhouse gases in Siberia and future research needs, Boreal Environ. Res., 16, 337–362, 2011.

Kulmala, M., Petäjä, T., Nieminen, T., Sipilä, M., Manninen, H. E., Lehtipalo, K., Dal Maso, M., Aalto, P. P., Junninen, H., and Paasonen, P.: Measurement of the nucleation of atmospheric aerosol particles, Nat. Protoc., 7, 1651–1667, https://doi.org/10.1038/nprot.2012.091, 2012.

Kulmala, M., Kontkanen, J., Junninen, H., Lehtipalo, K., Manninen, H. E., Nieminen, T., Petäjä, T., Sipilä, M., Schobesberger, S., Rantala, P., Franchin, A., Jokinen, T., Järvinen, E., Äijälä, M., Kangasluoma, J., Hakala, J., Aalto, P., Paasonen, P., Mikkilä, J., Vanhanen, J., Aalto, J., Hakola, H., Makkonen, U., Ruuskanen, T., Mauldin, R. r., Duplissy, J., Vehkamäki, H., Bäck, J., Kortelainen, A., Riipinen, I., Kurtén, T., Johnston, M., Smith, J., Ehn, M., Mentel, T., Lehtinen, K., Laaksonen, A., Kerminen, V., and Worsnop, D.: Direct observations of atmospheric aerosol nucleation, Science, 339, 943–946, https://doi.org/10.1126/science.1227385, 2013.

Kulmala, M., Petäjä, T., Kerminen, V.-M., Kujansuu, J., Ruuskanen, T., Ding, A., Nie, W., Hu, M., Wang, Z., Wu, Z., Wang, L., and Worsnop, D. R.: On secondary new particle formation in China, Front. Env. Sci. Eng., 10, 8, https://doi.org/10.1007/s11783-016-0850-1, 2016.

Kulmala, M., Kerminen, V.-M., Petäjä, T., Ding, A., and Wang, L.: Atmospheric gas-to-particle conversion: why NPF events are observed in megacities?, Faraday Discuss., 200, 271–288, 2017.

Leino, K., Nieminen, T., Manninen, H. E., Petäjä, T., Kerminen, V.-M., and Kulmala, M.: Intermediate ions as a strong indicator of new particle formation bursts in a boreal forest, Boreal Environ. Res., 21, 274–286, 2016.

Leino, K., Lampilahti, J., Poutanen, P., Väänänen, R., Manninen, A., Buenrostro Mazon, S., Dada, L., Nikandrova, A., Wimmer, D., Aalto, P. P., Ahonen, L. R., Enroth, J., Kangasluoma, J., Keronen, P., Korhonen, F., Laakso, H., Matilainen, T., Sivola, E., Manninen, H. E., Lehtipalo, K., Kerminen, V.-M., Petäjä, T., and Kulmala, M.: Vertical profiles of sub-3 nm particles over the boreal forest, Atmos. Chem. Phys. Discuss., https://doi.org/10.5194/acp-2018-605, in review, 2018.

Manninen, H. E., Petäjä, T., Asmi, E., Riipinen, I., Nieminen, T., Mikkilä, J., Hõrrak, U., Mirme, A., Mirme, S., Laakso, L., Kerminen, V.-M., and Kulmala, M.: Long-term field measurements of charged and neutral clusters using Neutral cluster and Air Ion Spectrometer (NAIS), Boreal Environ. Res, 14, 591–605, 2009.

Manninen, H. E., Nieminen, T., Asmi, E., Gagné, S., Häkkinen, S., Lehtipalo, K., Aalto, P., Vana, M., Mirme, A., Mirme, S., Hõrrak, U., Plass-Dülmer, C., Stange, G., Kiss, G., Hoffer, A., Töro, N., Moerman, M., Henzing, B., de Leeuw, G., Brinkenberg, M., Kouvarakis, G. N., Bougiatioti, A., Mihalopoulos, N., O'Dowd, C., Ceburnis, D., Arneth, A., Svenningsson, B., Swietlicki, E., Tarozzi, L., Decesari, S., Facchini, M. C., Birmili, W., Sonntag, A., Wiedensohler, A., Boulon, J., Sellegri, K., Laj, P., Gysel, M., Bukowiecki, N., Weingartner, E., Wehrle, G., Laaksonen, A., Hamed, A., Joutsensaari, J., Petäjä, T., Kerminen, V.-M., and Kulmala, M.: EUCAARI ion spectrometer measurements at 12 European sites – analysis of new particle formation events, Atmos. Chem. Phys., 10, 7907–7927, https://doi.org/10.5194/acp-10-7907-2010, 2010.

Manninen, H. E., Mirme, S., Mirme, A., Petäjä, T., and Kulmala, M.: How to reliably detect molecular clusters and nucleation mode particles with Neutral cluster and Air Ion Spectrometer (NAIS), Atmospheric Measurement Techniques, 9, 3577–3605, https://doi.org/10.5194/amt-9-3577-2016, 2016.

Merikanto, J., Spracklen, D. V., Mann, G. W., Pickering, S. J., and Carslaw, K. S.: Impact of nucleation on global CCN, Atmos. Chem. Phys., 9, 8601–8616, https://doi.org/10.5194/acp-9-8601-2009, 2009.

Mirme, S. and Mirme, A.: The mathematical principles and design of the NAIS – a spectrometer for the measurement of cluster ion and nanometer aerosol size distributions, Atmos. Meas. Tech., 6, 1061–1071, https://doi.org/10.5194/amt-6-1061-2013, 2013.

Nieminen, T., Asmi, A., Dal Maso, M., Aalto, P. P., Keronen, P., Petäjä, T., Kulmala, M., and Kerminen, V.-M.: Trends in atmospheric new-particle formation: 16 years of observations in a boreal-forest environment, Boreal Env. Res., 19, 191–214, 2014.

Nieminen, T., Yli-Juuti, T., Manninen, H. E., Petäjä, T., Kerminen, V.-M., and Kulmala, M.: Technical note: New particle formation event forecasts during PEGASOS–Zeppelin Northern mission 2013 in Hyytiälä, Finland, Atmos. Chem. Phys., 15, 12385–12396, https://doi.org/10.5194/acp-15-12385-2015, 2015.

Orfanidis, S. J.: Introduction to signal processing, Prentice-Hall, Inc., 1995.

Paasonen, P., Peltola, M., Kontkanen, J., Junninen, H., Kerminen, V.-M., and Kulmala, M.: Comprehensive analysis of particle growth rates from nucleation mode to cloud condensation nuclei in boreal forest, Atmos. Chem. Phys., 18, 12085–12103, https://doi.org/10.5194/acp-18-12085-2018, 2018.

Rose, C., Zha, Q., Dada, L., Yan, C., Lehtipalo, K., Junninen, H., Mazon, S. B., Jokinen, T., Sarnela, N., Sipilä, M., Petäjä, T., Kerminen, V.-M., Bianchi, F., and Kulmala, M.: Observations of biogenic ion-induced cluster formation in the atmosphere, Science Advances, 4, eaar5218, https://doi.org/10.1126/sciadv.aar5218, 2018.

Salma, I., Németh, Z., Kerminen, V.-M., Aalto, P., Nieminen, T., Weidinger, T., Molnár, Á., Imre, K., and Kulmala, M.: Regional effect on urban atmospheric nucleation, Atmos. Chem. Phys., 16, 8715–8728, https://doi.org/10.5194/acp-16-8715-2016, 2016.

Sogacheva, L., Dal Maso, M., Kerminen, V.-M., and Kulmala, M.: Probability of nucleation events and aerosol particle concentration in different air mass types arriving at Hyytiälä, southern Finland, based on back trajectories analysis, Boreal Env. Res., 10, 479–491, 2005.

Spracklen, D. V., Carslaw, K. S., Merikanto, J., Mann, G. W., Reddington, C. L., Pickering, S., Ogren, J. A., Andrews, E., Baltensperger, U., Weingartner, E., Boy, M., Kulmala, M., Laakso, L., Lihavainen, H., Kivekäs, N., Komppula, M., Mihalopoulos, N., Kouvarakis, G., Jennings, S. G., O'Dowd, C., Birmili, W., Wiedensohler, A., Weller, R., Gras, J., Laj, P., Sellegri, K., Bonn, B., Krejci, R., Laaksonen, A., Hamed, A., Minikin, A., Harrison, R. M., Talbot, R., and Sun, J.: Explaining global surface aerosol number concentrations in terms of primary emissions and particle formation, Atmos. Chem. Phys., 10, 4775–4793, https://doi.org/10.5194/acp-10-4775-2010, 2010.

Wang, Z., Wu, Z., Yue, D., Shang, D., Guo, S., Sun, J., Ding, A., Wang, L., Jiang, J., and Guo, H.: New particle formation in China: Current knowledge and further directions, Sci. Total Environ., 577, 258–266, 2017.

Wimmer, D., Buenrostro Mazon, S., Manninen, H. E., Kangasluoma, J., Franchin, A., Nieminen, T., Backman, J., Wang, J., Kuang, C., Krejci, R., Brito, J., Goncalves Morais, F., Martin, S. T., Artaxo, P., Kulmala, M., Kerminen, V.-M., and Petäjä, T.: Ground-based observation of clusters and nucleation-mode particles in the Amazon, Atmos. Chem. Phys., 18, 13245–13264, https://doi.org/10.5194/acp-18-13245-2018, 2018.

Yli-Juuti, T., Nieminen, T., Hirsikko, A., Aalto, P. P., Asmi, E., Hõrrak, U., Manninen, H. E., Patokoski, J., Dal Maso, M., Petäjä, T., Rinne, J., Kulmala, M., and Riipinen, I.: Growth rates of nucleation mode particles in Hyytiälä during 2003–2009: variation with particle size, season, data analysis method and ambient conditions, Atmos. Chem. Phys., 11, 12865–12886, https://doi.org/10.5194/acp-11-12865-2011, 2011.

# Paper II

Atmos. Chem. Phys., 17, 6227–6241, 2017
www.atmos-chem-phys.net/17/6227/2017/
doi:10.5194/acp-17-6227-2017


Atmospheric Chemistry and Physics
Open Access
EGU

# Long-term analysis of clear-sky new particle formation events and nonevents in Hyytiälä

**Lubna Dada[1], Pauli Paasonen[1], Tuomo Nieminen[1,2], Stephany Buenrostro Mazon[1], Jenni Kontkanen[1], Otso Peräkylä[1], Katrianne Lehtipalo[1,4], Tareq Hussein[1,5], Tuukka Petäjä[1], Veli-Matti Kerminen[1], Jaana Bäck[3], and Markku Kulmala[1]**

[1]Department of Physics, University of Helsinki, P.O. Box 64, 00014 Helsinki, Finland
[2]Department of Applied Physics, University of Eastern Finland, P.O. Box 1627, 70211 Kuopio, Finland
[3]Department of Forest Sciences, University of Helsinki, P.O. Box 27, 00014 Helsinki, Finland
[4]Laboratory of Atmospheric Chemistry, Paul Scherrer Institute (PSI), 5232 Villigen PSI, Switzerland
[5]Department of Physics, the University of Jordan, Amman 11942, Jordan

*Correspondence to:* Lubna Dada (lubna.dada@helsinki.fi)

Received: 26 September 2016 – Discussion started: 19 October 2016
Revised: 23 March 2017 – Accepted: 25 April 2017 – Published: 22 May 2017

**Abstract.** New particle formation (NPF) events have been observed all around the world and are known to be a major source of atmospheric aerosol particles. Here we combine 20 years of observations in a boreal forest at the SMEAR II station (Station for Measuring Ecosystem–Atmosphere Relations) in Hyytiälä, Finland, by building on previously accumulated knowledge and by focusing on clear-sky (non-cloudy) conditions. We first investigated the effect of cloudiness on NPF and then compared the NPF event and nonevent days during clear-sky conditions. In this comparison we considered, for example, the effects of calculated particle formation rates, condensation sink, trace gas concentrations and various meteorological quantities in discriminating NPF events from nonevents. The formation rate of 1.5 nm particles was calculated by using proxies for gaseous sulfuric acid and oxidized products of low volatile organic compounds, together with an empirical nucleation rate coefficient. As expected, our results indicate an increase in the frequency of NPF events under clear-sky conditions in comparison to cloudy ones. Also, focusing on clear-sky conditions enabled us to find a clear separation of many variables related to NPF. For instance, oxidized organic vapors showed a higher concentration during the clear-sky NPF event days, whereas the condensation sink (CS) and some trace gases had higher concentrations during the nonevent days. The calculated formation rate of 3 nm particles showed a notable difference between the NPF event and nonevent days during clear-sky conditions, especially in winter and spring. For springtime, we are able to find a threshold equation for the combined values of ambient temperature and CS, (CS ($s^{-1}$) $> -3.091 \times 10^{-5} \times T$ (in Kelvin) $+ 0.0120$), above which practically no clear-sky NPF event could be observed. Finally, we present a probability distribution for the frequency of NPF events at a specific CS and temperature.

## 1 Introduction

The effects of atmospheric aerosol particles on the climate system, human health and environmental interactions have raised interest in various phenomena associated with the formation, growth and loss of these particles (Pöschl, 2005; Seinfeld and Pandis, 2012; Apte et al., 2015). While primary emissions are a very important source of atmospheric aerosol particles, especially in terms of the aerosol mass loading, the particle number concentration is greatly affected by atmospheric new particle formation (NPF). During the last couple of decades, NPF has been observed to take place almost all over the world (Kulmala et al., 2004a; Zhang et al., 2011; Bianchi et al., 2016; Kontkanen et al., 2016a, 2017). Atmospheric NPF is thought to be the dominant source of the total particle number concentration (Kulmala et al., 2016) and a major source of cloud condensation nuclei in the global tro-

posphere (Merikanto et al., 2009; Yu et al., 2010; Kerminen et al., 2012; Salma et al., 2016).

Understanding the NPF phenomenon requires understanding its precursors and pathways involved under different atmospheric conditions. For instance, high concentrations of low-volatility vapors result in a higher probability for NPF (Nieminen et al., 2015), whereas a high relative humidity and condensation sink (CS) tend to suppress NPF (Hyvönen et al., 2005; Nieminen et al., 2014). Recent laboratory experiments have shown the importance of sulfuric acid and low-volatile oxidized organic vapors to NPF (Metzger et al., 2010; Kirkby et al., 2011; Petäjä et al., 2011; Kulmala et al., 2013; Ehn et al., 2014; Riccobono et al., 2014). Additionally, atmospheric observations confirm the importance of these precursor vapors in the initial steps of NPF and in the further growth of newly formed particles (Kulmala et al., 1998; Smith et al., 2005; Kerminen et al., 2010; Paasonen et al., 2010; Ahlm et al., 2012; Bzdek et al., 2014; Nieminen et al., 2014; Vakkari et al., 2015). The Station for Measuring Forest Ecosystem–Atmosphere Relations (SMEAR II), located in Hyytiälä, southern Finland, compiles almost 21 years of particle number size distribution and extensive complementary data, providing the longest size distribution time series in the world, and hence allows for robust NPF analysis which is not readily possible at other sites. The station is located in a homogenous Scots pine forest far from major pollution sources. Hyytiälä is therefore classified as a background site representative of the semi-clean Northern Hemisphere boreal forests.

Many studies have investigated the role of different variables in causing, enhancing or preventing new particle formation (Hyvönen et al., 2005; Baranizadeh et al., 2014; Nieminen et al., 2014). In particular, Baranizadeh et al. (2014) studied the effect of cloudiness on NPF events observed at SMEAR II in Hyytiälä. They concluded, in agreement with some other studies, that clouds tend to attenuate or interrupt NPF events (Sogacheva et al., 2008; Boulon et al., 2010; Baranizadeh et al., 2014; Nieminen et al., 2015). In this study, we eliminated one variable that limits NPF (cloudiness) in order to provide a better insight into the other quantities related to atmospheric NPF. Based on 20 years of observations and data analysis for the SMEAR II station in Hyytiälä, we aim to (i) quantify the effect of cloudiness on new particle formation frequency, (ii) characterize the differences between NPF event and nonevent days during clear-sky conditions, (iii) explore the connections between new particle formation rates calculated from precursor vapor proxies and the occurrence of NPF events, (iv) formulate an equation that predicts whether a clear-sky day with specific temperature and CS is classified as an event, (v) use the clear-sky data set to calculate the NPF probability distribution based on temperature and CS.

## 2 Materials and methods

### 2.1 Measurements

The data used for the analysis in this study are from the University of Helsinki SMEAR II station (Hari and Kulmala, 2005). The station provides long-term continuous comprehensive measurements of quantities describing atmospheric–forest–ecosystem interactions. The SMEAR II station is located in the boreal forest in Hyytiälä, southern Finland (61°51′ N, 24°17′ E, 181 m a.s.l.), 220 km NW of Helsinki. Tampere (200 000 inhabitants) is the largest city nearest to the station and is located 60 km SW of the site. Being far from major human activities and surrounded by a homogenous Scots pine belt, Hyytiälä is considered a rural background site due to the low levels of air pollutants (Asmi et al., 2011). A more detailed overview of the measurements at the station can be found in Hari and Kulmala (2005) and Nieminen et al. (2014).

In this study, the data analysis is based on four types of measurements: (i) aerosol particle number size distributions, (ii) concentration of the trace gases (CO, NO, $NO_2$, $NO_x$, $SO_2$ and $O_3$), (iii) meteorological parameters (solar radiation, temperature and relative humidity) and (iv) precursor vapor concentrations from previously developed proxies. The collection of data started in January 1996. Trace gas concentrations are measured at six different heights on a 74 m-high mast (extended to 126 m in summer 2010). Gas concentrations used in this study are collected from the middle level on the mast above the forest (at 16.8 m).

The aerosol number size distributions were measured with a twin DMPS (Differential Mobility Particle Sizer) system (Aalto et al., 2001) for the size ranges 3–500 nm until year 2004 and 3–1000 nm from 2005 onwards. These data were used to classify days as NPF events and nonevents following the method proposed by Dal Maso et al. (2005). The size distributions obtained from the DMPS measurements were used to calculate the CS, which is equal to the rate at which nonvolatile vapors condense onto a pre-existing aerosol particle population (Kulmala et al., 2012).

The CO concentration is measured with one infrared light absorption analyzer (API 300EU, Teledyne Monitor Labs, Englewood, CO, USA). The NO and $NO_x$ concentrations are monitored with a chemiluminescence analyzer (TEI 42C TL, Thermo Fisher Scientific, Waltham, MA, USA). The $NO_2$ concentration is calculated from the difference $NO_x$–NO. The detection limit is about 0.05 ppb. $SO_2$ measurements are made through a UV fluorescence analyzer (TEI 43 CTL, Thermo Fisher Scientific, Waltham, MA, USA) that has a detection limit of 0.1 ppb. The $O_3$ concentration is measured with an UV light absorption analyzer (TEI 49C, Thermo Fisher Scientific, Waltham, MA, USA) that has a detection limit of about 1 ppb. The data for trace gases are available as 30 min arithmetic means.

Solar radiation in the wavelengths of UV-B (280–320 nm) and global radiation (0.30–4.8 µm) are monitored using pyranometers (SL 501A UVB, Solar Light, Philadelphia, PA, USA; Reeman TP 3, Astrodata, Tõravere, Tartumaa, Estonia until June 2008, and Middleton Solar SK08, Middleton Solar, Yarraville, Australia since June 2008) above the forest at 18 m. The air temperature is measured with 4-wire PT-100 sensors, and the relative humidity (in percent) is measured with relative humidity sensors (Rotronic Hygromet MP102H with Hygroclip HC2-S3, Rotronic AG, Bassersdorf, Switzerland). These data are provided as 30 min averages.

## 2.2 Data analysis

### 2.2.1 New particle formation events classification

The formation of new aerosol particles in Hyytiälä is typically observed in the time window of several hours around noon, while this phenomenon seems to be rare during nighttime (Junninen et al., 2008; Buenrostro Mazon et al., 2016). Accordingly, aerosol number size distribution data from the DMPS measurements at around this time window are used for classifying individual days as new particle formation event or nonevent days. The classification follows the guidelines presented by Kulmala et al. (2012) and the procedure presented in Dal Maso et al. (2005). The latter uses a decision criterion based on the presence of particles < 25 nm in diameter and their consequent growth to Aitken mode. Event days are days on which sub-25 nm particle formation and growth are observed. Nonevent days are days on which neither modes are present. Undefined days are the days which do not fit either criterion.

### 2.2.2 Selecting noncloudy days

The cloudiness parameter ($P$) is the ratio of measured global radiation (Rd) divided by the theoretical global irradiance (Rg):

$$P = \frac{\mathrm{Rd}}{\mathrm{Rg}}. \quad (1)$$

The theoretical maximum of global radiation (Rg) is calculated by taking into consideration the latitude of the measurement station and the seasonal solar cycle. While a complete cloud coverage is classified as $P < 0.3$, a clear-sky is classified as $P > 0.7$ (Perez et al., 1990; Sogacheva et al., 2008; Sánchez et al., 2012). In Hyytiälä, the great majority of NPF events are initiated during the morning hours after sunrise, but before noon (Dada et al., 2017). Since the time of sunrise varies widely in Hyytiälä between the different seasons, the time window 09:00–12:00 seems a reasonable compromise for considering whether NPF occurred or not. We found that NPF events occurring outside our selected time window were very few. Accordingly, in this work, the days were classified as cloudy or clear-sky days based on the median value of $P$ during 09:00–12:00 each day, corresponding to the time window for new particle formation. The median value ensures that at least half of our selected time window is clear-sky while the rest can vary between clear-sky and minor scattered clouds. The median is also useful because NPF is a regional-scale phenomenon, so for instance, scattered clouds on an otherwise sunny day affecting the local radiation measurements (and leading to a momentarily drop in $P$) do not usually interrupt the regional NPF process. Clear-sky days were those with a median of $P > 0.7$ between 09:00 and 12:00 and are the focus of this study. For consistency, the variables compared in our study are taken from the same time window, 09:00–12:00.

### 2.2.3 Sulfuric acid and oxidized organics proxies

The gaseous sulfuric acid concentration is estimated from a pseudo-steady-state-approximation proxy developed by Petäjä et al. (2009). This proxy takes into consideration the sulfuric acid source and sink terms as

$$[\mathrm{H_2SO_4}]_{\mathrm{proxy}} = k \cdot \frac{[\mathrm{SO_2}] \cdot \mathrm{UVB}}{\mathrm{CS}}. \quad (2)$$

Here, UVB ($\mathrm{W\,m^{-2}}$) is the fraction of the UV radiation reaching the earth after being screened by ozone (280–320 nm). The coefficient $k$ ($\mathrm{m^2\,W^{-1}\,s^{-1}}$) is obtained from the comparison of the proxy concentration to the available measured $H_2SO_4$ data and has a median value of $9.9 \times 10^{-7}\,\mathrm{m^2\,W^{-1}\,s^{-1}}$.

The concentration of monoterpene oxidation products, called oxidized organic compounds (OxOrg) here, is estimated using a proxy developed by Kontkanen et al. (2016b). This proxy is calculated by using the concentrations of different oxidants (the measured ozone concentration $[O_3]$ and parameterizations for the hydroxyl and nitrate radical concentration, [OH] and $[NO_3]$, respectively) and their reaction rates, $k_i$, with the monoterpenes. The MT $_{\mathrm{proxy}}$ (in this case $\mathrm{MT_{proxy1,doy}}$) is calculated by taking into account the effect of temperature-driven emissions, the mixing of the boundary layer and the oxidation of monoterpenes (Kontkanen et al., 2016b).

$$\left[\mathrm{OxOrg}\right]_{\mathrm{proxy}} = \frac{\left(k_{\mathrm{OH+MT}}[\mathrm{OH}] + k_{\mathrm{O_3+MT}}[\mathrm{O_3}] + k_{\mathrm{NO_3+MT}}[\mathrm{NO_3}]\right) \cdot \mathrm{MT_{proxy}}}{\mathrm{CS}} \quad (3)$$

### 2.2.4 Particle formation rates

The formation rate of nucleation mode particles ($J_{3,C}$, particle diameter > 3 nm) was calculated based on the method suggested by Kerminen and Kulmala's equation (Kerminen and Kulmala, 2002). This quantity is a function of the calculated formation rate of 1.5 nm-sized particles ($J_{1.5,C}$), their growth rate (GR) and the CS:

$$J_{3,C} = J_{1.5,C} \exp\left(-\gamma \frac{\mathrm{CS'}}{\mathrm{GR_{1.5-3}}}\left(\frac{1}{1.5} - \frac{1}{3}\right)\right), \quad (4)$$

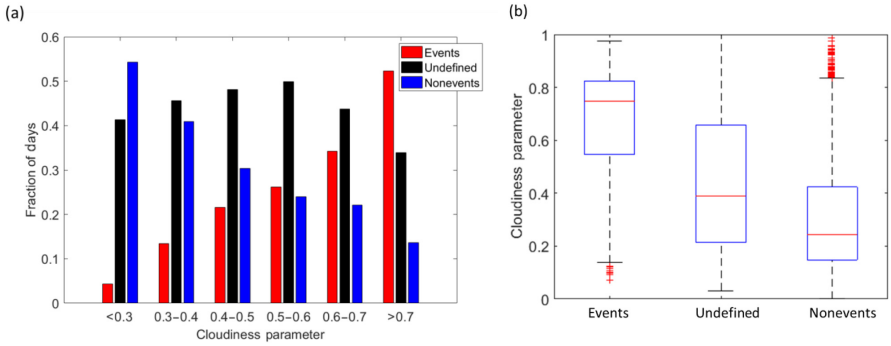


**Figure 1.** **(a)** Figure showing the fraction of days which are classified as NPF events, nonevents and undefined days during different sky cloudiness conditions. **(b)** Daily (09:00–12:00) medians and percentiles of cloudiness recorded during NPF event, undefined and nonevent days. The red line represents the median of the data and the lower and upper edges of the box represent 25th and 75th percentiles of the data, respectively. The length of the whiskers represent 1.5× interquartile range which includes 99.3 % of the data. Data outside the whiskers are considered outliers and are marked with red crosses.

where $\gamma$ is a coefficient with an approximate value of $0.23\,m^3\,nm^2\,s^{-1}$. The value of $J_{1.5,C}$ was calculated by assuming heteromolecular nucleation between SA and OxOrg as follows:

$$J_{1.5,C} = K_{het}[H_2SO_4]_{proxy}\left[OxOrg\right]_{proxy}. \quad (5)$$

The heterogeneous nucleation coefficient used in Eq. (5) is the median estimated coefficient for Hyytiälä scaled from Paasonen et al. (2010): $K_{het} = 9.2 \times 10^{-14}\,cm^3\,s^{-1}$. The scaling was made in order to fit the current data. The median value of [OxOrg] during the event days in April and May was found to be $1.6 \times 10^7\,cm^{-3}$ (Paasonen et al., 2010), whereas the revised median value of [OxOrg] by Kontkanen et al. (2016b) is $1.3 \times 10^8\,cm^{-3}$. The scaling factor is the ratio between new and original [OxOrg] (0.1194). Accordingly, while the value of $K_{het}$ from Paasonen et al. (2010) is $1.1 \times 10^{-14}\,cm^3\,s^{-1}$, after the scaling by 0.1194 we obtain the revised $K_{het} = 9.2 \times 10^{-14}\,cm^3\,s^{-1}$.

The particle growth rate over the particle diameter range of 1.5–3 nm was calculated by taking into account the size of the condensing vapor molecule size and the thermal speed of the particle (Nieminen et al., 2010). The growth rates (1.5–3 nm) were calculated as 30 min averages and as the sum of the growth rates due to the sulfuric acid (SA) vapor and OxOrg vapor condensation. The density of the particle was assumed to be constant ($1440\,kg\,m^{-3}$). For SA, we first determined the SA concentration needed to make the particles grow at the rate of 1 nm/h by taking into account the mass of hydrated SA at the present RH and its density (Kurtén et al., 2007). Then, we calculated the GR of the particles due to SA condensation by using the SA proxy concentration. The same method was used for GR due to OxOrg condensation, where the vapor density was assumed to be $1200\,kg\,m^{-3}$ (Hallquist et al., 2009; Kannosto et al., 2008). Similarly, the GR due to OxOrg was calculated by using OxOrg proxy concentrations divided by the concentration needed for $1\,nm\,h^{-1}$ GR.

#### 2.2.5 Calculation of backward air mass trajectories

Air mass trajectories were calculated using the Hybrid Single-Particle Lagrangian Integrated Trajectory (HYSPLIT_4) model at 96 h backward trajectories at 100, 250 and 500 m arrival heights once per hour.

## 3 Results and discussion

### 3.1 Effect of cloudiness on NPF

We studied NPF events as a function of cloudiness. Figure 1a shows the fraction of event, nonevent and undefined days as a function of cloudiness parameter. We can see that clear-sky conditions favor the occurrence of NPF: the fewer clouds there were, the higher was the fraction of NPF event days. For instance, for days with the cloudiness parameter of 0.3 or less, the fraction of event days was less than 0.1 of the total classified days. However, the fraction of NPF event days reached a maximum of around 0.55 during complete clear-sky conditions ($P > 0.7$), with 877 days classified as NPF events, 560 undefined days and only 229 as nonevents. On the NPF event days, the median cloudiness parameter $P$ during the time window 09:00–12:00 was found to be 0.75 (Fig. 1b), while the nonevent days were characterized by lower values of $P$ (a median of around 0.25). Also, 75 % of the NPF event days were found to have a cloudiness parameter larger than 0.5. The pattern found in Fig. 1a follows from the fact that radiation seems essential for NPF at this site, as the events occur almost solely during daylight hours (Kulmala et al., 2004b). Also, NPF is favored under abundant radiation conditions since the main components of

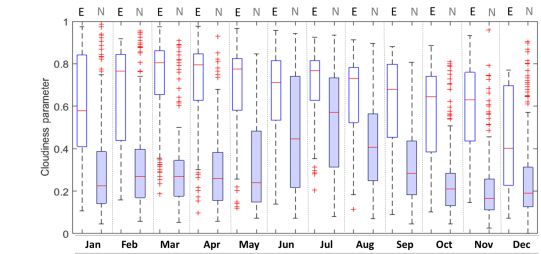


| | Jan | Feb | Mar | Apr | May | Jun | Jul | Aug | Sep | Oct | Nov | Dec |
|---|---|---|---|---|---|---|---|---|---|---|---|---|
| E | 27 | 68 | 277 | 296 | 267 | 162 | 94 | 110 | 188 | 115 | 30 | 17 |
| N | 316 | 218 | 143 | 125 | 110 | 138 | 192 | 162 | 158 | 229 | 308 | 318 |
| E ($P>0.7$) | 9 | 30 | 165 | 180 | 151 | 83 | 59 | 60 | 82 | 43 | 10 | 5 |
| N ($P>0.7$) | 18 | 18 | 16 | 10 | 11 | 31 | 68 | 21 | 9 | 6 | 4 | 17 |

**Figure 2.** Monthly variation of cloudiness daily (09:00–12:00) medians and percentiles recorded during NPF events (E; white) and nonevents (N; shaded). Numbers below the plot correspond to the number of data points included in each box plot. Number of clear-sky events (E ($P>0.7$)) and clear-sky nonevents (N ($P>0.7$)) accompany the plot. See Fig. 1 for an explanation of symbols.

freshly formed particles are mainly formed photochemically (Petäjä et al., 2009; Ehn et al., 2014). The fraction of undefined days, however, remained constant regardless of cloudiness conditions.

Our results emphasize the fact that radiation favors the occurrence of NPF, while clouds tend to decrease the probability of NPF. Undefined days were observed under cloudiness conditions that fell between those for NPF events and nonevents. In general, undefined days can be interrupted NPF events or unclassified plumes of small particles due to pollution (Buenrostro Mazon et al., 2009). The interruption of a NPF event can be due to a change in the measured air mass or to the attenuation of solar radiation caused by the appearance of a cloud during the event. We will not consider undefined days further in our analyses.

The monthly variation of daily median cloudiness parameter within the time window of 09:00–12:00 during the classified days is shown in Fig. 2. Spring showed the best separation between the events and nonevents in terms of the cloudiness parameter, while the separation became weaker during the summer and especially for June and July. Taken together, Figs. 1 and 2 emphasize the observation that the presence of clouds decreases the probability of NPF events.

### 3.2 General character of NPF on clear-sky days

Upon visualizing the cloudiness conditions during events and nonevents, we chose a fixed constraint for clear-sky conditions ($P>0.7$) during the time window of NPF (09:00–12:00) and will focus on other parameters that distinguish NPF events from nonevents in the following.

The monthly distribution of the event fraction on clear-sky days appeared as double peaks in spring and autumn, with spring having a higher fraction of events (Fig. 3a). The minimum fraction of NPF events was recorded in December.

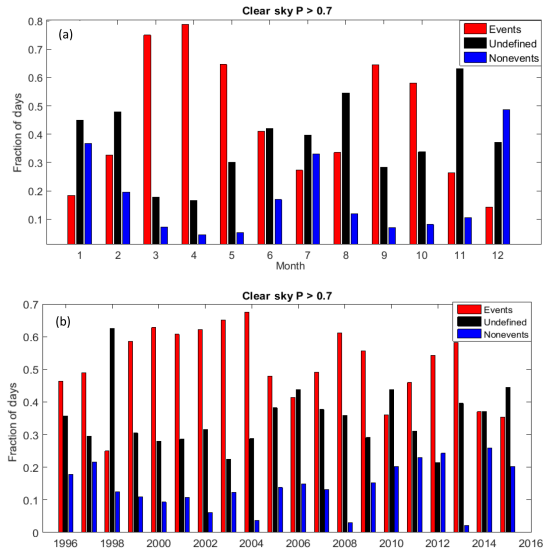


**Figure 3. (a)** Monthly and **(b)** yearly fraction of clear-sky days classified as NPF events, undefined and nonevents. In 1998, global radiation data are limited to 5.4 %, leading to the classification bias.

The fraction of nonevent days peaked in winter with another peak in summer. The total number of NPF events varied from year to year between 1996 and 2015. However, this variation did not show any specific trend of frequency (Fig. 3b), which is in agreement with previous statistics reported from studies that did not consider clear-sky classification (Nieminen et al., 2014).

#### 3.2.1 Backward air mass trajectories during clear-sky NPF events and nonevents

Since NPF is most frequent in spring, we dedicated our focus to this season (Fig. 3a). The springtime medians and percentiles of air mass trajectories arriving at Hyytiälä during clear-sky NPF events and nonevents were calculated 96 h backward in time at the 100, 250 and 500 m arrival heights for the years 1996–2015. The medians and similarly the percentiles were calculated by taking the median compass direction at every point on the trajectory (1 h between every two points), arriving every half an hour at Hyytiälä. The trajectories arriving at Hyytiälä at these three heights were quite similar, and those arriving at the 500 m height are shown in Fig. 4. Medians and percentiles of the routes were calculated by taking the median of the trajectories at every half hour for springtime NPF event days and nonevent days separately. During the NPF event days, the measured air masses were found to originate mainly from the north and passed over Scandinavia before arriving at Hyytiälä. Similarly to previously reported results, air masses arriving from the north and

**Table 1.** Correlation coefficients between different meteorological parameters, gas concentrations and condensation sink (CS) during clear-sky events and nonevents during spring (March–May, 1996–2015) and time window 09:00–12:00. High positive and negative correlations are marked in bold.

| | CS | $T$ | RH | CO | $NO_x$ | $SO_2$ | $O_3$ |
|---|---|---|---|---|---|---|---|
| Events | | | | | | | |
| CS | 1 | | | | | | |
| $T$ | 0.28 | 1 | | | | | |
| RH | −0.06 | −0.64 | 1 | | | | |
| CO | 0.33 | −0.37 | 0.26 | 1 | | | |
| $NO_x$ | 0.53 | −0.19 | 0.21 | 0.47 | 1 | | |
| $SO_2$ | 0.4 | −0.29 | 0.14 | 0.36 | 0.58 | 1 | |
| $O_3$ | 0.23 | 0.52 | −0.51 | −0.06 | −0.08 | −0.08 | 1 |
| Nonevents | | | | | | | |
| CS | 1 | | | | | | |
| $T$ | 0.15 | 1 | | | | | |
| RH | −0.12 | **−0.81** | 1 | | | | |
| CO | 0.53 | **−0.68** | 0.5 | 1 | | | |
| $NO_x$ | 0.34 | −0.51 | 0.45 | **0.7** | 1 | | |
| $SO_2$ | 0.23 | −0.55 | 0.42 | 0.56 | 0.41 | 1 | |
| $O_3$ | 0.43 | 0.62 | −0.64 | −4E-04 | −0.07 | −0.13 | 1 |

north-west directions result in clean air with low pollutant (particulate matter and trace gas) concentrations (Nieminen et al., 2015). During NPF the nonevent days, air masses originated from more polluted areas in Europe and Russia, resulting in elevated levels of condensation sink and other air pollutants in Hyytiälä, as also seen in previous studies (Sogacheva et al., 2005).

### 3.3 Influences of CS, meteorological parameters and trace gases

In Fig. 5a we present the monthly variation of condensation sink during NPF events and nonevents under daytime clear-sky conditions. NPF events tended to be favored by low values of CS throughout the year. In all months except during summer, the 75th percentile of the event day values of CS was lower than the 25th percentile of the nonevent day values of CS. On the NPF event days, CS had its maximum in summer, which might be one of the main reasons for the local minimum in the NPF event frequency during the summer months (Fig. 3a). However, the monthly cycle of CS during nonevent days had two maxima, one in spring and another one in autumn, which might suggest that during these seasons, high values of CS prevented NPF occurring on particular days. The difference in the value of CS between the NPF event and nonevent days was the highest in March and the lowest during the summer months.

Figure 5b shows the monthly temperature conditions ($T$) during the daytime NPF events and nonevents. While higher temperatures favored NPF during months when the average temperature was below 273.15 K (0 °C; months 1, 2, 3, 11 and 12), the opposite was true at average temperatures above 273.15 K (0 °C). From our data set, clear-sky events occurred within temperatures ranging between 252 K (−21 °C) and 300 K (25 °C). Days with higher or lower temperatures than the range mentioned above are found to be nonevents. Accordingly, both very high and very low temperatures were not favorable conditions for NPF. Although an increase in the ambient temperature results in higher concentrations of monoterpenes due to increased emissions, thereby favoring new particle formation and growth (Kulmala et al., 2004a), Fig. 5b shows that very high temperatures tend to suppress NPF. This latter feature is at least partly related to the positive relation between the ambient temperature and pre-existing aerosol loading (and hence CS) in Hyytiälä (Liao et al., 2014), even though it might also be attributed to the increase in vapor evaporation coefficients, which results in less stable clusters at high temperatures (Paasonen et al., 2012).

As with an earlier study (Hamed et al., 2011), our results indicate that NPF is favored by low values of ambient relative humidity in Hyytiälä (Fig. 5c). This observation does not conflict with chamber experiments (e.g., Duplissy et al., 2016) or theory (Merikanto et al., 2016; Vehkamäki et al., 2002), which suggest higher nucleation rates at higher values of RH, because binary $H_2SO_4$–water nucleation is not expected take place in Hyytiälä. Other studies have proposed that increased RH limits some VOC (Volatile Organic Compounds) ozonolysis reactions, preventing the formation of come condensable vapors necessary for nucleation (Boy and Kulmala, 2002). This might partially explain the observed anti-correlation between RH and particle formation rates. Therefore, it seems plausible that RH affects NPF via atmospheric chemistry rather than by changing the sink term for condensing vapors and small clusters. Additionally, we found clear differences in how trace gas concentrations were associated with RH between the NPF event and nonevent days (Table 1). For instance, $O_3$ showed a strong negative correlation with RH during events and nonevents. However, during nonevent days, a positive correlation appears between RH and each of CO, $SO_2$ and $NO_x$ while the correlation between them seems to be absent during event days. Our results show that air masses coming from central Europe and passing over the Baltic Sea tend to have higher values of RH.

After looking at the characteristics of clear-sky NPF event and nonevent days in terms of meteorological parameters and CS, we looked at the variation of trace gas (CO, $SO_2$, $NO_x$ and $O_3$) concentrations during these conditions (Fig. 6). Out of these gases, at least $SO_2$ and $O_3$ are expected to enhance NPF, $SO_2$ as a precursor for sulfuric acid and $O_3$ as an oxidant forming ELVOCs (extremely low volatile organic compounds; Donahue et al., 2012; Ehn et al., 2014). However, none of these vapors seemed to have higher concentrations during NPF event days. This suggests that, as tracers of pollution, these gases are strongly linked with high anthropogenic CS, so air masses with high trace gas concentrations often do not result in NPF in Hyytiälä.

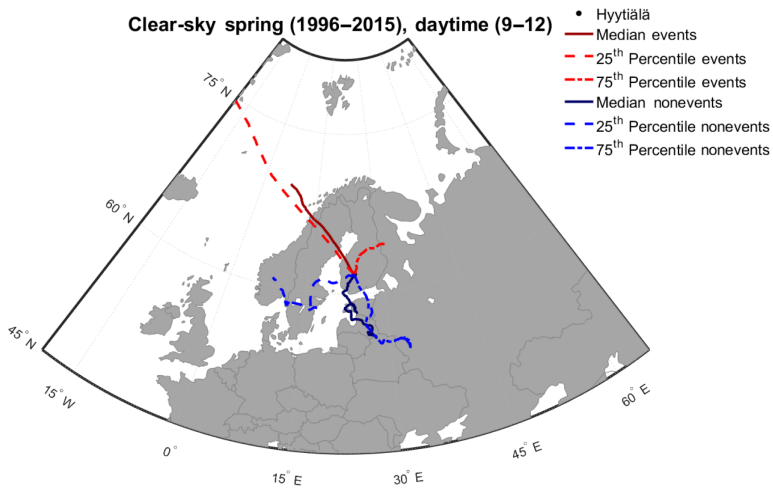


**Figure 4.** Median and percentiles of 96 h backward air mass trajectories arriving at Hyytiälä during springtime (09:00–12:00).

### 3.4 Connection of nucleating precursor vapors with new particle formation rate

#### 3.4.1 Precursor vapor proxies

In this study, we determined $J_{1.5,C}$ using the proxies for both SA and OxOrg. The monthly variations of these precursors (in the time window 09:00–12:00) are shown in Fig. 7. During clear-sky conditions, the SA proxy tended to have the highest median daytime values during the winter months with a maximum in February (Fig. 7a). Contrary to this, the seasonal distribution of the SA proxy reported in Hyytiälä appears as double peaks with an absolute maximum in spring and a smaller one in autumn when presenting the data, without excluding cloudy days (Nieminen et al., 2014). During winter, both condensation sink and boundary layer height are lower than in the summer (Paasonen et al., 2013), which might explain the higher concentrations of SA during the winter months.

Being a function of temperature, the OxOrg proxy concentration was generally found to follow the monthly cycle of the ambient temperature. The median value of [OxOrg] was higher on NPF events days in every month compared with nonevent days (Fig. 7b). The largest difference in [OxOrg] between the NPF events and nonevents, in terms of its median value, was recorded for January and the least difference was recorded for May. It is to be noted that the proxy values represent the measured values less accurately during winter than during the other periods (Kontkanen et al., 2016b).

#### 3.4.2 Particle formation rates

The calculated new particle formation rate, $J_{1.5,C}$, approximated with Eq. (5) shows a similar behavior to the [OxOrg] (see Figs. 7 and 8), being higher for the clear-sky NPF event days in comparison with nonevent days. Also, the difference in the value of $J_{1.5,C}$ between the NPF events and nonevents was highest in the winter and lowest in summer. The monthly cycle of $J_{1.5,C}$ closely followed that of [OxOrg], as the latter had a higher seasonal variability than the sulfuric acid proxy concentration, thereby being capable of affecting the seasonal pattern of $J_{1.5,C}$ (Fig. 8a). The diurnal cycle of $J_{1.5,C}$ during the NPF event days showed an increase along with sunrise, a peak at midday and decrease along with sunset. However, for nonevent days the $J_{1.5,C}$ value was relatively constant throughout the day and had clearly lower values than during the NPF event days (Fig. 8b).

Since previous studies have shown that there is a clear difference in observed $J_3$ between the event and nonevent days and much less difference in observed $J_{1.5}$ (Kulmala et al., 2013), we decided to focus on $J_3$ in our event to nonevent discrimination. Previous studies which did not consider clear-sky conditions have reported values of observed springtime $J_3$ between 0.01 and 5 $\mathrm{cm^{-3}\,s^{-1}}$ (median = 0.94 $\mathrm{cm^{-3}\,s^{-1}}$) during the period of active NPF (Kulmala et al., 2013). Our values of $J_{3,C}$ fit between the extremes of these values for the springtime and time window 09:00 to 12:00, with a slightly higher median value of 1.9 $\mathrm{cm^{-3}\,s^{-1}}$ (Figs. 9a, b). The formation rate of 3 nm particles is not only affected by the new particle formation rate ($J_{1.5}$) but also by the scavenging of newly formed particles by coagulation into pre-existing particles. We found that, in general, the values of $J_{3,C}$ calculated using Eqs. (4) and (5) were higher on NPF event days compared with nonevent days in all months (Fig. 9a). The difference between the event and nonevent days was the largest in winter and decreased towards summer. However, the diurnal cycles of percentiles and medians of $J_{3,C}$ during each month

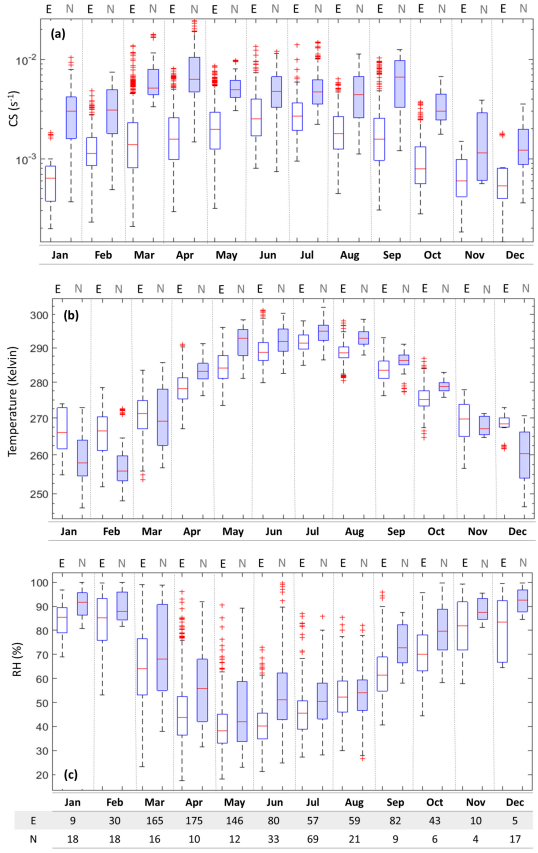


**Figure 5.** Median and percentiles of monthly variation (09:00–12:00) at $P > 0.7$ of **(a)** CS, **(b)** temperature and **(c)** RH during NPF events (E, white) and nonevents (N, shaded). See Fig. 1 for explanation of symbols.

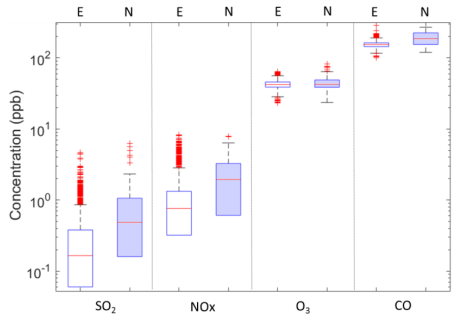


**Figure 6.** Springtime (months 3, 4, 5) medians and percentiles of trace gases during clear-sky events (E, white) and nonevents (n, shaded) during daytime (09:00–12:00). See Fig. 1 for explanation of symbols.

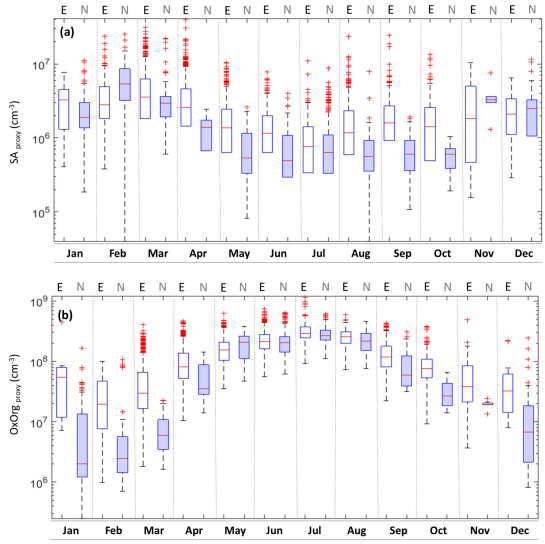


**Figure 7.** Monthly variation of medians and percentiles of **(a)** SA proxy and **(b)** OxOrg proxy at $P > 0.7$ during the time window 09:00–12:00 of NPF events (E, white) and nonevents (N, shaded). See Fig. 1 for explanation of symbols.

peaked around noon for both NPF events and nonevents. One example is presented in Fig. 9b, showing that $J_{3,C}$ tended to increase after sunrise, peak at about midday and diminish after sunset. This kind of diurnal cycle was similar for all months. Hourly values of $J_{3,C}$ calculated during the NPF event days were higher than those during the nonevent days. During the spring months, the difference in the median $J_{3,C}$ between the NPF events and nonevents, calculated for every half an hour, appeared to increase at about 10:00 and then started to decrease again at about 13:00 (Fig. 9b). On NPF event days, in comparison to springtime $J_{1.5,C}$ which peaked at around 10:45 (Fig. 8b), $J_{3,C}$ peaked typically about half an hour later. This time delay indicates how long it takes for the particles to grow from 1.5 to 3 nm. This growth is a critical step of NPF (Kulmala et al., 2013) and it depends on concentrations of available vapor precursors.

In Fig. 10 we present the median diurnal cycles of $J_{3,C}$ and CS during classified clear-sky NPF events and nonevents. The diurnal cycle was calculated by taking the median CS at every half hour throughout the season. On the NPF event days, the CS had higher values during the nighttime and lower values during daytime with a minimum at noon. It is important to remember that $J$ was calculated only for daytime when the SA proxy was available (UV-B radiation is needed for the proxy). On nonevent days, the values of CS showed no clear diurnal pattern, had practically

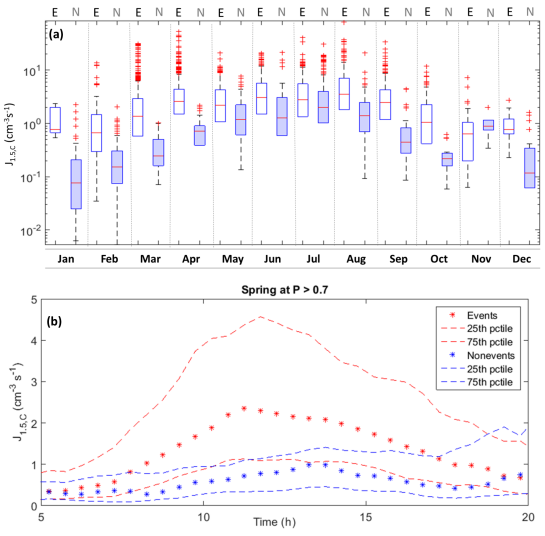


**Figure 8.** **(a)** Monthly variation of medians and percentiles of $J_{1.5,C}$ during the time window 09:00–12:00 of NPF events (E, white) and nonevents (N, shaded). See Fig. 1 for explanation of symbols. **(b)** The diurnal cycle of $J_{1.5,C}$ during spring. Nighttime is missing in this plot due to unavailable SA proxy which uses UVB to be calculated.

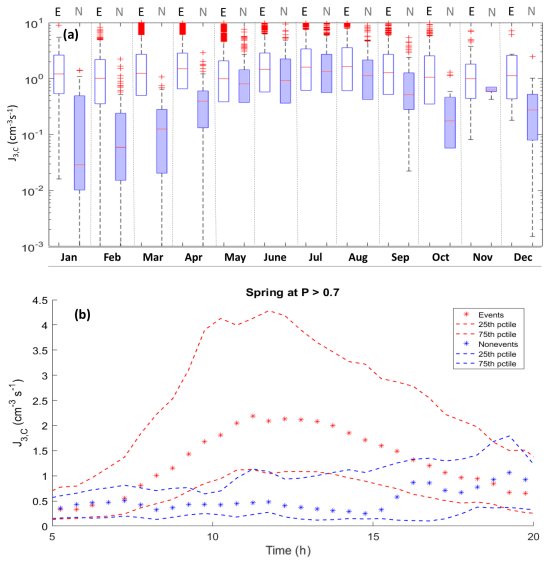


**Figure 9.** **(a)** Monthly variation of medians and percentiles of $J_{3,C}$ during the time window 09:00–12:00 of NPF events (E, white) and nonevents (N, shaded). See Fig. 1 for explanation of symbols. **(b)** The diurnal cycle of $J_{3,C}$ during spring. The nighttime is missing in this plot due to unavailable SA proxy which uses UVB to be calculated.

no difference between the daytime and nighttime hours and were roughly twice those recorded during the clear-sky NPF event days. The difference in CS between NPF events and nonevents follows from the distinctly different air masses arriving at Hyytiälä. For instance, it has been shown that air masses originating from the north and passing over Scandinavia have, on average, lower values of CS than the air masses passing over Russia and central Europe (Sogacheva et al., 2005; Nieminen et al., 2015).

On NPF event days, the median-approximated formation rate of 3 nm particles had its maximum value at about midday and was significantly higher than on nonevents days (Figs. 9b and 10). A clear negative relation could be seen between the median seasonal diurnal cycles of CS and $J_{3,C}$ on NPF event days (especially during spring daytime; Fig. 10). This kind of relation was not observed during nonevent days when these two quantities seemed to be independent of each other (Fig. 10). In summer, the median value of $J_{3,C}$ was roughly similar between NPF events and nonevents, whereas the median value of CS was almost 10 times higher during the nonevent days compared with event days. The high values of $J_{3,C}$ for the nonevent days in summer, despite the high CS values, seem to suggest that some other factor limits the actual NPF rate. One possibility is that freshly formed clusters are rapidly evaporated due to higher ambient temperatures (see Fig. 5b). This will be discussed in a more detail in the following section. Higher values of CS on nonevent days are expected, bearing in mind that these particles act as surfaces for scavenging precursor gases and freshly formed particles (Hussein et al., 2008). The association of a high CS with the lower NPF probability has been observed in many studies conducted in Hyytiälä (Boy and Kulmala, 2002; Hyvönen et al., 2005; Baranizadeh et al., 2014), as well as in other rural and urban areas, including Egbert and Toronto in Canada (Jun et al., 2014), Preila in Lithuania (Mordas et al., 2016), Po Valley in Italy (Hamed et al., 2007) and Budapest and K-puszta in Hungary (Salma et al., 2016).

### 3.4.3 Threshold separating the NPF events and nonevents

Since quite a visible separation could be observed in the calculated values of $J_{3,C}$ between the springtime clear-sky NPF events and nonevents, and since $J_{3,C}$ had its maximum at around midday, the plot of CS versus temperature at midday (11:00–12:00) in spring provides an equation that effectively separates the NPF events from nonevents during this season (Fig. 11). This equation was determined using a linear discriminant analysis (LDA) similar to Hyvönen et al. (2005). The equation provides a line that separates NPF events from nonevents at 95 % confidence towards nonevents. Based on their midday CS and temperature, the data point follows ei-

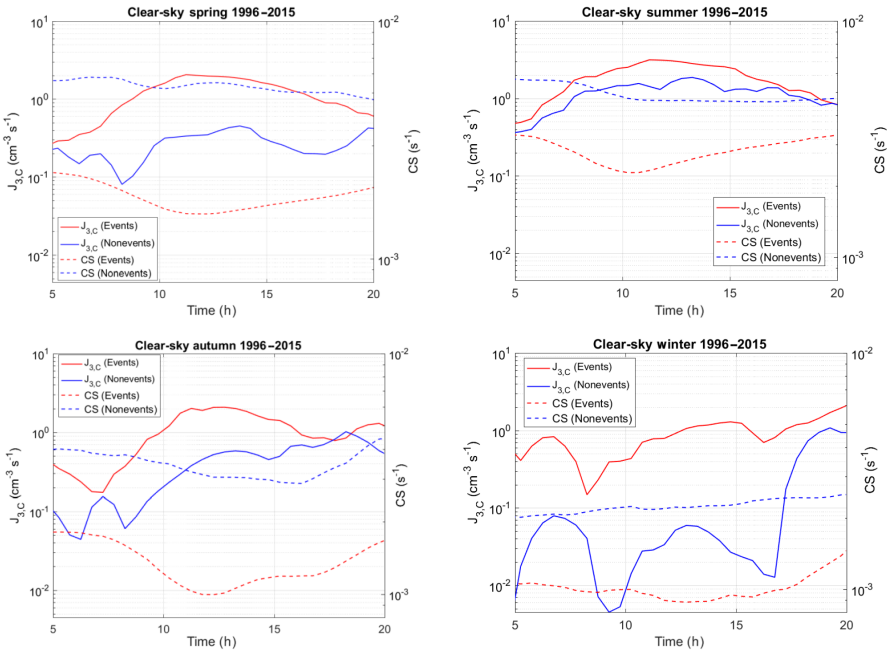


**Figure 10.** Diurnal cycle of median values of calculated formation rate of 3 nm particles ($J_{3,C}$) and condensation sink (CS) during different seasons for clear-sky events and nonevents.

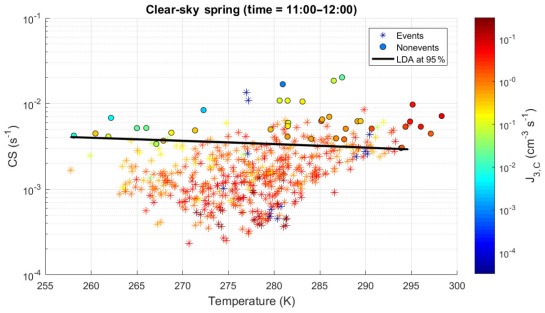


**Figure 11.** Relationship between temperature and CS during springtime (11:00–12:00) NPF clear-sky ($P > 0.7$) event days and nonevent days color-coded with $J_{3,C}$. Horizontal line is calculated from LDA at 95 % confidence relative to nonevents and is demonstrated by Eq. (6).

ther classes. More specifically, the days with

$$\mathrm{CS(s^{-1})} > -3.091 \times 10^{-5} \times T\,\mathrm{(in\ Kelvin)} + 0.0120 \qquad (6)$$

lie above the threshold line. Almost no nonevent days fall below this line (< 5 %). The points above the line were also characterized with higher trace gas concentrations and lower calculated formation rates of 3 nm particles than the rest of the points.

The separation between the clear-sky NPF events and nonevents in the CS versus $T$ plot was less evident in autumn and disappeared completely in the summer and winter (Fig. 12). Interestingly, a large number of NPF event days during these seasons still fell below the threshold line given by Eq. (6). Furthermore, we analyzed the effect of RH in separating the events from nonevents, similarly to the study done on RH by Hyvönen et al. (2005). We found that compared with CS versus temperature data, depicting CS versus RH (data not presented) did not work better for separating NPF events from nonevents during clear-sky conditions.

### 3.4.4 Probability of NPF events and nonevents

Since the biggest difference in the calculated 3 nm particle formation rates between the NPF events and nonevents was observed around noon (Fig. 9b), and since CS and temperature showed promising threshold values for predicting the occurrence of NPF nonevents during spring (up to 95 %) (Fig. 11), Fig. 13 presents the probability of having a NPF event in Hyytiälä at a specific CS and temperature within the time window 11:00–12:00. The probability was calculated by taking the fraction of events to the total events and nonevents in every cell which is 2.5 K on the $x$ axis and a

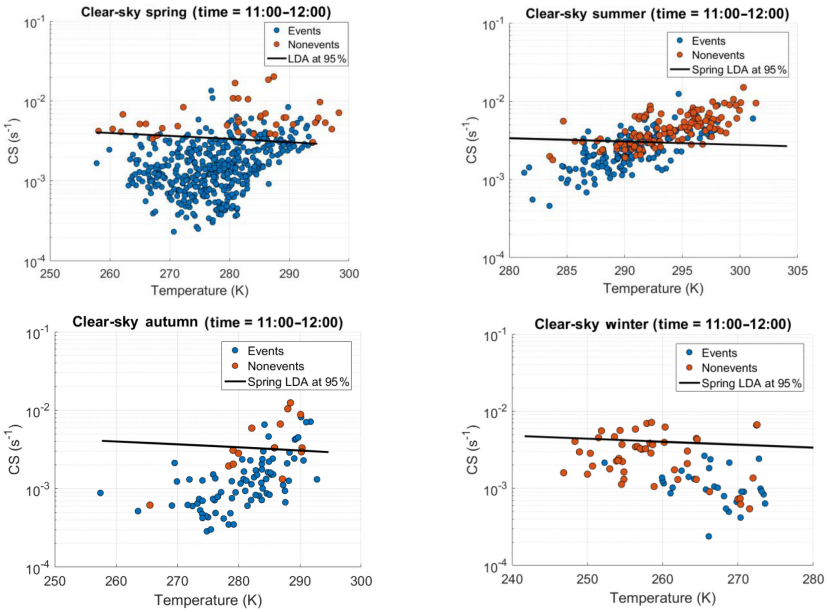


**Figure 12.** Relationship between CS and temperature (time window: 11:00–12:00) NPF clear-sky event days and nonevent days. Horizontal line is calculated from spring LDA at 95 % confidence relative to nonevents and is demonstrated by Eq. (6).

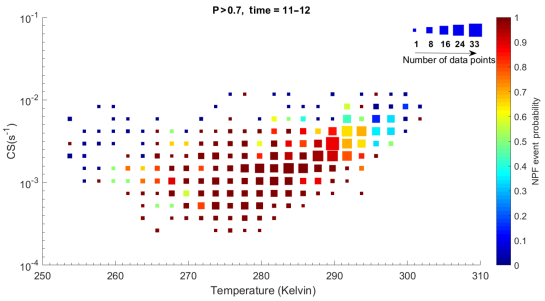


**Figure 13.** NPF probability distribution based on the CS and temperature conditions during clear-sky days (11:00–12:00). Marker size indicates number of days included in the probability calculation within every cell.

ratio of 1.14 on the $y$ axis between every two consecutive CS values. The highest probability of having a NPF event corresponded to conditions with moderate temperatures and low values of CS. At high values of CS, there was a zero probability for NPF regardless of the temperature. However, at moderate and low values of CS, the probability of having a NPF event decreases at lower temperatures. This could be explained by lower emissions of VOCs and thus lower OxOrg concentrations at lower temperatures. Similarly, the probability of NPF decreases at higher temperatures at constant values of CS. This latter feature might be attributed to conditions that are unfavorable for clustering due to high temperatures. Although previous studies have developed criteria for NPF probability which could work in diverse environments (Kuang et al., 2010), they did not explore the dependency of their parameter on atmospheric conditions.

## 4 Conclusions

In this study we combined 20 years of data collected at the SMEAR II station in order to characterize the conditions affecting the frequency of NPF events in that location. By focusing only on clear-sky conditions, we were able to get a new insight into differences between the NPF events and nonevents. In clear-sky conditions, the meteorological conditions, trace gas concentrations and other studied variables on NPF event days appeared to be similar to those presented in the previous studies which did not consider clear-sky classification. Furthermore, the monthly data refined the analysis so that the differences caused by different quantities became more visible compared the previous studies conducted for this site. Our work confirms the conclusions of Baranizadeh et al. (2014) with a complementary data set: NPF events and nonevents are typically associated with clear-sky and cloudy conditions, respectively.

Our results showed that using SA and OxOrg proxies to calculate the apparent formation rates of 1.5 and 3 nm par-

ticles works well in differentiating the clear-sky NPF events from nonevents. Moreover, during clear-sky conditions the effect of CS on attenuating or even preventing NPF was quite visible: CS was, on average, two times higher on the nonevent days compared with the NPF event days. Similarly, many other meteorological variables affected NPF. By using CS and ambient temperature, we were able to find a threshold above which no clear-sky NPF events occurred. This threshold is described with an equation that is able to separate 97.4 % of the NPF events from nonevents during springtime. In clear sky conditions, when there is plenty of radiation available, NPF events take place as long as the CS is low enough and temperature is moderate. Although a weaker separation was observed in the other seasons, considering only clear-sky conditions enabled us to form a map of the probability of having a NPF event within specific CS and temperature conditions. Using clear-sky conditions appears to bring us one step forward towards understanding NPF and predicting their occurrences in Hyytiälä. Our study serves as a basis of future detailed comparisons with observations to formulate even more robust conclusions.

*Data availability.* Data measured at the SMEAR II station are available on the following website: http://avaa.tdata.fi/web/smart/. The data are licensed under a Creative Commons 4.0 Attribution (CC BY) license. Backward air-mass trajectories are freely access from the transport model which is developed and provided by NOAA (National Oceanic and Atmospheric Administration) at (http://www.ready.noaa.gov/HYSPLIT.php). Input meteorological data required for 200 the model were collected from GDAS (Global Data Assimilation System) archives.

*Competing interests.* The authors declare that they have no conflict of interest.

*Acknowledgements.* This work was supported by the Academy of Finland Centre of Excellence program (grant no. 272041) and Nordic Top-level Research Initiative (TRI) Cryosphere-Atmosphere Interactions in a Changing Arctic Climate (CRAICC). Lubna Dada acknowledges the doctoral programme in Atmospheric Sciences (ATM-DP, University of Helsinki) for financial support. We also thank Ksenia Tabakova for providing air mass trajectory data.

Edited by: D. Spracklen
Reviewed by: two anonymous referees

## References

Aalto, P., Hämeri, K., Becker, E., Weber, R., Salm, J., Mäkelä, J. M., Hoell, C., O'dowd, C. D., Hansson, H.-C., Väkevä, M., Koponen, I. K., Buzorius, G., and Kulmala, M.: Physical characterization of aerosol particles during nucleation events, Tellus B, 53, 344–358 doi:10.1034/j.1600-0889.2001.530403.x, 2001.

Ahlm, L., Liu, S., Day, D. A., Russell, L. M., Weber, R., Gentner, D. R., Goldstein, A. H., DiGangi, J. P., Henry, S. B., Keutsch, F. N., VandenBoer, T. C., Markovic, M. Z., Murphy, J. G., Ren, X., and Scott, S.: Formation and growth of ultrafine particles from secondary sources in Bakersfield, California, J. Geophys. Res.-Atmos., 117, D00V08, doi:10.1029/2011JD017144, 2012.

Apte, J. S., Marshall, J. D., Cohen, A. J., and Brauer, M.: Addressing global mortality from ambient PM2. 5, Environ. Sci. Technol., 49, 8057–8066, doi:10.1021/acs.est.5b01236, 2015.

Asmi, A., Wiedensohler, A., Laj, P., Fjaeraa, A.-M., Sellegri, K., Birmili, W., Weingartner, E., Baltensperger, U., Zdimal, V., and Zikova, N.: Number size distributions and seasonality of submicron particles in Europe 2008–2009, Atmos. Chem. Phys., 11, 5505–5538, doi:10.5194/acp-11-5505-2011, 2011.

Baranizadeh, E., Arola, A., Hamed, A., Nieminen, T., Mikkonen, S., Virtanen, A., Kulmala, M., Lehtinen, K., and Laaksonen, A.: The effect of cloudiness on new-particle formation: investigation of radiation levels, Boreal Environ. Res., 19, 343–354, 2014.

Bianchi, F., Tröstl, J., Junninen, H., Frege, C., Henne, S., Hoyle, C., Molteni, U., Herrmann, E., Adamov, A., Bukowiecki, N., Chen, X., Duplissy, J., Gysel, M., Hutterli, M., Kangasluoma, J., Kontkanen, J., Kürten, A., Manninen, H. E., Münch, S., Peräkylä, O., Petäjä, T., Rondo, L., Williamson, C., Weingartner, E., Curtius, J., Worsnop, D. R., Kulmala, M., Dommen, J., and Baltensperger, U.: New particle formation in the free troposphere: A question of chemistry and timing, Science, 352, 1109–1112, doi:10.1126/science.aad5456, 2016.

Boulon, J., Sellegri, K., Venzac, H., Picard, D., Weingartner, E., Wehrle, G., Collaud Coen, M., Bütikofer, R., Flückiger, E., and Baltensperger, U.: New particle formation and ultrafine charged aerosol climatology at a high altitude site in the Alps (Jungfraujoch, 3580 m asl, Switzerland), Atmos. Chem. Phys., 10, 9333–9349, doi:10.5194/acp-10-9333-2010, 2010.

Boy, M. and Kulmala, M.: Nucleation events in the continental boundary layer: Influence of physical and meteorological parameters, Atmos. Chem. Phys., 2, 1–16, doi:10.5194/acp-2-1-2002, 2002.

Buenrostro Mazon, S., Riipinen, I., Schultz, D., Valtanen, M., Maso, M. D., Sogacheva, L., Junninen, H., Nieminen, T., Kerminen, V.-M., and Kulmala, M.: Classifying previously undefined days from eleven years of aerosol-particle-size distribution data from the SMEAR II station, Hyytiälä, Finland, Atmos. Chem. Phys., 9, 667–676, doi:10.5194/acp-9-667-2009, 2009.

Buenrostro Mazon, S., Kontkanen, J., Manninen, H. E., Nieminen, T., Kerminen, V.-M., and Kulmala, M.: A long-term comparison of nighttime cluster events and daytime ion formation in a boreal forest, Boreal Environ. Res., 21, 242–261, 2016.

Bzdek, B. R., Lawler, M. J., Horan, A. J., Pennington, M. R., DePalma, J. W., Zhao, J., Smith, J. N., and Johnston, M. V.: Molecular constraints on particle growth during new particle formation, Geophys. Res. Lett., 41, 6045–6054, doi:10.1021/ac100856j, 2014.

Dada, L., Chellapermal, R., Buenrostro Mazon, S., Junninen, H., Kerminen, V. M., Paasonen, P., and Kulmala, M.: Method for identifying NPF event start and end times as well as NPF types (ion-initiated, particle initiated, transported) using characteris-

tic nucleation-mode particles and air ions, Atmos. Chem. Phys. Dissc., in preparation, 2017.

Dal Maso, M., Kulmala, M., Riipinen, I., Wagner, R., Hussein, T., Aalto, P. P., and Lehtinen, K. E.: Formation and growth of fresh atmospheric aerosols: eight years of aerosol size distribution data from SMEAR II, Hyytiala, Finland, Boreal Environ. Res., 10, 323–336, 2005.

Donahue, N. M., Kroll, J., Pandis, S. N., and Robinson, A. L.: A two-dimensional volatility basis set – Part 2: Diagnostics of organic-aerosol evolution, Atmos. Chem. Phys., 12, 615–634, doi:10.5194/acp-12-615-2012, 2012.

Duplissy, J., Merikanto, J., Franchin, A., Tsagkogeorgas, G., Kangasluoma, J., Wimmer, D., Vuollekoski, H., Schobesberger, S., Lehtipalo, K., Flagan, R. C., Brus, D., Donahue, N. M., Vehkamäki, H., Almeida, J., Amorim, A., Barmet, P., Bianchi, F., Breitenlechner, M., Dunne, E. M., Guida, R., Henschel, H., Junninen, H., Kirkby, J., Kürten, A., Kupc, A., Määttänen, A., Makhmutov, V., Mathot, S., Nieminen, T., Onnela, A., Praplan, A. P., Riccobono, F., Rondo, L., Steiner, G., Tome, A., Walther, H., Baltensperger, U., Carslaw, K. S., Dommen, J., Hansel, A., Petäjä, T., Sipilä, M., Stratmann, F., Vrtala, A., Wagner, P. E., Worsnop, D. R.,, Curtius, and Kulmala, M.: Effect of ions on sulfuric acid-water binary particle formation: 2. Experimental data and comparison, J. Geophys. Res.-Atmos., 121, 1752–1775, doi:10.1002/2015JD023539, 2016.

Ehn, M., Thornton, J. A., Kleist, E., Sipilä, M., Junninen, H., Pullinen, I., Springer, M., Rubach, F., Tillmann, R., Lee, B., Lopez-Hilfiker, F., Andres, S., Acir, I.-H., Rissanen, M., Jokinen, T., Schobesberger, S., Kangasluoma, J., Kontkanen, J., Nieminen, T., Kurtén, T., Nielsen, L. B., Jørgensen, S., Kjaergaard, H. G., Canagaratna, M., Maso, M. D., Berndt, T., Petäjä, T., Wahner, A., Kerminen, V.-M., Kulmala, M., Worsnop, D. R., Wildt, J., and Mentel, T. F.: A large source of low-volatility secondary organic aerosol, Nature, 506, 476–479, doi:10.1038/nature13032, 2014.

Hallquist, M., Wenger, J., Baltensperger, U., Rudich, Y., Simpson, D., Claeys, M., Dommen, J., Donahue, N., George, C., and Goldstein, A.: The formation, properties and impact of secondary organic aerosol: current and emerging issues, Atmos. Chem. Phys., 9, 5155–5236, doi:10.5194/acp-9-5155-2009, 2009.

Hamed, A., Joutsensaari, J., Mikkonen, S., Sogacheva, L., Maso, M. D., Kulmala, M., Cavalli, F., Fuzzi, S., Facchini, M., and Decesari, S.: Nucleation and growth of new particles in Po Valley, Italy, Atmos. Chem. Phys., 7, 355–376, doi:10.5194/acp-7-355-2007, 2007.

Hamed, A., Korhonen, H., Sihto, S. L., Joutsensaari, J., Järvinen, H., Petäjä, T., Arnold, F., Nieminen, T., Kulmala, M., and Smith, J. N.: The role of relative humidity in continental new particle formation, J. Geophys. Res.-Atmos., 116, D3, 2011.

Hari, P. and Kulmala, M.: Station for measuring ecosystem-atmosphere relations, Boreal Environ. Res., 10, 315–322, 2005.

Hussein, T., Martikainen, J., Junninen, H., Sogacheva, L., Wagner, R., Dal Maso, M., Riipinen, I., Aalto, P. P., and Kulmala, M.: Observation of regional new particle formation in the urban atmosphere, Tellus B, 60, 509–521, doi:10.1111/j.1600-0889.2008.00365.x, 2008.

Hyvönen, S., Junninen, H., Laakso, L., Maso, M. D., Grönholm, T., Bonn, B., Keronen, P., Aalto, P., Hiltunen, V., Pohja, T., Launiainen, S., Hari, P., Mannila, H., and Kulmala, M.: A look at aerosol formation using data mining techniques, Atmos. Chem. Phys., 5, 3345–3356, doi:10.5194/acp-5-3345-2005, 2005.

Jun, Y.-S., Jeong, C.-H., Sabaliauskas, K., Leaitch, W. R., and Evans, G. J.: A year-long comparison of particle formation events at paired urban and rural locations, Atmos. Pollut. Res., 5, 447–454, doi:10.5094/APR.2014.052, 2014.

Junninen, H., Hulkkonen, M., Riipinen, I., Nieminen, T., Hirsikko, A., Suni, T., Boy, M., LEE, S. H., Vana, M., Tammet, H., KERMINEN, V.-M., and KULMALA, M.: Observations on nocturnal growth of atmospheric clusters, Tellus B, 60, 365–371, doi:10.1111/j.1600-0889.2008.00356.x, 2008.

Kannosto, J., Virtanen, A., Lemmetty, M., Mäkelä, J. M., Keskinen, J., Junninen, H., Hussein, T., Aalto, P., and Kulmala, M.: Mode resolved density of atmospheric aerosol particles, Atmos. Chem. Phys., 8, 5327–5337, doi:10.5194/acp-8-5327-2008, 2008.

Kerminen, V.-M. and Kulmala, M.: Analytical formulae connecting the "real" and the "apparent" nucleation rate and the nuclei number concentration for atmospheric nucleation events, J. Aerosol Sci., 33, 609–622, doi:10.1016/S0021-8502(01)00194-X, 2002.

Kerminen, V.-M., Petäjä, T., Manninen, H., Paasonen, P., Nieminen, T., Sipilä, M., Junninen, H., Ehn, M., Gagné, S., Laakso, L., Riipinen, I., Vehkamäki, H., Kurten, T., Ortega, I. K., Maso, M. D., Brus, D., Hyvärinen, A., Lihavainen, H., Leppä, J., Lehtinen, K. E. J., Mirme, A., Mirme, S., Hõrrak, U., Berndt, T., Stratmann, F., Birmili, W., Wiedensohler, A., Metzger, A., Dommen, J., Baltensperger, U., Kiendler-Scharr, A., Mentel, T. F., Wildt, J., Winkler, P. M., Wagner, P. E., Petzold, A., Minikin, A., Plass-Dülmer, C., Pöschl, U., Laaksonen, A., and Kulmala, M.: Atmospheric nucleation: highlights of the EUCAARI project and future directions, Atmos. Chem. Phys., 10, 10829–10848, doi:10.5194/acp-10-10829-2010, 2010.

Kerminen, V.-M., Paramonov, M., Anttila, T., Riipinen, I., Fountoukis, C., Korhonen, H., Asmi, E., Laakso, L., Lihavainen, H., Swietlicki, E., Svenningsson, B., Asmi, A., Pandis, S. N., Kulmala, M., and Petäjä, T.: Cloud condensation nuclei production associated with atmospheric nucleation: a synthesis based on existing literature and new results, Atmos. Chem. Phys., 12, 12037–12059, doi:10.5194/acp-12-12037-2012, 2012.

Kirkby, J., Curtius, J., Almeida, J., Dunne, E., Duplissy, J., Ehrhart, S., Franchin, A., Gagné, S., Ickes, L., Kürten, A., Kupc, A., Metzger, A., Riccobono, F., Rondo, L., Schobesberger, S., Georgios Tsagkogeorgas, Daniela Wimmer, Antonio Amorim, Bianchi, F., Martin Breitenlechner, André David, Josef Dommen, Downard, A., Ehn, M., Flagan, R. C., Haider, S., Hansel, A., Hauser, D., Jud, W., Junninen, H., Kreissl, F., Kvashin, A., Laaksonen, A., Lehtipalo, K., Lima, J., Lovejoy, E. R., Makhmutov, V., Mathot, S., Mikkilä, J., Minginette, P., Sandra Mogo, Nieminen, T., Onnela, A., Pereira, P., Petäjä, T., Schnitzhofer, R., Seinfeld, J. H., Sipilä, M., Stozhkov, Y., Stratmann, F., Tomé, A., Vanhanen, J., Viisanen, Y., Vrtala, A., Wagner, P. E., Walther, H., Weingartner, E., Wex, H., Winkler, P. M., Carslaw, K. S., Worsnop, D. R., Baltensperger, U., and Kulmala, M.: Role of sulphuric acid, ammonia and galactic cosmic rays in atmospheric aerosol nucleation, Nature, 476, 429–433, doi:10.1038/nature10343, 2011.

Kontkanen, J., Järvinen, E., Manninen, H. E., Lehtipalo, K., Kangasluoma, J., Decesari, S., Gobbi, G. P., Laaksonen, A., Petäjä, T., and Kulmala, M.: High concentrations of sub-3 nm clusters and frequent new particle formation observed in the Po Val-

ley, Italy, during the PEGASOS 2012 campaign, Atmos. Chem. Phys., 16, 1919–1935, doi:10.5194/acp-16-1919-2016, 2016a.

Kontkanen, J., Paasonen, P., Aalto, J., Bäck, J., Rantala, P., Petäjä, T., and Kulmala, M.: Simple proxies for estimating the concentrations of monoterpenes and their oxidation products at a boreal forest site, Atmos. Chem. Phys., 16, 13291–13307, doi:10.5194/acp-16-13291-2016, 2016b.

Kontkanen, J., Lehtipalo, K., Ahonen, L., Kangasluoma, J., Manninen, H. E., Hakala, J., Rose, C., Sellegri, K., Xiao, S., Wang, L., Qi, X., Nie, W., Ding, A., Yu, H., Lee, S., Kerminen, V. M., Petäjä, T., and Kulmala, M.: Measurements of sub-3 nm particles using a particle size magnifier in different environments: from clean mountain top to polluted megacities, Atmos. Chem. Phys., 17, 2163–2187, doi:10.5194/acp-17-2163-2017, 2017.

Kuang, C., Riipinen, I., Sihto, S.-L., Kulmala, M., McCormick, A., and McMurry, P.: An improved criterion for new particle formation in diverse atmospheric environments, Atmos. Chem. Phys., 10, 8469–8480, doi:10.5194/acp-10-8469-2010, 2010.

Kulmala, M., Toivonen, A., Mäkelä, J. M., and Laaksonen, A.: Analysis of the growth of nucleation mode particles observed in Boreal forest, Tellus B, 50, 449–462, 10.3402/tellusb.v50i5.16229, 1998.

Kulmala, M., Vehkamäki, H., Petäjä, T., Dal Maso, M., Lauri, A., Kerminen, V.-M., Birmili, W., and McMurry, P. H.: Formation and growth rates of ultrafine atmospheric particles: a review of observations, J. Aerosol Sci., 35, 143–176, doi:10.1016/j.jaerosci.2003.10.003, 2004a.

Kulmala, M., Suni, T., Lehtinen, K. E. J., Dal Maso, M., Boy, M., Reissell, A., Rannik, Ü., Aalto, P., Keronen, P., Hakola, H., Bäck, J., Hoffmann, T., Vesala, T., and Hari, P.: A new feedback mechanism linking forests, aerosols, and climate, Atmos. Chem. Phys., 4, 557–562, doi:10.5194/acp-4-557-2004, 2004b.

Kulmala, M., Petäjä, T., Nieminen, T., Sipilä, M., Manninen, H. E., Lehtipalo, K., Dal Maso, M., Aalto, P. P., Junninen, H., and Paasonen, P.: Measurement of the nucleation of atmospheric aerosol particles, Nat. Protoc., 7, 1651–1667, doi:10.1038/nprot.2012.091, 2012.

Kulmala, M., Kontkanen, J., Junninen, H., Lehtipalo, K., Manninen, H. E., Nieminen, T., Petäjä, T., Sipilä, M., Schobesberger, S., Rantala, P., Franchin, A., Jokinen, T., Järvinen, E., Äijälä, M., Kangasluoma, J., Hakala, J., Aalto, P., Paasonen, P., Mikkilä, J., Vanhanen, J., Aalto, J., Hakola, H., Makkonen, U., Ruuskanen, T., Mauldin, R. r., Duplissy, J., Vehkamäki, H., Bäck, J., Kortelainen, A., Riipinen, I., Kurtén, T., Johnston, M., Smith, J., Ehn, M., Mentel, T., Lehtinen, K., Laaksonen, A., Kerminen, V., and Worsnop, D.: Direct observations of atmospheric aerosol nucleation, Science, 339, 943–946, doi:10.1126/science.1227385, 2013.

Kulmala, M., Luoma, K., Virkkula, A., Petäjä, T., Paasonen, P., Kerminen, V.-M., Nie, W., Qi, X., Shen, Y., and Chi, X.: On the mode-segregated aerosol particle number concentration load, Boreal Environ. Res., 21 319–331, 2016.

Kurtén, T., Torpo, L., Ding, C. G., Vehkamäki, H., Sundberg, M. R., Laasonen, K., and Kulmala, M.: A density functional study on water-sulfuric acid-ammonia clusters and implications for atmospheric cluster formation, J. Geophys. Res.-Atmos., 112, D04210, doi:10.1029/2006JD007391, 2007.

Liao, L., Kerminen, V.-M., Boy, M., Kulmala, M., and Dal Maso, M.: Temperature influence on the natural aerosol budget over boreal forests, Atmos. Chem. Phys., 14, 8295–8308, doi:10.5194/acp-14-8295-2014, 2014.

Merikanto, J., Spracklen, D., Mann, G., Pickering, S., and Carslaw, K.: Impact of nucleation on global CCN, Atmos. Chem. Phys., 9, 8601–8616, doi:10.5194/acp-9-8601-2009, 2009.

Merikanto, J., Duplissy, J., Määttänen, A., Henschel, H., Donahue, N. M., Brus, D., Schobesberger, S., Kulmala, M., and Vehkamäki, H.: Effect of ions on sulfuric acid-water binary particle formation: 1. Theory for kinetic-and nucleation-type particle formation and atmospheric implications, J. Geophys. Res.-Atmos., 121, 1736–1751, doi:10.1002/2015JD023538, 2016.

Metzger, A., Verheggen, B., Dommen, J., Duplissy, J., Prevot, A. S., Weingartner, E., Riipinen, I., Kulmala, M., Spracklen, D. V., and Carslaw, K. S.: Evidence for the role of organics in aerosol particle formation under atmospheric conditions, P. the Natl. Acad. Sci. USA, 107, 6646–6651, doi:10.1073/pnas.0911330107, 2010.

Mordas, G., Plauškaitė, K., Prokopciuk, N., Dudoitis, V., Bozzetti, C., and Ulevicius, V.: Observation of new particle formation on Curonian Spit located between continental Europe and Scandinavia, J. Aerosol Sci., 97, 38–55, doi:10.1016/j.jaerosci.2016.03.002, 2016.

Nieminen, T., Lehtinen, K., and Kulmala, M.: Sub-10 nm particle growth by vapor condensation–effects of vapor molecule size and particle thermal speed, Atmos. Chem. Phys., 10, 9773–9779, doi:10.5194/acp-10-9773-2010, 2010, 2010.

Nieminen, T., Asmi, A., Dal Maso, M., Aalto, P. P., Keronen, P., Petäjä, T., Kulmala, M., and Kerminen, V.-M.: Trends in atmospheric new-particle formation: 16 years of observations in a boreal-forest environment, Boreal Environ. Res., 19, 191–214, 2014.

Nieminen, T., Yli-Juuti, T., Manninen, H., Petäjä, T., Kerminen, V.-M., and Kulmala, M.: Technical note: New particle formation event forecasts during PEGASOS–Zeppelin Northern mission 2013 in Hyytiälä, Finland, Atmos. Chem. Phys., 15, 12385–12396, doi:10.5194/acp-15-12385-2015, 2015.

Paasonen, P., Nieminen, T., Asmi, E., Manninen, H., Petäjä, T., Plass-Dülmer, C., Flentje, H., Birmili, W., Wiedensohler, A., Horrak, U., Metzger, A., Hamed, A., Laaksonen, A., Facchini, M. C., Kerminen, V.-M., and Kulmala, M.: On the roles of sulphuric acid and low-volatility organic vapours in the initial steps of atmospheric new particle formation, Atmos. Chem. Phys., 10, 11223–11242, doi:10.5194/acp-10-11223-2010, 2010.

Paasonen, P., Olenius, T., Kupiainen, O., Kurtén, T., Petäjä, T., Birmili, W., Hamed, A., Hu, M., Huey, L., Plass-Duelmer, C., Smith, J. N., Wiedensohler, A., Loukonen, V., McGrath, M. J., Ortega, I. K., Laaksonen, A., Vehkamäki, H., Kerminen, V.-M., and Kulmala, M.: On the formation of sulphuric acid–amine clusters in varying atmospheric conditions and its influence on atmospheric new particle formation, Atmos. Chem. Phys., 12, 9113–9133, doi:10.5194/acp-12-9113-2012, 2012.

Paasonen, P., Asmi, A., Petäjä, T., Kajos, M. K., Äijälä, M., Junninen, H., Holst, T., Abbatt, J. P., Arneth, A., Birmili, W., Gon, H. D. v. d., Hamed, A., Hoffer, A., Laakso, L., Laaksonen, A., Leaitch, W. R., Plass-Dülmer, C., Pryor, S. C., Räisänen, P., Swietlicki, E., Wiedensohler, A., Worsnop, D. R., Kerminen, V.-M., and Kulmala, M.: Warming-induced increase in aerosol number concentration likely to moderate climate change, Nat. Geosci., 6, 438–442, doi:10.1038/ngeo1800, 2013.

Perez, R., Ineichen, P., Seals, R., and Zelenka, A.: Making full use of the clearness index for parameterizing hourly insolation conditions, Solar Energ., 45, 111–114, doi:10.1016/0038-092X(90)90036-C, 1990.

Petäjä, T., Mauldin Iii, R., Kosciuch, E., McGrath, J., Nieminen, T., Paasonen, P., Boy, M., Adamov, A., Kotiaho, T., and Kulmala, M.: Sulfuric acid and OH concentrations in a boreal forest site, Atmos. Chem. Phys., 9, 7435–7448, doi:10.5194/acp-9-7435-2009, 2009.

Petäjä, T., Sipilä, M., Paasonen, P., Nieminen, T., Kurtén, T., Ortega, I. K., Stratmann, F., Vehkamäki, H., Berndt, T., and Kulmala, M.: Experimental observation of strongly bound dimers of sulfuric acid: Application to nucleation in the atmosphere, Physical review letters, 106, 228302, doi:10.1103/PhysRevLett.106.228302, 2011.

Pöschl, U.: Atmospheric aerosols: composition, transformation, climate and health effects, Angewandte Chemie International Edition, 44, 7520–7540, doi:10.1002/anie.200501122, 2005.

Riccobono, F., Schobesberger, S., Scott, C. E., Dommen, J., Ortega, I. K., Rondo, L., Almeida, J., Amorim, A., Bianchi, F., Breitenlechner, M., David, A., Downard, A., Dunne, E. M., Duplissy, J., Ehrhart, S., Flagan, R. C., Franchin, A., Hansel, A., Junninen, H., Kajos, M., Keskinen, H., Kupc, A., Kürten, A., Kvashin, A. N., Laaksonen, A., Lehtipalo, K., Makhmutov, V., Mathot, S., Nieminen, T., Onnela, A., Petäjä, T., Praplan, A. P., Santos, F. D., Schallhart, S., Seinfeld, J. H., Sipilä, M., Spracklen, D. V., Stozhkov, Y., Stratmann, F., Tomé, A., Tsagkogeorgas, G., Vaattovaara, P., Viisanen, Y., Vrtala, A., Wagner, P. E., Weingartner, E., Wex, H., Wimmer, D., Carslaw, K. S., Curtius, J., Donahue, N. M., Kirkby, J., Kulmala, M., Worsnop, D. R., and Baltensperger, U.: Oxidation products of biogenic emissions contribute to nucleation of atmospheric particles, Science, 344, 717–721, doi:10.1126/science.1243527, 2014.

Salma, I., Németh, Z., Kerminen, V.-M., Aalto, P., Nieminen, T., Weidinger, T., Molnár, Á., Imre, K., and Kulmala, M.: Regional effect on urban atmospheric nucleation, Atmos. Chem. Phys., 16, 8715–8728, doi:10.5194/acp-16-8715-2016, 2016.

Sánchez, G., Serrano, A., and Cancillo, M.: Effect of cloudiness on solar global, solar diffuse and terrestrial downward radiation at Badajoz (Southwestern Spain), Optica pura y aplicada, 45, 33–38, 2012.

Seinfeld, J. H. and Pandis, S. N.: Atmospheric chemistry and physics: from air pollution to climate change, John Wiley & Sons, 2012.

Smith, J. N., Moore, K. F., Eisele, F. L., Voisin, D., Ghimire, A. K., Sakurai, H., and McMurry, P. H.: Chemical composition of atmospheric nanoparticles during nucleation events in Atlanta, J. Geophys. Res.-Atmos., 110, D22S03, doi:10.1029/2005JD005912, 2005.

Sogacheva, L., Dal Maso, M., Kerminen, V.-M., and Kulmala, M.: Probability of nucleation events and aerosol particle concentration in different air mass types arriving at Hyytiälä, southern Finland, based on back trajectories analysis, Boreal Environ. Res., 10, 493–510, 2005.

Sogacheva, L., Saukkonen, L., Nilsson, E., Dal Maso, M., Schultz, D. M., De Leeuw, G., and Kulmala, M.: New aerosol particle formation in different synoptic situations at Hyytiälä, southern Finland, Tellus B, 60, 485–494, doi:10.1111/j.1600-0889.2008.00364.x, 2008.

Vakkari, V., Tiitta, P., Jaars, K., Croteau, P., Beukes, J. P., Josipovic, M., Kerminen, V. M., Kulmala, M., Venter, A. D., and Zyl, P. G.: Reevaluating the contribution of sulfuric acid and the origin of organic compounds in atmospheric nanoparticle growth, Geophys. Res. Lett., 42, 10486–10493, doi:10.1002/2015GL066459, 2015.

Vehkamäki, H., Kulmala, M., Napari, I., Lehtinen, K. E., Timmreck, C., Noppel, M., and Laaksonen, A.: An improved parameterization for sulfuric acid–water nucleation rates for tropospheric and stratospheric conditions, J. Geophys. Res.-Atmos., 107, 4622, doi:10.1029/2002JD002184, 2002.

Yu, F., Luo, G., Bates, T. S., Anderson, B., Clarke, A., Kapustin, V., Yantosca, R. M., Wang, Y., and Wu, S.: Spatial distributions of particle number concentrations in the global troposphere: Simulations, observations, and implications for nucleation mechanisms, J. Geophys. Res.-Atmos., 115, D17205, doi:10.1029/2009JD013473, 2010.

Zhang, R., Khalizov, A., Wang, L., Hu, M., and Xu, W.: Nucleation and growth of nanoparticles in the atmosphere, Chem. Rev., 112, 1957–2011, doi:10.1021/cr2001756, 2011.

# Paper III

ATMOSPHERIC SCIENCE

# Multicomponent new particle formation from sulfuric acid, ammonia, and biogenic vapors

Katrianne Lehtipalo[1,2,3*†], Chao Yan[1*], Lubna Dada[1], Federico Bianchi[1], Mao Xiao[2], Robert Wagner[1], Dominik Stolzenburg[4], Lauri R. Ahonen[1], Antonio Amorim[5], Andrea Baccarini[2], Paulus S. Bauer[4], Bernhard Baumgartner[4], Anton Bergen[6], Anne-Kathrin Bernhammer[7,8], Martin Breitenlechner[7‡], Sophia Brilke[4], Angela Buchholz[9], Stephany Buenrostro Mazon[1], Dexian Chen[10], Xuemeng Chen[1], Antonio Dias[5], Josef Dommen[2], Danielle C. Draper[11], Jonathan Duplissy[1], Mikael Ehn[1], Henning Finkenzeller[12], Lukas Fischer[7], Carla Frege[2], Claudia Fuchs[2], Olga Garmash[1], Hamish Gordon[13], Jani Hakala[1], Xucheng He[1], Liine Heikkinen[1], Martin Heinritzi[6], Johanna C. Helm[6], Victoria Hofbauer[10], Christopher R. Hoyle[2§], Tuija Jokinen[1], Juha Kangasluoma[1,14], Veli-Matti Kerminen[1], Changhyuk Kim[15‖], Jasper Kirkby[6,16], Jenni Kontkanen[1,17], Andreas Kürten[6], Michael J. Lawler[11], Huajun Mai[15], Serge Mathot[16], Roy L. Mauldin III[10,12], Ugo Molteni[2], Leonid Nichman[18¶], Wei Nie[1,19,20], Tuomo Nieminen[9], Andrea Ojdanic[4], Antti Onnela[16], Monica Passananti[1], Tuukka Petäjä[1,19], Felix Piel[6,7,8], Veronika Pospisilova[2], Lauriane L. J. Quéléver[1], Matti P. Rissanen[1], Clémence Rose[1#], Nina Sarnela[1], Simon Schallhart[1**], Simone Schuchmann[16], Kamalika Sengupta[13], Mario Simon[6], Mikko Sipilä[1], Christian Tauber[4], António Tomé[21], Jasmin Tröstl[2], Olli Väisänen[9], Alexander L. Vogel[2,6,22], Rainer Volkamer[12], Andrea C. Wagner[6], Mingyi Wang[10], Lena Weitz[6], Daniela Wimmer[1††], Penglin Ye[10,23], Arttu Ylisirniö[9], Qiaozhi Zha[1], Kenneth S. Carslaw[13], Joachim Curtius[6], Neil M. Donahue[1,10], Richard C. Flagan[15], Armin Hansel[1,7,8], Ilona Riipinen[17,24], Annele Virtanen[9], Paul M. Winkler[4], Urs Baltensperger[2], Markku Kulmala[1,14,25†], Douglas R. Worsnop[1,23]



**A major fraction of atmospheric aerosol particles, which affect both air quality and climate, form from gaseous precursors in the atmosphere. Highly oxygenated organic molecules (HOMs), formed by oxidation of biogenic volatile organic compounds, are known to participate in particle formation and growth. However, it is not well understood how they interact with atmospheric pollutants, such as nitrogen oxides ($NO_x$) and sulfur oxides ($SO_x$) from fossil fuel combustion, as well as ammonia ($NH_3$) from livestock and fertilizers. Here, we show how $NO_x$ suppresses particle formation, while HOMs, sulfuric acid, and $NH_3$ have a synergistic enhancing effect on particle formation. We postulate a novel mechanism, involving HOMs, sulfuric acid, and ammonia, which is able to closely reproduce observations of particle formation and growth in daytime boreal forest and similar environments. The findings elucidate the complex interactions between biogenic and anthropogenic vapors in the atmospheric aerosol system.**

## INTRODUCTION

Atmospheric new particle formation (NPF) can dominate regional concentrations of aerosol particles and cloud condensation nuclei (CCN) and significantly contribute to their global budgets (*1*–*3*). Because variations in CCN concentrations affect aerosol-cloud interactions and associated climate forcing, it is vital to understand both past changes to CCN since the industrial revolution and also expected future changes, as emissions from fossil fuel combustion decline in response to efforts to improve air quality and mitigate climate change (*4*).

NPF begins with the formation of molecular clusters from low-volatility vapors and continues with their subsequent growth to aerosol particles under favorable conditions (*5*, *6*). Sulfuric acid is believed to govern NPF in most environments, although it cannot alone explain the observed formation and growth rates (GRs) (*7*, *8*). Particle growth, on the other hand, has been closely linked to organic vapors (*9*), which are abundant in the continental boundary layers. Highly oxygenated organic molecules (HOMs) with exceedingly low vapor pressures can be involved at the very early stages of particle formation (*10*–*12*), but very few field studies have unambiguously observed NPF without sulfuric acid (*13*, *14*). Despite numerous laboratory and field studies, interactions between organic and inorganic constituents, as well as their relative roles in atmospheric NPF, remain highly uncertain. It is also crucial to resolve whether the strong enhancement of nucleation rates by ions, which was observed in the pure systems (*15*, *16*), occurs also when organic vapors interact with other compounds.

Recent laboratory experiments with comprehensive instrumentation and low contaminant levels have shown how NPF can proceed via a binary mechanism (water and sulfuric acid) (*16*–*18*), a ternary inorganic mechanism (water, sulfuric acid, and base) (*16*, *19*–*21*), or a ternary organic mechanism (water, sulfuric acid, and organics) (*10*, *11*, *22*) or by nucleation of HOMs alone, i.e., pure biogenic nucleation (*15*). These experiments have constrained the particle formation rates in these model systems; however, none of them have reproduced conditions of the daytime atmospheric boundary layer, especially the boreal forest where NPF is very common (*5*). Some of the main differences are that most of the previous laboratory experiments did not include $NO_x$ or they did not control the $NH_3$ concentrations.

$NO_x$ influences organic oxidation indirectly by changing the oxidant balance (OH versus ozone and $NO_3$) and directly by perturbing oxidation mechanisms, especially the branching of peroxy radical ($RO_2$) reactions, which is crucial in the production of HOMs. $NO_x$ can decrease yields of secondary organic aerosol (SOA) (*23*, *24*) and

suppress NPF from terpenes (*25*), possibly by shutting off $RO_2$ autoxidation leading to HOMs (*12*) and, instead, forming (relatively) more volatile organonitrates (ONs) (*23*). The oxidation of $SO_2$, on the other hand, leads to the formation of sulfuric acid, which has a very low vapor pressure. Sulfuric acid also clusters very efficiently with bases (*19*), but whether this happens in the presence of organics is not known until now. Thus, both enhancement and suppression of NPF by human activity is possible, depending on conditions.

## RESULTS

To simulate NPF and growth under realistic daytime conditions resembling those in the boreal forest (our reference being the Hyytiälä SMEAR II station in southern Finland), we performed experiments in the CLOUD (Cosmics Leaving OUtdoors Droplets) chamber at CERN (European Organization for Nuclear Research). All experiments were performed at 278 K and 38% relative humidity (RH) and included monoterpenes (MTs; $C_{10}H_{16}$). We used a 2:1 volume mixture of alpha-pinene and delta-3-carene, which are the two most abundant MTs in Hyytiälä (*26*). The ozone mixing ratio in the chamber was ca. 40 parts per billion by volume (ppbv), and the hydroxyl radical (OH) concentration was controlled with an ultraviolet (UV) light system (see Materials and Methods). We first performed experiments without $SO_2$ ($H_2SO_4$ concentration of $<2 \times 10^5$ cm$^{-3}$) and then added 0.5 to 5 ppbv of $SO_2$, leading to $1 \times 10^6$ to $7 \times 10^7$ cm$^{-3}$ of $H_2SO_4$ in the chamber. The experiments were conducted with various mixing ratios of $NO_x$ (=NO + $NO_2$, 0 to 5 ppbv) and ammonia [2 to 3000 parts per trillion by volume (pptv)], covering the range from very clean to polluted environments. Most experiments were first performed without ions in the chamber (neutral conditions, N) and then repeated with ionization from galactic cosmic rays (GCR conditions).

Figure 1 shows the step-by-step change in nucleation rates (*J*) when going from a single-component system toward a more realistic multicomponent mixture. Compared to the pure biogenic system with only MTs in the chamber, fewer new particles are formed when $NO_x$ is added and more particles are formed when $SO_2$ is added (Fig. 1 and figs. S1 and S2). A further increase is observed when ammonia is added to the chamber as well. To understand the mechanism and magnitude of these effects, we will first discuss the reduction of particle formation by $NO_x$ and then the increase by addition of $SO_2$ and $NH_3$ and finally show how each of these compounds are needed to explain NPF and growth in the multicomponent system.

### Effect of $NO_x$ on particle formation rates

We find that the particle formation rates largely follow the ratio of MT to $NO_x$ in the chamber (fig. S3), as reported in an earlier study, albeit for larger particles (*25*). However, to discover the underlying cause of this pattern, we need to understand what happens to HOMs when $NO_x$ is added to the chamber. Increasing the $NO_x$ concentration leads to a larger fraction of ONs among all HOMs and a significant decrease in dimers, although the total HOM concentration slightly increases. Therefore, the volatility distribution is shifted toward more volatile products. This is consistent with lower SOA mass yields from terpenes at high $NO_x$ concentrations (*23*, *24*).

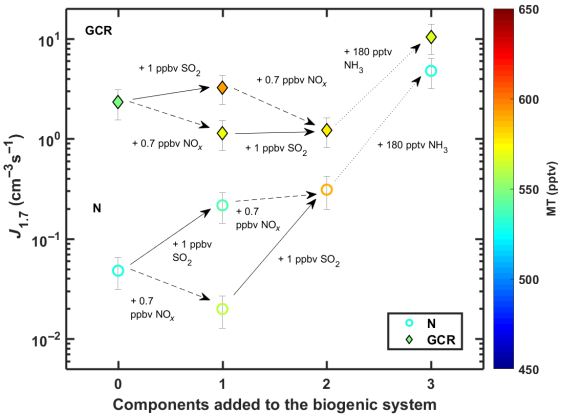


**Fig. 1. The effect of adding different vapors on biogenic nucleation rates ($J_{1.7}$).** All points have similar MT (530 to 590 pptv) and ozone (40 ppbv) mixing ratios. The leftmost points were measured with only MTs added to the chamber, and each step to the right represents addition of one more component to the system. Solid arrows describe the addition of ca. 1 ppbv of $SO_2$ (resulting in an $H_2SO_4$ concentration of $1 \times 10^7$ to $2 \times 10^7$ cm$^{-3}$), dashed arrows describe the addition of ca. 0.7 ppbv of $NO_x$, and dotted arrows describe the addition of ca. 180 pptv of $NH_3$. Circles are experiments at neutral conditions (N), and diamonds are experiments at GCR conditions. Colors of the symbols indicate the measured MT mixing ratio. The error bars describe the uncertainty in the nucleation rates, which was calculated similar to earlier CLOUD publications, taking into account both the systematic and statistical errors and run-to-run repeatability (see Supplementary Materials and Methods). See fig. S1 for the formation rate of 2.5-nm particles.

[1]Institute for Atmospheric and Earth System Research/Physics, Faculty of Science, University of Helsinki, P.O. Box 64, FI-00014 Helsinki, Finland. [2]Laboratory of Atmospheric Chemistry, Paul Scherrer Institute, 5232 Villigen PSI, Switzerland. [3]Finnish Meteorological Institute, Erik Palménin aukio 1, 00560 Helsinki, Finland. [4]Faculty of Physics, University of Vienna, Boltzmanngasse 5, 1090 Wien, Austria. [5]CENTRA and FCUL, Universidade de Lisboa, Campo Grande, 1749-016 Lisboa, Portugal. [6]Goethe University Frankfurt, Institute for Atmospheric and Environmental Sciences, Altenhöferallee 1, 60438 Frankfurt am Main, Germany. [7]University of Innsbruck, Institute for Ion and Applied Physics, 6020 Innsbruck, Austria. [8]Ionicon GesmbH, Innsbruck, Austria. [9]University of Eastern Finland, Department of Applied Physics, P.O. Box 1627, 70211 Kuopio, Finland. [10]Carnegie Mellon University Center for Atmospheric Particle Studies, 5000 Forbes Avenue, Pittsburgh, PA 15213, USA. [11]Department of Chemistry, University of California, Irvine, Irvine, CA 92697, USA. [12]Department of Chemistry and CIRES, University of Colorado, Boulder, CO 80309 USA. [13]University of Leeds, Leeds LS2 9JT, UK. [14]Aerosol and Haze Laboratory, Beijing University of Chemical Technology, Beijing, China. [15]California Institute of Technology, 210-41, Pasadena, CA 91125, USA. [16]CERN, CH-1211 Geneva, Switzerland. [17]Department of Environmental Science and Analytical Chemistry (ACES) and Bolin Centre for Climate Research, Stockholm University, 10691 Stockholm, Sweden. [18]School of Earth and Environmental Sciences, University of Manchester, Manchester M13 9PL, UK. [19]Joint International Research Laboratory of Atmospheric and Earth System Sciences, Nanjing University, Nanjing, China. [20]Collaborative Innovation Center of Climate Change, Jiangsu Province, China. [21]IDL, Universidade da Beira Interior, Covilhã, Portugal. [22]Laboratory of Environmental Chemistry, Paul Scherrer Institute, 5232 Villigen PSI, Switzerland. [23]Aerodyne Research Inc., 45 Manning Road, Billerica, MA 01821, USA. [24]Aerosol Physics, Faculty of Science, Tampere University of Technology, P.O. Box 692, 33101, Tampere, Finland. [25]Helsinki Institute of Physics, FI-00014 Helsinki, Finland.
*These authors contributed equally to this work.
†Corresponding author. Email: katrianne.lehtipalo@helsinki.fi (K.L.); markku.kulmala@helsinki.fi (M.K.)
‡Present address: Harvard University, 18 Oxford Street, Cambridge, MA 02138, USA.
§Present address: Institute for Atmospheric and Climate Science, ETH Zurich, Zurich, Switzerland.
||Present address: Department of Environmental Engineering, Pusan National University, Busan 46241, Republic of Korea.
¶Present address: Flight Research Laboratory, National Research Council, Canada.
#Present address: Laboratoire de Météorologie Physique CNRS UMR 6016, Observatoire de Physique du Globe de Clermont-Ferrand, Université Clermont Auvergne, France.
**Present address: Finnish Meteorological Institute, 00560 Helsinki, Finland.
††Present address: Faculty of Physics, University of Vienna, Boltzmanngasse 5, 1090 Wien, Austria.

In contrast to pure biogenic experiments (*15*), the nucleation rates in the presence of $NO_x$ do not correlate with the total HOM concentration (Fig. 2A). Therefore, we further divided the HOMs into four groups: non-nitrate HOM monomers ($C_{4-10}H_xO_y$), non-nitrate HOM dimers ($C_{11-20}H_xO_y$), ON monomers ($C_{4-10}H_xO_yN_{1-2}$), and ON dimers ($C_{11-20}H_xO_yN_{1-2}$). We find a clear difference in how non-nitrate HOMs and ONs relate to the nucleation rates (Fig. 2 and table S1). The nucleation rates correlate with non-nitrate HOMs (Pearson's correlation coefficient $R = 0.72$ for GCR experiments), especially with dimers ($R = 0.97$), but not with ONs ($R = -0.42$).

It should be noted that the effect of $NO_x$ chemistry on HOM formation, and the subsequent NPF, might depend on the organic molecule in question; alpha-pinene has been reported to behave differently with respect to SOA formation than some other MTs and sesquiterpenes (*24*, *27*). For any given volatile organic compound (VOC) concentration, the HOM yield and volatility distribution, both of which are altered by $NO_x$, matter for the NPF efficiency. Our results are specific to photo-oxidation, i.e., daytime conditions.

### Effect of $SO_2$ and $NH_3$ on particle formation rates

Let us next consider the addition of $SO_2$, which quickly forms $H_2SO_4$ in the chamber by OH oxidation under the presence of UV light. Without added ammonia (background $NH_3$ estimated to be ca. 2 pptv), $J$ shows no correlation with sulfuric acid ($R = -0.06$; table S1), consistent with an earlier CLOUD observation (*15*) that $H_2SO_4$ does not affect nucleation from alpha-pinene ozonolysis at $H_2SO_4 < 6 \times 10^6$ cm$^{-3}$. Our experiments with somewhat higher sulfuric acid concentration ($H_2SO_4 \geq 1 \times 10^7$ cm$^{-3}$) show consistently slightly higher $J$ at the same HOM concentration than the experiments without $SO_2$ (Figs. 1 and 2D). At low HOM dimer concentrations, the pure biogenic $J$ drops below the detection threshold, although particle formation could still be observed together with $H_2SO_4$ (Fig. 2D). This indicates that $H_2SO_4$ is able to interact with HOMs to form particles, as speculated earlier (*11*), but the mechanism is inefficient without $NH_3$ (or another base).

Ammonia strongly enhances nucleation rates (Fig. 1 and figs. S1, S2, and S4) when both $H_2SO_4$ and HOMs are present simultaneously. In general, experiments at higher $NH_3$ ($\geq$200 pptv) show up to two orders of magnitude higher $J$ than otherwise similar experiments without added $NH_3$ (Fig. 1 and fig. S4). The multicomponent experiments with all three precursors—MT, $H_2SO_4$, and $NH_3$—in the presence of $NO_x$ are able to qualitatively and quantitatively reproduce boreal forest nucleation and GRs (Fig. 3). The ternary inorganic mechanism ($H_2SO_4$, $NH_3$, and water) cannot explain them, as it produces very few particles at $H_2SO_4$ concentrations below $1 \times 10^7$ cm$^{-3}$ and temperatures of $\geq$278 K (*16*, *21*), although most NPF events in Hyytiälä occur at these conditions (Fig. 3A). The pure biogenic mechanism, on the other hand, does not show a similar $H_2SO_4$ dependency as observed in the atmosphere, and it produces significant nucleation rates ($J \geq 1$ cm$^{-3}$ s$^{-1}$) only without $NO_x$ or when $NO_x$ is low compared to MT concentrations ($MT/NO_x \geq 1$) (fig. S3). Thus, the nucleation rates detected during multicomponent experiments cannot be explained solely by the sum of ternary inorganic and pure biogenic nucleation (Fig. 3A).

### Particle formation and growth in multicomponent experiments

Combining the observations listed above, we postulate that the formation rates in the multicomponent system can be parametrized with the empirical formula

$$J = k_1[H_2SO_4]^a[NH_3]^b[HOM_{di}]^c \quad (1)$$

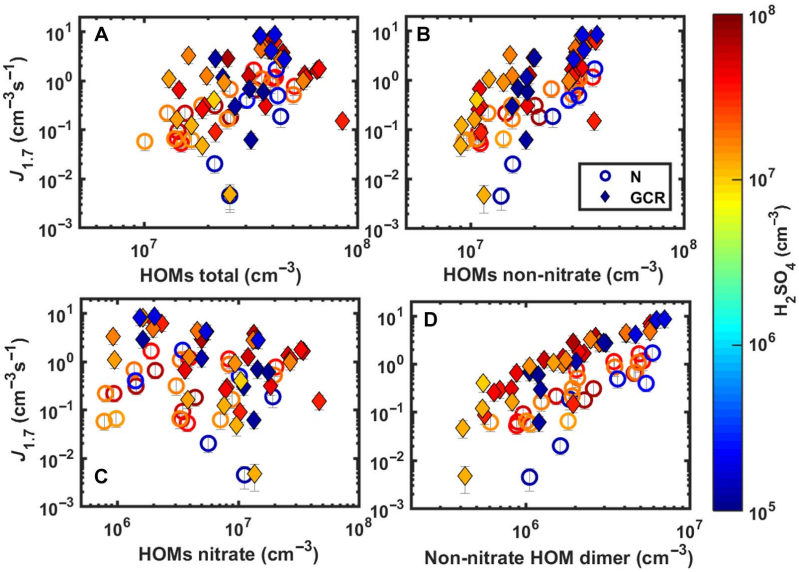


**Fig. 2. Relation of nucleation rates to different HOM categories.** Nucleation rates ($J_{1.7}$) as a function of the (**A**) total concentration of HOMs [regardless whether the molecule has nitrate group(s) or not], (**B**) non-nitrate HOMs, (**C**) nitrate HOMs (ONs), and (**D**) non-nitrate HOM dimers. Open circles refer to neutral experiments, closed diamonds refer to GCR experiments, and the color refers to the $H_2SO_4$ concentration (blue points were measured without added $SO_2$). All points were measured at 278 K and 38% RH, with varying MT concentrations (100 to 1500 pptv) and $NO_x$ levels (0 to 5 ppbv; $NO/NO_2$, about 0.6%) without added $NH_3$.

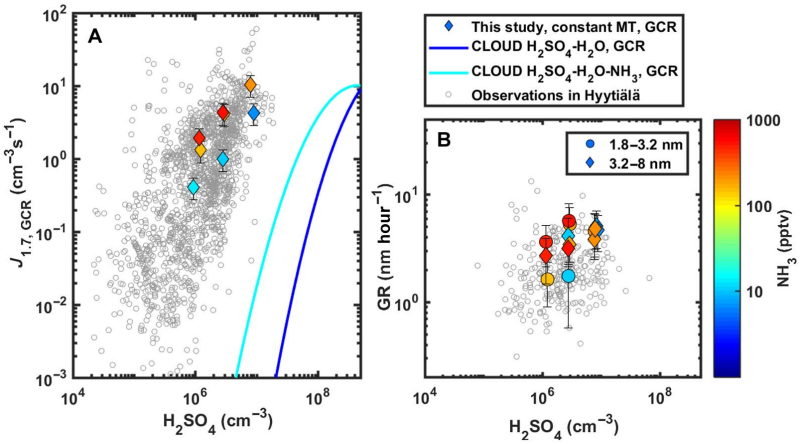


**Fig. 3. Nucleation and GRs at CLOUD compared to atmospheric observations in Hyytiälä.** Here, we chose a series of experiments with constant MT/$NO_x$ ratio (ca. 0.6, $NO/NO_2$ = 7%), while $H_2SO_4$ and $NH_3$ concentrations were varied across the range relevant for boreal forest. (**A**) Nucleation rates ($J_{1.7}$) at CLOUD (colored points) and ambient observations in Hyytiälä (*5*, *8*) (gray circles). The blue and cyan lines represent binary ($H_2SO_4$-$H_2O$) and ternary ($H_2SO_4$-$H_2O$-$NH_3$, 7 < [$NH_3$] < 40 pptv) nucleation, respectively, based on earlier CLOUD data (*21*), while the pure biogenic nucleation rate at similar MT/$NO_x$ ratio would be <1 $cm^{-3}$ $s^{-1}$ (fig. S3). (**B**) GRs of 1.8- to 3.2-nm-sized and 3.2- to 8-nm-sized particles in the same experiments compared to observations of initial GR in Hyytiälä (*40*).

where [$HOM_{di}$] is the concentration of non-nitrate HOM dimers and $k_1$, $a$, $b$, and $c$ are free parameters. This approach builds on the many observations showing that measured nucleation rates in the continental boundary layer seem to follow a power-law functional dependency on sulfuric acid concentration

$$J = k[H_2SO_4]^p \quad (2)$$

with the exponent $p$ varying between 1 and 2 (*6*–*8*). The prefactor $k$ varies considerably between different locations, as it includes the variation of nucleation rates due to external conditions ($T$, RH, etc.) and any conucleating vapors. On the basis of earlier CLOUD data showing the participation of oxidized organics in the first steps of particle formation (*11*), the parametrization was rewritten as

$$J = k_2[H_2SO_4]^p[\mathrm{BioOxOrg}]^q \quad (3)$$

Compared to Eq. 3, we have now included a dependency on ammonia and further defined the oxidized organics participating in particle formation to be mainly non-nitrate HOM dimers. In the next section, we will show that all of these species can participate in clustering simultaneously.

Using Eq. 1 with $a$ = 2, $b$ = $c$ = 1, we can find an extremely good correlation ($R$ = 0.96) between the modeled and measured formation rates for the set of neutral experiments at 10 < $NH_3$ < 3000 pptv, 5 × $10^6$ < $H_2SO_4$ < 6 × $10^7$ $cm^{-3}$, 100 < MT < 1200 pptv, 0.7 < $NO_x$ < 2.1 ppbv, and $O_3$ = 40 ppbv (Fig. 4 and fig. S5). Replacing [$HOM_{di}$] with [MT/$NO_x$] still gives a high correlation ($R$ = 0.92). However, using Eq. 3 with $p$ = 2, $q$ = 1 as in (*11*) and [BioOxOrg] = [HOMs], the correlation is worse, $R$ = 0.53, mainly due to varying $NO_x$ and $NH_3$ concentrations not included in the earlier parametrization (fig. S5). A more sophisticated multicomponent parametrization, which can be extended to a larger set of conditions ($T$, RH, ion concentration, etc.) and a wider range of vapor concentrations, is subject to future studies.

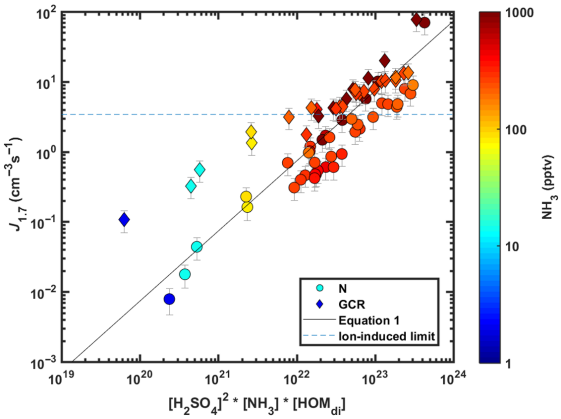


**Fig. 4. Nucleation rates ($J_{1.7}$) as a function of the product of the concentrations of $H_2SO_4$, $NH_3$, and non-nitrate HOM dimers.** Circles refer to neutral experiments, diamonds refer to GCR experiments, and the color refers to the $NH_3$ concentration. All points here were measured at 278 K and 38% RH. The MT mixing ratio was varied between 100 and 1200 pptv, $H_2SO_4$ concentration between 5 × $10^6$ and 6 × $10^7$ $cm^{-3}$, $NH_3$ between 2 and 3000 pptv, and $NO_x$ between 0.7 and 2.1 ppbv ($NO/NO_2$ = 0.6%). The dashed line gives the maximum rate from ion-induced nucleation based on the ion pair production rate in CLOUD under GCR conditions (*15*). The solid line is the multicomponent parametrization for neutral experiments based on Eq. 1 with $k$ = 7.4 × $10^{-23}$ $s^{-1}$ $pptv^{-1}$ $cm^6$.

The enhancement of $J$ due to ions decreases with increasing $NH_3$ concentration and $J$ (Fig. 4 and fig. S4) and is generally considerably weaker in the multicomponent system than in the acid-base or pure biogenic systems (*15*, *16*) at otherwise similar vapor concentrations (Fig. 1). This means that the neutral nucleation pathway is more efficient in the multicomponent system. In general, ion enhancement becomes weaker with increasing stability of the forming neutral

clusters, indicating that chemical interactions between different kinds of molecules become more important in cluster bonding. This might, at least partly, explain why field studies have found only minor contribution of ions to NPF in various environments (*5*, *13*, *28*), as multiple vapors are always present in the atmosphere.

The formation rate is not the only important factor governing NPF. The competition between the GR of newly formed particles and their loss rate governs the fraction of particles that eventually reach CCN sizes. Because particle losses are most severe in the beginning of the growth process, initial GRs in the sub–3-nm size range are especially critical (*29*). Particle GRs in our experiments, over the same ranges of gas concentrations as above, seem to follow a formula

$$\mathrm{GR} = k_1[\mathrm{H_2SO_4}]^a + k_2[\mathrm{H_2SO_4}]^b[\mathrm{NH_3}]^c + k_3[\mathrm{Org}]^d \quad (4)$$

where the first term can be interpreted as growth by condensation of sulfuric acid (*30*), the second term by sulfuric acid ammonia clusters (*31*), and the third term by oxidized organics (*32*). As we concentrate on the initial GRs, we chose [Org] to include only non-nitrate HOM dimers, which are the most relevant in this size range (<7 nm). Again, taking $a = b = c = d = 1$, we find a very good correlation especially for the size range 3.5 to 7 nm ($R = 0.94$) between modeled and measured GRs (fig. S6). It should be noted that the coefficients $k$ are size dependent and, especially, that for different size ranges a different subset of organic vapors is relevant for growth (*32*). As the particles grow, a wider range of vapors with different volatilities can contribute to the growth, and the third term grows progressively more important (fig. S6). This conforms to the present qualitative picture of the particle growth process in the boreal forest (*5*), and the measured values are in the same order of magnitude as those observed in Hyytiälä (Fig. 3B).

Here, we assume no interaction between organics and sulfuric acid or organics and ammonia in particle growth, which could be relevant in other conditions. However, when using measured sulfuric acid concentrations, we cannot accurately model the GRs without a term depending on $NH_3$ concentrations. This is consistent with the recent findings that bases can enhance initial GRs (*31*, *33*), e.g., due to a significant fraction of sulfuric acid bonded to acid-base clusters (*31*, *34*) and therefore not included in the sulfuric acid monomer measurement. It should be noted that reactive uptake, particle-phase reactions, and other growth mechanisms than nonreversible condensation can be important for growth at larger sizes.

## Composition of clusters during multicomponent experiments

We measured the chemical composition of freshly formed clusters with mass spectrometric methods, shown as a mass defect plot (Fig. 5A and fig. S7). The mass spectra from the multicomponent experiments are remarkably similar to those recorded in Hyytiälä during NPF (Fig. 5B) (*10*, *35*), indicating that the underlying chemistry in the chamber was very similar to that under ambient atmospheric conditions.

We find that HOMs, $H_2SO_4$, and $NH_3$ are able to cluster with each other in many different ways. Similar to pure biogenic experiments (*15*), we detect non-nitrate HOMs clustered with $NO_3^-$; but now we detect also ONs clustered with $NO_3^-$. Both non-nitrate HOMs and ONs are also capable of forming clusters with $HSO_4^-$. While the upper part of the mass defect plot (Fig. 5) is characterized by these organic clusters, the lower part is dominated by inorganic clusters. In addition to pure sulfuric acid clusters [$(H_2SO_4)_{0-3}HSO_{4,5}^-$)], we see sulfuric acid clusters containing ammonia, the largest one being $(H_2SO_4)_9(NH_3)_8HSO_4^-$. During ternary ($H_2SO_4$-$H_2O$-$NH_3$) nucleation, the entire spectrum is composed solely of those two compounds, up to 1500 Thomson (Th), with approximately one-to-one acid-base ratio (*10*). However, this is not the case in the multicomponent experiments or in the atmosphere. We believe that, once larger acid-base clusters are formed, they can interact with organics, creating very large clusters, whose identities cannot be resolved with current instrumentation due to their size and complex elemental composition. Some multicomponent HOM-$H_2SO_4$-$NH_3$-$NH_4^+$ clusters can be detected in the positive ion side. Positive ions are mainly composed of non-nitrate HOMs and ONs up to tetramer, with and without ammonia as core ion, and

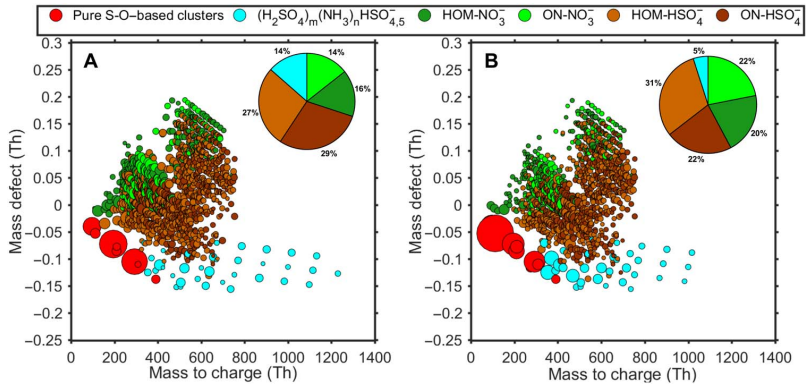


**Fig. 5. Negative ions and ion clusters detected during multicomponent NPF in the CLOUD chamber and in Hyytiälä.** The mass defect shows the difference between nominal and exact mass of the ions detected with the negative atmospheric pressure interface–time-of-flight mass spectrometer. (**A**). Data from the CLOUD chamber, averaged over several experiments (the orange and red points in Fig. 3) with $H_2SO_4$ ($1 \times 10^6$ to $1 \times 10^7$ $cm^{-3}$), $NO_x$ (1 ppb), and $NH_3$ (200 to 500 pptv). (**B**) Data from Hyytiälä during an NPF event on 5 April 2012. The colored symbols indicate the identified ions: pure sulfuric acid and S-O–based clusters (red), sulfuric acid–ammonia clusters (cyan), HOMs clustered with $NO_3^-$ (dark green), ONs clustered with $NO_3^-$ (light green), HOMs clustered with $HSO_4^-$ (light brown), and ON clustered with $HSO_4^-$ (dark brown). The symbol size corresponds to the relative signal intensity on a logarithmic scale. The pie charts give the fraction of all identified peaks, excluding the pure S-O–based peaks.

$H_2SO_4$-$NH_3$-$NH_4^+$ clusters (fig. S7). The clusters might also contain water molecules that evaporate during sampling.

## DISCUSSION

In summary, we have shown that sulfuric acid, ammonia, and organic vapors have a synergetic effect on NPF. Sulfuric acid, together with ammonia, can enhance particle formation in situations when the HOM concentration alone is not high enough to form substantial amounts of particles and enables the formed particles to grow past 3 nm before the biogenic vapors take over in the growth process. The efficiency of biogenic vapors to form aerosol particles strongly depends on the amount of non-nitrate HOMs formed; thus, higher $NO_x$ concentrations tend to suppress NPF and initial growth in environments similar to daytime boreal forest, while the growth of larger particles is less severely affected. Nucleation and GRs are sensitive to changes in any of the precursor vapor concentrations (HOMs, $H_2SO_4$, and $NH_3$) and the $NO_x$ concentration. This sensitivity can partly explain the wide range of observed atmospheric nucleation rates for a given sulfuric acid concentration.

We have measured three critical parameters associated with NPF: the nucleation rate, the GR, and the composition of the growing clusters. All three are consistent with observations in the atmosphere. Thus, we are able to reproduce the observations at daytime boreal forest conditions in the laboratory. The results from a chemical transport model (fig. S8) show that there is almost always sufficient $NH_3$ in the continental boundary layer to combine efficiently with $H_2SO_4$ and HOMs due to effective long-range transport of anthropogenic pollutants. This pattern favors the multicomponent mechanism over pure biogenic nucleation in the present-day atmosphere. The results presented here can almost certainly be extended to other chemical systems; specifically, HOMs can be produced from other organic vapors than MTs, and the stabilizing agent for sulfuric acid could be amines in addition to ammonia. Therefore, we believe that the multicomponent acid-base organic mechanism is dominant in the continental boundary layer in all relatively clean to moderately polluted present-day environments.

Possible future reductions in anthropogenic emissions of $SO_2$ and $NH_3$ may reduce particle formation involving $H_2SO_4$, while a reduction of $NO_x$ could possibly promote NPF from organic vapors. Thus, the climate effects of these measures depend strongly on which compounds are regulated. Understanding the complex interplay between different anthropogenic and biogenic vapors, their oxidants, and primary particles remains a key question in assessing the role of NPF in the global climate system.

## MATERIALS AND METHODS

### Experimental design

The objective of this study was to explore the conditions required to replicate daytime NPF and growth as it is observed at the Hyytiälä SMEAR II station, which is one of the most studied field sites in this respect, located in the boreal forest region in southern Finland (*36*). Most of the experiments were performed during September to December 2015 (CLOUD10 campaign) at the CLOUD facility (see below) at CERN, Geneva. To find the correct combination of condensable vapors, we first measured nucleation and GRs in the presence of pure biogenic precursors only (mixture of alpha-pinene and delta-3-carene). The total MT mixing ratio was varied between 100 and 1500 pptv. The background sulfuric acid concentration for those experiments was $<2 \times 10^5$ cm$^{-3}$. Then, 1 to 5 ppbv of $SO_2$ were added to study the influence of sulfuric acid on pure biogenic nucleation, resulting in sulfuric acid concentrations of $5 \times 10^6$ to $6 \times 10^7$ cm$^{-3}$. The measurements at different $SO_2$-MT concentration pairs were repeated at four different mixing ratios of nitrogen oxides in the chamber 0, 0.7, 2, and 5 ppbv, with a $NO/NO_2$ ratio of ca. 0.6%. Here, we aimed to produce a similar fraction of ONs from all HOMs, as is observed in Hyytiälä during NPF. Last, we added ammonia (10 to 3000 pptv) to the chamber and repeated a subset of experiments in the presence of all the precursors (MTs, $SO_2$, and $NH_3$) and $NO_x$. The estimated background $NH_3$ mixing ratio in the chamber (i.e., before $NH_3$ addition) is ca. 2 pptv (*21*, *37*).

In fall 2016, additional experiments were performed during the CLOUD11 campaign at lower $H_2SO_4$ concentrations ($1 \times 10^6$ to $2 \times 10^7$ cm$^{-3}$), two MT mixing ratios (600 and 1200 pptv), and three $NH_3$ levels (~10, 200, and 500 pptv). Between CLOUD10 and CLOUD11 campaigns, the UV light system in the chamber was enhanced (see below), enabling using a 7% $NO/NO_2$ ratio with 1 ppbv of total $NO_x$, typical of daytime Hyytiälä (*38*). Figures 3 and 5 and fig. S7 show data from the CLOUD11 campaign. Although the relation between $J$ and HOMs and $H_2SO_4$ and $NH_3$ was explored at a $NO/NO_2$ ratio lower than 7% (Figs. 1, 2, and 4), we believe that this affects mainly the fraction of non-nitrate to nitrate HOMs in the chamber and not the particle formation process from the product molecules.

To study the neutral and ion-induced nucleation pathway separately, most of the experiments were conducted first at neutral and then at GCR (see below) conditions. All of the experiments for this study were performed at 278 K and 38% RH.

It should be noted that our current study differs in several important ways from Riccobono *et al.* (*11*) and Schobesberger *et al.* (*10*), which also show quantitative agreement of the nucleation rates from a chamber study with ambient observations, in the absence of added $NH_3$. First, and most importantly, the experiments in those studies focused on second-generation products formed via oxidation of pinanediol, a very low vapor pressure surrogate for first-generation alpha-pinene oxidation products, so the chemical system was different. The SOA mass yields from pinanediol are much higher than those from alpha-pinene itself, and it is plausible that the oxidation products require less stabilization than the first-generation products studied here. Second, those experiments did not include $NO_x$, which at least partly compensates the enhancing effect from $NH_3$. Moreover, the mass spectra in the study of Riccobono *et al.* (*11*) revealed some clusters including $NH_3$ and dimethylamine at the low pptv level. Further experiments would be required to assess the enhancement of $J$ by trace concentrations of amines in a HOM-$H_2SO_4$ system.

### The CLOUD facility

The CLOUD chamber (*16*, *17*) is a temperature-controlled stainless steel cylinder with a volume of 26.1 m$^3$ located at CERN, Geneva, Switzerland. To ensure cleanliness, all inner surfaces of the chamber are electropolished. Before each campaign, the chamber was rinsed with ultrapure water and subsequently heated to 373 K. While cooling down to operating temperature, the chamber was flushed with humidified synthetic air containing several ppmv (parts per million by volume) of ozone. Thus, the background total VOC concentration is in the sub-ppbv level (*39*) and the contamination from condensable vapors is mostly below the detection limit of our instruments [sub-pptv (*15*)]. A sophisticated gas supply system was used to carefully control the amounts of trace gases added to the chamber.

A high voltage field cage (±30 kV) inside the chamber can be switched on to remove all ions from the chamber (referred to as "neutral conditions," N). When the electric field is off, natural GCRs are creating ions in the chamber, as is the situation in the atmosphere. This is referred to as "GCR conditions." Ion concentrations in the chamber can be artificially increased by using the pion beam from the CERN Proton Synchrotron (3.5 GeV/c). This is called "π conditions" (not used in this study).

The chamber was equipped with several UV light systems. In all the experiments described in this study, so-called UVH light (4 × 200 W Hamamatsu Hg-Xe lamps producing light in the wavelength range of 250 to 450 nm) was used to produce OH. In CLOUD10, additionally, a UV laser (4-W excimer laser; KrF, 248 nm) was used in some of the experiments to achieve higher $H_2SO_4$ concentrations. Between the CLOUD10 and CLOUD11 campaigns, the intensity of the UVH light was increased by renewing and shortening the optical fibers, which deliver the light into the chamber. Therefore, the use of the UV laser was not necessary, as the UVH system could supply the same wavelengths. In CLOUD11, also a UV-sabre (400-W UVS3, centered on 385 nm) was available, with the main purpose to form NO from $NO_2$. Thus, the NO/$NO_2$ ratio could be controlled by changing the UV-sabre light intensity. The $NO_2$ photolysis frequency, $j_{NO2}$, was characterized using $NO_2$ actinometry and varying the UV-sabre intensity. In CLOUD10, we injected NO directly into the chamber (leading to a constant NO/$NO_2$). More details of the facility can be found elsewhere (*16*, *17*).

The instruments used to record chamber conditions, gas and particle concentration, as well as methods to calculate particle formation and GRs were similar to previous CLOUD publications, and they are described in Supplementary Materials and Methods.

### Statistical analysis

The correlation coefficients mentioned in the text and some figure captions were calculated with Matlab using function corrcoef, which gives Pearson's correlation coefficient and the associated *P* values for testing the null hypothesis that there is no relationship between the observed phenomena. The correlation is considered significant when *P* is smaller than 0.05. The correlation coefficients, *P* values, and sample sizes between the nucleation rates ($J_{1.7}$) and different gas phase precursor concentrations are summarized in table S1 separately for neutral and GCR experiments before and after $NH_3$ addition.

## SUPPLEMENTARY MATERIALS

Supplementary material for this article is available at http://advances.sciencemag.org/cgi/content/full/4/12/eaau5363/DC1

Supplementary Materials and Methods

Fig. S1. The effect of different additional vapors on the NPF rates ($J_{2.5}$).

Fig. S2. The effect of different additional vapors on the biogenic nucleation rate ($J_{1.7}$) at different $NO_x$ concentrations.

Fig. S3. Nucleation rates ($J_{1.7}$) as a function of the MT to $NO_x$ ratio (MT/$NO_x$).

Fig. S4. Nucleation rates ($J_{1.7}$) as a function of $NH_3$ mixing ratio.

Fig. S5. Modeled versus measured nucleation rates.

Fig. S6. Modeled versus measured GRs.

Fig. S7. Positive ions and ion clusters detected during multicomponent NPF in the CLOUD chamber.

Fig. S8. Global annual mean concentrations of vapors involved in NPF.

Table S1. Pearson's correlation coefficient (*R*) between $J_{1.7}$ and the concentration of different precursors in the chamber.

References (*41*–*56*)

## REFERENCES AND NOTES


1. D. V. Spracklen, K. S. Carslaw, M. Kulmala, V.-M. Kerminen, G. W. Mann, S.-L. Sihto, The contribution of boundary layer nucleation events to total particle concentrations on regional and global scales. *Atmos. Chem. Phys.* **6**, 5631–5648 (2006).
2. D. M. Westervelt, J. R. Pierce, I. Riipinen, W. Trivitayanurak, A. Hamed, M. Kulmala, A. Laaksonen, S. Decesari, P. J. Adams, Formation and growth of nucleated particles into cloud condensation nuclei: Model-measurement comparison. *Atmos. Chem. Phys.* **13**, 7645–7663 (2013).
3. E. M. Dunne, E. M. Dunne, H. Gordon, A. Kürten, J. Almeida, J. Duplissy, C. Williamson, I. K. Ortega, K. J. Pringle, A. Adamov, U. Baltensperger, P. Barmet, F. Benduhn, F. Bianchi, M. Breitenlechner, A. Clarke, J. Curtius, J. Dommen, N. M. Donahue, S. Ehrhart, R. C. Flagan, A. Franchin, R. Guida, J. Hakala, A. Hansel, M. Heinritzi, T. Jokinen, J. Kangasluoma, J. Kirkby, M. Kulmala, A. Kupc, M. J. Lawler, K. Lehtipalo, V. Makhmutov, G. Mann, S. Mathot, J. Merikanto, P. Miettinen, A. Nenes, A. Onnela, A. Rap, C. L. Reddington, F. Riccobono, N. A. Richards, M. P. Rissanen, L. Rondo, N. Sarnela, S. Schobesberger, K. Sengupta, M. Simon, M. Sipilä, J. N. Smith, Y. Stozkhov, A. Tomé, J. Tröstl, P. E. Wagner, D. Wimmer, P. M. Winkler, D. R. Worsnop, K. S. Carslaw, Global atmospheric particle formation from CERN CLOUD measurements. *Science* **354**, 1119–1124 (2016).
4. J. Rogelj, S. Rao, D. L. McCollum, S. Pachauri, Z. Klimont, V. Krey, K. Riahi, Air-pollution emission ranges consistent with the representative concentration pathways. *Nat. Clim. Chang.* **4**, 446–450 (2014).
5. M. Kulmala, J. Kontkanen, H. Junninen, K. Lehtipalo, H. E. Manninen, T. Nieminen, T. Petäjä, M. Sipilä, S. Schobesberger, P. Rantala, A. Franchin, T. Jokinen, E. Järvinen, M. Äijälä, J. Kangasluoma, J. Hakala, P. P. Aalto, P. Paasonen, J. Mikkilä, J. Vanhanen, J. Aalto, H. Hakola, U. Makkonen, T. Ruuskanen, R. L. Mauldin III, J. Duplissy, H. Vehkamäki, J. Bäck, A. Kortelainen, I. Riipinen, T. Kurtén, M. V. Johnston, J. N. Smith, M. Ehn, T. F. Mentel, K. E. J. Lehtinen, A. Laaksonen, V.-M. Kerminen, D. R. Worsnop, Direct observations of atmospheric aerosol nucleation. *Science* **339**, 943–946 (2013).
6. R. Zhang, A. Khalizov, L. Wang, M. Hu, W. Xu, Nucleation and growth of nanoparticles in the atmosphere. *Chem. Rev.* **112**, 1957–2011 (2012).
7. R. J. Weber, J. J. Marti, P. H. McMurry, F. L. Eisele, D. J. Tanner, A. Jefferson, Measured atmospheric new particle formation rates: Implications for nucleation mechanisms. *Chem. Eng. Commun.* **151**, 53–64 (1996).
8. S.-L. Sihto, M. Kulmala, V.-M. Kerminen, M. Dal Maso, T. Petäjä, I. Riipinen, H. Korhonen, F. Arnold, R. Janson, M. Boy, A. Laaksonen, K. E. J. Lehtinen, Atmospheric sulphuric acid and aerosol formation: Implications from atmospheric measurements for nucleation and early growth mechanisms. *Atmos. Chem. Phys.* **6**, 4079–4091 (2006).
9. I. Riipinen, T. Yli-Juuti, J. R. Pierce, T. Petäjä, D. R. Worsnop, M. Kulmala, N. M. Donahue, The contribution of organics to atmospheric nanoparticle growth. *Nat. Geosci.* **5**, 453–458 (2012).
10. S. Schobesberger, H. Junninen, F. Bianchi, G. Lönn, M. Ehn, K. Lehtipalo, J. Dommen, S. Ehrhart, I. K. Ortega, A. Franchin, T. Nieminen, F. Riccobono, M. Hutterli, J. Duplissy, J. Almeida, A. Amorim, M. Breitenlechner, A. J. Downard, E. M. Dunne, R. C. Flagan, M. Kajos, H. Keskinen, J. Kirkby, A. Kupc, A. Kürten, T. Kurtén, A. Laaksonen, S. Mathot, A. Onnela, A. P. Praplan, L. Rondo, F. D. Santos, S. Schallhart, R. Schnitzhofer, M. Sipilä, A. Tomé, G. Tsagkogeorgas, H. Vehkamäki, D. Wimmer, U. Baltensperger, K. S. Carslaw, J. Curtius, A. Hansel, T. Petäjä, M. Kulmala, N. M. Donahue, D. R. Worsnop, Molecular understanding of atmospheric particle formation from sulfuric acid and large oxidized organic molecules. *Proc. Natl. Acad. Sci. U.S.A.* **110**, 17223–17228 (2013).
11. F. Riccobono, S. Schobesberger, C. E. Scott, J. Dommen, I. K. Ortega, L. Rondo, J. Almeida, A. Amorim, F. Bianchi, M. Breitenlechner, A. David, A. Downard, E. M. Dunne, J. Duplissy, S. Ehrhart, R. C. Flagan, A. Franchin, A. Hansel, H. Junninen, M. Kajos, H. Keskinen, A. Kupc, A. Kürten, A. N. Kvashin, A. Laaksonen, K. Lehtipalo, V. Makhmutov, S. Mathot, T. Nieminen, A. Onnela, T. Petäjä, A. P. Praplan, F. D. Santos, S. Schallhart, J. H. Seinfeld, M. Sipilä, D. V. Spracklen, Y. Stozhkov, F. Stratmann, A. Tomé, G. Tsagkogeorgas, P. Vaattovaara, Y. Viisanen, A. Vrtala, P. E. Wagner, E. Weingartner, H. Wex, D. Wimmer, K. S. Carslaw, J. Curtius, N. M. Donahue, J. Kirkby, M. Kulmala, D. R. Worsnop, U. Baltensperger, Oxidation products of biogenic emissions contribute to nucleation of atmospheric particles. *Science* **344**, 717–721 (2014).
12. M. Ehn, J. A. Thornton, E. Kleist, M. Sipilä, H. Junninen, I. Pullinen, M. Springer, F. Rubach, R. Tillmann, B. Lee, F. Lopez-Hilfiker, S. Andres, I.-H. Acir, M. Rissanen, T. Jokinen, S. Schobesberger, J. Kangasluoma, J. Kontkanen, T. Nieminen, T. Kurtén, L. B. Nielsen, S. Jørgensen, H. G. Kjaergaard, M. Canagaratna, M. Dal Maso, T. Berndt, T. Petäjä, A. Wahner, V.-M. Kerminen, M. Kulmala, D. R. Worsnop, J. Wildt, T. F. Mentel, A large source of low-volatility secondary organic aerosol. *Nature* **506**, 476–479 (2014).
13. F. Bianchi, J. Tröstl, H. Junninen, C. Frege, S. Henne, C. R. Hoyle, U. Molteni, E. Herrmann, A. Adamov, N. Bukowiecki, X. Chen, J. Duplissy, M. Gysel, M. Hutterli, J. Kangasluoma, J. Kontkanen, A. Kürten, H. E. Manninen, S. Münch, O. Peräkylä, T. Petäjä, L. Rondo, C. Williamson, E. Weingartner, J. Curtius, D. R. Worsnop, M. Kulmala, J. Dommen, U. Baltensperger, New particle formation in the free troposphere: A question of chemistry and timing. *Science* **352**, 1109–1112 (2016).

14. M. Sipilä, N. Sarnela, T. Jokinen, H. Henschel, H. Junninen, J. Kontkanen, S. Richters, J. Kangasluoma, A. Franchin, O. Peräkylä, M. P. Rissanen, M. Ehn, H. Vehkamäki, T. Kurten, T. Berndt, T. Petäjä, D. Worsnop, D. Ceburnis, V.-M. Kerminen, M. Kulmala, C. O'Dowd, Molecular-scale evidence of aerosol particle formation via sequential addition of $HIO_3$. *Nature* **537**, 532–534 (2016).
15. J. Kirkby, J. Duplissy, K. Sengupta, C. Frege, H. Gordon, C. Williamson, M. Heinritzi, M. Simon, C. Yan, J. Almeida, J. Tröstl, T. Nieminen, I. K. Ortega, R. Wagner, A. Adamov, A. Amorim, A.-K. Bernhammer, F. Bianchi, M. Breitenlechner, S. Brilke, X. Chen, J. Craven, A. Dias, S. Ehrhart, R. C. Flagan, A. Franchin, C. Fuchs, R. Guida, J. Hakala, C. R. Hoyle, T. Jokinen, H. Junninen, J. Kangasluoma, J. Kim, M. Krapf, A. Kürten, A. Laaksonen, K. Lehtipalo, V. Makhmutov, S. Mathot, U. Molteni, A. Onnela, O. Peräkylä, F. Piel, T. Petäjä, A. P. Praplan, K. Pringle, A. Rap, N. A. D. Richards, I. Riipinen, M. P. Rissanen, L. Rondo, N. Sarnela, S. Schobesberger, C. E. Scott, J. H. Seinfeld, M. Sipilä, G. Steiner, Y. Stozhkov, F. Stratmann, A. Tomé, A. Virtanen, A. L. Vogel, A. C. Wagner, P. E. Wagner, E. Weingartner, D. Wimmer, P. M. Winkler, P. Ye, X. Zhang, A. Hansel, J. Dommen, N. M. Donahue, D. R. Worsnop, U. Baltensperger, M. Kulmala, K. S. Carslaw & J. Curtius, Ion-induced nucleation of pure biogenic particles. *Nature* **533**, 521–526 (2016).
16. J. Kirkby, J. Curtius, J. Almeida, E. Dunne, J. Duplissy, S. Ehrhart, A. Franchin, S. Gagné, L. Ickes, A. Kürten, A. Kupc, A. Metzger, F. Riccobono, L. Rondo, S. Schobesberger, G. Tsagkogeorgas, D. Wimmer, A. Amorim, F. Bianchi, M. Breitenlechner, A. David, J. Dommen, A. Downard, M. Ehn, R. C. Flagan, S. Haider, A. Hansel, D. Hauser, W. Jud, H. Junninen, F. Kreissl, A. Kvashin, A. Laaksonen, K. Lehtipalo, J. Lima, E. R. Lovejoy, V. Makhmutov, S. Mathot, J. Mikkilä, P. Minginette, S. Mogo, T. Nieminen, A. Onnela, P. Pereira, T. Petäjä, R. Schnitzhofer, J. H. Seinfeld, M. Sipilä, Y. Stozhkov, F. Stratmann, A. Tomé, J. Vanhanen, Y. Viisanen, A. Vrtala, P. E. Wagner, H. Walther, E. Weingartner, H. Wex, P. M. Winkler, K. S. Carslaw, D. R. Worsnop, U. Baltensperger, M. Kulmala, Role of sulphuric acid, ammonia and galactic cosmic rays in atmospheric aerosol nucleation. *Nature* **476**, 429–433 (2011).
17. J. Duplissy, J. Merikanto, A. Franchin, G. Tsagkogeorgas, J. Kangasluoma, D. Wimmer, H. Vuollekoski, S. Schobesberger, K. Lehtipalo, R. C. Flagan, D. Brus, N. M. Donahue, H. Vehkamäki, J. Almeida, A. Amorim, P. Barmet, F. Bianchi, M. Breitenlechner, E. M. Dunne, R. Guida, H. Henschel, H. Junninen, J. Kirkby, A. Kürten, A. Kupc, A. Määttänen, V. Makhmutov, S. Mathot, T. Nieminen, A. Onnela, A. P. Praplan, F. Riccobono, L. Rondo, G. Steiner, A. Tome, H. Walther, U. Baltensperger, K. S. Carslaw, J. Dommen, A. Hansel, T. Petäjä, M. Sipilä, F. Stratmann, A. Vrtala, P. E. Wagner, D. R. Worsnop, J. Curtius, M. Kulmala, Effect of ions on sulfuric acid-water binary particle formation: 2. Experimental data and comparison with QC-normalized classical nucleation theory. *J. Geophys. Res. Atmos.* **121**, 1752–1775 (2016).
18. H. Yu, L. Dai, Y. Zhao, V. P. Kanawade, S. N. Tripathi, X. Ge, M. Chen, S.-H. Lee, Laboratory observations of temperature and humidity dependencies of nucleation and growth rates of sub-3nm particles. *J. Geophys. Res. Atmos.* **122**, 1919–1929 (2017).
19. J. Almeida, S. Schobesberger, A. Kürten, I. K. Ortega, O. Kupiainen-Määttä, A. P. Praplan, A. Adamov, A. Amorim, F. Bianchi, M. Breitenlechner, A. David, J. Dommen, N. M. Donahue, A. Downard, E. Dunne, J. Duplissy, S. Ehrhart, R. C. Flagan, A. Franchin, R. Guida, J. Hakala, A. Hansel, M. Heinritzi, H. Henschel, T. Jokinen, H. Junninen, M. Kajos, J. Kangasluoma, H. Keskinen, A. Kupc, T. Kurtén, A. N. Kvashin, A. Laaksonen, K. Lehtipalo, M. Leiminger, J. Leppä, V. Loukonen, V. Makhmutov, S. Mathot, M. J. McGrath, T. Nieminen, T. Olenius, A. Onnela, T. Petäjä, F. Riccobono, I. Riipinen, M. Rissanen, L. Rondo, T. Ruuskanen, F. D. Santos, N. Sarnela, S. Schallhart, R. Schnitzhofer, J. H. Seinfeld, M. Simon, M. Sipilä, Y. Stozhkov, F. Stratmann, A. Tomé, J. Tröstl, G. Tsagkogeorgas, P. Vaattovaara, Y. Viisanen, A. Virtanen, A. Vrtala, P. E. Wagner, E. Weingartner, H. Wex, C. Williamson, D. Wimmer, P. Ye, T. Yli-Juuti, K. S. Carslaw, M. Kulmala, J. Curtius, U. Baltensperger, D. R. Worsnop, H. Vehkamäki, J. Kirkby, Molecular understanding of sulphuric acid-amine particle nucleation in the atmosphere. *Nature* **502**, 359–363 (2013).
20. C. N. Jen, P. H. McMurry, D. R. Hanson, Stabilization of sulfuric acid dimers by ammonia, methylamine, dimethylamine, and trimethylamine. *J. Geophys. Res. Atmos.* **119**, 7502–7514 (2014).
21. A. Kürten, F. Bianchi, J. Almeida, O. Kupiainen-Määttä, E. M. Dunne, J. Duplissy, C. Williamson, P. Barmet, M. Breitenlechner, J. Dommen, N. M. Donahue, R. C. Flagan, A. Franchin, H. Gordon, J. Hakala, A. Hansel, M. Heinritzi, L. Ickes, T. Jokinen, J. Kangasluoma, J. Kim, J. Kirkby, A. Kupc, K. Lehtipalo, M. Leiminger, V. Makhmutov, A. Onnela, I. K. Ortega, T. Petäjä, A. P. Praplan, F. Riccobono, M. P. Rissanen, L. Rondo, R. Schnitzhofer, S. Schobesberger, J. N. Smith, G. Steiner, Y. Stozhkov, A. Tomé, J. Tröstl, G. Tsagkogeorgas, P. E. Wagner, D. Wimmer, P. Ye, U. Baltensperger, K. Carslaw, M. Kulmala, J. Curtius, Experimental particle formation rates spanning tropospheric sulfuric acid and ammonia abundances, ion production rates, and temperatures. *J. Geophys. Res. Atmos.* **121**, 12377–12400 (2016).
22. R. Y. Zhang, I. Suh, J. Zhao, D. Zhang, E. C. Fortner, X. Tie, L. T. Molina, M. J. Molina, Atmospheric new particle formation enhanced by organic acids. *Science* **304**, 1487–1490 (2004).
23. A. A. Presto, K. E. Hartz, N. M. Donahue, Secondary organic aerosol production from terpene ozonolysis. 2. Effect of NOx concentration. *Environ. Sci. Technol.* **39**, 7046–7054 (2005).
24. N. L. Ng, P. S. Chhabra, A. W. H. Chan, J. D. Surratt, J. H. Kroll, A. J. Kwan, D. C. McCabe, P. O. Wennberg, A. Sorooshian, S. M. Murphy, N. F. Dalleska, R. C. Flagan, J. H. Seinfeld, Effect of NOx level on secondary organic aerosol (SOA) formation from the photooxidation of terpenes. *Atmos. Chem. Phys.* **7**, 5159–5174 (2007).
25. J. Wildt, T. F. Mentel, A. Kiendler-Scharr, T. Hoffmann, S. Andres, M. Ehn, E. Kleist, P. Müsgen, F. Rohrer, Y. Rudich, M. Springer, R. Tillmann, A. Wahner, Suppression of new particle formation from monoterpene oxidation by $NO_x$. *Atmos. Chem. Phys.* **14**, 2789–2804 (2014).
26. J. Rinne, H. Hakola, T. Laurila, U. Rannik, Canopy scale monoterpene emissions of *Pinus sylvestris* dominated forests. *Atmos. Environ.* **34**, 1099–1107 (2000).
27. J. L. Fry, D. C. Draper, K. C. Barsanti, J. N. Smith, J. Ortega, P. M. Winkler, M. J. Lawler, S. S. Brown, P. M. Edwards, R. C. Cohen, L. Lee, Secondary organic aerosol formation and organic nitrate yield from NO3 oxidation of biogenic hydrocarbons. *Environ. Sci. Technol.* **48**, 11944–11953 (2014).
28. H. E. Manninen, T. Nieminen, E. Asmi, S. Gagné, S. Häkkinen, K. Lehtipalo, P. Aalto, M. Vana, A. Mirme, S. Mirme, U. Hörrak, C. Plass-Dülmer, G. Stange, G. Kiss, A. Hoffer, N. Töro, M. Moerman, B. Henzing, G. De Leeuw, M. Brinkenberg, G. N. Kouvarakis, A. Bougiatioti, N. Mihalopoulos, C. O'Dowd, D. Ceburnis, A. Arneth, B. Svenningsson, E. Swietlicki, L. Tarozzi, S. Decesari, M. C. Facchini, W. Birmili, A. Sonntag, A. Wiedensohler, J. Boulon, K. Sellegri, P. Laj, M. Gysel, N. Bukowiecki, E. Weingartner, G. Wehrle, A. Laaksonen, A. Hamed, J. Joutsensaari, T. Petäjä, V. M. Kerminen, M. Kulmala, EUCAARI ion spectrometer measurements at 12 European sites-analysis of new particle formation events. *Atmos. Chem. Phys.* **10**, 7907–7927 (2010).
29. C. Kuang, M. Chen, J. Zhao, J. Smith, P. H. McMurry, J. Wang, Size and time-resolved growth rate measurements of 1 to 5 nm freshly formed atmospheric nuclei. *Atmos. Chem. Phys.* **12**, 3573–3589 (2012).
30. T. Nieminen, K. E. J. Lehtinen, M. Kulmala, Sub-10 nm particle growth by vapor condensation - effects of vapor molecule size and particle thermal speed. *Atmos. Chem. Phys.* **10**, 9773–9779 (2010).
31. K. Lehtipalo, L. Rondo, J. Kontkanen, S. Schobesberger, T. Jokinen, N. Sarnela, A. Kürten, S. Ehrhart, A. Franchin, T. Nieminen, F. Riccobono, M. Sipilä, T. Yli-Juuti, J. Duplissy, A. Adamov, L. Ahlm, J. Almeida, A. Amorim, F. Bianchi, M. Breitenlechner, J. Dommen, A. J. Downard, E. M. Dunne, R. C. Flagan, R. Guida, J. Hakala, A. Hansel, W. Jud, J. Kangasluoma, V.-M. Kerminen, H. Keskinen, J. Kim, J. Kirkby, A. Kupc, O. Kupiainen-Määttä, A. Laaksonen, M. J. Lawler, M. Leiminger, S. Mathot, T. Olenius, I. K. Ortega, A. Onnela, T. Petäjä, A. Praplan, M. P. Rissanen, T. Ruuskanen, F. D. Santos, S. Schallhart, R. Schnitzhofer, M. Simon, J. N. Smith, J. Tröstl, G. Tsagkogeorgas, A. Tomé, P. Vaattovaara, H. Vehkamäki, A. E. Vrtala, P. E. Wagner, C. Williamson, D. Wimmer, P. M. Winkler, A. Virtanen, N. M. Donahue, K. S. Carslaw, U. Baltensperger, I. Riipinen, J. Curtius, D. R. Worsnop, M. Kulmala, The effect of acid–base clustering and ions on the growth of atmospheric nano-particles. *Nat. Commun.* **7**, 11594 (2016).
32. J. Tröstl, W. K. Chuang, H. Gordon, M. Heinritzi, C. Yan, U. Molteni, L. Ahlm, C. Frege, F. Bianchi, R. Wagner, M. Simon, K. Lehtipalo, C. Williamson, J. S. Craven, J. Duplissy, A. Adamov, J. Almeida, A.-K. Bernhammer, M. Breitenlechner, S. Brilke, A. Dias, S. Ehrhart, R. C. Flagan, A. Franchin, C. Fuchs, R. Guida, M. Gysel, A. Hansel, C. R. Hoyle, T. Jokinen, H. Junninen, J. Kangasluoma, H. Keskinen, J. Kim, M. Krapf, A. Kürten, A. Laaksonen, M. Lawler, M. Leiminger, S. Mathot, O. Möhler, T. Nieminen, A. Onnela, T. Petäjä, F. M. Piel, P. Miettinen, M. P. Rissanen, L. Rondo, N. Sarnela, S. Schobesberger, K. Sengupta, M. Sipilä, J. N. Smith, G. Steiner, A. Tomè, A. Virtanen, A. C. Wagner, E. Weingartner, D. Wimmer, P. M. Winkler, P. Ye, K. S. Carslaw, J. Curtius, J. Dommen, J. Kirkby, M. Kulmala, I. Riipinen, D. R. Worsnop, N. M. Donahue, U. Baltensperger, The role of low-volatility organic compounds in initial particle growth in the atmosphere. *Nature* **533**, 527–531 (2016).
33. H. Yu, R. McGraw, S.-H. Lee, Effects of amines on formation of sub-3 nm particles and their subsequent growth. *Geophys. Res. Lett.* **39**, L02807 (2012).
34. A. Kürten, T. Jokinen, M. Simon, M. Sipilä, N. Sarnela, H. Junninen, A. Adamov, J. Almeida, A. Amorim, F. Bianchi, M. Breitenlechner, J. Dommen, N. M. Donahue, J. Duplissy, S. Ehrhart, R. C. Flagan, A. Franchin, J. Hakala, A. Hansel, M. Heinritzi, M. Hutterli, J. Kangasluoma, J. Kirkby, A. Laaksonen, K. Lehtipalo, M. Leiminger, V. Makhmutov, S. Mathot, A. Onnela, T. Petäjä, A. P. Praplan, F. Riccobono, M. P. Rissanen, L. Rondo, S. Schobesberger, J. H. Seinfeld, G. Steiner, A. Tomé, J. Tröstl, P. M. Winkler, C. Williamson, D. Wimmer, P. Ye, U. Baltensperger, K. S. Carslaw, M. Kulmala, D. R. Worsnop, J. Curtius, Neutral molecular cluster formation of sulfuric acid–dimethylamine observed in real time under atmospheric conditions. *Proc. Natl. Acad. Sci. U.S.A.* **111**, 15019–15024 (2014).
35. F. Bianchi, O. Garmash, X. He, C. Yan, S. Iyer, I. Rosendahl, Z. Xu, P. Rissanen Matti, M. Riva, R. Taipale, N. Sarnela, T. Petäjä, R. Worsnop Douglas, M. Kulmala, M. Ehn, H. Junninen, The role of highly oxygenated molecules (HOMs) in determining the composition of ambient ions in the boreal forest. *Atmos. Chem. Phys.* **17**, 13819–13831 (2017).
36. P. Hari, M. Kulmala, Station for measuring ecosystem-atmosphere relations (SMEAR II). *Boreal Environ. Res.* **10**, 315–322 (2005).
37. A. P. Praplan, F. Bianchi, J. Dommen, U. Baltensperger, Dimethylamine and ammonia measurements with ion chromatography during the CLOUD4 campaign. *Atmos. Meas. Tech.* **5**, 2161–2167 (2012).

38. M. Boy, M. Kulmala, T. M. Ruuskanen, M. Pihlatie, A. Reissell, P. P. Aalto, P. Keronen, M. Dal Maso, H. Hellen, H. Hakola, R. Jansson, M. Hanke, F. Arnold, Sulphuric acid closure and contribution to nucleation mode particle growth. *Atmos. Chem. Phys.* **5**, 863–878 (2005).
39. R. Schnitzhofer, A. Metzger, M. Breitenlechner, W. Jud, M. Heinritzi, L.-P. de Menezes, J. Duplissy, R. Guida, S. Haider, J. Kirkby, S. Mathot, P. Minginette, A. Onnela, H. Walther, A. Wasem, A. Hansel; The Cloud Team, Characterisation of organic contaminants in the CLOUD chamber at CERN. *Atmos. Meas. Tech.* **7**, 2159–2168 (2014).
40. T. Yli-Juuti, O. P. Tikkanen, H. E. Manninen, T. Nieminen, M. Kulmala, Analysis of sub-3 nm particle growth in connection with sulfuric acid in a boreal forest. *Boreal Environ. Res.* **21**, 287–298 (2016).
41. J. Vanhanen, J. Mikkilä, K. Lehtipalo, M. Sipilä, H. E. Manninen, E. Siivola, T. Petäjä, M. Kulmala, Particle size magnifier for nano-CN detection. *Aerosol Sci. Tech.* **45**, 533–542 (2011).
42. K. Lehtipalo, J. Leppa, J. Kontkanen, J. Kangasluoma, A. Franchin, D. Wimmer, S. Schobesberger, H. Junninen, T. Petaja, M. Sipila, J. Mikkila, J. Vanhanen, R. Worsnop Douglas, M. Kulmala, Methods for determining particle size distribution and growth rates between 1 and 3 nm using the Particle Size Magnifier. *Boreal Environ. Res.* **19**, 215–236 (2014).
43. D. Stolzenburg, G. Steiner, P. M. Winkler, A DMA-train for precision measurement of sub-10 nm aerosol dynamics. *Atmos. Meas. Tech.* **10**, 1639–1651 (2017).
44. S. Mirme, A. Mirme, The mathematical principles and design of the NAIS - a spectrometer for the measurement of cluster ion and nanometer aerosol size distributions. *Atmos. Meas. Tech.* **6**, 1061–1071 (2013).
45. T. Jokinen, M. Sipilä, H. Junninen, M. Ehn, G. Lönn, J. Hakala, T. Petäjä, R. L. Mauldin III, M. Kulmala, D. R. Worsnop, Atmospheric sulphuric acid and neutral cluster measurements using CI-APi-TOF. *Atmos. Chem. Phys.* **12**, 4117–4125 (2012).
46. H. Junninen, M. Ehn, T. Petäjä, L. Luosujärvi, T. Kotiaho, R. Kostiainen, U. Rohner, M. Gonin, K. Fuhrer, M. Kulmala, D. R. Worsnop, A high-resolution mass spectrometer to measure atmospheric ion composition. *Atmos. Meas. Tech.* **3**, 1039–1053 (2010).
47. M. Heinritzi, M. Simon, G. Steiner, C. W. Andrea, A. Kürten, A. Hansel, J. Curtius, Characterization of the mass-dependent transmission efficiency of a CIMS. *Atmos. Meas. Tech.* **9**, 1449–1460 (2016).
48. F. L. Eisele, D. J. Tanner, Measurement of the gas-phase concentration of $H_2SO_4$ and methane sulfonic-acid and estimates of $H_2SO_4$ production and loss in the atmosphere. *J. Geophys. Res. Atmos.* **98**, 9001–9010 (1993).
49. D. R. Hanson, P. H. McMurry, J. Jiang, D. Tanner, L. G. Huey, Ambient pressure proton transfer mass spectrometry: Detection of amines and ammonia. *Environ. Sci. Technol.* **45**, 8881–8888 (2011).
50. A. Kürten, L. Rondo, S. Ehrhart, J. Curtius, Performance of a corona ion source for measurement of sulfuric acid by chemical ionization mass spectrometry. *Atmos. Meas. Tech.* **4**, 437–443 (2011).
51. A. Kürten, A. Bergen, M. Heinritzi, M. Leiminger, V. Lorenz, F. Piel, M. Simon, R. Sitals, C. W. Andrea, J. Curtius, Observation of new particle formation and measurement of sulfuric acid, ammonia, amines and highly oxidized organic molecules at a rural site in central Germany. *Atmos. Chem. Phys.* **16**, 12793–12813 (2016).
52. M. Breitenlechner, L. Fischer, M. Hainer, M. Heinritzi, J. Curtius, A. Hansel, PTR3: An instrument for studying the lifecycle of reactive organic carbon in the atmosphere. *Anal. Chem.* **89**, 5825–5832 (2017).
53. J. Kangasluoma, A. Samodurov, M. Attoui, A. Franchin, H. Junninen, F. Korhonen, T. Kurtén, H. Vehkamäki, M. Sipilä, K. Lehtipalo, D. R. Worsnop, T. Petäjä, M. Kulmala, Heterogeneous nucleation onto ions and neutralized ions: Insights into sign-preference. *J. Phys. Chem. C* **120**, 7444–7450 (2016).
54. R. Wagner, H. E. Manninen, A. Franchin, K. Lehtipalo, S. Mirme, G. Steiner, T. Petäjä, M. Kulmala, On the accuracy of ion measurements using a Neutral cluster and Air Ion Spectrometer. *Boreal Environ. Res.* **21**, 230–241 (2016).
55. T. Olenius, I. Riipinen, K. Lehtipalo, H. Vehkamaki, Growth rates of atmospheric molecular clusters based on appearance times and collision-evaporation fluxes: Growth by monomers. *J. Aerosol Sci.* **78**, 55–70 (2014).
56. J. Kontkanen, T. Olenius, K. Lehtipalo, H. Vehkamäki, M. Kulmala, K. E. J. Lehtinen, Growth of atmospheric clusters involving cluster-cluster collisions: Comparison of different growth rate methods. *Atmos. Chem. Phys.* **16**, 5545–5560 (2016).



**Acknowledgments:** We thank CERN for supporting CLOUD with technical and financial resources, and for providing a particle beam from the CERN Proton Synchrotron. We thank P. Carrie, L.-P. De Menezes, J. Dumollard, K. Ivanova, F. Josa, I. Krasin, R. Kristic, A. Laassiri, O. S. Maksumov, B. Marichy, H. Martinati, S. V. Mizin, R. Sitals, A. Wasem, and M. Wilhelmsson for their contributions to the experiment. We thank tofTools team for providing programs for mass spectrometry analysis. **Funding:** This research has received funding from the EC Seventh Framework Programme and European Union's Horizon 2020 Programme [Marie Curie ITN (no. 316662 "CLOUD-TRAIN") MSCA-IF (no. 656994 "nano-CAVa"), MC-COFUND (grant nos. 600377 and 665779), and ERC (project no. 692891 "DAMOCLES," no. 638703 "COALA," no. 616075 "NANODYNAMITE," no. 335478 "QAPPA," no. 742206 "ATM-GP," and no. 714621 "GASPARCON")], the German Federal Ministry of Education and Research (project nos. 01LK0902A, 01LK1222A, and 01LK1601A), the Swiss National Science Foundation [project nos. 200021_140663, 206021_144947/1, 20FI20_159851, 200020_172602, 20FI20_172622, 200021_169090, and the Starting Grant IPR-SHOP (BSSGI0_155846)], the Academy of Finland (Center of Excellence no. 307331 and project nos. 139995, 137749, 299574, 251007, 296628, and 306853), the Finnish Funding Agency for Technology and Innovation, the Väisälä Foundation, the Nessling Foundation, the Austrian Science Fund (FWF; project no. J3951-N36), the Austrian research funding association (FFG, project no. 846050), the Portuguese Foundation for Science and Technology (project no. CERN/FP/116387/2010), the Swedish Research Council Formas (project no. 2015-749), Knut and Alice Wallenberg Foundation (Academy Fellowship AtmoRemove), Vetenskapsrådet (grant no. 2011-5120), the Presidium of the Russian Academy of Sciences and Russian Foundation for Basic Research (grant nos. 08-02-91006-CERN and 12-02-91522-CERN), the U.S. National Science Foundation (grant nos. AGS1136479, AGS1447056, AGS1439551, CHE1012293, AGS1649147, and AGS1602086), the Wallace Research Foundation, the U.S. Department of Energy (grant DE-SC0014469), the NERC GASSP (project no. NE/J024252/1m), the Royal Society (Wolfson Merit Award), UK Natural Environment Research Council (grant no. NE/K015966/1), Dreyfus Award (EP-11-117), the French National Research Agency, the Nord-Pas de Calais, and European Funds for Regional Economic Development Labex-Cappa (grant no. ANR-11-LABX-0005-01). **Author contributions:** K.L., C.Y., D.R.W., and M.K. designed the experiments and wrote the paper. K.L., C.Y., L.D., F.B., M.X., R.W., and D.S. analyzed the main datasets. All other authors contributed to the design of the facility and preparation of the instruments or data collection and analysis and commented on the manuscript. **Competing interests:** The authors declare that they have no competing interests. **Data and materials availability:** All data needed to evaluate the conclusions in the paper are present in the paper and/or the Supplementary Materials. Additional data related to this paper may be requested from the authors.

Submitted 20 June 2018
Accepted 15 November 2018
Published 12 December 2018
10.1126/sciadv.aau5363

**Citation:** K. Lehtipalo, C. Yan, L. Dada, F. Bianchi, M. Xiao, R. Wagner, D. Stolzenburg, L. R. Ahonen, A. Amorim, A. Baccarini, P. S. Bauer, B. Baumgartner, A. Bergen, A.-K. Bernhammer, M. Breitenlechner, S. Brilke, A. Buchholz, S. B. Mazon, D. Chen, X. Chen, A. Dias, J. Dommen, D. C. Draper, J. Duplissy, M. Ehn, H. Finkenzeller, L. Fischer, C. Frege, C. Fuchs, O. Garmash, H. Gordon, J. Hakala, X. He, L. Heikkinen, M. Heinritzi, J. C. Helm, V. Hofbauer, C. R. Hoyle, T. Jokinen, J. Kangasluoma, V.-M. Kerminen, C. Kim, J. Kirkby, J. Kontkanen, A. Kürten, M. J. Lawler, H. Mai, S. Mathot, R. L. Mauldin III, U. Molteni, L. Nichman, W. Nie, T. Nieminen, A. Ojdanic, A. Onnela, M. Passananti, T. Petäjä, F. Piel, V. Pospisilova, L. L. J. Quéléver, M. P. Rissanen, C. Rose, N. Sarnela, S. Schallhart, S. Schuchmann, K. Sengupta, M. Simon, M. Sipilä, C. Tauber, A. Tomé, J. Tröstl, O. Väisänen, A. L. Vogel, R. Volkamer, A. C. Wagner, M. Wang, L. Weitz, D. Wimmer, P. Ye, A. Ylisirniö, Q. Zha, K. S. Carslaw, J. Curtius, N. M. Donahue, R. C. Flagan, A. Hansel, I. Riipinen, A. Virtanen, P. M. Winkler, U. Baltensperger, M. Kulmala, D. R. Worsnop, Multicomponent new particle formation from sulfuric acid, ammonia, and biogenic vapors. *Sci. Adv.* **4**, eaau5363 (2018).

ScienceAdvances

# Multicomponent new particle formation from sulfuric acid, ammonia, and biogenic vapors

Katrianne Lehtipalo, Chao Yan, Lubna Dada, Federico Bianchi, Mao Xiao, Robert Wagner, Dominik Stolzenburg, Lauri R. Ahonen, Antonio Amorim, Andrea Baccarini, Paulus S. Bauer, Bernhard Baumgartner, Anton Bergen, Anne-Kathrin Bernhammer, Martin Breitenlechner, Sophia Brilke, Angela Buchholz, Stephany Buenrostro Mazon, Dexian Chen, Xuemeng Chen, Antonio Dias, Josef Dommen, Danielle C. Draper, Jonathan Duplissy, Mikael Ehn, Henning Finkenzeller, Lukas Fischer, Carla Frege, Claudia Fuchs, Olga Garmash, Hamish Gordon, Jani Hakala, Xucheng He, Liine Heikkinen, Martin Heinritzi, Johanna C. Helm, Victoria Hofbauer, Christopher R. Hoyle, Tuija Jokinen, Juha Kangasluoma, Veli-Matti Kerminen, Changhyuk Kim, Jasper Kirkby, Jenni Kontkanen, Andreas Kürten, Michael J. Lawler, Huajun Mai, Serge Mathot, Roy L. Mauldin III, Ugo Molteni, Leonid Nichman, Wei Nie, Tuomo Nieminen, Andrea Ojdanic, Antti Onnela, Monica Passananti, Tuukka Petäjä, Felix Piel, Veronika Pospisilova, Lauriane L. J. Quéléver, Matti P. Rissanen, Clémence Rose, Nina Sarnela, Simon Schallhart, Simone Schuchmann, Kamalika Sengupta, Mario Simon, Mikko Sipilä, Christian Tauber, António Tomé, Jasmin Tröstl, Olli Väisänen, Alexander L. Vogel, Rainer Volkamer, Andrea C. Wagner, Mingyi Wang, Lena Weitz, Daniela Wimmer, Penglin Ye, Arttu Ylisirniö, Qiaozhi Zha, Kenneth S. Carslaw, Joachim Curtius, Neil M. Donahue, Richard C. Flagan, Armin Hansel, Ilona Riipinen, Annele Virtanen, Paul M. Winkler, Urs Baltensperger, Markku Kulmala and Douglas R. Worsnop

*Sci Adv* **4** (12), eaau5363.
DOI: 10.1126/sciadv.aau5363

# Paper IV

Atmos. Chem. Phys., 18, 13231–13243, 2018
https://doi.org/10.5194/acp-18-13231-2018


Atmospheric Chemistry and Physics
Open Access
EGU

# The role of $H_2SO_4$-$NH_3$ anion clusters in ion-induced aerosol nucleation mechanisms in the boreal forest

**Chao Yan[1], Lubna Dada[1], Clémence Rose[1], Tuija Jokinen[1], Wei Nie[1,2], Siegfried Schobesberger[1,3], Heikki Junninen[1,4], Katrianne Lehtipalo[1], Nina Sarnela[1], Ulla Makkonen[5], Olga Garmash[1], Yonghong Wang[1], Qiaozhi Zha[1], Pauli Paasonen[1], Federico Bianchi[1], Mikko Sipilä[1], Mikael Ehn[1], Tuukka Petäjä[1,2], Veli-Matti Kerminen[1], Douglas R. Worsnop[1,6], and Markku Kulmala[1,2,7]**

[1]Institute for Atmospheric and Earth System Research / Physics, Faculty of Science, University of Helsinki, P. O. Box 64, 00014, Helsinki, Finland
[2]Joint International Research Laboratory of Atmospheric and Earth System Sciences, School of Atmospheric Sciences, Nanjing University, Nanjing, 210046, China
[3]Department of Applied Physics, University of Eastern Finland, 70211 Kuopio, Finland
[4]Institute of Physics, University of Tartu, Ülikooli 18, 50090 Tartu, Estonia
[5]Finnish Meteorological Institute, 00560 Helsinki, Finland
[6]Aerodyne Research, Inc., Billerica, MA 01821, USA
[7]Aerosol and Haze Laboratory, Beijing Advanced Innovation Center for Soft Matter Science and Engineering, Beijing University of Chemical Technology, Beijing, 100029, China

**Correspondence:** Chao Yan (chao.yan@helsinki.fi)

Received: 19 February 2018 – Discussion started: 10 April 2018
Revised: 11 August 2018 – Accepted: 22 August 2018 – Published: 13 September 2018

**Abstract.** New particle formation (NPF) provides a large source of atmospheric aerosols, which affect the climate and human health. In recent chamber studies, ion-induced nucleation (IIN) has been discovered as an important pathway of forming particles; however, atmospheric investigation remains incomplete. For this study, we investigated the air anion compositions in the boreal forest in southern Finland for three consecutive springs, with a special focus on $H_2SO_4$-$NH_3$ anion clusters. We found that the ratio between the concentrations of highly oxygenated organic molecules (HOMs) and $H_2SO_4$ controlled the appearance of $H_2SO_4$-$NH_3$ clusters ($3 < no.S < 13$): all such clusters were observed when [HOM] / [$H_2SO_4$] was smaller than 30. The number of $H_2SO_4$ molecules in the largest observable cluster correlated with the probability of ion-induced nucleation (IIN) occurrence, which reached almost 100 % when the largest observable cluster contained six or more $H_2SO_4$ molecules. During selected cases when the time evolution of $H_2SO_4$-$NH_3$ clusters could be tracked, the calculated ion growth rates exhibited good agreement across measurement methods and cluster (particle) sizes. In these cases, $H_2SO_4$-$NH_3$ clusters alone could explain ion growth up to 3 nm (mobility diameter). IIN events also occurred in the absence of $H_2SO_4$-$NH_3$, implying that other NPF mechanisms also prevail at this site, most likely involving HOMs. It seems that $H_2SO_4$ and HOMs both affect the occurrence of an IIN event, but their ratio ([HOMs] / [$H_2SO_4$]) defines the primary mechanism of the event. Since that ratio is strongly influenced by solar radiation and temperature, the IIN mechanism ought to vary depending on conditions and seasons.

## 1 Introduction

Atmospheric aerosol particles are known to influence human health and the climate (Heal et al., 2012; Stocker et al., 2013). New particle formation (NPF) from gas-phase precursors contributes to a major fraction of the global cloud condensation nuclei population (Merikanto et al., 2009; Kerminen et al., 2012; Dunne et al., 2016; Gordon et al., 2017) and provides an important source of particulate air pollutants in many urban environments (Guo et al., 2014).

Although NPF is an abundant phenomenon and has been observed in different places around the globe within the boundary layer (Kulmala et al., 2004), the detailed mechanisms at each location may differ and are still largely unknown. Experiments done in the CLOUD chamber (Cosmics Leaving Outside Droplets) at CERN explored different NPF mechanisms on a molecular level, including sulfuric acid ($H_2SO_4$) and ammonia ($NH_3$) nucleation (Kirkby et al., 2011), $H_2SO_4$ and dimethylamine) nucleation (Almeida et al., 2013), and pure biogenic nucleation (Kirkby et al., 2016) from highly oxygenated organic molecules (HOMs) (Ehn et al., 2014). While chamber experiments can mimic some properties of ambient observations (Schobesberger et al., 2013), it is still unclear to what extent these chamber findings can be applied to understand NPF in the more complex atmosphere, mostly due to the challenges in atmospheric measurements and characterization of the nucleating species.

In the aforementioned chamber studies, ions have been shown to play a crucial role in enhancing new particle formation, which is known as ion-induced nucleation (IIN). The importance of IIN varies significantly depending on the temperature as well as the concentration and composition of the ion species. For instance, big $H_2SO_4$ ion clusters were not found in the sulfur-rich air mass from Atlanta, suggesting the minor role of IIN (Eisele et al., 2006). Similar conclusions were drawn based on the observations in Boulder (Iida et al., 2006) and Hyytiälä (e.g., Manninen et al., 2010), although the suggested importance of IIN in cold environments, such as upper troposphere, cannot be excluded (Lovejoy et al., 2004; Kürten et al., 2016). Recently, the CLOUD experiments have revealed that the importance of IIN can be negligible in the $H_2SO_4$-dimethylamine system (Almeida et al., 2013), moderate in the $H_2SO_4$-$NH_3$ system (Kirkby et al., 2011), and dominating in the pure HOMs system (Kirkby et al., 2016). However, it is also important to note that the ion-pair concentration in Hyytiälä is lower than in the CLOUD chamber, which partly explains its smaller contribution of IIN (Wagner et al., 2017).

The recently developed atmospheric-pressure interface time-of-flight mass spectrometer (APi-TOF) (Junninen et al., 2010) has been used for measuring ion composition at the SMEAR II station in Hyytiälä since 2009. Ehn et al. (2010) first showed that the negative ion population varied significantly, with $H_2SO_4$ clusters dominating during the day and HOM-$NO_3^-$ clusters doing so during the night. This variation was further studied by Bianchi et al. (2017), who grouped HOM-containing ions by separating the HOMs into non-nitrate- and nitrate-containing species as well as into ion adducts with $HSO_4^-$ or $NO_3^-$. At nighttime, HOMs may form negatively charged clusters containing up to 40 carbons (Bianchi et al., 2017; Frege et al., 2018). In the daytime, $H_2SO_4$ and $H_2SO_4$-$NH_3$ clusters appear to be the most prominent negative ions (Schobesberger et al., 2015, 2013). However, they have not yet been thoroughly studied regarding their appearance and their plausible links to atmospheric IIN.

Along with the changes in temperature and in ion concentration and composition, the importance of IIN is expected to vary considerably. In this study, we revisit the ion measurement in Hyytiälä, aiming to connect our current understanding of the formation of ion clusters to the significance of IIN, with a special focus on the fate of $H_2SO_4$-$NH_3$ clusters. We also extend our analysis to ions other than $H_2SO_4$ clusters, i.e., HOMs, and identify their role in IIN, in addition to other measured parameters on site. Finally, this study confirms the consistency between chamber findings and atmospheric observations, even though it seems that at least two separate mechanisms alternately control the IIN in Hyytiälä.

## 2 Materials and methods

For this study, we used data collected at the Station for Measuring Forest Ecosystem-Atmospheric Relations (SMEAR II station), in Hyytiälä, southern Finland (Hari and Kulmala, 2005). In this study, our data sets were obtained from intensive campaigns in three consecutive springs (2011–2013). The exact time periods of the APi-TOF measurements are 22 March until 24 May 2011, 31 March until 28 April 2012, and 7 April until 8 June 2013. For 134 days we were able to extend our analysis to include (i) ion composition and chemical characterization using the APi-TOF (Junninen et al., 2010), (ii) particle and ion number size distribution using a neutral cluster and air ion spectrometer (NAIS) (e.g., Mirme and Mirme 2013), (iii) concentrations of $H_2SO_4$ and HOMs measured by the chemical-ionization atmospheric-pressure interface time-of-flight mass spectrometer (CI-APi-TOF; see, e.g., Jokinen et al. (2012), Ehn et al. (2014), and Yan et al. (2016)), and (iv) other relevant parameters, e.g., $NH_3$ (Makkonen et al., 2014), temperature, and cloudiness (Dada et al., 2017).

### 2.1 Measurement of atmospheric ions

The composition of atmospheric anions was measured using the atmospheric-pressure interface time-of-flight mass spectrometer (APi-TOF) (Junninen et al., 2010). The instrument was situated inside a container in the forest, directly sampling the air outside. To minimize the sampling losses, we firstly drew the air at a greater flow rate within a wide tube (40 mm inner diameter), and another 30 cm long coaxial tube (10 mm outer diameter and 8 mm inner diameter) inside the wider one was used to draw 5 L $min^{-1}$ towards the APi-TOF, 0.8 L $min^{-1}$ of which entered through the pinhole. After entering the pinhole, the ions were focused and guided through two quadrupoles and one ion lens and finally detected by the time-of-flight mass spectrometer.

Unlike the commonly used chemical-ionization mass spectrometer (CIMS), the APi-TOF does not do any ioniza-

tion, so it only measures the naturally charged ions in the sample. In the atmosphere, the ion composition is affected by the proton affinity of the species: molecules with the lowest proton affinity are more likely to lose the proton and thus become negatively charged after colliding many times with other species; similarly, molecules with the highest proton affinity would probably become positively charged ions. In addition to the proton affinity, the neutral concentration also plays a role in determining the ion composition by affecting the collision frequency. Due to the limited ionization rate in the atmosphere, there is always a competition between different species in taking the charges. For example, $H_2SO_4$ often dominates the spectrum in the daytime when it is abundant, while at nighttime nitrate ions and their cluster with HOMs are always prominent due to the low chances of colliding with the $H_2SO_4$. Since the signal strength of an ion in the APi-TOF depends not only on the abundance of the respective neutral molecules but also on the availability of other charge-competing species, it is very important to note that the APi-TOF cannot quantify the neutral species.

One important virtue of APi-TOF is that it does not introduce extra energy during sampling, which ensures the sample is least affected when compared to other measurement techniques such as CIMS although fragmentation cannot be fully avoided inside the instrument (Schobesberger et al., 2013). Because of this, it is a well-suited instrument to directly measure the composition of weakly bonded clusters in the atmosphere.

The APi-TOF data were processed with the tofTools package (version 6.08) (Junninen et al., 2010). Since the ion signal in APi-TOF is usually weak, a 5 h integration time was used, after which the signals of $H_2SO_4$-$NH_3$ clusters and HOMs were fitted (see Fig. 1). For HOM signals, we used the same peaks reported in Bianchi et al. (2017), and the total signal of HOM ions is the sum of all identified HOMs.

It should also be mentioned that the voltage tuning of the instrument was not the same in the years we analyzed, which led to differences in the ion transmission efficiency function. For example, we noticed that in 2011, the largest $H_2SO_4$-$NH_3$ clusters contained 6 $H_2SO_4$ molecules, whereas more than 10 $H_2SO_4$ were observed in the clusters in other years. This was very likely due to the very low ion transmission in the mass range larger than about 700 Th for the measurements in 2011. However, this should not affect our results and conclusions because clusters consisting of six $H_2SO_4$ molecules had little difference from larger clusters in affecting the IIN in terms of occurrence probability (see more details in Sect. 3.3.1).

### 2.2 Measurement of $H_2SO_4$ and HOMs

The concentrations of $H_2SO_4$ and HOMs were measured by the chemical-ionization atmospheric-pressure interface time-of-flight mass spectrometer (CI-APi-TOF). The details of the quantification method for $H_2SO_4$ can be found in Jokinen et al. (2012) and those for HOMs in Kirkby et al., 2016. For all data, we applied the same calibration coefficient ($1.89 \times 10^{10}$ cm$^{-3}$) reported by Jokinen et al. (2012).

Although the tuning of the CI-APi-TOF was not exactly the same during the measurement period included in this study, no systematic difference was found in the concentrations of $H_2SO_4$ and HOMs from different years.

### 2.3 Measurements of ion and particle size distribution

The mobility distribution of charged particles and air ions in the range 3.2–0.0013 cm$^2$ V$^{-1}$ s$^{-1}$ (corresponding to mobility diameter 0.8–42 nm) were measured together with the size distribution of total particles in the range $\sim$ 2.5–42 nm using a NAIS (Airel Ltd.; Mirme and Mirme, 2013). The instrument has two identical differential mobility analyzers (DMAs) which allow for the simultaneous monitoring of positive and negative ions. In order to minimize the diffusion losses in the sampling lines, each analyzer has a sample flow rate of 30 L min$^{-1}$ and a sheath flow rate of 60 L min$^{-1}$. In "particle mode", when measuring total particle concentration, neutral particles are charged by ions produced from a corona discharge in a "pre-charging" unit before they are detected in the DMAs. The charging ions used in this process were previously reported to influence the total particle concentrations below $\sim$ 2 nm (Asmi et al., 2008; Manninen et al., 2010); for that reason, only the particle concentrations above 2.5 nm were used in the present work. Also, each measurement cycle, i.e., 2 min in ion mode and 2 min in particle mode, is followed by an offset measurement, during which the background signal of the instrument is determined and then subtracted from measured ion and particle concentrations. In addition, particle size distributions between 3 and 990 nm were measured with a differential mobility particle sizer (DMPS) described in detail in Aalto et al. (2001). Based on earlier work by Kulmala et al. (2001), these data were used to calculate the condensation sink (CS), which represents the rate of loss of condensing vapors on preexisting particles.

### 2.4 Measurement of the meteorological parameter

The meteorological variables used as supporting data in the present work were measured on a mast, all with a time resolution of 1 min. Temperature and relative humidity were measured at 16.8 m using a PT-100 sensor and relative humidity sensors (Rotronic Hygromet MP102H with Hygroclip HC2-S3, Rotronic AG, Bassersdorf, Switzerland), respectively. Global radiation was measured at 18 m with a pyranometer (Middleton Solar SK08, Middleton Solar, Yarraville, Australia) and further used to calculate the cloudiness parameter, as done previously by Dada et al. (2017, and references therein). This parameter is defined as the ratio of measured global radiation to theoretical global irradiance so that parameter values $< 0.3$ correspond to a complete cloud

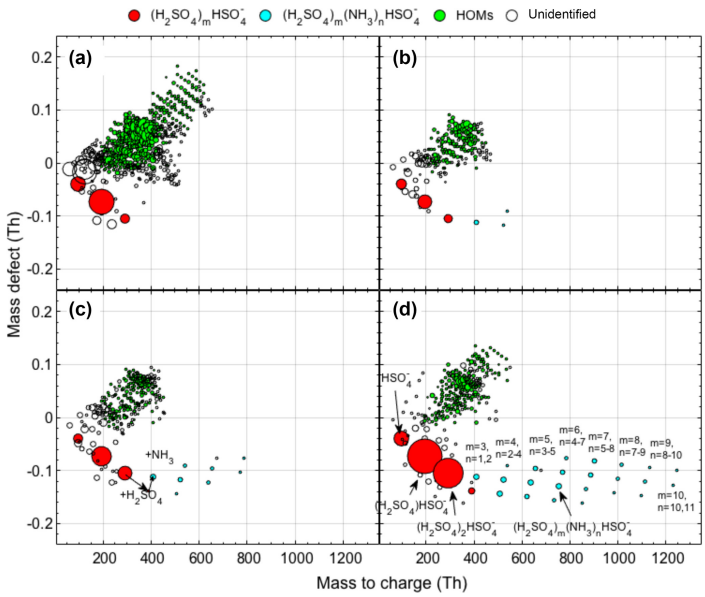


**Figure 1.** Mass defect plot showing the composition of ion clusters on four separate days. **(a)** $NH_3$-free clusters; **(b, c, d)** $H_2SO_4$-$NH_3$ clusters with different maximum number of $H_2SO_4$ molecules. The circle size is linearly proportional to the logarithm of the signal intensity.

coverage, while values $> 0.7$ are representative of clear-sky conditions.

### 2.5 Calculation of particle formation rates and growth rates

The formation rate of 2.5 nm particles includes both neutral and charged particles, and it was calculated from the following equation:

$$J_{2.5} = \frac{dN_{2.5-3.5}}{dt} + \mathrm{CoagS}_{2.5} \times N_{2.5-3.5} + \frac{1}{1\,\mathrm{nm}}\mathrm{GR}_{1.5-3} \times N_{2.5-3.5}, \quad (1)$$

where $N_{2.5-3.5}$ is the particle concentration between 2.5 and 3.5 nm measured with the NAIS in particle mode, $\mathrm{CoagS}_{2.5}$is the coagulation sink of 2.5 nm particles, as derived from DMPS measurements, and $\mathrm{GR}_{1.5-3}$ is the particle growth rate calculated from NAIS measurements in ion mode. Calculating the formation rate of 2.5 nm ions or charged particles includes two additional terms to account for the loss of 2.5–3.5 nm ions due to their recombination with sub −3.5 nm ions of the opposite polarity (fourth term of Eq. 2) and the gain of ions caused by the attachment of sub −2.5 nm ions on 2.5–3.5 nm neutral clusters (fifth term of Eq. 2):

$$J^{\pm}_{2.5} = \frac{dN^{\pm}_{2.5-3.5}}{dt} + \mathrm{CoagS}_{2.5} \times N^{\pm}_{2.5-3.5} + \frac{1}{1\,\mathrm{nm}}\mathrm{GR}_{1.5-3} \times N^{\pm}_{2.5-3.5} + \alpha \times N^{\pm}_{2.5-3.5}N^{\mp}_{<3.5} - \beta \times N_{2.5-3.5}N^{\pm}_{<2.5}, \quad (2)$$

where $N^{\pm}_{2.5-3.5}$ is the concentration of positive or negative ions between 2.5 and 3.5 nm, $N^{\pm}_{<2.5}$ is the concentration of sub −2.5 nm ions of the same polarity, and $N^{\mp}_{<3.5}$ is the concentration of sub −3.5 nm ions of the opposite polarity, all measured with the NAIS in ion mode; $\alpha$ and $\beta$ are the ion–ion recombination and the ion-neutral attachment coefficients, respectively, and were assumed to be equal to $1.6 \times 10^{-6}\,\mathrm{cm^3\,s^{-1}}$ and $0.01 \times 10^{-6}\,\mathrm{cm^3\,s^{-1}}$, respectively. We consider these values to be reasonable approximations, keeping in mind that the exact values of both $\alpha$ and $\beta$ depend on a number of variables, including the ambient temperature, pressure, and relative humidity as well as the sizes of the colliding objects (ion–ion or ion–aerosol particle) (e.g., Hoppel, 1985; Tammet and Kulmala, 2005; Franchin et al., 2015).

$\mathrm{GR}_{1.5-3}$ were calculated from NAIS data in ion mode using the "maximum" method introduced by (Hirsikko et al., 2005). Briefly, the peaking time of the ion concentration in each size bin of the selected diameter range was first determined by fitting a Gaussian to the concentration. The growth rate was then determined by a linear least square fit through the times. The uncertainty in the peak time determination

was reported as the Gaussian's mean 67 % confidence interval and was further taken into account in the growth rate determination.

A similar approach was used to estimate the early growth rate of the $H_2SO_4$-$NH_3$ clusters detected with the APi-TOF. Prior to growth rate calculation, we first converted cluster masses into diameters in order to get growth rate values in $nm\,h^{-1}$ instead of $amu\,h^{-1}$. For that purpose, we applied the conversion from Ehn et al. (2011), using a cluster density of $1840\,kg\,m^{-3}$. The time series of the cluster signals were then analyzed in the same way as ion or particle concentrations using the maximum method from Hirsikko et al. (2005), and the growth rate was calculated using the procedure outlined above. Our ability to determine the early cluster growth rate from APi-TOF measurements was strongly dependent on the strength of the signal of the different $H_2SO_4$-$NH_3$ clusters. As a consequence, the reported growth rates characterize a size range which might vary slightly between the events, falling in a range between 1 and 1.7 nm.

## 3 Results and discussion

### 3.1 Daytime ion composition

We examined the daytime ion composition of 134 days from three consecutive springs (2011–2013) in Hyytiälä. Consistent with the findings by previous studies showing that $H_2SO_4$ clusters are the most abundant ions in the daytime (Ehn et al., 2010; Bianchi et al., 2017), we found that $NH_3$-free $H_2SO_4$ clusters can contain up to three $H_2SO_4$ molecules when counting the $HSO_4^-$ also as one $H_2SO_4$ molecule ($(H_2SO_4)_2HSO_4^-$) and that $NH_3$ is always present in clusters containing four or more $H_2SO_4$ molecules. The latter feature suggests the important role of $NH_3$ as a stabilizer in growing $H_2SO_4$ clusters (Kirkby et al., 2011). $NH_3$-free clusters (at least dimers $H_2SO_4HSO_4^-$) were observed on 116 measurement days, but the signal intensity varied from day to day. Bigger clusters that contained $NH_3$ were observed on 39 days, containing a maximum of 4 to 13 $H_2SO_4$ per cluster. Figure 1 provides four examples of daytime ion spectra, including an $NH_3$-free case (Fig. 1a) and three cases with a different maximum size of $H_2SO_4$-$NH_3$ clusters (Fig. 1b–d), illustrating the significant variations in signal and maximum size of $H_2SO_4$-$NH_3$ clusters. In the $NH_3$-free case, a larger number of HOM clusters (green circles) was observed, indicating a competition between $H_2SO_4$ and HOMs in taking the charges. The largest detected cluster during the measurement was $(H_2SO_4)_{12}\,(NH_3)_{13}HSO_4^-$, which corresponds to a mobility-equivalent diameter of about 1.7 nm according to the conversion method (Ehn et al., 2011) and is big enough to be detected by particle counters. Since the observed formation of such large $H_2SO_4$-$NH_3$ clusters is essentially the initial step of IIN, we anticipate that the variation in $H_2SO_4$-$NH_3$ clusters will influence the occurrence of IIN.

### 3.2 The determining parameters for $H_2SO_4$-$NH_3$ cluster formation

To find out the dominating parameters that affect the formation of $H_2SO_4$-$NH_3$ clusters, we performed a correlation analysis that included the ambient temperature, relative humidity (RH), wind speed, wind direction, CS, and the gas-phase concentrations of $NH_3$, $H_2SO_4$, and HOMs. Among all the examined parameters, we found that the ratio between concentrations of HOMs and $H_2SO_4$ had the most pronounced influence on the appearance of $H_2SO_4$-$NH_3$ clusters. As shown in Fig. 2, all $H_2SO_4$-$NH_3$ clusters were detected when [HOMs] / [$H_2SO_4$] was smaller than 30. No such dependence was observed for only [HOMs] or [$H_2SO_4$]. This implies that the appearance of $H_2SO_4$-$NH_3$ clusters is primarily controlled by the competition between $H_2SO_4$ and HOMs in getting the charges. More specifically, $HSO_4^-$, the main charge carrier in the daytime, may either collide with neutral $H_2SO_4$ to form large clusters to accommodate $NH_3$ or collide with HOMs, which prevents the former process. In addition, a reasonable correlation was found between [HOMs] / [$H_2SO_4$] and temperature, likely explained by the emission of volatile organic compounds (VOCs) increasing with temperature, leading to higher HOMs concentrations, whereas the formation of $H_2SO_4$ is not strongly temperature-dependent. This observation indicates that the formation of $H_2SO_4$-$NH_3$ clusters may vary seasonally: we expect to see them more often in cold seasons when HOM concentrations are low and less often in warm seasons.

Parameters other than [HOMs] / [$H_2SO_4$] and temperature seemed to have little influence on the formation of $H_2SO_4$-$NH_3$ clusters. Interestingly, we found that $NH_3$ was even lower when $H_2SO_4$-$NH_3$ clusters were observed, indicating that the $NH_3$ concentration is not the limiting factor for forming $H_2SO_4$-$NH_3$ clusters (also see Sect. 3.4). In addition, $H_2SO_4$-$NH_3$ clusters were observed in a wide range of RH spanning from 20 % to 90 %, suggesting that RH does not affect the cluster formation. Besides, no clear influence from CS, wind speed, or wind direction was observed.

### 3.3 The relation between $H_2SO_4$-$NH_3$ clusters and IIN

#### 3.3.1 The effect of cluster size on the probability of IIN events

We identified IIN events using data from the NAIS (ion mode) by observing an increase in the concentration of sub-2 nm ions (Rose et al., 2018) and classified 67 IIN events out of the 134 days of measurements. We defined the IIN probability as the number of days when IIN events were identified out of the total number of days that were counted. For example, the overall IIN probably is 50 % (67 out of 134 days). We found that the maximum observed size of $H_2SO_4$-$NH_3$ clusters may affect the occurrence of IIN. Our conclusion is complementary to previous theories which stated that the critical

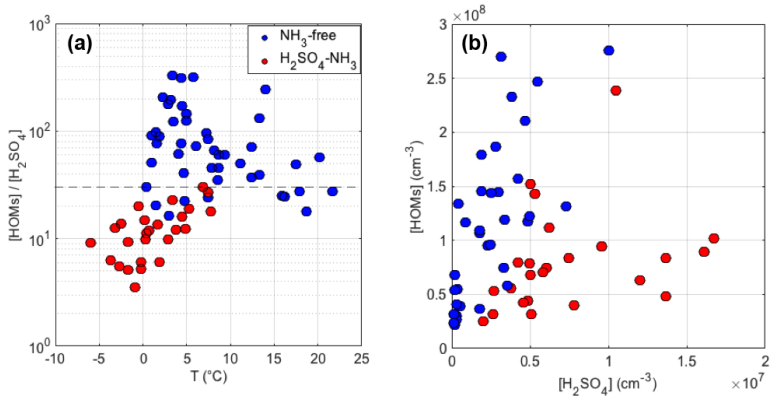


**Figure 2.** The effect of the concentration of HOMs, $H_2SO_4$, their ratio ([HOM] / [$H_2SO_4$]), and temperature on the appearance of $H_2SO_4$-$NH_3$ clusters.

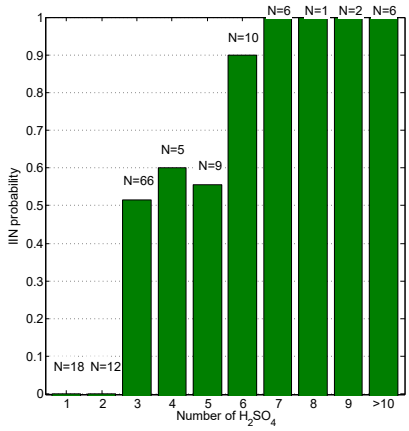


**Figure 3.** The maximum number of $H_2SO_4$ molecules observed in clusters and the respective IIN probability. The days when it was unclear if IIN occurred was counted as nonevent days. *N* denotes the number of days when such clusters were the largest observed.

step of particle nucleation is the formation of initial clusters that are big enough for condensational growth to outcompete evaporation (Kulmala et al., 2013). To further understand the size dependency of IIN probability, we investigated the IIN probability when different maximum sizes of $H_2SO_4$-$NH_3$ clusters were observed. As illustrated in Fig. 3, the IIN probability increases dramatically when larger $H_2SO_4$-$NH_3$ clusters were observed: IIN events were never observed when only $HSO_4^-$ or $H_2SO_4HSO_4^-$ were present, whereas the IIN probability increased to about 50 %–60 % when the largest clusters contained three to five $H_2SO_4$ molecules. IIN occurred in 24 out of 25 days (96 %) when the largest clusters consisted of no less than six $H_2SO_4$ molecules. Thus, it is evident that the occurrence of IIN is related to the size and thus the stability of $H_2SO_4$-$NH_3$ clusters and that a cluster consisting of six $H_2SO_4$ molecules seems to lie on the threshold size of triggering nucleation.

### 3.3.2 Continuous growth from clusters to 3 nm particles

Although the strong connection between the size of $H_2SO_4$-$NH_3$ clusters and the occurrence of IIN was confirmed, it is challenging to directly observe the growth of these clusters in the atmosphere, limited by the inhomogeneity of the ambient air and low concentrations of atmospheric ions. Combining APi-TOF and NAIS measurements, we were able to follow the very first steps of the cluster growth for eight of the detected events. In Fig. 4a and b, we present two examples in which the continuous growth of $H_2SO_4$-$NH_3$ clusters to 3 nm (mobility diameter) particles was directly evaluated using the maximum-time method. The maximum times, determined from APi-TOF and NAIS data independently, fall nicely into the same linear fit. The continuity of the growth and the linearity of the fit suggests that the current mechanism ($H_2SO_4$-$NH_3$, acid–base) explains the formation and growth of sub-3 nm ion clusters in these cases. In most cases, the calculation of cluster GR from APi-TOF measurement suffered from large uncertainties, but a weak positive correlation can be observed between the cluster growth rate and $H_2SO_4$ concentration (Fig. 4c). This correlation is likely due to the collision of $H_2SO_4$ with existing $H_2SO_4$-$NH_3$ clusters being the limiting step for cluster growth when $NH_3$ is abundant enough to follow up immediately (Schobesberger et al., 2015).

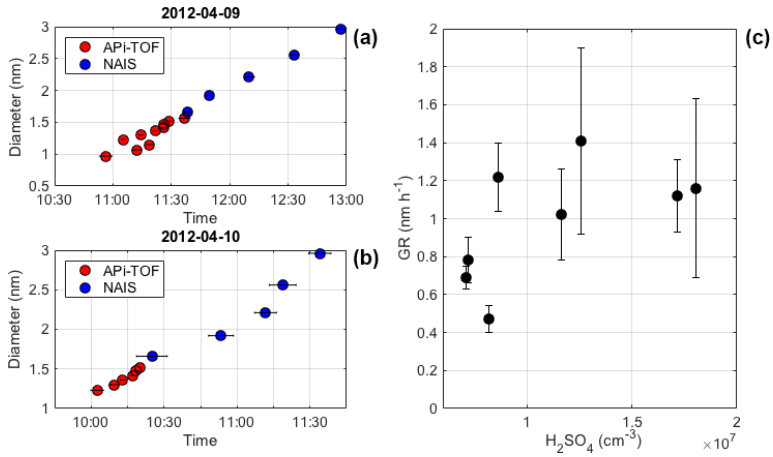


**Figure 4.** Cluster growth rate determined from APi-TOF **(a)** and NAIS **(b)** measurements using the maximum-time method; the correlation between growth rates and concentrations of $H_2SO_4$ molecules **(c)**.

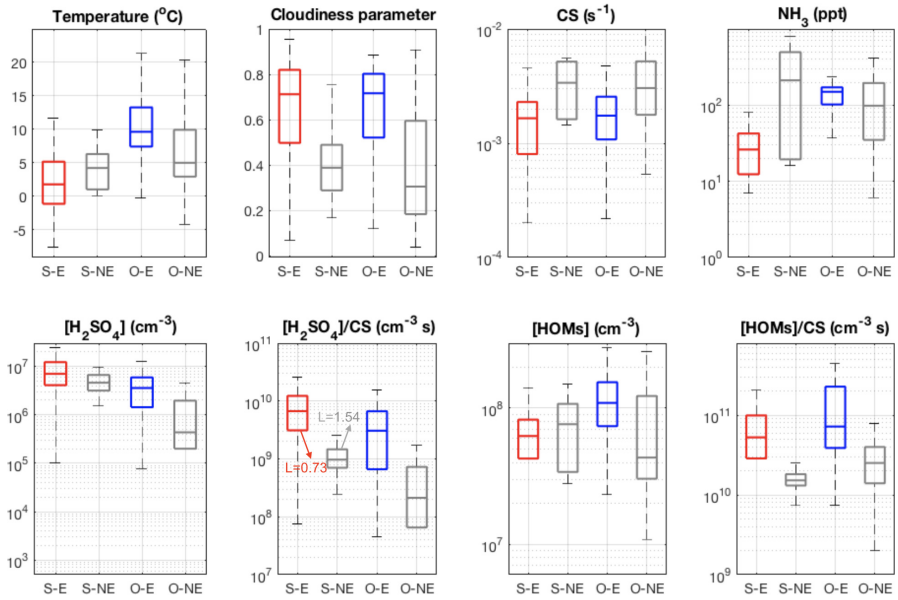


**Figure 5.** Comparison of different parameters for $H_2SO_4-NH_3$-involved events (S–E, red bars), nonevents with the presence of $H_2SO_4-NH_3$ clusters (S–NE, first column of black bars), other events (O–E, blue bars), and other nonevents (O–NE, second column of black bars).

### 3.4 Evidence for other IIN mechanisms

For the 134 days of measurements, we were able to identify 67 IIN events using the NAIS data, out of which $H_2SO_4$-$NH_3$ clusters were observed on 32 days, implying that at least 35 IIN events were likely driven by mechanism(s) other than $H_2SO_4$-$NH_3$. In Fig. 5, we classified the days according to the types of IIN observation: 32 IIN events involving $H_2SO_4-NH_3$ (S–E), 3 nonevents with the presence of $H_2SO_4$-$NH_3$ clusters (S–NE), 35 IIN events involving other mechanisms (O–E), 41 other nonevent days (O–NE), and 23 days with unclear types. We further present the respective

statistics of additional measurements for the first four types of days, including the concentrations of plausible precursor vapors, condensation sinks, and meteorological parameters. It should be noted that the S–NE has only three days; thus, the statistics on this type of day might not be fully representative.

Consistent with the previous discussion (Fig. 2), low temperatures are conducive to IIN events via the $H_2SO_4$-$NH_3$ mechanism whilst being the highest other type of events (O–E) (Fig. 5a). The clear-sky parameter (100 % – clear sky; 0 % – cloudiness) shows a noticeably higher value during both event types compared to the nonevent cases (Fig. 5b), indicating that photochemistry-related processes are important for all events. Moreover, the CS is obviously lower for both types of events than on nonevent days (Fig. 5c). Although a strong effect of CS on the appearance of $H_2SO_4$-$NH_3$ clusters has not been noticed, it is a most important parameter in regulating the occurrence of IIN. Similar effects of cloudiness and CS on governing the occurrence of NPF have been reported by Dada et al. (2017) based on long-term data sets.

Remarkably, $NH_3$ has very low concentrations during $H_2SO_4$-$NH_3$ events in comparison to the other type of events (Fig. 5d). This is likely due to high $NH_3$ concentrations coinciding with higher temperature and thus elevated HOMs concentration or the lower stability of $H_2SO_4$-$NH_3$ clusters at high temperatures that can evaporate $NH_3$ back to the atmosphere. This observation rules out the addition of $NH_3$ as a limiting step in the $H_2SO_4$-$NH_3$ nucleation mechanism, but the participation of $NH_3$ in the other type of events cannot be excluded.

$H_2SO_4$ has the highest concentrations during the $H_2SO_4$-$NH_3$-involved events (Fig. 5e), but the concentration of $H_2SO_4$ in S–NE days is not much lower, suggesting that the occurrence of $H_2SO_4$-$NH_3$-involved events is not solely controlled by the $H_2SO_4$ concentration. The incorporating the effect of CS ($[H_2SO_4]$ / CS) significantly improves the separation (Fig. 5f). McMurry and colleagues (Mcmurry et al., 2005) introduced a parameter $L$ (Eq. 3) to quantitatively evaluate the likelihood of NPF, and they found that NPF mostly occurred when $L$ is smaller than 1. A similar result has been reported by Kuang et al. (2010), and a slightly different threshold $L$ value of 0.7 was determined.

$$L = \frac{\mathrm{CS}}{[\mathrm{H_2SO_4}]} \times \frac{1}{\beta_{11}} \quad (3)$$

Here, $L$ is a dimensionless parameter representing the probability that NPF will not occur, and $\beta_{11}$ is the collision rate between $H_2SO_4$ vapor molecules, which is characterized as $4.4 \times 10^{-10}\,\mathrm{cm^3\,s^{-1}}$. Our results suggest a consistent $L$ that most (75 percentile) S–E cases happen when $L$ is lower than 0.73 and most (75 percentile) S–NE cases are observed when $L$ is larger than 1.54.

HOM concentrations are highest in the case of other events, revealing that HOMs play a key role in this mechanism (Fig. 5f), although the contribution of $H_2SO_4$ in this HOM-involving IIN mechanism cannot be excluded. Similar to the $H_2SO_4$-$NH_3$-driven cases, incorporating the CS better distinguishes the event and nonevent cases.

Overall, our results suggest that the concentrations of $H_2SO_4$ and HOMs, together with the CS, govern the occurrence of IIN, whereas their ratio determines the exact underlying mechanism (Fig. 2). Although $H_2SO_4$-$NH_3$ and HOMs clearly drives the S–E and O–E events, respectively, we cannot exclude the later participation of HOMs in S–E cases or $H_2SO_4$ in O–E cases. Different NPF mechanisms have also been identified at the Jungfraujoch station (Bianchi et al., 2016; Frege et al., 2018) when influenced by different air masses. At the SMEAR II station, on the other hand, our results suggest that the natural variation in temperature is already sufficient to modify the NPF mechanism by modulating the biogenic VOC emissions.

### 3.5 Contribution of IIN to total nucleation rate

In order to obtain further insight into the importance of IIN during our measurements, we compared the formation rate of 2.5 nm ions, $J_{\mathrm{ION}} = J^{\pm}_{2.5}$ (see Eq. 2), to the total formation rate of 2.5 nm particles, $J_{\mathrm{TOT}} = J_{2.5}$ (see Eq. 1). The ratio $J_{\mathrm{ION}}/J_{\mathrm{TOT}}$ is equal to the charged fraction of the 2.5 nm particle formation rate. In analyzing field measurements, a similar ratio at a certain particle size (typically 2 nm) has commonly been used to estimate the contribution of ion-induced nucleation to the total nucleation rate (see Hirsikko et al., 2011, and references therein). It should be noted that $J_{\mathrm{ION}}/J_{\mathrm{TOT}}$ represents only a lower limit for the contribution of ion-induced nucleation, as this ratio does not take into account the potential neutralization of growing charged sub −2.5 nm particles by ion–ion recombination (e.g., Kontkanen et al., 2013; Wagner et al., 2017). At present, measuring the true contribution of ion-induced nucleation to the total nucleation rate is possible only in the CLOUD chamber (Wagner et al., 2017).

We were able to calculate $J_{\mathrm{ION}}$ and $J_{\mathrm{TOT}}$ for 57 (out of 67) cases, and the ratio $J_{\mathrm{ION}}/J_{\mathrm{TOT}}$ varied from 4 to 45 %, showing a clear correlation with the HOM signal (Fig. 6a). This indicates the participation of HOMs even in $H_2SO_4$-$NH_3$-driven cases. In addition, most of the high $J_{\mathrm{ION}}/J_{\mathrm{TOT}}$ ratios were observed at moderate or low $H_2SO_4$ concentrations; e.g., $J_{\mathrm{ION}}/J_{\mathrm{TOT}} > 15\,\%$ was only observed when $[H_2SO_4] < 6 \times 10^6\,\mathrm{cm^{-3}}$. These observations indicate that HOMs are important in high $J_{\mathrm{ION}}/J_{\mathrm{TOT}}$ cases, while during events driven by $H_2SO_4$-$NH_3$ clusters, low $J_{\mathrm{ION}}/J_{\mathrm{TOT}}$ is more often observed. Accordingly, the median value of $J_{\mathrm{ION}}/J_{\mathrm{TOT}}$ for the $H_2SO_4$-$NH_3$ cases is about 12 % and is clearly higher (18 %) in HOM-driven events (Fig. 6d). Figures 6b and c reveal that both $J_{\mathrm{ION}}$ and $J_{\mathrm{TOT}}$ values are in fact higher in $H_2SO_4$-$NH_3$ cases, but the neutral nucleation pathway is relatively more enhanced, leading to the lower ratio. These results suggest that ion-induced nucleation plays a more important role in the events driven by HOMs than in

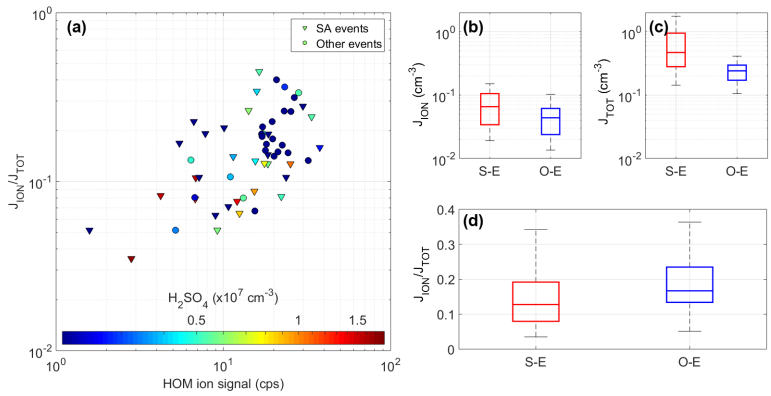


**Figure 6.** Formation rate 2.5 nm ions and total particles (both ions and neutral clusters) under different nucleation mechanisms. **(a)** Charged fraction of the formation rate of 2.5 nm particles as a function of the total signal of HOM ions color-coded by the $H_2SO_4$ concentration, and **(b, c, d)** the differences in $J_{ION}$, $J_{TOT}$, and $J_{ION}/J_{TOT}$ between the $H_2SO_4$–$NH_3$-involved events (S–E) and other events (O–E).

the events driven by $H_2SO_4$-$NH_3$. A plausible explanation is that $NH_3$ performs well in stabilizing $H_2SO_4$ molecules during the clustering process, whereas ions are a relatively more important stabilizing agent for HOM clustering.

## 4 Summary

We investigated the formation of $H_2SO_4$-$NH_3$ anion clusters measured by APi-TOF during three springs from 2011 to 2013 in a boreal forest in southern Finland and their connection to IIN. The abundance and maximum size of $H_2SO_4$-$NH_3$ clusters showed great variability. Out of the total 134 measurement days, $H_2SO_4$-$NH_3$ clusters were only seen during 39 days. The appearance of these clusters was mainly regulated by the concentration ratio between HOMs and $H_2SO_4$, which can be changed by temperature by modulating the HOM production.

We found that the maximum observable size of $H_2SO_4$-$NH_3$ clusters has a strong influence on the probability of an IIN event to occur. More specifically, when clusters containing six or more $H_2SO_4$ molecules were detected, IIN was observed at almost 100 % probability. We further compared the cluster ion growth rates from APi-TOF and NAIS using the maximum-time method. In these $H_2SO_4$-$NH_3$-driven cases when we could robustly define the track of the cluster evolution, the cluster growth was continuous and near linear for cluster sizes up to 3 nm, suggesting co-condensation of $H_2SO_4$ and $NH_3$ as the sole growth mechanism. This does not exclude the possibility that organics could also participate in the growth process in Hyytiälä on other days.

In addition, we noticed that there was a mechanism driving the IIN, and HOMs are most likely to be the responsible species, although $H_2SO_4$ and $NH_3$ might also participate in this mechanism. Such a mechanism was responsible for at least 35 IIN events during the measurement days and is expected to be the prevailing one in higher-temperature seasons.

The contribution of IIN to the total rates of NPF differs between events driven by $H_2SO_4$-$NH_3$ and by HOMs. IIN plays a bigger role in HOM-driven events, likely due to a relatively stronger stabilizing effect of ions. Since the production of HOMs and $H_2SO_4$ are strongly modulated by solar radiation and/or temperature, seasonal variation in IIN can be expected, not only in terms of frequency but also in terms of the underlying mechanisms and hence in terms of the enhancing effect of ions. This information should be considered in aerosol formation modeling in future works.

*Data availability.* The processed APi-TOF data, as well as other relevant parameters, are available at: https://doi.org/10.5281/zenodo.1408617 (Chao, 2018). For the raw mass spectrometer data, please contact the first author via email: chao.yan@helsinki.fi

*Author contributions.* CY and LD wrote the paper. CY, LD, and CR analyzed the main datasets. TJ, SS, HJ, and UM collected the data. All listed coauthors contributed to the manuscript by useful scientific discussions or comments.

*Competing interests.* The authors declare that they have no conflict of interest.

*Acknowledgements.* This work was partially funded by the Academy of Finland (1251427, 1139656, 296628, 306853, Finnish centre of excellence 1141135), the EC Seventh Framework Program and European Union's Horizon 2020 program (Marie Curie ITN no. 316662 "CLOUD-TRAIN", no. 656994 "Nano-CAVa",

no. 227463 “ATMNUCLE”, no. 638703 “COALA”, no. 714621 “GASPARCON”, and no. 742206 “ATM-GTP”), and the European Regional Development Fund project “MOBTT42”. We thank the tofTools team for providing tools for mass spectrometry analysis.

Edited by: Gordon McFiggans
Reviewed by: two anonymous referees

## References

Aalto, P., Hämeri, K., Becker, E., Weber, R., Salm, J., Mäkelä, J. M., Hoell, C., O'Dowd, C. D., Karlsson, H., and Hansson, H. C.: Physical characterization of aerosol particles during nucleation events, Tellus B, 53, 344–358, 2001.

Almeida, J., Schobesberger, S., Kuerten, A., Ortega, I. K., Kupiainen-Maatta, O., Praplan, A. P., Adamov, A., Amorim, A., Bianchi, F., Breitenlechner, M., David, A., Dommen, J., Donahue, N. M., Downard, A., Dunne, E., Duplissy, J., Ehrhart, S., Flagan, R. C., Franchin, A., Guida, R., Hakala, J., Hansel, A., Heinritzi, M., Henschel, H., Jokinen, T., Junninen, H., Kajos, M., Kangasluoma, J., Keskinen, H., Kupc, A., Kürten, T., Kvashin, A. N., Laaksonen, A., Lehtipalo, K., Leiminger, M., Leppa, J., Loukonen, V., Makhmutov, V., Mathot, S., McGrath, M. J., Nieminen, T., Olenius, T., Onnela, A., Petaja, T., Riccobono, F., Riipinen, I., Rissanen, M., Rondo, L., Ruuskanen, T., Santos, F. D., Sarnela, N., Schallhart, S., Schnitzhofer, R., Seinfeld, J. H., Simon, M., Sipila, M., Stozhkov, Y., Stratmann, F., Tome, A., Troestl, J., Tsagkogeorgas, G., Vaattovaara, P., Viisanen, Y., Virtanen, A., Vrtala, A., Wagner, P. E., Weingartner, E., Wex, H., Williamson, C., Wimmer, D., Ye, P., Yli-Juuti, T., Carslaw, K. S., Kulmala, M., Curtius, J., Baltensperger, U., Worsnop, D. R., Vehkamaki, H., and Kirkby, J.: Molecular understanding of sulphuric acid-amine particle nucleation in the atmosphere, Nature, 502, 359–363, https://doi.org/10.1038/nature12663, 2013.

Asmi, E., Sipilä, M., Manninen, H. E., Vanhanen, J., Lehtipalo, K., Gagné, S., Neitola, K., Mirme, A., Mirme, S., Tamm, E., Uin, J., Komsaare, K., Attoui, M., and Kulmala, M.: Results of the first air ion spectrometer calibration and intercomparison workshop, Atmos. Chem. Phys., 9, 141–154, https://doi.org/10.5194/acp-9-141-2009, 2009.

Bianchi, F., Tröstl, J., Junninen, H., Frege, C., Henne, S., Hoyle, C. R., Molteni, U., Herrmann, E., Adamov, A., Bukowiecki, N., Chen, X., Duplissy, J., Gysel, M., Hutterli, M., Kangasluoma, J., Kontkanen, J., Kürten, A., Manninen, H. E., Münch, S., Perä kylä , O., Petä jä , T., Rondo, L., Williamson, C., Weingartner, E., Curtius, J., Worsnop, D. R., Kulmala, M., Dommen, J., and Baltensperger, U.: New particle formation in the free troposphere: A question of chemistry and timing, Science, 352, 1109–1112, 2016.

Bianchi, F., Garmash, O., He, X., Yan, C., Iyer, S., Rosendahl, I., Xu, Z., Rissanen, M. P., Riva, M., Taipale, R., Sarnela, N., Petäjä, T., Worsnop, D. R., Kulmala, M., Ehn, M., and Junninen, H.: The role of highly oxygenated molecules (HOMs) in determining the composition of ambient ions in the boreal forest, Atmos. Chem. Phys., 17, 13819–13831, https://doi.org/10.5194/acp-17-13819-2017, 2017.

Chao, Y.: The role of H2SO4-NH3 anion clusters in ion-induced aerosol nucleation mechanisms in the boreal forest, available at: https://zenodo.org/record/1408617, 2018.

Dada, L., Paasonen, P., Nieminen, T., Buenrostro Mazon, S., Kontkanen, J., Peräkylä, O., Lehtipalo, K., Hussein, T., Petäjä, T., Kerminen, V.-M., Bäck, J., and Kulmala, M.: Long-term analysis of clear-sky new particle formation events and non-events in Hyytiälä, Atmos. Chem. Phys., 17, 6227–6241, https://doi.org/10.5194/acp-17-6227-2017, 2017.

Dunne, E. M., Gordon, H., Kurten, A., Almeida, J., Duplissy, J., Williamson, C., Ortega, I. K., Pringle, K. J., Adamov, A., Baltensperger, U., Barmet, P., Benduhn, F., Bianchi, F., Breitenlechner, M., Clarke, A., Curtius, J., Dommen, J., Donahue, N. M., Ehrhart, S., Flagan, R. C., Franchin, A., Guida, R., Hakala, J., Hansel, A., Heinritzi, M., Jokinen, T., Kangasluoma, J., Kirkby, J., Kulmala, M., Kupc, A., Lawler, M. J., Lehtipalo, K., Makhmutov, V., Mann, G., Mathot, S., Merikanto, J., Miettinen, P., Nenes, A., Onnela, A., Rap, A., Reddington, C. L., Riccobono, F., Richards, N. A., Rissanen, M. P., Rondo, L., Sarnela, N., Schobesberger, S., Sengupta, K., Simon, M., Sipila, M., Smith, J. N., Stozkhov, Y., Tome, A., Trostl, J., Wagner, P. E., Wimmer, D., Winkler, P. M., Worsnop, D. R., and Carslaw, K. S.: Global atmospheric particle formation from CERN CLOUD measurements, Science, 354, 1119–1124, https://doi.org/10.1126/science.aaf2649, 2016.

Eisele, F., Lovejoy, E., Kosciuch, E., Moore, K., Mauldin, R., Smith, J., McMurry, P., and Iida, K.: Negative atmospheric ions and their potential role in ion-induced nucleation, J. Geophys. Res.-Atmos., 111, 2006.

Ehn, M., Junninen, H., Petäjä, T., Kurtén, T., Kerminen, V.-M., Schobesberger, S., Manninen, H. E., Ortega, I. K., Vehkamäki, H., Kulmala, M., and Worsnop, D. R.: Composition and temporal behavior of ambient ions in the boreal forest, Atmos. Chem. Phys., 10, 8513–8530, https://doi.org/10.5194/acp-10-8513-2010, 2010.

Ehn, M., Junninen, H., Schobesberger, S., Manninen, H. E., Franchin, A., Sipila, M., Petaja, T., Kerminen, V. M., Tammet, H., Mirme, A., Mirme, S., Horrak, U., Kulmala, M., and Worsnop, D. R.: An Instrumental Comparison of Mobility and Mass Measurements of Atmospheric Small Ions, Aerosol Sci. Tech., 45, 522–532, https://doi.org/10.1080/02786826.2010.547890, 2011.

Ehn, M., Kleist, E., Junninen, H., Petäjä, T., Lönn, G., Schobesberger, S., Dal Maso, M., Trimborn, A., Kulmala, M., Worsnop, D. R., Wahner, A., Wildt, J., and Mentel, Th. F.: Gas phase formation of extremely oxidized pinene reaction products in chamber and ambient air, Atmos. Chem. Phys., 12, 5113–5127, https://doi.org/10.5194/acp-12-5113-2012, 2012.

Ehn, M., Thornton, J. A., Kleist, E., Sipila, M., Junninen, H., Pullinen, I., Springer, M., Rubach, F., Tillmann, R., Lee, B., Lopez-Hilfiker, F., Andres, S. Y., , Acir, I. H., Rissanen, M., Jokinen, T., Schobesberger, S., Kangasluoma, J., Kontkanen, J., Nieminen, T., Kürten, T., Nielsen, L. B., Jorgensen, S., Kjaergaard, H. G., Canagaratna, M., Dal Maso, M., Berndt, T., Petaja, T., Wahner, A., Kerminen, V. M., Kulmala, M., Worsnop, D. R., Wildt, J., and Mentel, T. F.: A large source of low-volatility secondary organic aerosol, Nature, 506, 476–480, https://doi.org/10.1038/nature13032, 2014.

Franchin, A., Ehrhart, S., Leppä, J., Nieminen, T., Gagné, S., Schobesberger, S., Wimmer, D., Duplissy, J., Riccobono, F., Dunne, E. M., Rondo, L., Downard, A., Bianchi, F., Kupc, A., Tsagkogeorgas, G., Lehtipalo, K., Manninen, H. E., Almeida, J., Amorim, A., Wagner, P. E., Hansel, A., Kirkby, J., Kürten, A., Donahue, N. M., Makhmutov, V., Mathot, S., Metzger, A., Petäjä, T., Schnitzhofer, R., Sipilä, M., Stozhkov, Y., Tomé, A., Kerminen, V.-M., Carslaw, K., Curtius, J., Baltensperger, U., and Kulmala, M.: Experimental investigation of ion-ion recombination under atmospheric conditions, Atmos. Chem. Phys., 15, 7203–7216, https://doi.org/10.5194/acp-15-7203-2015, 2015.

Frege, C., Ortega, I. K., Rissanen, M. P., Praplan, A. P., Steiner, G., Heinritzi, M., Ahonen, L., Amorim, A., Bernhammer, A.-K., Bianchi, F., Brilke, S., Breitenlechner, M., Dada, L., Dias, A., Duplissy, J., Ehrhart, S., El-Haddad, I., Fischer, L., Fuchs, C., Garmash, O., Gonin, M., Hansel, A., Hoyle, C. R., Jokinen, T., Junninen, H., Kirkby, J., Kürten, A., Lehtipalo, K., Leiminger, M., Mauldin, R. L., Molteni, U., Nichman, L., Petäjä, T., Sarnela, N., Schobesberger, S., Simon, M., Sipilä, M., Stolzenburg, D., Tomé, A., Vogel, A. L., Wagner, A. C., Wagner, R., Xiao, M., Yan, C., Ye, P., Curtius, J., Donahue, N. M., Flagan, R. C., Kulmala, M., Worsnop, D. R., Winkler, P. M., Dommen, J., and Baltensperger, U.: Influence of temperature on the molecular composition of ions and charged clusters during pure biogenic nucleation, Atmos. Chem. Phys., 18, 65–79, https://doi.org/10.5194/acp-18-65-2018, 2018.

Gordon, H., Kirkby, J., Baltensperger, U., Bianchi, F., Breitenlechner, M., Curtius, J., Dias, A., Dommen, J., Donahue, N. M., Dunne, E. M., Duplissy, J., Ehrhart, S., Flagan, R. C., Frege, C., Fuchs, C., Hansel, A., Hoyle, C. R., Kulmala, M., Kürten, A., Lehtipalo, K., Makhmutov, V., Molteni, U., Rissanen, M. P., Stozhov, Y., Tröstl, J., Tsakogeorgas, G., Wagner, R., Williamson, C., Wimmer, D., Winkler, P. M., Yan, C., and Carslaw, K. S.: Causes and importance of new particle formation in the present-day and preindustrial atmospheres, J. Geophys. Res.-Atmos., 122, 8739–8760, 2017.

Guo, S., Hu, M., Zamora, M. L., Peng, J., Shang, D., Zheng, J., Du, Z., Wu, Z., Shao, M., Zeng, L., Molina, M. J., and Zhang, R.: Elucidating severe urban haze formation in China, P. Natl. Acad. Sci. USA, 111, 17373–17378, https://doi.org/10.1073/pnas.1419604111, 2014.

Hari, P. and Kulmala, M.: Station for measuring ecosystem-atmosphere relations, Bor. Environ. Res., 10, 315–322, 2005.

Heal, M., Kumar, P., and Harrison, R.: Particles, air quality, policy and health, Chem. Soc. Rev., 41, 6606–6630, 2012.

Hirsikko, A., Laakso, L., Hõrra, U., Aalto, P. P., Kerminen, V. M., and Kulmala, M.: Annual and size dependent variation of growth rates and ion concentrations in boreal forest, Boreal Environ. Res., 10, 357–369, 2005.

Hirsikko, A., Nieminen, T., Gagné, S., Lehtipalo, K., Manninen, H. E., Ehn, M., Hõrrak, U., Kerminen, V.-M., Laakso, L., McMurry, P. H., Mirme, A., Mirme, S., Petäjä, T., Tammet, H., Vakkari, V., Vana, M., and Kulmala, M.: Atmospheric ions and nucleation: a review of observations, Atmos. Chem. Phys., 11, 767–798, https://doi.org/10.5194/acp-11-767-2011, 2011.

Hoppel, W. A.: Ion-aerosol attachment coefficients, ion depletion, and the charge distribution on aerosols, J. Geophys. Res., 90, 5917–5923, 1985.

Iida, K., Stolzenburg, M., McMurry, P., Dunn, M. J., Smith, J. N., Eisele, F., and Keady, P.: Contribution of ion-induced nucleation to new particle formation: Methodology and its application to atmospheric observations in Boulder, Colorado, J. Geophys. Res.-Atmos., 111, D23201, https://doi.org/10.1029/2006JD007167, 2006.

Jokinen, T., Sipilä, M., Junninen, H., Ehn, M., Lönn, G., Hakala, J., Petäjä, T., Mauldin III, R. L., Kulmala, M., and Worsnop, D. R.: Atmospheric sulphuric acid and neutral cluster measurements using CI-APi-TOF, Atmos. Chem. Phys., 12, 4117–4125, https://doi.org/10.5194/acp-12-4117-2012, 2012.

Junninen, H., Ehn, M., Petäjä, T., Luosujärvi, L., Kotiaho, T., Kostiainen, R., Rohner, U., Gonin, M., Fuhrer, K., Kulmala, M., and Worsnop, D. R.: A high-resolution mass spectrometer to measure atmospheric ion composition, Atmos. Meas. Tech., 3, 1039–1053, https://doi.org/10.5194/amt-3-1039-2010, 2010.

Kerminen, V.-M., Paramonov, M., Anttila, T., Riipinen, I., Fountoukis, C., Korhonen, H., Asmi, E., Laakso, L., Lihavainen, H., Swietlicki, E., Svenningsson, B., Asmi, A., Pandis, S. N., Kulmala, M., and Petäjä, T.: Cloud condensation nuclei production associated with atmospheric nucleation: a synthesis based on existing literature and new results, Atmos. Chem. Phys., 12, 12037–12059, https://doi.org/10.5194/acp-12-12037-2012, 2012.

Kirkby, J., Curtius, J., Almeida, J., Dunne, E., Duplissy, J., Ehrhart, S., Franchin, A., Gagné, S., Ickes, L., Kürten, A., Kupc, A., Metzger, A., Riccobono, F., Rondo, L., Schobesberger, S., Tsagkogeorgas, G., Wimmer, D., Amorim, A., Bianchi, F., Breitenlechner, M., David, A., Dommen, J., Downard, A., Ehn, M., Flagan, R. C., Haider, S., Hansel, A., Hauser, D., Jud, W., Junninen, H., Kreissl, F., Kvashin, A., Laaksonen, A., Lehtipalo, K., Lima, J., Lovejoy, E. R., Makhmutov, V., Mathot, S., Mikkilä, J., Minginette, P., Mogo, S., Nieminen, T., Onnela, A., Pereira, P., Petäjä, T., Schnitzhofer, R., Seinfeld, J. H., Sipilä, M., Stozhkov, Y., Stratmann, F., Tomé, A., Vanhanen, J., Viisanen, Y., Vrtala, A., Wagner, P. E., Walther, H., Weingartner, E., Wex, H., Winkler, P. M., Carslaw, K. S., Worsnop, D. R., Baltensperger, U., and Kulmala, M.: Role of sulphuric acid, ammonia and galactic cosmic rays in atmospheric aerosol nucleation, Nature, 476, 429–433, https://doi.org/10.1038/nature10343, 2011.

Kirkby, J., Duplissy, J., Sengupta, K., Frege, C., Gordon, H., Williamson, C., Heinritzi, M., Simon, M., Yan, C., Almeida, J., Tröstl, J., Nieminen, T., Ortega, I. K., Wagner, R., Adamov, A., Amorim, A., Bernhammer, A.-K., Bianchi, F., Breitenlechner, M., Brilke, S., Chen, X., Craven, J., Dias, A., Ehrhart, S., Flagan, R. C., Franchin, A., Fuchs, C., Guida, R., Hakala, J., Hoyle, C. R., Jokinen, T., Junninen, H., Kangasluoma, J., Kim, J., Krapf, M., Kürten, A., Laaksonen, A., Lehtipalo, K., Makhmutov, V., Mathot, S., Molteni, U., Onnela, A., Peräkylä, O., Piel, F., Petäjä, T., Praplan, A. P., Pringle, K., Rap, A., Richards, N. A. D., Riipinen, I., Rissanen, M. P., Rondo, L., Sarnela, N., Schobesberger, S., Scott, C. E., Seinfeld, J. H., Sipilä, M., Steiner, G., Stozhkov, Y., Stratmann, F., Tomé, A., Virtanen, A., Vogel, A. L., Wagner, A. C., Wagner, P. E., Weingartner, E., Wimmer, D., Winkler, P. M., Ye, P., Zhang, X., Hansel, A., Dommen, J., Donahue, N. M., Worsnop, D. R., Baltensperger, U., Kulmala, M., Carslaw, K. S., and Curtius, J.: Ion-induced nucleation of pure biogenic particles, Nature, 533, 521–526, https://doi.org/10.1038/nature17953, 2016.

Kontkanen, J., Lehtinen, K. E. J., Nieminen, T., Manninen, H. E., Lehtipalo, K., Kerminen, V.-M., and Kulmala, M.: Estimating the contribution of ion-ion recombination to sub-2 nm cluster concentrations from atmospheric measurements, Atmos. Chem. Phys., 13, 11391–11401, https://doi.org/10.5194/acp-13-11391-2013, 2013.

Kuang, C., Riipinen, I., Sihto, S.-L., Kulmala, M., McCormick, A. V., and McMurry, P. H.: An improved criterion for new particle formation in diverse atmospheric environments, Atmos. Chem. Phys., 10, 8469–8480, https://doi.org/10.5194/acp-10-8469-2010, 2010.

Kulmala, M., Maso, M. D., Mäkelä, J. M., Pirjola, L., Väkevä, M., Aalto, P., Miikkulainen, P., Hämeri, K., and O'Dowd, C. D.: On the formation, growth and composition of nucleation mode particles, Tellus B, 53, 479–490, 2001.

Kulmala, M., Vehkamäki, H., Petäjä, T., Dal Maso, M., Lauri, A., Kerminen, V.-M., Birmili, W., and McMurry, P. H.: Formation and growth rates of ultrafine atmospheric particles: a review of observations, J. Aerosol Sci., 35, 143–176, 2004.

Kulmala, M., Petaja, T., Nieminen, T., Sipila, M., Manninen, H. E., Lehtipalo, K., Dal Maso, M., Aalto, P. P., Junninen, H., Paasonen, P., Riipinen, I., Lehtinen, K. E., Laaksonen, A., and Kerminen, V. M.: Measurement of the nucleation of atmospheric aerosol particles, Nat. Protocol., 7, 1651–1667, https://doi.org/10.1038/nprot.2012.091, 2012.

Kulmala, M., Kontkanen, J., Junninen, H., Lehtipalo, K., Manninen, H. E., Nieminen, T., Petäjä, T., Sipilä, M., Schobesberger, S., Rantala, P., Franchin, A., Jokinen, T., Järvinen, E., Äijälä, M., Kangasluoma, J., Hakala, J., Aalto, P. P., Paasonen, P., Mikkilä, J., Vanhanen, J., Aalto, J., Hakola, H., Makkonen, U., Ruuskanen, T., Mauldin, R. L., Duplissy, J., Vehkamäki, H., Bäck, J., Kortelainen, A., Riipinen, I., Kurtén, T., Johnston, M. V., Smith, J. N., Ehn, M., Mentel, T. F., Lehtinen, K. E. J., Laaksonen, A., Kerminen, V.-M., and Worsnop, D. R.: Direct Observations of Atmospheric Aerosol Nucleation, Science, 339, 943–946, https://doi.org/10.1126/science.1227385, 2013.

Kürten, A., Bianchi, F., Almeida, J., Kupiainen-Määttä, O., Dunne, E. M., Duplissy, J., Williamson, C., Barmet, P., Breitenlechner, M., Dommen, J., Donahue, N. M., Flagan, R. C., Franchin, A., Gordon, H., Hakala, J., Hansel, A., Heinritzi, M., Ickes, L., Jokinen, T., Kangasluoma, J., Kim, J., Kirkby, J., Kupc, A., Lehtipalo, K., Leiminger, M., Makhmutov, V., Onnela, A., Ortega, I. K., Petäjä, T., Praplan, A. P., Riccobono, F., Rissanen, M. P., Rondo, L., Schnitzhofer, R., Schobesberger, S., Smith, J. N., Steiner, G., Stozhkov, Y., Tomé, A., Tröstl, J., Tsagkogeorgas, G., Wagner, P. E., Wimmer, D., Ye, P., Baltensperger, U., Carslaw, K., Kulmala, M., and Curtius, J.: Experimental particle formation rates spanning tropospheric sulfuric acid and ammonia abundances, ion production rates, and temperatures, J. Geophys. Res.-Atmos., 121, 12377–12400, https://doi.org/10.1002/2015jd023908, 2016.

Lovejoy, E., Curtius, J., and Froyd, K.: Atmospheric ion-induced nucleation of sulfuric acid and water (1984–2012), J. Geophys. Res.-Atmos., 109, 109, D08204, doi:10.1029/2003JD004460, 2004.

Makkonen, U., Virkkula, A., Hellen, H., Hemmila, M., Sund, J., Aijala, M., Ehn, M., Junninen, H., Keronen, P., Petaja, T., Worsnop, D. R., Kulmala, M., and Hakola, H.: Semi-continuous gas and inorganic aerosol measurements at a boreal forest site: seasonal and diurnal cycles of $NH_3$, HONO and $HNO_3$, Boreal Environ. Res., 19, 311–328, 2014.

Manninen, H. E., Nieminen, T., Asmi, E., Gagné, S., Häkkinen, S., Lehtipalo, K., Aalto, P., Vana, M., Mirme, A., Mirme, S., Hõrrak, U., Plass-Dülmer, C., Stange, G., Kiss, G., Hoffer, A., Töro, N., Moerman, M., Henzing, B., de Leeuw, G., Brinkenberg, M., Kouvarakis, G. N., Bougiatioti, A., Mihalopoulos, N., O'Dowd, C., Ceburnis, D., Arneth, A., Svenningsson, B., Swietlicki, E., Tarozzi, L., Decesari, S., Facchini, M. C., Birmili, W., Sonntag, A., Wiedensohler, A., Boulon, J., Sellegri, K., Laj, P., Gysel, M., Bukowiecki, N., Weingartner, E., Wehrle, G., Laaksonen, A., Hamed, A., Joutsensaari, J., Petäjä, T., Kerminen, V.-M., and Kulmala, M.: EUCAARI ion spectrometer measurements at 12 European sites – analysis of new particle formation events, Atmos. Chem. Phys., 10, 7907–7927, https://doi.org/10.5194/acp-10-7907-2010, 2010.

Mcmurry, P. H., Fink, M., Sakurai, H., Stolzenburg, M. R., Mauldin, R. L., Smith, J., Eisele, F., Moore, K., Sjostedt, S., and Tanner, D.: A criterion for new particle formation in the sulfur-rich Atlanta atmosphere, J. Geophys. Res.-Atmos., 110, 2935–2948, 2005.

Merikanto, J., Spracklen, D. V., Mann, G. W., Pickering, S. J., and Carslaw, K. S.: Impact of nucleation on global CCN, Atmos. Chem. Phys., 9, 8601–8616, https://doi.org/10.5194/acp-9-8601-2009, 2009.

Mirme, S. and Mirme, A.: The mathematical principles and design of the NAIS – a spectrometer for the measurement of cluster ion and nanometer aerosol size distributions, Atmos. Meas. Tech., 6, 1061–1071, https://doi.org/10.5194/amt-6-1061-2013, 2013.

Riccobono, F., Schobesberger, S., Scott, C. E., Dommen, J., Ortega, I. K., Rondo, L., Almeida, J., Amorim, A., Bianchi, F., Breitenlechner, M., David, A., Downard, A., Dunne, E. M., Duplissy, J., Ehrhart, S., Flagan, R. C., Franchin, A., Hansel, A., Junninen, H., Kajos, M., Keskinen, H., Kupc, A., Kürten, A., Kvashin, A. N., Laaksonen, A., Lehtipalo, K., Makhmutov, V., Mathot, S., Nieminen, T., Onnela, A., Petaja, T., Praplan, A. P., Santos, F. D., Schallhart, S., Seinfeld, J. H., Sipila, M., Spracklen, D. V., Stozhkov, Y., Stratmann, F., Tome, A., Tsagkogeorgas, G., Vaattovaara, P., Viisanen, Y., Vrtala, A., Wagner, P. E., Weingartner, E., Wex, H., Wimmer, D., Carslaw, K. S., Curtius, J., Donahue, N. M., Kirkby, J., Kulmala, M., Worsnop, D. R., and Baltensperger, U.: Oxidation products of biogenic emissions contribute to nucleation of atmospheric particles, Science, 344, 717–721, https://doi.org/10.1126/science.1243527, 2014.

Rose, C., Zha, Q., Dada, L., Yan, C., Lehtipalo, K., Junninen, H., Mazon, S. B., Jokinen, T., Sarnela, N., Sipila, M., Petaja, T., Kerminen, V. M., Bianchi, F., and Kulmala, M.: Observations of biogenic ion-induced cluster formation in the atmosphere, Sci. Adv., 4, 5218, https://doi.org/10.1126/sciadv.aar5218, 2018.

Schobesberger, S., Junninen, H., Bianchi, F., Lonn, G., Ehn, M., Lehtipalo, K., Dommen, J., Ehrhart, S., Ortega, I. K., Franchin, A., Nieminen, T., Riccobono, F., Hutterli, M., Duplissy, J., Almeida, J., Amorim, A., Breitenlechner, M., Downard, A. J., Dunne, E. M., Flagan, R. C., Kajos, M., Keskinen, H., Kirkby, J., Kupc, A., Kürten, A., Kürten, T., Laaksonen, A., Mathot, S., Onnela, A., Praplan, A. P., Rondo, L., Santos, F. D., Schallhart, S., Schnitzhofer, R., Sipila, M., Tome, A., Tsagkogeorgas, G., Vehkamaki, H., Wimmer, D., Baltensperger, U., Carslaw, K. S., Curtius, J., Hansel, A., Petaja, T., Kulmala, M., Donahue,

N. M., and Worsnop, D. R.: Molecular understanding of atmospheric particle formation from sulfuric acid and large oxidized organic molecules, P. Natl. Acad. Sci. USA, 110, 17223–17228, https://doi.org/10.1073/pnas.1306973110, 2013.

Schobesberger, S., Franchin, A., Bianchi, F., Rondo, L., Duplissy, J., Kürten, A., Ortega, I. K., Metzger, A., Schnitzhofer, R., Almeida, J., Amorim, A., Dommen, J., Dunne, E. M., Ehn, M., Gagné, S., Ickes, L., Junninen, H., Hansel, A., Kerminen, V.-M., Kirkby, J., Kupc, A., Laaksonen, A., Lehtipalo, K., Mathot, S., Onnela, A., Petäjä, T., Riccobono, F., Santos, F. D., Sipilä, M., Tomé, A., Tsagkogeorgas, G., Viisanen, Y., Wagner, P. E., Wimmer, D., Curtius, J., Donahue, N. M., Baltensperger, U., Kulmala, M., and Worsnop, D. R.: On the composition of ammonia-sulfuric-acid ion clusters during aerosol particle formation, Atmos. Chem. Phys., 15, 55–78, https://doi.org/10.5194/acp-15-55-2015, 2015.

Stocker, T., Qin, D., Plattner, G., Tignor, M., Allen, S., Boschung, J., Nauels, A., Xia, Y., Bex, B., and Midgley, B.: in: IPCC, 2013, Climate change 2013, The physical science basis. Contribution of working group I to the fifth assessment report of the intergovernmental panel on climate change, 2013.

Tammet, H. and Kulmala, M.: Simulation tool for atmospheric aerosol nucleation bursts, J. Aerosol Sci., 36, 173–196, 2005.

Wagner, R., Yan, C., Lehtipalo, K., Duplissy, J., Nieminen, T., Kangasluoma, J., Ahonen, L. R., Dada, L., Kontkanen, J., Manninen, H. E., Dias, A., Amorim, A., Bauer, P. S., Bergen, A., Bernhammer, A.-K., Bianchi, F., Brilke, S., Mazon, S. B., Chen, X., Draper, D. C., Fischer, L., Frege, C., Fuchs, C., Garmash, O., Gordon, H., Hakala, J., Heikkinen, L., Heinritzi, M., Hofbauer, V., Hoyle, C. R., Kirkby, J., Kürten, A., Kvashnin, A. N., Laurila, T., Lawler, M. J., Mai, H., Makhmutov, V., Mauldin III, R. L., Molteni, U., Nichman, L., Nie, W., Ojdanic, A., Onnela, A., Piel, F., Quéléver, L. L. J., Rissanen, M. P., Sarnela, N., Schallhart, S., Sengupta, K., Simon, M., Stolzenburg, D., Stozhkov, Y., Tröstl, J., Viisanen, Y., Vogel, A. L., Wagner, A. C., Xiao, M., Ye, P., Baltensperger, U., Curtius, J., Donahue, N. M., Flagan, R. C., Gallagher, M., Hansel, A., Smith, J. N., Tomé, A., Winkler, P. M., Worsnop, D., Ehn, M., Sipilä, M., Kerminen, V.-M., Petäjä, T., and Kulmala, M.: The role of ions in new particle formation in the CLOUD chamber, Atmos. Chem. Phys., 17, 15181–15197, https://doi.org/10.5194/acp-17-15181-2017, 2017.

Yan, C., Nie, W., äijälä, M., Rissanen, M. P., Canagaratna, M. R., Massoli, P., Junninen, H., Jokinen, T., Sarnela, N., Häme, S. A. K., Schobesberger, S., Canonaco, F., Yao, L., Prévôt, A. S. H., Petäjä, T., Kulmala, M., Sipilä, M., Worsnop, D. R., and Ehn, M.: Source characterization of highly oxidized multifunctional compounds in a boreal forest environment using positive matrix factorization, Atmos. Chem. Phys., 16, 12715–12731, https://doi.org/10.5194/acp-16-12715-2016, 2016.

# Paper V

ATMOSPHERIC SCIENCE

# Observations of biogenic ion-induced cluster formation in the atmosphere

Clémence Rose,[1]* Qiaozhi Zha,[1†] Lubna Dada,[1†] Chao Yan,[1] Katrianne Lehtipalo,[1] Heikki Junninen,[1,2] Stephany Buenrostro Mazon,[1] Tuija Jokinen,[1] Nina Sarnela,[1] Mikko Sipilä,[1] Tuukka Petäjä,[1,3,4] Veli-Matti Kerminen,[1] Federico Bianchi,[1,5] Markku Kulmala[1,3,5]*



**A substantial fraction of aerosols, which affect air quality and climate, is formed from gaseous precursors. Highly oxygenated organic molecules (HOMs) are essential to grow the newly formed particles and have been evidenced to initiate ion-induced nucleation in chamber experiments in the absence of sulfuric acid. We investigate this phenomenon in the real atmosphere using an extensive set of state-of-the-art ion and mass spectrometers deployed in a boreal forest environment. We show that within a few hours around sunset, HOMs resulting from the oxidation of monoterpenes are capable of forming and growing ion clusters even under low sulfuric acid levels. In these conditions, we hypothesize that the lack of photochemistry and essential vapors prevents the organic clusters from growing past 6 nm. However, this phenomenon might have been a major source of particles in the preindustrial atmosphere and might also contribute to particle formation in the future and consequently affect the climate.**

## INTRODUCTION

Atmospheric new particle formation (NPF) is a significant source of particles and cloud condensation nuclei (CCN) (*1*) and in turn affects both air quality and climate. It has been commonly believed that sulfuric acid ($H_2SO_4$) is essential to initiate the process in most environments (*2*, *3*). However, typical daytime $H_2SO_4$ concentrations are usually too low to explain the observed particle formation and growth rates, indicating that additional vapors are needed to sustain the process (*2*, *4*, *5*). These vapors are most likely highly oxygenated organic molecules (HOMs) resulting from the oxidation of volatile organic compounds (VOCs) (*5*–*8*), either from anthropogenic or biogenic (BVOC) origin. Bianchi *et al.* (*9*) recently reported the first direct atmospheric evidence for the contribution of these compounds, probably from anthropogenic origin, in the early nucleation stage. Correspondingly, using the CERN Cosmics Leaving Outdoor Droplets (CLOUD) facilities, Kirkby *et al.* (*10*) were able to show evidence for ion-induced nucleation of pure biogenic particles initiated by HOMs produced by the ozonolysis of α-pinene. Implementing these chamber findings into a global model suggested that pure biogenic nucleation may be able to explain a significant source of particles in pristine environments at the present time and might have also dominated both nucleation and atmospheric CCN formation in the preindustrial era, when $H_2SO_4$ concentrations were much lower (*11*). However, although circumstantial evidence for pure biogenic nucleation is well demonstrated in the latter study, a direct observation of this process in the ambient atmosphere is still lacking. In particular, most of the studies conducted so far to document the chemical composition of ions in relation to the occurrence of NPF were performed using daytime measurements conducted in the boreal forest in Hyytiälä, Southern Finland, when $H_2SO_4$ has been shown to play a major role in cluster formation (*2*). Also, although chamber experiments can well mimic atmospheric observations (*6*, *12*), they cannot fully achieve the complexity of the real atmosphere. For instance, the experiments discussed by Kirkby *et al.* (*10*) were conducted in the absence of $NO_x$. Recently, Bianchi *et al.* (*13*) have extensively analyzed the chemical composition of the negative ions in the boreal forest, where they identified many HOMs clustered with $NO_3^-$ and $HSO_4^-$. Ion clusters containing up to 40 carbon atoms were detected during nighttime, but a possible link with NPF was not investigated.

## RESULTS

### Identification of the evening ion cluster formation events

The aim of our work was to investigate the occurrence of the pure biogenic ion cluster formation in the real atmosphere. For that, we analyzed measurements performed between 9 April 2013 and 15 June 2013 with an extensive set of state-of-the-art ion and mass spectrometers at the boreal Station for Measuring Forest Ecosystem–Atmosphere Relations (SMEAR) II station in Hyytiälä, Southern Finland. BVOC emissions have been reported to be dominated by monoterpenes (*14*) and to produce large amounts of HOMs (*15*, *16*) at this site. Keeping in mind that sulfuric acid–driven pathways are dominating daytime nucleation in Hyytiälä (*2*), we focus here on the occurrence of evening events leading to the formation and growth of intermediate ions, also referred to as ion clusters or charged clusters. Studying evening-time ion cluster formation processes also enabled us to focus on HOM production in absence of NO, which then resembles the conditions discussed by Kirkby *et al.* (*10*) at close proximity.

We started the identification of the ion cluster formation events by filtering out all evenings with precipitation detected after 1600 [local time, universal time (UT) +2] to exclude all potential rain-induced events from our analysis (*17*). Consistent with previous observations at the site (*18*–*20*), 25 of the 32 evenings included in our analysis were classified as evening events (~78%), during which we identified a distinct rise in the 1.5- to 2.5-nm ion concentration measured with a Neutral cluster and Air Ion Spectrometer (NAIS; see Materials and Methods

[1]Institute for Atmospheric and Earth System Research/Physics, Faculty of Science, University of Helsinki, P.O. Box 64, FIN-00014 Helsinki, Finland. [2]Institute of Physics, University of Tartu, Ülikooli 18, EE-50090 Tartu, Estonia. [3]Joint International Research Laboratory of Atmospheric and Earth System Sciences, School of Atmospheric Sciences, Nanjing University, Nanjing 210046, P.R. China. [4]Tyumen State University, 6 Volodarskogo Street, 625003 Tyumen, Russia. [5]Aerosol and Haze Laboratory, Beijing University of Chemical Technology, North Third Ring Road East 15, Chaoyang District, Beijing 100029, P.R. China.
*Corresponding author. Email: c.rose@opgc.univ-bpclermont.fr (C.R.); markku.kulmala@helsinki.fi (M.K.)
†These authors contributed equally to this work.

for a detailed description of the instrumental setup), with similar observations for both polarities (Fig. 1). Three evenings were classified as nonevent, and the last four were considered as undefined. Because our mass spectrometer was operated to measure negative ions, we proceeded by analyzing only negatively charged clusters from the NAIS. Owing to this last information, ion data discussed in the next sections will implicitly refer to negative polarity only.

The median concentration of 1.5- to 2.5-nm ions was 28 $cm^{-3}$ at the beginning of the events and reached 180 $cm^{-3}$ at the event peak time, with a major contribution of sub–2-nm clusters. As reported in Table 1, the formation rate of 1.5-nm charged clusters ($J^{-}_{1.5}$; also, see Materials and Methods) was on average ~3 times higher compared to that in daytime NPF events observed at the same site (*2*). Cluster growth rates in the size range of 1.5 to 3 nm were also higher than those usually measured during daytime NPF events (*21*). However, in contrast to daytime, as expected from the ion concentrations in the aforementioned size bins, we did not observe the growth of ion clusters past a few nanometers during the evening events, similar to earlier publications (*18*–*20*). The limited growth of the clusters was additionally highlighted by the sharp decrease of the cluster formation rate as the cluster size increases, as illustrated in fig. S1. The observed events were further classified into three classes based on the size of the clusters at the end of their growth process (Fig. 1 and Table 1). These three event types will be hereafter referred to as Minimum, (final cluster size, <3 nm), Medium (final cluster size, between 3 and 4 nm), and Maximum (final cluster size, >4 nm) growth events, with Minimum growth events being the most frequent. As presented in Table 1, the detection of ion clusters at larger sizes during Maximum growth events (up to NAIS channel with a mean diameter of 6 nm) consistently coincided with higher cluster formation and early growth rates compared to other event types, with average $J^{-}_{1.5}$ being, for instance, ~2.7 times higher than that measured during Minimum growth events.

On event evenings, the median start time of ion cluster formation was 1815, that is, on average, 2 hours before sunset, with no clear distinction between different event types (fig. S2). The earliest events were observed to start slightly after 1600. Most of the Minimum growth events (67%)

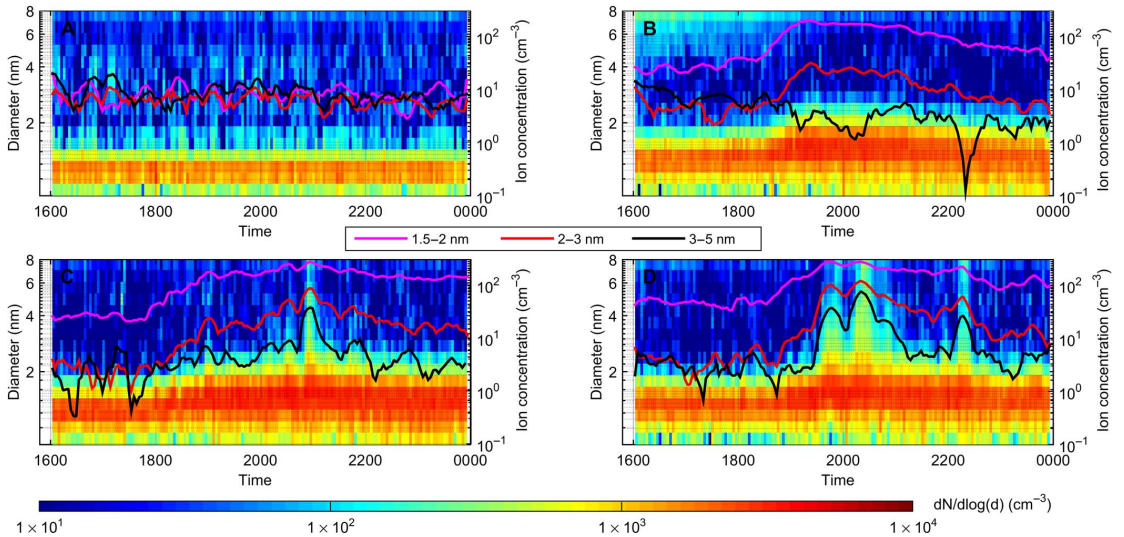


**Fig. 1. Classification of the charged cluster formation events.** Classification was performed using NAIS surface plots and time series of ions concentration in various size ranges, including 1.5 to 2 nm, 2 to 3 nm, and 3 to 5 nm. (**A**) Nonevent evening on 12 April. (**B**) Minimum growth event on 21 April. (**C**) Medium growth event on 12 May. (**D**) Maximum growth event on 8 May.

**Table 1. Characteristics of the observed evening events.** All 25 events were classified into three groups (Minimum, Medium, and Maximum growth events) based on the size of the clusters at the end of the growth process (second column). The number of events in each class is indicated in the first column. Cluster ion (1.5 nm) formation rates ($J^{-}_{1.5}$) and cluster growth rate in the range of 1.5 to 3 nm ($GR_{1.5–3}$) are reported in the third and fourth columns, respectively. The reported values are given as mean ± 1σ, either calculated from all events or from events of the specified type.

| Type of events (frequency) | Final cluster size | $J^{-}_{1.5}$ (×10$^{-1}$ cm$^{-3}$) | $GR_{1.5–3}$ (nm hour$^{-1}$) |
|---|---|---|---|
| All events | — | 2.6 ± 2.3 | 2.8 ± 1.4 |
| Minimum growth events (18) | <3 nm | 2.1 ± 1.6 | 2.5 ± 1.3 |
| Medium growth events (4) | Between 3 and 4 nm | 3.5 ± 2.7 | 3.2 ± 0.9 |
| Maximum growth events (3) | >4 nm | 5.5 ± 3.9 | 4.0 ± 2.1 |

were peaking after daylight had completely disappeared, whereas by contrast, half of the Medium growth events and most of Maximum growth events (two of three) were on average peaking slightly before sunset, up to almost 1 hour before dark.

### Evidence for the major implication of monoterpene oxidation products in the early stage of ion cluster formation

Concurrent with the occurrence of evening events, we observed a build-up of naturally charged HOM compounds using an atmospheric pressure interface–time-of-flight mass spectrometer (APi-TOF; Fig. 2). Assuming monoterpenes ($C_{10}H_{16}$) are the dominant precursors for HOMs at this site (*16*), the mass/charge (*m/z*) range was divided into three subranges for the present study. We defined monomers (carbon numbers 9 and 10), dimers (carbon numbers 16 to 20), and trimers (carbon numbers 27 to 30) to be the sum of HOM peaks in the ranges of *m/z* = 300 to 400 Thomson (Th), 500 to 650 Th, and 750 to 850 Th, respectively. The averaged time evolution of the mass spectra calculated from all event evenings shows that monomers typically dominated the mass spectrum until 1900, after which dimers and trimers progressively took over (Fig. 2A). As demonstrated earlier by Yan *et al.* (*15*), the aforementioned modifications of the mass spectrum could be, to a large extent, explained by the diurnal variation of the oxidation mechanisms responsible for the formation of HOMs. In particular, active photochemistry during daytime supports the production of NO and $HO_2$, which are known to be efficient peroxy radical ($RO_2$) terminators and in turn prevent the formation of dimers, which are closed-shell molecules assumed to be formed through the reaction between two $RO_2$ (*22*). On the other hand, the absence of the abovementioned terminators during evening-time and nighttime hours supports the appearance of dimers and in turn trimers because those most likely result from the clustering of monomers and dimers (*23*). The average molecular growth rate resulting from this progressive HOMs build-up process was estimated to be 181.8 atomic mass unit (amu) $hour^{-1}$ between 1800 and 2100 (Fig. 2A; also, see Materials and Methods). Assuming an average density of 1400 kg $m^{-3}$ for the clusters, this growth rate is equivalent to 0.14 nm $hour^{-1}$, comparable to daytime values reported for the same size range by Kulmala *et al.* (*2*). The HOMs build-up is further illustrated in Fig. 2B, which shows one example of a mass defect plot [that is, the difference between the exact mass and the nominal mass (*24*)], during which it was possible to detect tetramers, that is, HOMs containing up to 40 carbon atoms. According to Frege *et al.* (*23*), those probably result from the collision of two dimers.

We investigated the relationship between the observations of the ion and mass spectrometers by checking the correlation between the APi-TOF signal of selected mass ranges and the charged cluster concentration measured with the NAIS in different size bins. Among the most possible combinations (table S1), strong correlations were found between the concentrations of 1.44-nm ions and HOM dimers ($R^2$ = 0.84; Fig. 3A) and between the concentrations of 1.66-nm ions and HOM trimers ($R^2$ = 0.65; Fig. 3B), consistent with expectations from the mass-to-diameter conversion. The tight connection between the HOMs build-up and the formation of charged clusters was further supported by the similar temporal variation of $J^-_{1.5}$ and HOM dimers signal (Fig. 3C). The median HOM dimers and trimers signals were on average ~2 times higher during the active cluster formation period, that is, ~1900 to 2200, compared to the same period on nonevent evenings (fig. S3, A and C, and table S2A). In addition, although similar signal intensities were observed during all the events regardless of their type, the highest HOM dimers and trimers signals were detected during

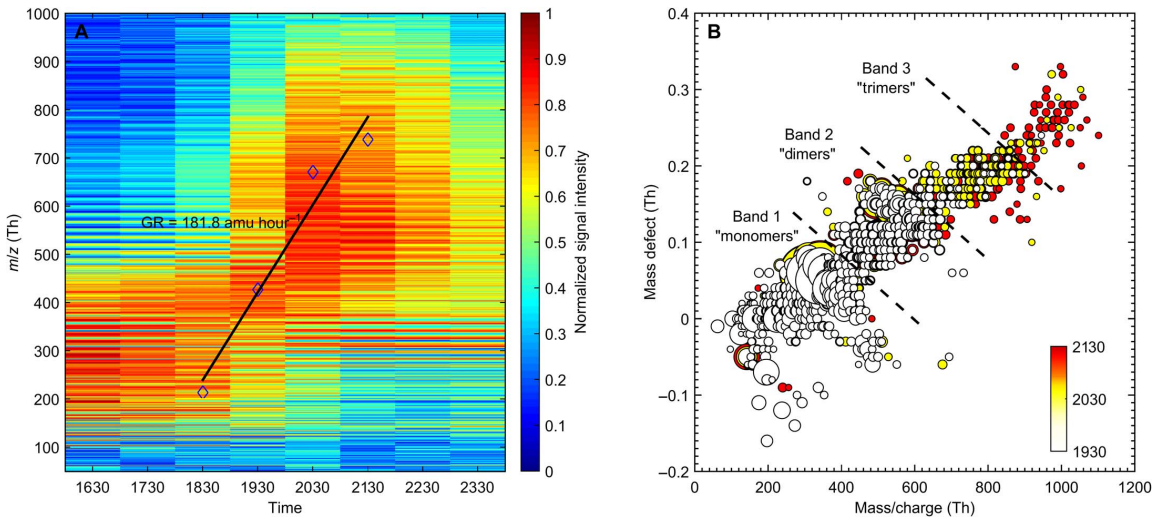


**Fig. 2. Build-up process of naturally negatively charged HOMs.** (**A**) Averaged time evolution of the mass spectra calculated from all 25 event evenings between 1600 and 0000 (local time, UT +2). The solid line and corresponding diamonds illustrate the molecular growth rate resulting from the HOMs build-up process. (**B**) Mass defect plot for the cluster formation event detected on 20 April. The mass defect, that is, the difference between the exact mass and the nominal mass, is shown on the ordinate. The area of the dots is proportional to the intensity of the observed signal, and the color scale indicates the time at which each of the three mass spectra was measured. The presence of HOM monomers, dimers, and trimers is evidenced on the mass defect plot and their progressive appearance from 1930 to 2130. By contrast, clusters resulting from based-stabilized nucleation of $H_2SO_4$ with $NH_3$ or amines are not observed at any time.

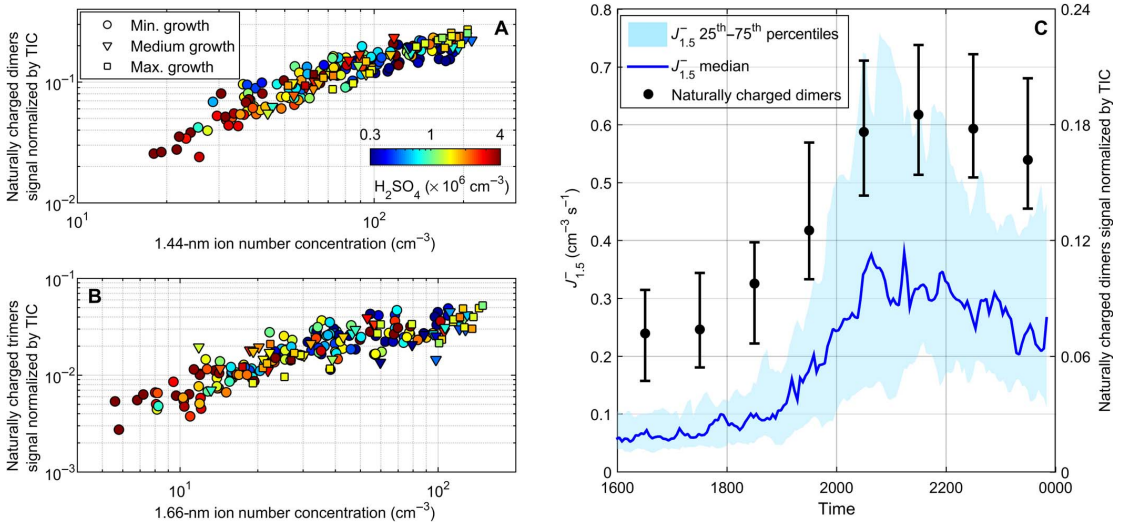


**Fig. 3. Relationship between ion and mass spectrometers observations.** (**A**) Normalized HOM dimers signal as a function of 1.44-nm negative ion number concentration. Concentrations and signal intensities are 1-hour averages from all event evenings between 1600 and 0000. (**B**) Same as (A) with HOM trimers and 1.66-nm negatively charged clusters. (**C**) Averaged time series of the HOM dimers signal normalized by total ion count (TIC) and formation rate of 1.5-nm negatively charged clusters on event evenings. Black circles represent the median of the normalized HOM dimers signal, whereas lower and upper limits of the error bars represent the 25th and 75th percentiles, respectively.

the active cluster formation period on Maximum growth event evenings. By contrast, similar signals were measured for monomers on event and nonevent evenings (fig. S4 and table S2A), suggesting that monomers were not directly connected to the occurrence of the evening events. The latter supports previous observations reported by Kulmala *et al.* (*2*) during daytime NPF. Also, Mohr *et al.* (*25*) have discussed the importance of HOM dimers in atmospheric NPF.

In addition, sulfuric acid was measured with an APi-TOF equipped with a nitrate ion-based chemical ionization (CI) inlet (CI-APi-TOF). As evidenced in Fig. 3, $H_2SO_4$ concentration was below ~$4 \times 10^6$ cm$^{-3}$ during the observed events, with a median level of $8.4 \times 10^5$ cm$^{-3}$ (fig. S5 and table S2A). These values are slightly higher compared to those reported by Kirkby *et al.* (*10*) during ion-induced nucleation of pure biogenic particles in the CLOUD chamber, and thus, we cannot totally exclude participation of $H_2SO_4$ in the evening events in Hyytiälä. However, at these concentrations, $H_2SO_4$ is neither expected to efficiently participate in the cluster formation process nor significantly influence the formation rates (*9*, *10*), at least without the involvement of bases such as ammonia ($NH_3$) or amines (*4*, *26*). As anticipated, the cluster formation rates measured during evening time in Hyytiälä were several orders of magnitude higher compared to those expected from binary ion induced nucleation of $H_2SO_4$–$H_2O$ in similar conditions (*4*, *27*). Also, as illustrated on Fig. 2B, the mass defect plots obtained during the observed evening events did not indicate the formation of $H_2SO_4$–$NH_3$ nor $H_2SO_4$–amine clusters and contrasted with those characteristic of base-stabilized nucleation of $H_2SO_4$ in the presence of $NH_3$ or amines (*12*). This indicates that $H_2SO_4$-driven pathways, that is, both acid-base and $H_2SO_4$–$H_2O$ binary nucleation, could not dominate the evening-time formation of ion clusters, which was instead driven by monoterpene oxidation products that we detected with the APi-TOF. A strong implication of $H_2SO_4$ in the cluster formation process together with HOMs was also unlikely because $HSO_4^-$-HOM clusters were only observed during daytime in Hyytiälä, whereas HOMs were rather clustered with nitrate radical during the night (*13*). Instead, slightly higher $H_2SO_4$ concentrations observed on event evenings were most likely explained by increased amounts of stabilized Criegee intermediates, whose production was previously reported to be tightly connected to that of HOMs (*28*). All in all, our observations thus present the first direct evidence of an atmospheric ion cluster (1.5 to 3 nm) formation pathway dominated by biogenic HOMs.

## Further insights into the chemical specificities of the HOMs involved in ion cluster formation

We further investigated the chemical specificities of the dimers involved in the formation of the charged clusters. On the basis of earlier work by Yan *et al.* (*15*), we used two subsets of peaks: the ozonolysis products of monoterpenes (that is, non-nitrate HOM dimers) and organonitrate HOM dimers (that is, nitrogen-containing compounds; table S3). The median signal of the non-nitrate HOM dimers was on average ~3 times higher during the active ion cluster formation period compared to the same time period on nonevent evenings, with the highest signals recorded during Maximum growth events (table S2A). In addition, a strong correlation was observed between the number concentration of 1.44-nm ion clusters and the signal of non-nitrate dimers ($R^2$ = 0.75; Fig. 4A). By contrast, because of an important variability of their signal, organonitrate dimers did not fully correlate with the 1.44-nm ion number concentration ($R^2$ = 0.07; Fig. 4B), and the difference between event and nonevent evening median signals was not as pronounced as for non-nitrate compounds (fig. S6C and table S2A). As a result, non-nitrate HOM dimers were more abundant relative to organonitrates

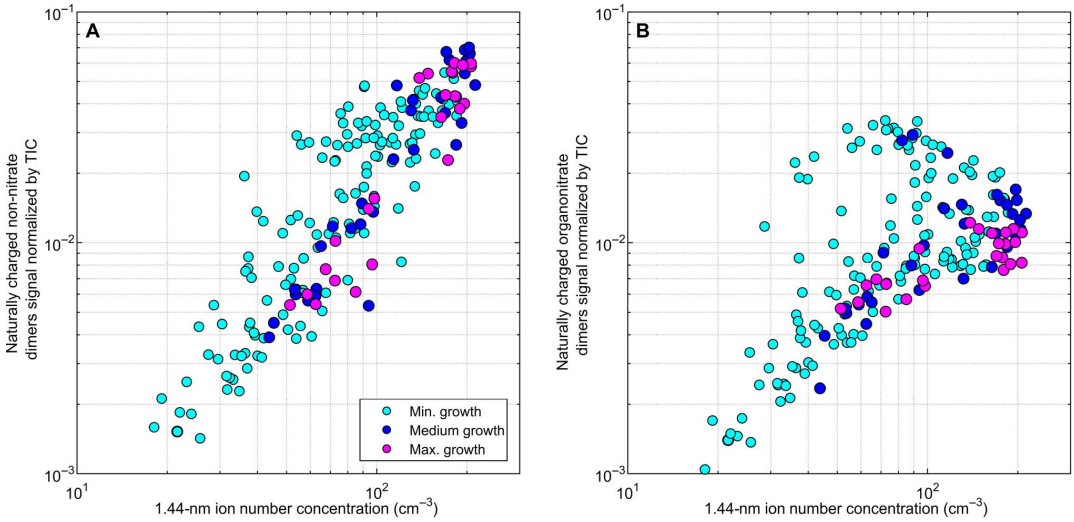


**Fig. 4. Insights into the identification of the charged HOMs involved in the formation of negatively charged clusters.** Normalized signals of (**A**) non-nitrate and (**B**) organonitrate HOM dimers as a function of 1.44-nm negative ion number concentration. Concentrations and signal intensities are 1-hour averages from all event evenings between 1600 and 0000.

during Maximum growth events, suggesting that nitrogen-containing compounds could be less efficient in forming and growing the clusters than non-nitrate compounds.

### Effect of various atmospheric parameters on HOMs production and subsequent ion cluster formation

To further identify the conditions favoring the production of HOMs and subsequent formation of organic clusters, we investigated the time evolution of several meteorological and atmospheric variables. For simplicity, we compare Maximum growth events and nonevent evenings in Fig. 5 while showing all event types in fig. S7 and table S2B. The medians of monoterpene and ozone concentrations were ~4 and 1.5, respectively, times higher during the active cluster formation period on Maximum growth events compared to the same time period on nonevent evenings, when temperature and global radiation were also higher (Fig. 5, A and B, and table S2B). In contrast to the abovementioned HOM-source related variables, relative humidity and condensation sink (CS) had median values ~2.5 and 4 times lower on event evenings, respectively (Fig. 5C and table S2B). The former observation related to monoterpene and ozone concentrations supported an enhanced production of $RO_2$ on event evenings and subsequent higher probability of $RO_2$–$RO_2$ reaction. This, together with lower CS, most likely explains the higher dimer signals measured on those specific evenings compared to nonevent evenings. Explicitly combining the aforementioned variables in a proxy describing the formation of monoterpene ozonolysis products further highlighted their synergistic effect, both on the occurrence of cluster formation and on the ability of the ion clusters to grow (Fig. 5D, fig. S7, and table S2B; see Materials and Methods). On Maximum growth event evenings, the conditions favored the formation of monoterpene ozonolysis products compared to other evenings, which most probably explained the higher formation and early growth rates of organic ion clusters on those specific evenings (Table 1). The survival probability of the clusters increased as well, resulting in the observation of larger clusters compared to other evenings.

## DISCUSSION

Consistent with previous observations at the site (*18*–*20*), we report the frequent (~78%) evening-time formation of charged clusters at the boreal SMEAR II station in Hyytiälä during spring 2013. Our results demonstrate, for the first time, that the first step of ion-induced NPF, that is, initial ion cluster formation and growth, can be active under atmospheric conditions in a system dominated by biogenic vapors at very low $H_2SO_4$ concentrations.

As pointed out earlier in this work, the growth of the ion clusters up to 3 nm was on average faster during evening events compared to that in daytime NPF events at the same site (*21*). This observation is most likely explained by the fact that dimers, which are more efficiently produced in the evening, represent a significant fraction of the extremely low VOCs (ELVOCs) shown to be the major organic contributor to cluster growth in this size range (*8*). Nevertheless, in contrast to daytime, the growth of observed ion clusters did not exceed 6 nm. Instrumental limitations prevent a complete understanding of the reasons for this limited growth. We are currently unable to measure the chemical composition of clusters after they have grown out of the size range where they can be detected by ion mass spectrometers, such as the APi-TOF (>~2 nm), and before they are sufficiently large to be characterized by aerosol mass spectrometers (<~ 100 nm). As a result, the compounds, which are involved in the growth of these "intermediate"-sized particles, have not been directly characterized yet. Using a dynamic volatility basis set model, Tröstl *et al.* (*8*) were able to demonstrate that, besides ELVOCs, low VOCs (LVOCs) are needed to explain observed particle growth past 2 nm. Among other sources, the reaction of first-generation oxidation products of monoterpenes with OH radicals was

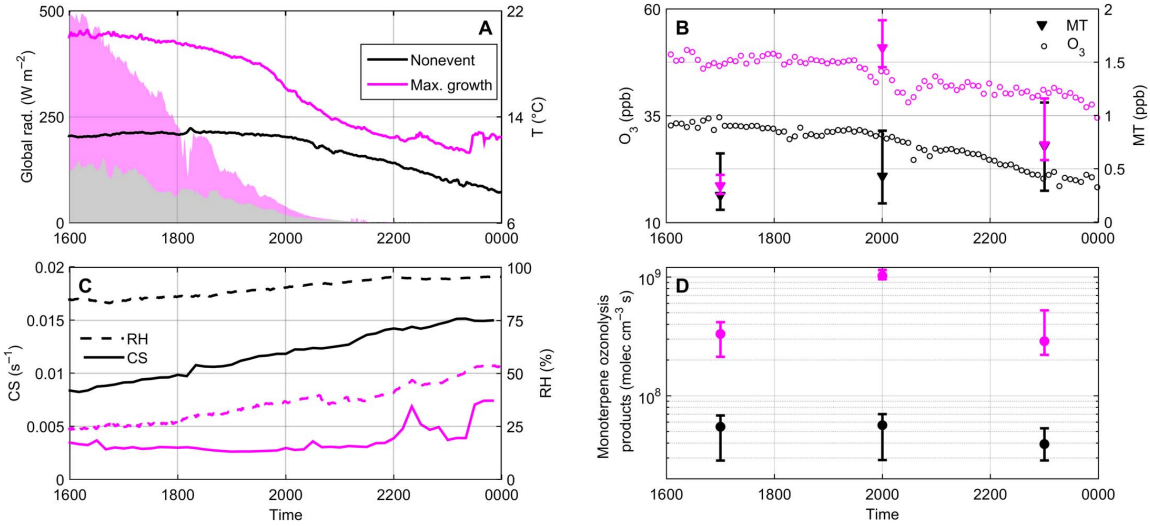


**Fig. 5. The effect of various parameters on HOMs production and subsequent ion cluster formation.** Throughout, colors indicate evening type, that is, nonevent (black) or Maximum growth events (magenta). In (**A**) to (**C**), when not specified, reported values are medians calculated over all the evenings belonging to each class. (A) Global radiation (left ordinate) and temperature (right ordinate). (B) Ozone (left ordinate) and monoterpene (right ordinate) concentrations. In addition to median concentrations (triangles), the 25th and 75th percentiles are also reported for monoterpene concentration, corresponding respectively to the lower and upper limits of the error bars. (C) CS (left ordinate) and relative humidity (right ordinate). (**D**) Proxy for the concentration of monoterpene ozonolysis products. Markers stand for median values, whereas lower and upper limits of the error bars represent the 25th and 75th percentiles, respectively.

reported to produce these compounds in the atmosphere (*8*, *12*). We thus hypothesize that during evening events, when solar radiation is progressively diminishing, the photochemical processes responsible for OH production are inhibited and that less LVOCs are produced, which might be one the main reasons for the limited cluster growth. In addition, the decreasing of ozonolysis products of monoterpenes after 2000 (Fig. 5, B and D) limits the growth of particles during the night.

Our observations, however, do not preclude the possibility of atmospheric clusters growing further in a system dominated by biogenic vapors when photochemistry is active and produces enough HOMs. The observations reported by Kirkby *et al.* (*10*) and Tröstl *et al.* (*8*) slightly differ from our results because ozonolysis alone was able to support particle growth beyond 20 nm in the CLOUD chamber. This might be, at least partly, related to lower CS in the chamber or the absence of $NO_x$ during the discussed experiments, which meant that all the produced HOMs were nitrogen-free. However, in Hyytiälä, cluster formation and further growth seem to be decoupled processes (*2*).

Assessing the effect of biogenic cluster formation pathways on a global scale will require multiple observations, including, for instance, the analysis of daytime events detected in pristine environments such as the Amazon forest (*29*). Providing a comprehensive description of biogenic ion cluster formation pathways from atmospheric observations will, above all, improve the understanding of preindustrial climate and predictions of future climate. In climate model simulations, an accurate representation of this source of biogenic particles is especially needed to simulate preindustrial conditions because they form the baseline to calculate the radiative forcing caused by anthropogenic emissions. Getting more insight into the formation of pure biogenic particles will also help predict future climate change because this process will most likely be favored by a strong reduction of anthropogenic $SO_2$ and $NO_x$ emissions and the simultaneous increase of BVOC emissions caused by warmer temperatures (*30*, *31*). The intensification of various stressors for plants, such as heat waves, droughts, and infestation, would also cause additional emissions of BVOCs (*32*), which might result in even larger amounts of HOMs leading to higher significance of biogenic NPF in low-$H_2SO_4$ environments.

## MATERIALS AND METHODS

### Instrumental setup

Measurements were performed during spring 2013 (9 April to 15 June) at the SMEAR II station located in Hyytiälä, Southern Finland (61°510°N, 24°170°E, 180 m above sea level) (*33*). The site is mainly surrounded by a Scots pine forest representative of the boreal coniferous forest where BVOC emissions are dominated by monoterpenes (*14*), among which α-pinene is a major HOM precursor (*6*).

Monoterpene volume mixing ratios (VMRs) were continuously monitored at the station with a quadrupole proton transfer reaction mass spectrometer (PTR-MS; Ionicon Analytik GmbH) (*34*) dedicated to real-time monitoring of VMRs down to tens of parts per thousand. Sampling was performed every 3 hours, and monoterpene concentrations were derived from the signal obtained at $m/z$ = 137. The instrumental background was determined every 3 hours using a zero-air generator producing VOC-free air (Parker ChromGas, model 3501). More details about the instrument setup and data analysis can be found in the study of Rantala *et al.* (*35*).

The detection of ion cluster formation events was achieved from the analysis of the ion size distributions measured with a NAIS (Airel) (*36*). In "ion mode," the NAIS simultaneously provides the concentration of both positive and negative ions in the mobility range of 3.2 to

0.0013 $cm^2V^{-1}s^{-1}$, corresponding to 0.8 to 42 nm. In "particle mode," the instrument measures the number size distribution of total particles in the range of ~2 to 42 nm. Measurements were performed with a time resolution of 3 min. In addition, particle number size distributions in the size range of 3 to 1000 nm were measured using a differential mobility particle sizer (DMPS) with a time resolution of 10 min. On the basis of a previous work by Kulmala *et al.* (*37*), the DMPS particle number size distributions were further used to calculate the CS, which describes the loss rate of vapors related to their condensation on aerosols particles.

The chemical composition of naturally charged ions was measured with an APi-TOF (Aerodyne Research Inc. and TOFWERK AG) (*38*) mass spectrometer. The APi-TOF consists of a TOF mass spectrometer capable of determining *m/z* with a resolution >3000 Th/Th in high vacuum conditions, coupled to an APi unit designed to sample ions from ambient pressure at ~0.8 liters/min. During the campaign conducted in spring 2013, the instrument was operated to characterize negative ions. The measurements discussed in this study are given as 1-hour averages, all normalized with respect to the TIC to avoid effects related to changes in the TIC, even if they are minimal (see fig. S8).

To evaluate $H_2SO_4$ concentration, a second APi-TOF was equipped with a nitrate ion-based CI inlet [CI-APi-TOF (*39*)]. The CI inlet allowed for the artificial charging of neutral molecules by $NO_3^-$ ions. Those were produced by exposing clean air (sheath flow) containing nitric acid ($HNO_3$) to α radiation (10-megabecquerel $^{241}Am$ source) or x-rays, and they were guided into the sample flow by an electric field, where they further ionized neutral molecules. Ionized molecules then enter the TOF mass analyzer through a critical orifice. The CI-APi-TOF calibration was based on $H_2SO_4$ detection. The measurements discussed in this study are given as 30-min averages. Both APi-TOF and CI-APi-TOF measurements were analyzed using the MATLAB-based software package tofTools (6.07) developed at the University of Helsinki (*38*).

Ozone concentration was monitored with an analyzer based on the absorption of ultraviolet light (Thermo Environmental Instruments 49C, Thermo Fisher Scientific). Measurements were performed with a time resolution of 1 min, and detection limit of the instrument is about 1 part per billion. Global radiation (0.3 to 4.8 μm) was measured with a pyranometer (Middleton Solar SK08, Middleton Solar). Temperature was measured using a PT-100 sensor, and relative humidity was monitored with relative humidity sensors (Rotronic HygroMet MP102H with Hygroclip HC2-S3, Rotronic AG). All were measured with a time resolution of 1 min.

Particle and ion number size distributions, together with the chemical composition of negative ions and $H_2SO_4$ concentration, were measured at ground level. Other abovementioned measurements were in contrast performed on a mast. Data from the lowest height (4.2 m) were used in the present work for consistency with measurements conducted at ground level, except for global radiation, which was measured at 18 m.

## Determination of the ion cluster formation and growth rates from NAIS measurements

The formation rate of 1.5-nm negative ions ($J_{1.5}^-$) was calculated according to Kulmala *et al.* (*40*)

$$J_{1.5}^- = \frac{dN_{1.5-2.5}^-}{dt} + \mathrm{CoagS}_{1.5} \times N_{1.5-2.5}^- + \frac{\mathrm{GR}_{1.5-3}}{3-1.5} \times N_{1.5-2.5}^- + \alpha \times N_{1.5-2.5}^- \times N_{<2.5}^+ - \chi \times N_{1.5-2.5} \times N_{<1.5}^- \quad (1)$$

$N_{1.5-2.5}^-$ is the number concentration of 1.5- to 2.5-nm negative ions, $N_{<2.5}^+$ is the number concentration of positive ions smaller than 2.5 nm, and $N_{<1.5}^-$ is the number concentration of negative ions smaller than 1.5 nm, all derived from NAIS measurements. $CoagS_{1.5}$ is the coagulation sink of 1.5-nm charged clusters due to their coagulation on larger pre-existing particles and was calculated using the particle number size distributions measured with the DMPS.

$GR_{1.5-3}$ is the growth rate of the ion clusters between 1.5 and 3 nm. The growth rates were calculated separately for the two polarities using the ion size distributions measured with the NAIS and following the "appearance time" method described in details in Lehtipalo *et al.* (*41*). The growth rate values used in the present work were averaged from the two polarities.

The fourth term of Eq. 1 represents the loss of 1.5- to 2.5-nm negative ions due to their recombination with sub–2.5 nm positive ions, whereas the fifth term represents the gain of ions caused by the attachment of sub–1.5 nm negative ions on 1.5- to 2.5-nm neutral clusters. The number concentration of 1.5- to 2.5-nm neutral clusters $N_{1.5-2.5}$ needed for the calculation of this last term was not available for all the events. However, in their recent study, Mazon *et al.* (*18*) have shown that the attachment term only accounted for <2% to the overall value of $J_2^-$. Assuming a similar effect on the calculation of $J_{1.5}^-$, the fifth term of Eq. 1 was thus neglected. The value of $1.6 \times 10^{-6}$ $cm^3s^{-1}$ was used for the recombination rate coefficient α (*42*).

## Determination of the early ion cluster growth rate from Api-TOF measurements

For this study, we used the APi-TOF spectra, which were collected every hour between 1600 and 0000. The average of all event evenings shown on Fig. 2A was calculated by taking the mean of all spectra collected at each hour. Before the averaging step, each spectrum was converted from high-resolution *m/z* to unit mass resolution, after which every unit mass was then divided by its maximum signal on each day individually. The resulting normalized spectra allowed for the comparison of the evolution pattern of the signal of each unit mass between the different evenings regardless of potential day-to-day changes in the absolute intensity of the signal.

The early ion cluster growth rate was determined from the averaged mass spectrum shown on Fig. 2A. For each hour in the time range of 1600 to 0000, we first identified the masses with the highest normalized signal intensity and then plotted the probability distribution by fitting a Gaussian to these masses. The growth rate was then determined by a linear least-square fit through the mean of the Gaussians obtained at each hour. The growth rate calculation was restricted to the period of 1800 to 2100. The uncertainty on the growth rate calculation arising from the last linear-fitting step was 117.5 amu $hour^{-1}$ (95% confidence bound). This value is at the lower limit of the actual uncertainty because other factors were likely to affect the determination of the growth rate, including the mass calibration of the instrument (which directly determines the location of the peaks on the mass axis), the averaging and the normalization of the mass spectra, and the use of a probability distribution. However, the effects of these last factors were complex to quantify and were thus left behind for further investigation.

To compare the growth rate derived from APi-TOF measurements (in amu $hour^{-1}$) with those reported in the literature (in nm $hour^{-1}$), we converted APi-TOF–derived atomic mass units per hour values to nanometers per hour values. We based the mass-to-diameter conversion on Tammet (*43*), using a cluster density of 1400 kg $m^{-3}$. A similar value was recently used by Tröstl *et al.* (*8*). The mean masses of the Gaussians used

to determine the growth rate from APi-TOF measurements were converted according to this method. The growth rate in nanometers per hour was then determined by a linear least-square fit through these diameters, being 0.14 nm hour$^{-1}$ (±0.12 nm hour$^{-1}$, 95% confidence bounds derived from linear fitting).

### Proxy for monoterpene ozonolysis products

The concentration of ozonolysis products of monoterpenes was calculated based on their production in the reaction with ozone and their loss by condensation on pre-existing aerosol particles. The production term was calculated from the measured concentrations of ozone ([$O_3$]) and monoterpenes ([MT]) taking into account the reaction rate between them ($k_{O3+MT}$), whereas the sink term was represented by the CS calculated from the DMPS number size distributions (*37*)

$$[\text{Monoterpene ozonolysis products}] = \frac{k_{O_3+MT} \times [O_3] \times [MT]}{CS} \quad (2)$$

The reaction rate $k_{O3+MT}$ was determined following the methodology previously suggested by Kontkanen *et al.* (*44*). Briefly, to get the correct diurnal cycle, $k_{O3+MT}$ was first calculated from a temperature-dependent relation developed for α-pinene. The obtained values were then modulated using monthly mean rates to take into account the seasonal changes in the composition of monoterpenes.

## SUPPLEMENTARY MATERIALS

Supplementary material for this article is available at http://advances.sciencemag.org/cgi/content/full/4/4/eaar5218/DC1

fig. S1. Ion cluster formation rates.
fig. S2. Time of sunset and beginning and event peak times for each of the 25 events.
fig. S3. Naturally charged HOM dimers and trimers.
fig. S4. Naturally charged HOM monomers.
fig. S5. Sulfuric acid concentration.
fig. S6. Non-nitrate and organonitrate HOM dimers.
fig. S7. Conditions favoring HOMs production and subsequent ion cluster formation.
fig. S8. Evolution of the APi-TOF TIC during the course of the measurement campaign.
table S1. Relationship between the observations of the ion and mass spectrometers.
table S2. Characterization of the active cluster formation period.
table S3. Subsets of compounds representative of non-nitrate and organonitrate HOM dimers.

## REFERENCES AND NOTES


1. J. Merikanto, D. V. Spracklen, G. W. Mann, S. J. Pickering, K. S. Carslaw, Impact of nucleation on global CCN. *Atmos. Chem. Phys.* **9**, 8601–8616 (2009).
2. M. Kulmala, J. Kontkanen, H. Junninen, K. Lehtipalo, H. E. Manninen, T. Nieminen, T. Petäjä, M. Sipilä, S. Schobesberger, P. Rantala, A. Franchin, T. Jokinen, E. Järvinen, M. Äijälä, J. Kangasluoma, J. Hakala, P. P. Aalto, P. Paasonen, J. Mikkilä, J. Vanhanen, J. Aalto, H. Hakola, U. Makkonen, T. Ruuskanen, R. L. Mauldin III, J. Duplissy, H. Vehkamäki, J. Bäck, A. Kortelainen, I. Riipinen, T. Kurtén, M. V. Johnston, J. N. Smith, M. Ehn, T. F. Mentel, K. E. J. Lehtinen, A. Laaksonen, V.-M. Kerminen, D. R. Worsnop, Direct observations of atmospheric aerosol nucleation. *Science* **339**, 943–946 (2013).
3. M. Sipilä, T. Berndt, T. Petäjä, D. Brus, J. Vanhanen, F. Stratmann, J. Patokoski, R. L. Mauldin III, A.-P. Hyvärinen, H. Lihavainen, M. Kulmala, The role of sulfuric acid in atmospheric nucleation. *Science* **327**, 1243–1246 (2010).
4. J. Kirkby, J. Curtius, J. Almeida, E. Dunne, J. Duplissy, S. Ehrhart, A. Franchin, S. Gagné, L. Ickes, A. Kürten, A. Kupc, A. Metzger, F. Riccobono, L. Rondo, S. Schobesberger, G. Tsagkogeorgas, D. Wimmer, A. Amorim, F. Bianchi, M. Breitenlechner, A. David, J. Dommen, A. Downard, M. Ehn, R. C. Flagan, S. Haider, A. Hansel, D. Hauser, W. Jud, H. Junninen, F. Kreissl, A. Kvashin, A. Laaksonen, K. Lehtipalo, J. Lima, E. R. Lovejoy, V. Makhmutov, S. Mathot, J. Mikkilä, P. Minginette, S. Mogo, T. Nieminen, A. Onnela, P. Pereira, T. Petäjä, R. Schnitzhofer, J. H. Seinfield, M. Sipilä, Y. Stozhkov, F. Stratmann, A. Tomé, J. Vanhanen, Y. Viisanen, A. Vrtala, P. E. Wagner, H. Walther, E. Weingartner, H. Wex, P. M. Winkler, K. S. Carslaw, D. R. Worsnop, U. Baltensperger, M. Kulmala, Role of sulphuric acid, ammonia and galactic cosmic rays in atmospheric aerosol nucleation. *Nature* **476**, 429–433 (2011).
5. M. Kulmala, A. Toivonen, J. M. Mäkelä, A. Laaksonen, Analysis of the growth of nucleation mode particles observed in Boreal forest. *Tellus B* **50**, 449–462 (1998).
6. M. Ehn, J. A. Thornton, E. Kleist, M. Sipilä, H. Junninen, I. Pullinen, M. Springer, F. Rubach, R. Tillmann, B. Lee, F. Lopez-Hilfiker, S. Andres, I.-H. Acir, M. Rissanen, T. Jokinen, S. Schobesberger, J. Kangasluoma, J. Kontkanen, T. Nieminen, T. Kurtén, L. B. Nielsen, S. Jørgensen, H. G. Kjaergaard, M. Canagaratna, M. Dal Maso, T. Berndt, T. Petäjä, A. Wahner, V.-M. Kerminen, M. Kulmala, D. R. Worsnop, J. Wildt, T. F. Mentel, A large source of low-volatility secondary organic aerosol. *Nature* **506**, 476–479 (2014).
7. I. Riipinen, T. Yli-Juuti, J. R. Pierce, T. Petäjä, D. R. Worsnop, M. Kulmala, N. M. Donahue, The contribution of organics to atmospheric nanoparticle growth. *Nat. Geosci.* **5**, 453–458 (2012).
8. J. Tröstl, W. K. Chuang, H. Gordon, M. Heinritzi, C. Yan, U. Molteni, L. Ahlm, C. Frege, F. Bianchi, R. Wagner, M. Simon, K. Lehtipalo, C. Williamson, J. S. Craven, J. Duplissy, A. Adamov, J. Almeida, A.-K. Bernhammer, M. Breitenlechner, S. Brilke, A. Dias, S. Ehrhart, R. C. Flagan, A. Franchin, C. Fuchs, R. Guida, M. Gysel, A. Hansel, C. R. Hoyle, T. Jokinen, H. Junninen, J. Kangasluoma, H. Keskinen, J. Kim, M. Krapf, A. Kürten, A. Laaksonen, M. Lawler, M. Leiminger, S. Mathot, O. Möhler, T. Nieminen, A. Onnela, T. Petäjä, F. M. Piel, P. Miettinen, M. P. Rissanen, L. Rondo, N. Sarnela, S. Schobesberger, K. Sengupta, M. Sipilä, J. N. Smith, G. Steiner, A. Tomè, A. Virtanen, A. C. Wagner, E. Weingartner, D. Wimmer, P. M. Winkler, P. Ye, K. S. Carslaw, J. Curtius, J. Dommen, J. Kirkby, M. Kulmala, I. Riipinen, D. R. Worsnop, N. M. Donahue, U. Baltensperger, The role of low-volatility organic compounds in initial particle growth in the atmosphere. *Nature* **533**, 527–531 (2016).
9. F. Bianchi, J. Tröstl, H. Junninen, C. Frege, S. Henne, C. R. Hoyle, U. Molteni, E. Herrmann, A. Adamov, N. Bukowiecki, X. Chen, J. Duplissy, M. Gysel, M. Hutterli, J. Kangasluoma, J. Kontkanen, A. Kürten, H. E. Manninen, S. Münch, O. Peräkylä, T. Petäjä, L. Rondo, C. Williamson, E. Weingartner, J. Curtius, D. R. Worsnop, M. Kulmala, J. Dommen, U. Baltensperger, New particle formation in the free troposphere: A question of chemistry and timing. *Science* **352**, 1109–1112 (2016).
10. J. Kirkby, J. Duplissy, K. Sengupta, C. Frege, H. Gordon, C. Williamson, M. Heinritzi, M. Simon, C. Yan, J. Almeida, J. Tröstl, T. Nieminen, I. K. Ortega, R. Wagner, A. Adamov, A. Amorim, A.-K. Bernhammer, F. Bianchi, M. Breitenlechner, S. Brilke, X. Chen, J. Craven, A. Dias, S. Ehrhart, R. C. Flagan, A. Franchin, C. Fuchs, R. Guida, J. Hakala, C. R. Hoyle, T. Jokinen, H. Junninen, J. Kangasluoma, J. Kim, M. Krapf, A. Kürten, A. Laaksonen, K. Lehtipalo, V. Makhmutov, S. Mathot, U. Molteni, A. Onnela, O. Peräkylä, F. Piel, T. Petäjä, A. P. Praplan, K. Pringle, A. Rap, N. A. D. Richards, I. Riipinen, M. P. Rissanen, L. Rondo, N. Sarnela, S. Schobesberger, C. E. Scott, J. H. Seinfield, M. Sipilä, G. Steiner, Y. Stozhkov, F. Stratmann, A. Tomé, A. Virtanen, A. L. Vogel, A. C. Wagner, P. E. Wagner, E. Weingartner, D. Wimmer, P. M. Winkler, P. Ye, X. Zhang, A. Hansel, J. Dommen, N. M. Donahue, D. R. Worsnop, U. Baltensperger, M. Kulmala, K. S. Carslaw, J. Curtius, Ion-induced nucleation of pure biogenic particles. *Nature* **533**, 521–526 (2016).
11. H. Gordon, K. Sengupta, A. Rap, J. Duplissy, C. Frege, C. Williamson, M. Heinritzi, M. Simon, C. Yan, J. Almeida, J. Tröstl, T. Nieminen, I. K. Ortega, R. Wagner, E. M. Dunne, A. Adamov, A. Amorim, A.-K. Bernhammer, F. Bianchi, M. Breitenlechner, S. Brilke, X. Chen, J. S. Craven, A. Dias, S. Ehrhart, L. Fischer, R. C. Flagan, A. Franchin, C. Fuchs, R. Guida, J. Hakala, C. R. Hoyle, T. Jokinen, H. Junninen, J. Kangasluoma, J. Kim, J. Kirkby, M. Krapf, A. Kürten, A. Laaksonen, K. Lehtipalo, V. Makhmutov, S. Mathot, U. Molteni, S. A. Monks, A. Onnela, O. Peräkylä, F. Piel, T. Petäjä, A. P. Praplan, K. J. Pringle, N. A. D. Richards, M. P. Rissanen, L. Rondo, N. Sarnela, S. Schobesberger, C. E. Scott, J. H. Seinfield, S. Sharma, M. Sipilä, G. Steiner, Y. Stozhkov, F. Stratmann, A. Tomé, A. Virtanen, A. L. Vogel, A. C. Wagner, P. E. Wagner, E. Weingartner, D. Wimmer, P. M. Winkler, P. Ye, X. Zhang, A. Hansel, J. Dommen, N. M. Donahue, D. R. Worsnop, U. Baltensperger, M. Kulmala, J. Curtius, K. S. Carslaw, Reduced anthropogenic aerosol radiative forcing caused by biogenic new particle formation. *Proc. Natl. Acad. Sci. U.S.A.* **113**, 12053–12058 (2016).
12. S. Schobesberger, H. Junninen, F. Bianchi, G. Lönn, M. Ehn, K. Lehtipalo, J. Dommen, S. Ehrhart, I. K. Ortega, A. Franchin, T. Nieminen, F. Riccobono, M. Hutterli, J. Duplissy, J. Almeida, A. Amorim, M. Breitenlechner, A. J. Downard, E. M. Dunne, R. C. Flagan, M. Kajos, H. Keskinen, J. Kirkby, A. Kupc, A. Kürten, T. Kurtén, A. Laaksonen, S. Mathot, A. Onnela, A. P. Praplan, L. Rondo, F. D. Santos, S. Schallhart, R. Schnitzhofer, M. Sipilä, A. Tomé, G. Tsagkogeorgas, H. Vehkamäki, D. Wimmer, U. Baltensperger, K. S. Carslaw, J. Curtius, A. Hansel, T. Petäjä, M. Kulmala, N. M. Donahue, D. R. Worsnop, Molecular understanding of atmospheric particle formation from sulfuric acid and large oxidized organic molecules. *Proc. Natl. Acad. Sci. U.S.A.* **110**, 17223–17228 (2013).
13. F. Bianchi, O. Garmash, X. He, C. Yan, S. Iyer, I. Rosendahl, Z. Xu, M. P. Rissanen, M. Riva, R. Taipale, N. Sarnela, T. Petäjä, D. R. Worsnop, M. Kulmala, M. Ehn, H. Junninen, The role of highly oxygenated molecules (HOMs) in determining the composition of ambient ions in the boreal forest. *Atmos. Chem. Phys.* **17**, 13819–13831 (2017).
14. H. Hakola, V. Tarvainen, J. Bäck, H. Ranta, B. Bonn, J. Rinne, M. Kulmala, Seasonal variation of mono- and sesquiterpene emission rates of Scots pine. *Biogeosciences* **3**, 93–101 (2006).

15. C. Yan, W. Nie, M. Äijälä, M. P. Rissanen, M. R. Canagaratna, P. Massoli, H. Junninen, T. Jokinen, N. Sarnela, S. A. K. Häme, S. Schobesberger, F. Canonaco, L. Yao, A. S. H. Prévôt, T. Petäjä, M. Kulmala, M. Sipilä, D. R. Worsnop, M. Ehn, Source characterization of highly oxidized multifunctional compounds in a boreal forest environment using positive matrix factorization. *Atmos. Chem. Phys.* **16**, 12715–12731 (2016).
16. M. Ehn, E. Kleist, H. Junninen, T. Petäjä, G. Lönn, S. Schobesberger, M. Dal Maso, A. Trimborn, M. Kulmala, D. R. Worsnop, A. Wahner, J. Wildt, T. F. Mentel, Gas phase formation of extremely oxidized pinene reaction products in chamber and ambient air. *Atmos. Chem. Phys.* **12**, 5113–5127 (2012).
17. H. Tammet, U. Hõrrak, M. Kulmala, Negatively charged nanoparticles produced by splashing of water. *Atmos. Chem. Phys.* **9**, 357–367 (2009).
18. S. B. Mazon, J. Kontkanen, H. E. Manninen, T. Nieminen, V.-M. Kerminen, M. Kulmala, A long-term comparison of nighttime cluster events and daytime ion formation in a boreal forest. *Boreal Environ. Res.* **21**, 242–261 (2016).
19. H. Junninen, M. Hulkkonen, I. Riipinen, T. Nieminen, A. Hirsikko, T. Suni, M. Boy, S.-H. Lee, M. Vana, H. Tammet, V.-M. Kerminen, M. Kulmala, Observations on nocturnal growth of atmospheric clusters. *Tellus B* **60**, 365–371 (2008).
20. K. Lehtipalo, M. Sipilä, H. Junninen, M. Ehn, T. Berndt, M. K. Kajos, D. R. Worsnop, T. Petäjä, M. Kulmala, Observations of Nano-CN in the Nocturnal Boreal Forest. *Aerosol Sci. Technol.* **45**, 499–509 (2011).
21. T. Yli-Juuti, T. Nieminen, A. Hirsikko, P. P. Aalto, E. Asmi, U. Hõrrak, H. E. Manninen, J. Patokoski, M. Dal Maso, T. Petäjä, J. Rinne, M. Kulmala, I. Riipinen, Growth rates of nucleation mode particles in Hyytiälä during 2003–2009: Variation with particle size, season, data analysis method and ambient conditions. *Atmos. Chem. Phys.* **11**, 12865–12886 (2011).
22. M. P. Rissanen, T. Kurtén, M. Sipilä, J. A. Thornton, J. Kangasluoma, N. Sarnela, H. Junninen, S. Jørgensen, S. Schallhart, M. K. Kajos, R. Taipale, M. Springer, T. F. Mentel, T. Ruuskanen, T. Petäjä, D. R. Worsnop, H. G. Kjaergaard, M. Ehn, The formation of highly oxidized multifunctional products in the ozonolysis of cyclohexene. *J. Am. Chem. Soc.* **136**, 15596–15606 (2014).
23. C. Frege, I. K. Ortega, M. P. Rissanen, A. P. Praplan, G. Steiner, M. Heinritzi, L. Ahonen, A. Amorim, A.-K. Bernhammer, F. Bianchi, S. Brilke, M. Breitenlechner, L. Dada, A. Dias, J. Duplissy, S. Ehrhart, I. El-Haddad, L. Fischer, C. Fuchs, O. Garmash, M. Gonin, A. Hansel, C. R. Hoyle, T. Jokinen, H. Junninen, J. Kirkby, A. Kürten, K. Lehtipalo, M. Leiminger, R. L. Mauldin, U. Molteni, L. Nichman, T. Petäjä, N. Sarnela, S. Schobesberger, M. Simon, M. Sipilä, D. Stolzenburg, A. Tomé, A. L. Vogel, A. C. Wagner, R. Wagner, M. Xiao, C. Yan, P. Ye, J. Curtius, N. M. Donahue, R. C. Flagan, M. Kulmala, D. R. Worsnop, P. M. Winkler, J. Dommen, U. Baltensperger, Influence of temperature on the molecular composition of ions and charged clusters during pure biogenic nucleation. *Atmos. Chem. Phys.* **18**, 65–79 (2018).
24. M. Ehn, H. Junninen, T. Petäjä, T. Kurtén, V.-M. Kerminen, S. Schobesberger, H. E. Manninen, I. K. Ortega, H. Vehkamäki, M. Kulmala, D. R. Worsnop, Composition and temporal behavior of ambient ions in the boreal forest. *Atmos. Chem. Phys.* **10**, 8513–8530 (2010).
25. C. Mohr, F. D. Lopez-Hilfiker, T. Yli-Juuti, A. Heitto, A. Lutz, M. Hallquist, E. L. D'Ambro, M. P. Rissanen, L. Hao, S. Schobesberger, M. Kulmala, R. L. Mauldin III, U. Makkonen, M. Sipilä, T. Petäjä, J. A. Thornton, Ambient observations of dimers from terpene oxidation in the gas phase: Implications for new particle formation and growth. *Geophys. Res. Lett.* **44**, 2958–2966 (2017).
26. J. Almeida, S. Schobesberger, A. Kürten, I. K. Ortega, O. Kupiainen-Määttä, A. P. Praplan, A. Adamov, A. Amorim, F. Bianchi, M. Breitenlechner, A. David, J. Dommen, N. M. Donahue, A. Downard, E. Dunne, J. Duplissy, S. Ehrhart, R. C. Flagan, A. Franchin, R. Guida, J. Hakala, A. Hansel, M. Heinritzi, H. Henschel, T. Jokinen, H. Junninen, M. Kajos, J. Kangasluoma, H. Keskinen, A. Kupc, T. Kurtén, A. N. Kvashin, A. Laaksonen, K. Lehtipalo, M. Leiminger, J. Leppä, V. Loukonen, V. Makhmutov, S. Mathot, M. J. McGrath, T. Nieminen, T. Olenius, A. Onnela, T. Petäjä, F. Riccobono, I. Riipinen, M. Rissanen, L. Rondo, T. Ruuskanen, F. D. Santos, N. Sarnela, S. Schallhart, R. Schnitzhofer, J. H. Seinfeld, M. Simon, M. Sipilä, Y. Stozhkov, F. Stratmann, A. Tomé, J. Tröstl, G. Tsagkogeorgas, P. Vaattovaara, Y. Viisanen, A. Virtanen, A. Vrtala, P. E. Wagner, E. Weingartner, H. Wex, C. Williamson, D. Wimmer, P. Ye, T. Yli-Juuti, K. S. Carslaw, M. Kulmala, J. Curtius, U. Baltensperger, D. R. Worsnop, H. Vehkamäki, J. Kirkby, Molecular understanding of sulphuric acid–amine particle nucleation in the atmosphere. *Nature* **502**, 359–363 (2013).
27. J. Duplissy, J. Merikanto, A. Franchin, G. Tsagkogeorgas, J. Kangasluoma, D. Wimmer, H. Vuollekoski, S. Schobesberger, K. Lehtipalo, R. C. Flagan, D. Brus, N. M. Donahue, H. Vehkamäki, J. Almeida, A. Amorim, P. Barmet, F. Bianchi, M. Breitenlechner, E. M. Dunne, R. Guida, H. Henschel, H. Junninen, J. Kirkby, A. Kürten, A. Kupc, A. Määttänen, V. Makhmutov, S. Mathot, T. Nieminen, A. Onnela, A. P. Praplan, F. Riccobono, L. Rondo, G. Steiner, A. Tome, H. Walther, U. Baltensperger, K. S. Carslaw, J. Dommen, A. Hansel, T. Petäjä, M. Sipilä, F. Stratmann, A. Vrtala, P. E. Wagner, D. R. Worsnop, J. Curtius, M. Kulmala, Effect of ions on sulfuric acid-water binary particle formation: 2. Experimental data and comparison with QC-normalized classical nucleation theory. *J. Geophys. Res. Atmos.* **121**, 1752–1775 (2016).
28. R. L. Mauldin III, T. Berndt, M. Sipilä, P. Paasonen, T. Petäjä, S. Kim, T. Kurtén, F. Stratmann, V.-M. Kerminen, M. Kulmala, A new atmospherically relevant oxidant of sulphur dioxide. *Nature* **488**, 193–196 (2012).
29. S. T. Martin, M. O. Andreae, D. Althausen, P. Artaxo, H. Baars, S. Borrmann, Q. Chen, D. K. Farmer, A. Guenther, S. S. Gunthe, J. L. Jimenez, T. Karl, K. Longo, A. Manzi, T. Müller, T. Pauliquevis, M. D. Petters, A. J. Prenni, U. Pöschl, L. V. Rizzo, J. Schneider, J. N. Smith, E. Swietlicki, J. Tota, J. Wang, A. Wiedensohler, S. R. Zorn, An overview of the Amazonian Aerosol Characterization Experiment 2008 (AMAZE-08). *Atmos. Chem. Phys.* **10**, 11415–11438 (2010).
30. G. Lin, J. E. Penner, C. Zhou, How will SOA change in the future? *Geophys. Res. Lett.* **43**, 1718–1726 (2016).
31. J. Rogelj, S. Rao, D. L. McCollum, S. Pachauri, Z. Klimont, V. Krey, K. Riahi, Air-pollution emission ranges consistent with the representative concentration pathways. *Nat. Clim. Chang.* **4**, 446–450 (2014).
32. D. F. Zhao, A. Buchholz, R. Tillmann, E. Kleist, C. Wu, F. Rubach, A. Kiendler-Scharr, Y. Rudich, J. Wildt, T. F. Mentel, Environmental conditions regulate the impact of plants on cloud formation. *Nat. Commun.* **8**, 14067 (2017).
33. P. Hari, M. Kulmala, Station for measuring ecosystem-atmosphere relations (SMEAR II). *Boreal Environ. Res.* **10**, 315–322 (2005).
34. R. Taipale, T. M. Ruuskanen, J. Rinne, M. K. Kajos, H. Hakola, T. Pohja, M. Kulmala, Technical Note: Quantitative long-term measurements of VOC concentrations by PTR-MS - measurement, calibration, and volume mixing ratio calculation methods. *Atmos. Chem. Phys.* **8**, 6681–6698 (2008).
35. P. Rantala, J. Aalto, R. Taipale, T. M. Ruuskanen, J. Rinne, Annual cycle of volatile organic compound exchange between a boreal pine forest and the atmosphere. *Biogeosciences* **12**, 5753–5770 (2015).
36. S. Mirme, A. Mirme, The mathematical principles and design of the NAIS – a spectrometer for the measurement of cluster ion and nanometer aerosol size distributions. *Atmos. Meas. Tech.* **6**, 1061–1071 (2013).
37. M. Kulmala, M. Dal Maso, J. M. Mäkelä, L. Pirjola, M. Väkevä, P. Aalto, P. Miikkulainen, K. Hämeri, C. D. O'Dowd, On the formation, growth and composition of nucleation mode particles. *Tellus B* **53**, 479–490 (2001).
38. H. Junninen, M. Ehn, T. Petäjä, L. Luosujärvi, T. Kotiaho, R. Kostiainen, U. Rohner, M. Gonin, K. Fuhrer, M. Kulmala, D. R. Worsnop, A high-resolution mass spectrometer to measure atmospheric ion composition. *Atmos. Meas. Tech.* **3**, 1039–1053 (2010).
39. T. Jokinen, M. Sipilä, H. Junninen, M. Ehn, G. Lönn, J. Hakala, T. Petäjä, R. L. Mauldin III, M. Kulmala, D. R. Worsnop, Atmospheric sulphuric acid and neutral cluster measurements using CI-APi-TOF. *Atmos. Chem. Phys.* **12**, 4117–4125 (2012).
40. M. Kulmala, T. Petäjä, T. Nieminen, M. Sipilä, H. E. Manninen, K. Lehtipalo, M. Dal Maso, P. P. Aalto, H. Junninen, P. Paasonen, I. Riipinen, K. E. J. Lehtinen, A. Laaksonen, V.-M. Kerminen, Measurement of the nucleation of atmospheric aerosol particles. *Nat. Protoc.* **7**, 1651–1667 (2012).
41. K. Lehtipalo, J. Leppä, J. Kontkanen, J. Kangasluoma, A. Franchin, D. Wimmer, S. Schobesberger, H. Junninen, T. Petäjä, M. Sipilä, J. Mikkilä, J. Vanhanen, D. R. Worsnop, M. Kulmala, Methods for determining particle size distribution and growth rates between 1 and 3 nm using the Particle Size Magnifier. *Boreal Environ. Res.* **19**, 215–236 (2014).
42. H. Tammet, M. Kulmala, Simulation tool for atmospheric aerosol nucleation bursts. *J. Aerosol Sci.* **36**, 173–196 (2005).
43. H. Tammet, Size and mobility of nanometer particles, clusters and ions. *J. Aerosol Sci.* **26**, 459–475 (1995).
44. J. Kontkanen, P. Paasonen, J. Aalto, J. Bäck, P. Rantala, T. Petäjä, M. Kulmala, Simple proxies for estimating the concentrations of monoterpenes and their oxidation products at a boreal forest site. *Atmos. Chem. Phys.* **16**, 13291–13307 (2016).


**Acknowledgments:** We acknowledge T. Nieminen, H. Manninen, J. Kontkanen, and M. Riva for useful discussions. We also acknowledge the personnel of the Hyytiälä Forestry Field Station and all researchers and students involved in the measurement campaign discussed in the present manuscript for help during field measurements. We thank the tofTools team for providing tools for mass spectrometry analysis. **Funding:** This work was funded by the Academy of Finland Centre of Excellence Program (grant no. 272041), the Doctoral Programme in Atmospheric Sciences (University of Helsinki), the European Research Council [ERC; GASPARCON (Molecular steps of gas-to-particle conversion: From oxidation to precursors, clusters and secondary aerosol particles) grant no. 714621], and the ERC under the European Union's Horizon 2020 Research and Innovation Programme (grant agreement no. 742206). In addition, K.L. acknowledges funding from European Commission's Horizon 2020 programme (Marie Skłodowska-Curie Actions–Individual Fellowships project NanoCAVa, no. 656994), and F.B. acknowledges funding from the Swiss National Science Foundation (grant P2EZP2_168787). **Author contributions:** M.K., T.P., K.L., and M.S. organized and designed the intensive measurement campaign. N.S., T.J., and H.J. conducted the measurements. H.J. contributed to the analytic tools. C.R., Q.Z., L.D., C.Y., S.B.M., and F.B.

analyzed the data. C.R., L.D., V.-M.K., and K.L. wrote the manuscript. **Competing interests:** The authors declare they have no competing interests. **Data and materials availability:** All data needed to evaluate the conclusions in the paper are present in the paper and/or the Supplementary Materials. Additional data related to this paper may be requested from the authors. Raw data including meteorological variables, ozone and monoterpene concentrations, and particle size distributions from DMPS are available at https://avaa.tdata.fi/web/smart/smear. In addition, a time series of HOMs signal from APi-TOF and sulfuric acid concentration from CI-APi-TOF are available from the authors upon request.

Submitted 17 November 2017
Accepted 12 March 2018
Published 25 April 2018
10.1126/sciadv.aar5218

**Citation:** C. Rose, Q. Zha, L. Dada, C. Yan, K. Lehtipalo, H. Junninen, S. B. Mazon, T. Jokinen, N. Sarnela, M. Sipilä, T. Petäjä, V.-M. Kerminen, F. Bianchi, M. Kulmala, Observations of biogenic ion-induced cluster formation in the atmosphere. *Sci. Adv.* **4**, eaar5218 (2018).

# Observations of biogenic ion-induced cluster formation in the atmosphere

Clémence Rose, Qiaozhi Zha, Lubna Dada, Chao Yan, Katrianne Lehtipalo, Heikki Junninen, Stephany Buenrostro Mazon, Tuija Jokinen, Nina Sarnela, Mikko Sipilä, Tuukka Petäjä, Veli-Matti Kerminen, Federico Bianchi and Markku Kulmala

*Sci Adv* **4** (4), eaar5218.
DOI: 10.1126/sciadv.aar5218